Johannes Gutenberg-University Mainz
Institute of Geosciences

- Partial melting within the lower crust –
Constraints from bulk rock geochemical data and trace element mineral analyses of granulites and migmatites from Central Finland

Dissertation zur Erlangung des Doktorgrades der Mathematisch-Naturwissenschaftlichen Fakultät der Johannes Gutenberg-Universität, Mainz

submitted by Dipl. Geol. Franziska Nehring

Mainz, Juni 2007

Table of contents

Summary **I**

Zusammenfassung **V**

Part I: Laser-ablation ICP-MS analysis of siliceous rock glasses fused on an Iridium strip heater using MgO dilution **1**
(Franziska Nehring, Dorrit E. Jacob, Matthias G. Barth, Stephen F. Foley)

Part II: - Internal differentiation of the Archean continental crust - Fluid-controlled melting of granulites and TTG-amphibolite associations in Central Finland **23**
(Franziska Nehring, Stephen F. Foley, Pentti Hölttä, Alfons van den Kerkhof)

Part III: Trace element partitioning in the granulite facies **76**
(Franziska Nehring, Stephen F. Foley, Pentti Hölttä)

Summary

The PhD thesis at hand predominantly concerns geochemical constraints on recycling and partial melting of Archean continental crust. A natural example of such processes was found in the Iisalmi area of Central Finland. The rocks from this area are Middle to Late Archean in age and experienced metamorphism and partial melting between 2.7-2.63 Ga.

The work is based on extensive field work, carried out in cooperation with the Geological Survey of Finland. It is furthermore founded on bulk rock geochemical data as well as *in-situ* analyses of minerals. All geochemical data were obtained at the Institute of Geosciences, University of Mainz using X-ray fluorescence (major elements), solution ICP-MS and laser ablation-ICP-MS (trace elements) for bulk rock geochemical analyses. Mineral analyses were accomplished by electron microprobe and laser ablation ICP-MS. Fluid inclusions in minerals were studied by microscope on a heating-freezing-stage at the Geoscience Center, University Göttingen.

The thesis is subdivided into three major parts. **Part I** focuses on the development of a new analytical method for bulk rock trace element determination. **Part II** uses the bulk rock geochemical data and the results from fluid inclusion studies for discrimination of melting processes observed in different rock types from the working area. **Part III** of the thesis describes how analyses of minerals from a specific rock type (granulite) can be used to determine partition coefficients between different minerals and between minerals and melt suitable for lower crustal conditions.

Part I: Laser-ablation ICP-MS analysis of siliceous rock glasses fused on an Iridium strip heater using MgO dilution

Laser ablation-ICP-MS of bulk rock samples requires fusion of rock powder on an Iridium strip heater in order to produce homogeneous glasses for ablation. This method is easily applicable for mafic rock samples whose melts have low viscosities and homogenize quickly at temperatures of ~1200°C. Highly viscous melts of felsic samples prevent melting and homogenization at comparable temperatures. **Part I** describes how fusion of felsic samples can be enabled by addition of MgO to the rock powder and adjustment of melting temperature and melting duration to the respective rock composition. Data obtained by this method from geochemical reference

materials (AGV-2, GSP-2, JG-1a) usually agree within 10 % with published values. Similar accordance was observed between data from solution ICP-MS and laser ablation-ICP-MS of natural rock samples. Advantages of the fusion method are lower detection limits compared to XRF analyses and avoidance of wet-chemical processing and use of strong acids as in solution ICP-MS as well as smaller sample volumes compared to the other methods. Thus, the method is an user-friendly analytical tool that can be easily adopted wherever laser ablation-ICP-MS is used for data acquisition.

Part II: - Internal differentiation of the Archean continental crust - Fluid-controlled melting of granulites and TTG-amphibolite associations in Central Finland

Part II focuses on the conclusions about crustal recycling and crustal melting that can be drawn from the field work, bulk rock data and fluid inclusion studies. The working area comprises mafic and intermediate granulites that are hosted by upper-amphibolite facies migmatitic gneisses of the typical Archean association 'tonalite-trondhjemite-granodiorite' (TTG). Amphibolites of variable extension are interspersed with the TTG gneisses.

Fluid inclusion studies demonstrate a major change in fluid composition from CO_2-dominated fluids in granulites to aqueous fluids in TTG gneisses and associated amphibolites. Carbonic inclusions in granulites were captured during peak metamorphism but experienced retrograde density resetting. Their presence suggests that dry conditions were reached during metamorphism and melting of the mafic and intermediate precursor rocks of the granulites. Partial melts were generated in this dry environment by dehydration melting of amphibole that in addition to tonalitic melts simultaneously produced the typical anhydrous minerals assemblages of granulites (grt + cpx + pl ± amph or opx + cpx + pl + amph). Trace element modelling showed that mafic granulites are residues of 10-30 % melt extraction from amphibolitic precursor rocks. The maximum degree of melting in intermediate granulites was ~10 % as inferred from modal abundances of amphibole, clinopyroxene and orthopyroxene.

Carbonic inclusions are absent in upper-amphibolite facies migmatites whereas aqueous inclusion with up to 20 wt% NaCl are abundant. This suggests that melting within TTG gneisses and amphibolites took place in the presence of an aqueous fluid phase that enabled melting at the wet solidus at temperatures of 700-750°C. The stability of plagioclase decreases in the presence

of an aqueous fluid such that the melting reaction becomes pl + qtz → melt. The strong disruption of pre-metamorphic structures in some outcrops suggests that the maximum amount of melt in TTG gneisses was ~25 vol%.

The presence of leucosomes in all rock types is taken as the principle evidence for melt formation. However, mineralogical appearance as well as major and trace element composition of many leucosomes imply that leucosomes seldom represent frozen *in-situ* melts. They are better considered as remnants of the melt channel network, e.g. ways on which melts escaped from the system. Nevertheless, leucosome composition is related to host rock composition what can be concluded for instance from the Na/Ca ratios of leucosomes. Tonalitic leucosomes are formed in calcic precursor rocks (mafic granulites, amphibolites) whereas leucosomes from the more sodic TTG gneisses show affinities towards trondhjemite.

Part III: Trace element partitioning in the granulite facies

Mineral analyses were undertaken to constrain distribution of trace elements among granulite facies minerals and between minerals and melt. Furthermore, these data yield evidence for melt removal and melt metasomatism.

According to electron microprobe analyses prograde amphiboles in granulites are pargasites and edenites. Clinopyroxene is augitic-diopsidic (X_{Mg} 0.6-0.8, X_{Wo} 0.4-0.5). The mineralogical assemblage furthermore comprises enstatitic orthopyroxene (X_{Mg} 0.45-0.7) and garnet with X_{Alm} 0.5-0.62 and X_{Grs} 0.15-0.28. Plagioclase has a more variable composition ranging between plagioclase with X_{An} 0.5-0.7 in mafic granulites and more sodic plagioclase (X_{An} 0.25-0.5) in intermediate granulites.

The trace element analyses by laser ablation-ICP-MS show coherent distribution among the principal mineral phases independent of rock composition. REE contents in amphibole are about 3 times higher than REE contents in clinopyroxene from the same sample. This remarkable consistency has to be taken into consideration in models of lower crustal melting where amphibole is replaced by clinopyroxene in the course of melting. Equilibrium distribution of the REE is also observed between garnet and clinopyroxene or garnet and amphibole intergrown with each other. However equilibrium between matrix clinopyroxene / amphibole and garnet was not obtained which suggests a late stage growth of garnet and slow diffusion and equilibration of the REE during metamorphism.

The data provide a first set of distribution coefficients of the transition metals (Sc, V, Cr, Ni) in the lower crust. In addition, analyses of ilmenite and apatite demonstrate the strong influence of accessory phases on trace element distribution. Apatite contains high amounts of REE and Sr while ilmenite incorporates about 20-30 times higher amounts of Nb and Ta than amphibole.

Mineral / melt partition coefficients were derived from predictive models, comparison with published data and actually observed ratios between minerals and melt (leucosome). Thereby a self-consistent set of mineral / melt partition coefficients was derived which is applicable for models of melting of mafic and intermediate rocks under lower crustal conditions.

Granulite patches from a melt-rich environment (diatexite) contain the most sodic plagioclase, show enrichment of potassium in amphiboles and frequently comprise potassic feldspar. This points to an addition of alkalis to these samples. Furthermore, amphiboles from such granulite patches are enriched in incompatible trace elements (Rb, Nb, Ta, Th) and contain the highest amounts of REE with noticeable negative Eu anomaly. These geochemical features of granulite patches within diatexite are interpreted as a result of metasomatism and refertilization by a percolating melt phase. A high melt / restite ratio in diatexites is inferred from the high proportion of leucocratic material (leucosomes) in these outcrops. Despite the fact that also this leucocratic material has residual features (see part II), its large volumetric amount points to an increased melt flow through these rocks. Thus, the melt signature became imprinted on minerals in granulite patches which were disrupted and dislocated from the granulite host and became incorporated in the melt phase.

Zusammenfassung

Die vorliegende Dissertation beschäftigt sich mit geochemischen Prozessen, die im Zusammenhang mit partiellen Schmelzvorgängen in archaischen Krustenblöcken stehen. Ein natürliches Beispiel für krustales Schmelzen in unterschiedlichen Gesteinsarten bietet die Gegend um Iisalmi in Zentral-Finnland. Die Gesteine dieses Gebietes haben einen mittel- bis spät-archaischen Ursprung und wurden im Zeitraum vor 2.7-2.63 Milliarden Jahren metamorph überprägt und partiell geschmolzen.

Die Arbeit basiert auf umfangreichen Geländearbeiten, welche in Zusammenarbeit mit dem Geologischen Dienst von Finnland ausgeführt wurden. Anschließende geochemische Analysen der Haupt- und Spurenelemente des Gesamtgesteins wurden mittels Röntgenfluoreszenz sowie mittels Flüssig-ICP-MS und Laser-Ablations-ICP-MS am Institut für Geowissenschaften der Universität Mainz durchgeführt. Zur Untersuchung der Mineralphasen wurden die Elektronenmikrosonde und ebenfalls die Laser-Ablations-ICP-MS am selbigen Institut verwendet. Fluideinschlüsse in Mineralen wurden mikroskopisch am Geowissenschaftichen Zentrum der Universität Göttingen untersucht.

1. Teil: Herstellung von Silizium-reichen Gesteinsgläsern auf einem heizbaren Iridium-Streifen und Analyse der Gläser mittels Laser-Ablations-ICP-MS

Um die Laser-Ablations-ICP-MS für die Analyse von Gesamtgesteinsproben nutzen zu können, wird das Gesteinspulver auf einem heizbaren Iridium-Streifen zu einem homogenen Gesteinsglas geschmolzen. Diese Methode ist besonders für mafische Gesteinsproben geeignet, deren niedrig viskose Schmelzen bereits bei 1200°C Schmelztemperatur homogenisieren. Dagegen verhindert die hohe Viskosität der Schmelzen felsischer Gesteinsproben mit höherem SiO_2-Gehalt eine Homogenisierung der Schmelze bei vergleichbaren Temperaturen. Um felsische Proben dennoch zu homogenen Gesteinsgläsern zu verarbeiten, wurde eine Methode erprobt, in der dem Gesteinspulver Magnesiumoxid zugesetzt wird, welches die Viskosität deutlich verringert. Zudem werden die Schmelztemperaturen und Schmelzintervalle auf die jeweilige Gesteinszusammensetzung angepasst. Analysen von geochemischen Referenzmaterialien (AGV-2, GSP-2, JG-1a), die mit dieser Methode angefertigt wurden, ergaben eine Übereinstimmung mit publizierten Werten innerhalb von 10 %. Der Vergleich von Analysen der Laser-Ablations-ICP-

MS und Analysen mittels Röntgenfluoreszenz und Flüssig-ICP-MS von den Gesteinsproben aus dem Untersuchungsgebiet ergab eine ähnliche Übereinstimmung.

Vorteile der Schmelzmethode gegenüber Spurenelementanalysen mittels Röntgenfluoreszenz sind die deutlich niedrigeren Nachweisgrenzen der ICP-MS. Die einfache Durchführbarkeit des Schmelzprozesses bietet zudem einen analytischen Vorteil gegenüber nasschemischen Aufschlussverfahren unter dem Einsatz starker Säuren für die Flüssig-ICP-MS. Die Methode ist daher besonders empfehlenswert für Fragestellungen, in denen Laser-Ablations-ICP-MS für ein breites Probenspektrum eingesetzt werden soll.

2. Teil: - Differentierung archaischer kontinentaler Kruste -
Einfluss der Fluidzusammensetzung auf Schmelzprozesse in Granuliten und TTG-Amphibolit-Vergesellschaftungen in Zentral-Finnland

Im Arbeitsgebiet treten mafische und intermediäre Granulite umgeben von migmatitischen Gneisen der oberen Amphibolitfazies auf. Diese Gneise gehören der typisch archaischen Paragenese ‘Tonalit-Trondhjemit-Granodiorit’ (TTG) an, sind jedoch zudem von Amphiboliten variabler Ausdehnung durchsetzt.

Die Untersuchung von Fluideinschlüssen in Mineralen ergab einen deutlichen Wechsel von CO_2-Einschlüssen in Granuliten zu wässrigen Einschlüssen in der TTG-Serie und den Amphiboliten. Die hohe Anzahl der CO_2-Einschlüsse spricht für trockene Bedingungen während der Metamorphose und des partiellen Schmelzens der mafischen und intermediären Ausgangsgesteine der Granulite. Partielle Schmelzen entstanden unter diesen Bedingungen durch Dehydrationsschmelzreaktionen von Amphibol, welche parallel zur Entstehung der typischen wasserfreien Mineralparagenesen (grt + cpx + pl ± amph or opx + cpx + pl + amph) der Granulite führte. Modellierungen der Spurenelementmuster zeigen, dass mafische Granulite Restite eines amphibolitischen Ausgangsgesteins sind, die 10-30 % einer tonalitischen Schmelze verloren haben. In den intermediären Granuliten sprechen die Verhältnisse von Amphibol zu Klinopyroxen und Amphibol zu Orthopyroxen für einen Schmelzgrad von maximal 10 %.

Während CO_2-Einschlüsse in der TTG-Serie und den zwischengelagerten Amphiboliten fehlen, treten wässrigen Einschlüsse mit 8-18 eq. wt% NaCl in großer Anzahl auf. Daraus kann geschlussfolgert werden, dass partielles Schmelzen in der TTG-Serie und Amphiboliten durch die Gegenwart eines wässrigen Fluids bei Temperaturen von 700-750°C ermöglicht wurde. In der

Gegenwart von wässrigen Lösungen ist die Stabilität von Plagioklas stark herabgesetzt, und Schmelze entsteht daher durch die Reaktion pl + qtz → Schmelze. Die starke Zerstörung prämetamorpher Strukturen deutet auf einen Volumenanteil von bis zu 25 % Schmelze in einigen Aufschlüssen hin.

Leukosome, welche in allen untersuchten Gesteinsarten auftreten, werden als ehemalige Schmelzbahnen angesehen. Das Na/Ca Verhältnis der Leukosome spiegelt das Verhältnis im jeweiligen Muttergestein wider. Tonalitische Schmelzen sind daher charakteristisch für CaO-reiche Gesteine (mafische Granulite, Amphibolite), während eher trondhjemitische Schmelzen in der Na_2O reicheren TTG-Serie entstehen. Die mineralogische Erscheinung und die Seltenerdmuster der Leukosome deuten darauf hin, dass Leukosome nicht die Gesamtschmelze darstellen. Sie bestehen vielmehr aus früh kristallisiertem Plagioklas und Quartz, während die fraktionierte Schmelze das System verlassen hat.

3. Teil: Spurenelementverteilung in der Granulit-Fazies

Die mineral-chemischen Untersuchungen dienen dazu, die Verteilung von Spurenelementen zwischen unterschiedlichen Mineralphasen sowie zwischen Mineralen und Schmelze unter granulitfaziellen Bedingungen zu verstehen. Sie können weiterhin genutzt werden, um die metasomatische Überprägung des Restits durch perkolierende Schmelzen nachzuvollziehen.

Anhand von Elektronenmikrosondenanalysen wurden die Amphibole in Granuliten als Edenite und Pargasite klassifiziert. Klinopyroxene sind Augite (X_{Mg} 0.6-0.8), Orthopyroxene ist intermediär mit X_{Mg}= 0.5-0.7 und Granat ist Fe-reich (X_{Alm} 0.5-0.62). Plagioklas weist erhebliche Unterschiede in der Zusammensetzung auf. In CaO-reichen mafischen Granuliten besitzt der Plagioklas eine hohe Anorthitkomponente mit X_{An} 0.5-0.7, während X_{An} 0.25-0.5 in den CaO-armen intermediären Granuliten vorherrscht.

Unabhängig von der Gesamtgesteinszusammensetzung sind die Spurenelemente konstant zwischen den vorherrschenden Mineralphasen verteilt. Insbesondere fällt das Verhältnis von 3fach höheren Seltenerd-Konzentrationen in Amphibol gegenüber Klinopyroxen auf, welches bei der Modellierung von chemischen Prozessen in der Unterkruste Beachtung finden sollte. Die Verteilung der Seltenen Erden zeigt weiterhin, dass große Granatporphyroblasten nur mit den direkt mit ihnen verwachsenen Klinopyroxen und Amphibol, jedoch nicht mit der gesamten Matrix im Gleichgewicht stehen. Das Ungleichgewicht zwischen Granat und Matrix deutet auf

ein spätes Wachstum der Granatporphyroblasten sowie langsame Diffusion der Seltenen Erden und somit verhinderte Gleichgewichtseinstellung hin.

Neben den Verteilungsmustern der Seltenen Erden wurden auch Verteilungskoeffizienten für die Übergangsmetalle bestimmt (Sc, V, Cr, Ni), für die bisher wenige Literaturangaben existierten. Analysen von Ilmenite und Apatite demonstrierten zudem den starken Einfluß von akzessorischen Mineralien auf die Spurenelementverteilung. Apatite besitzt hohe Gehalte an Seltenen Erden und Sr, während Ilmenite 20-30-mal höhere Gehalte an Nb und Ta als Amphibol aufweist.

Es wurden Verteilungskoeffizienten zwischen Mineralen und Schmelzen durch die Anwendung rechnerischer Methoden, sowie durch den Vergleich mit Literaturangaben und tatsächlich beobachteten Verhältnissen in Mineral und Schmelze (Leukosomen) ermittelt. Dadurch war es möglich, eine Reihe in sich konsistenter Schmelzverteilungskoeffizienten zu formulieren, die in der Modellierung von Schmelzen mafischer und intermediärer Gesteine unter den Druck-Temperatur-Bedingungen der Unterkruste Anwendung finden können.

Kleine Bruchstücke von Granuliten wurden in Aufschlüssen mit einem hohen Volumenanteil von Schmelze gefunden (Diatexite). Die Minerale dieser Bruchstücke weisen eine Anreicherung von Alkalien auf, die sich in niedrigen Anorthitgehalten der Plagioklase, erhöhten Kalium-Gehalten der Amphibole und dem seltenen Auftreten von Kalifeldspat manifestiert. Zudem sind die Amphibole dieser Proben an inkompatiblen Spurenelementen (Rb, Nb, Ta, Th) angereichert und besitzen hohe Gehalte der Seltenen Erden mit deutlich entwickelten negativen Eu-Anomalien. Diese Merkmale deuten auf eine metasomatische Überprägung der Minerale durch eine Schmelze hin. Obwohl das leukokrate Material der Aufschlüsse (Leukosom) größtenteils eine residuale Zusammensetzung aufweist, deutet sein hoher Volumenanteil auf einen großen Durchsatz an Schmelze hin. Diese Schmelze überprägte die Spurenelementmuster der Minerale in Granulitfetzen, die aus dem ursprünglichen Gesteinsverband herausgelöst und in die Schmelze inkorporiert wurden.

Part I

Laser-ablation ICP-MS analysis of siliceous rock glasses fused on an Iridium strip heater using MgO dilution.

Franziska Nehring, Dorrit E. Jacob, Matthias G. Barth, Stephen F. Foley

Abstract 2

1. Introduction and summary of previous studies 2

2. Experimental 4

2.1 Instruments and analytical procedure 4

2.2 Samples and sample preparation 6

3. Results 7

3.1 Homogeneity and accuracy of analyses of reference materials 7

3.2 Comparison of scanning mode ablation with spot ablation 13

3.3 Application of LA-ICP-MS on glass beads to natural rock samples 14

3.4 Comparison with alternative methods for trace element analysis of bulk rocks 17

References 20

Abstract

Trace element determination in rocks by fusion on an Iridium strip heater followed by LA-ICP-MS analysis of the glass beads is extended here to SiO_2-rich rocks; rapid fusion of samples with >55 wt% SiO_2 is facilitated by dilution by high purity MgO. The method developed here can rapidly and accurately determine numerous trace elements in a large range of rock compositions in a short time (about 50 samples/day). Systematic evaluation for a large range of rock compositions (natural rocks and reference materials AGV-2, GSP-2, JG-1a) with SiO_2 contents between 45-80 wt% shows that reproducibility and accuracy within 10% can be routinely achieved for most of the 28 trace elements investigated (Rb, Sr, Cs, Ba, Ti, Zr, Hf, Nb, Ta, Sc, V, Cr, Ni, Pb, Th, U, REE). The 40 mg sample size is smaller than for XRF, INAA or solution-ICP-MS, detection limits are lower and trace element palettes more complete than XRF and INAA. This microchemical method is thus attractive for the analysis of all natural geological materials as well as for experimental applications with small samples. Samples with SiO_2-contents >55 wt% require hot and long melting to achieve homogeneous glasses and eliminate all residual minerals, particularly refractory accessory phases. Melting conditions of 1600°C and 20 s for samples are recommended for SiO_2-contents between 55-70 wt%, whereas 1800°C and 20-30 s are often required for samples with >70 wt% SiO_2. Problems are encountered for Pb and Cs due to volatilization on the Ir-strip, for Sc due to interferences, and Zr and Hf due to their sequestration in refractory accessory minerals.

1. Introduction and summary of previous studies

Precise determination of bulk rock trace element contents is required for most geochemical studies. Several standard analytical techniques for trace element analysis are available (e.g. XRF, ICP-MS, INAA), which have particular advantages and disadvantages in routine use. Amongst the disadvantages are the need for chemical dissolution of samples and problems of incomplete dissolution (ICP-MS), high detection limits (XRF) or time consuming processing (INAA). A relatively new and rather simple microanalytical tool for trace element determination is direct fusion of rock powder on an Iridium strip heater and analysis of trace elements by LA-ICP-MS (Laser Ablation Inductively Coupled Mass Spectrometry). This method provides low detection limits for a large range of elements and can be performed rapidly and easily, by-passing the need for sample dissolution. This is an improvement over the use of lithium borate glasses by Eggins

(2003), whose analysis by ICP-MS eliminates the possibility of Li determination and may contaminate the instrument for Li analysis in other samples.

The Ir-strip fusion method was first described by Nicholls (1974) for determination of major element concentrations on glass beads by electron microprobe and was later extended with slight modification (Tungsten strips) to determine trace element concentrations (Fedorowich et al., 1993). The procedure is well established and unproblematic for mafic compositions (<55 wt% SiO_2) that can easily be fused at 1200°C with routine accuracies better than 10 % (pers. comm. K.P. Jochum, Max-Planck-Institute for Chemistry, Mainz). Fusion of siliceous samples is more problematic, because rapid homogenization during melting on the strip is hindered by high melt viscosities. Homogeneity in such samples can only be obtained by applying high melting temperatures (1700-1800°C) and long fusion times (60-120 s) combined with stirring at high temperatures, but this is disadvantageous for elements with high volatility.

Another approach to facilitate rapid fusion and homogeneity is dilution of high SiO_2-concentrations by addition of high-purity MgO (Gumann et al., 2003, Gumann, 2004). These authors focused on glass beads of granitic materials for the analysis of major elements by electron microprobe, and discovered that homogeneous beads are best obtained by two sequences of grinding MgO and sample material together in an agate mortar and fusing on the Ir-strip. They documented accuracies better than 5 % except for MgO, and encountered problems with trace elements in geochemical reference material JG2; LREE-contents were generally too low, whereas Ni and Cu contents were contaminated by the strip heater electrodes.

In this study, we use an improved Ir-strip heater design with computer-controlled heating and melting under an Ar atmosphere to systematically evaluate melting behaviour of a wide range of rock compositions (55-80 wt% SiO_2) and the behaviour of trace element concentrations on the sample / MgO mixing ratio, melting time and melting temperature. The study also employed three commercially available international reference materials (AGV-2, GSP-2 and JG-1a).

2. Experimental

2.1 Instruments and analytical procedure

The Iridium strip heater consists of an Iridium strip (20 x 0.5 x 0.05 mm in size) clamped between the poles of a 3 V / 250 A electric source, enabling resistance heating (Fig. 1). The heating assemblage is located in a closed chamber flooded with Argon during melting to suppress oxidation of the sample. Temperature is computer-controlled by adjusting the electrical current according to a calibration of melting temperature using a pyrometer. Melts are quenched by a cold argon jet located immediately beneath the Iridium strip.

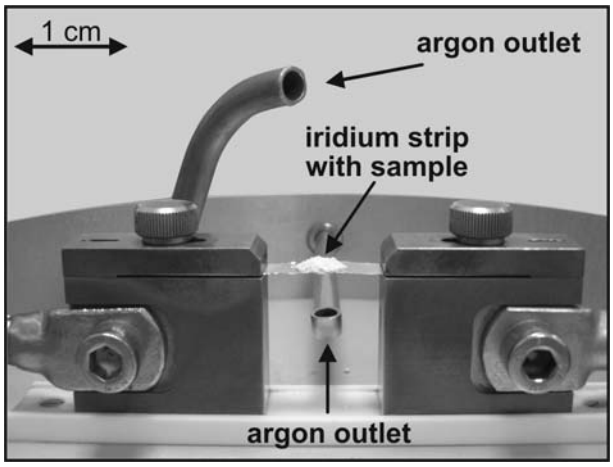

Fig. 1:
The strip heater cell at the Department of Geosciences, University, Mainz, showing the Iridium strip clamped between two copper electrodes. During fusion and quenching, argon flows through the cell via two outlets to prevent oxidation. An Ar jet directly below the Ir strip helps to quench the glass.

LA-ICP-MS measurements were performed at the Department of Geosciences, University of Mainz with an Agilent 7500ce quadrupole ICP-MS coupled with a NewWave Research UP-213 laser. Data acquisition was accomplished in peak-jumping mode with one point per peak and 10 ms dwell time. LA-ICP-MS operating parameters are given in Table 1. Background measurements were performed for each analysis for 60 s prior to ablation. Plasma conditions were adjusted to oxide formation rates below 0.5 % (monitored using the 248/232 mass ratio), so that no further oxide corrections were necessary. Either ^{43}Ca or ^{44}Ca were used as internal standards for the geochemical reference materials and most natural samples, whereas ^{29}Si was used as internal standard for samples with less than 1 wt% CaO. Certified glass reference material NIST SRM 612 served as the external standard and was measured at the beginning and at the end of each group of unknowns as well as after every tenth to fifteenth sample measurement during long runs to monitor instrumental drift. Data reduction was carried out using "Glitter" software. Detection limits generally range between 0.001 and 0.5 $\mu g g^{-1}$. The elemental concentrations of NIST SRM 612 were taken from Pearce et al. (1997) except for Zr for which

the preferred value given in the GeoReM database (Jochum et al., 2005) was used. Measured trace elements in NIST SRM 612 have a reproducibility better than 5 % (exceptions are Cs, Pb, Th and U at <10 %) and correspond within 5 % to recommended values.

Table 1: LA-ICP-MS operating parameters

Laser	New Wave UP 213, Nd:YAG Laser
Wavelength	213 nm
Pulse Energy	0.36 – 0.45 mJ
Repetition rate	spot: 10 Hz line scan: 20 Hz / 20 µm/s
Spot size	100 µm
ICP-MS	Agilent 7500ce
Forward Power	1200 W
Plasma Gas Flow (Ar)	15 l min^{-1}
Carrier Gas Flow (Ar)	1.2 l min^{-1}
Cone Material	Ni
ThO^+/Th^+	< 0.5 %

Instrument performance and stability were monitored by repeated measurements of USGS basaltic reference glass BCR-2G during the analytical sessions. Reproducibility on BCR-2G is better than 10 % except for Ni (16 %) and Pb (11 %), and measured concentrations generally agree within 10 %.

In addition to the determinations on Ir-strip glasses, several samples were analysed for comparative purposes for rare earth elements (REE) and Y by solution ICP-MS after Li-metaborate fusion (Mareels, 2004), and for Sc, V, Cr, Ni, Zr, Sr and Ba by XRF (MagiXPro) on pressed powder tablets. After Li-metaborate fusion the material was dissolved in 0.42 M HNO_3. Solutions were analysed at the Department of Geosciences at the University of Mainz using a VG Elemental Plasma Quad 3 following routine methods. Quantification of element concentration was carried out by external calibration using reference material AGV-2 processed in the same way as the samples. In and Re were added as internal standards to the sample solutions for instrumental drift correction.

2.2 Samples and sample preparation

Geochemical reference materials AGV-2 and GSP-2 (United States Geological Survey, USGS) as well as JG-1a (Geological Survey of Japan, GSJ) were used for the experiments. AGV-2 is an andesite with a SiO_2 content of 59.3 wt%. GSP-2 and JG-1a are granodiorites with SiO_2 contents of 66.6 wt% and 72.3 wt%, respectively. The natural rock samples cover a range of SiO_2-contents from 45 - 80 wt% SiO_2, and represent igneous and metamorphic rocks typical of the continental crust (see Part II). In addition, paragneisses, sandstones and litharenites (Meinhold et al., 2007) were included to test the applicability of the strip heater method to sedimentary rocks.

All samples were milled in an agate rotary mill before fusion. About 40 mg of mafic and intermediate samples with up to 55 wt% SiO_2 were fused directly at 1100-1400 °C at a current of 110-120 A (140-170 W) for 10 s. Samples with >55 wt% SiO_2 were dried at 1000 °C for 15 min to reduce degassing during the fusion process. Afterwards high purity MgO powder was added to reduce the SiO_2 content of the mixture to ~55 wt%. Trace elements in the MgO as determined by solution ICP-MS are in the range of 0.00002–0.2 $\mu g g^{-1}$ (pers. comm. G. Brey, Institute Geosciences, University Frankfurt on Main.). The mixtures were blended for several minutes in an agate mortar adding a few drops of acetone. This procedure has the advantage of producing a very fine powder that was easier to fuse than the routinely milled rock powder. About 40 mg of the mixtures were fused for 10 s, 30 s and 70 s using a current of 116-125 A (160-190 W, 1200-1600 °C). At 1600°C quench crystals occurred in compositions with more than 70 wt% SiO_2 but even the most siliceous samples yielded homogeneous clear, translucent glass beads at 1800 °C (135 A / 220 W). Therefore, melting conditions were chosen according to initial SiO_2 contents as 1200°C for mafic, undiluted samples, 1600 °C for samples with less than 70 wt% and 1800 °C for samples with more than 70 wt% SiO_2. We also applied grinding of primary glass beads and re-melting of the glass powder. Glass powders melted easily and always produced optically homogeneous beads. For analysis by LA-ICP-MS, beads were stuck onto a microscope slide using double-sided adhesive tape.

Melting of silicic glasses is accompanied by degassing of the sample and formation of vesicles in the melt. Degassing can be a result of release of crystal-bound water as well as of water absorbed by the powders during grinding; the latter is indicated by the fact that vesicle formation during fusion of glass powders is especially strong.

3. Results

3.1 Homogeneity and accuracy of analyses of reference materials

Homogeneous results can be achieved in the three reference materials (Fig. 2-4) by adjusting the fusion conditions to the SiO_2-content of the sample. For the elements Sr, Ba, Th, U, Ti, Nb, Ta, Th and the REE (Rare Earth Elements), accuracy is usually within 10 % of the reference value (Table 2-4). Reproducibility is also within 10 %, which may partly be due to similar fractionation to the internal standard Ca during laser ablation (Guillong & Günther, 2002, Kuhn et al., 2004). Homogeneity of REE in reference material JG-1a and highly siliceous samples is only achieved under the highest temperature fusion conditions applied (1800°C and 30 s), whereas the behaviour of Sr, Ba, Th, U, Nb and Ta is evidently not influenced by fusion conditions. This may be due to storage of the REE in refractory accessory phases (zircon, apatite, monazite, allanite) that do not easily dissolve in the melt. Similary, REE contents in reference material GSP-2 only agree with the reference values if the fusion process is prolonged (30-70 s) or the glass beads are reground and molten again.

Inhomogenously distributed Zr and Hf contents in the glass beads of GSP-2 and JG-1a are most likely related to incomplete melting of microscopic zircon crystals. Re-grinding and a second fusion cycle improved the homogeneity of these elements. However, similar improvements are obtained during hotter and prolonged fusion of the siliceous compositions, which is preferred to re-grinding and re-fusion.

Reproducibility of Cr and Ni contents is poorer at 10-15 %, which may be attributed to less well determined Ni and Cr concentrations in the reference materials (Table 3). Reference values for Cr and Ni contents of AGV-2 are documented with relative standard deviations (RSD%) of 12 % and 16 % respectively (Cr 17 $\mu g g^{-1} \pm 2 \mu g g^{-1}$; Ni 19 $\mu g g^{-1} \pm 3 \mu g g^{-1}$) and uncertainties are larger for GSP-2 (Cr ±30 %, Ni ±12 %) and JG-1a (Cr ±25 %, Ni ±27 %). Our values lie within the given RSD% of the reference materials.

Pb and Cs are depleted in the glass beads compared to the reference values, which is due to volatilization during melting. Their determination by the strip heater method is therefore not recommended. The loss of these elements increases with increasing fusion temperature and time and, hence, is especially strong if a second melting cycle is applied.

We investigated several degrees of dilution to the reference materials AGV-2 and GSP-2. The fusion procedure and the homogeneity of the glasses is not significantly improved by

dilution down to 50 wt% SiO_2. On the contrary, accuracy suffered slightly, probably due to mixing problems.

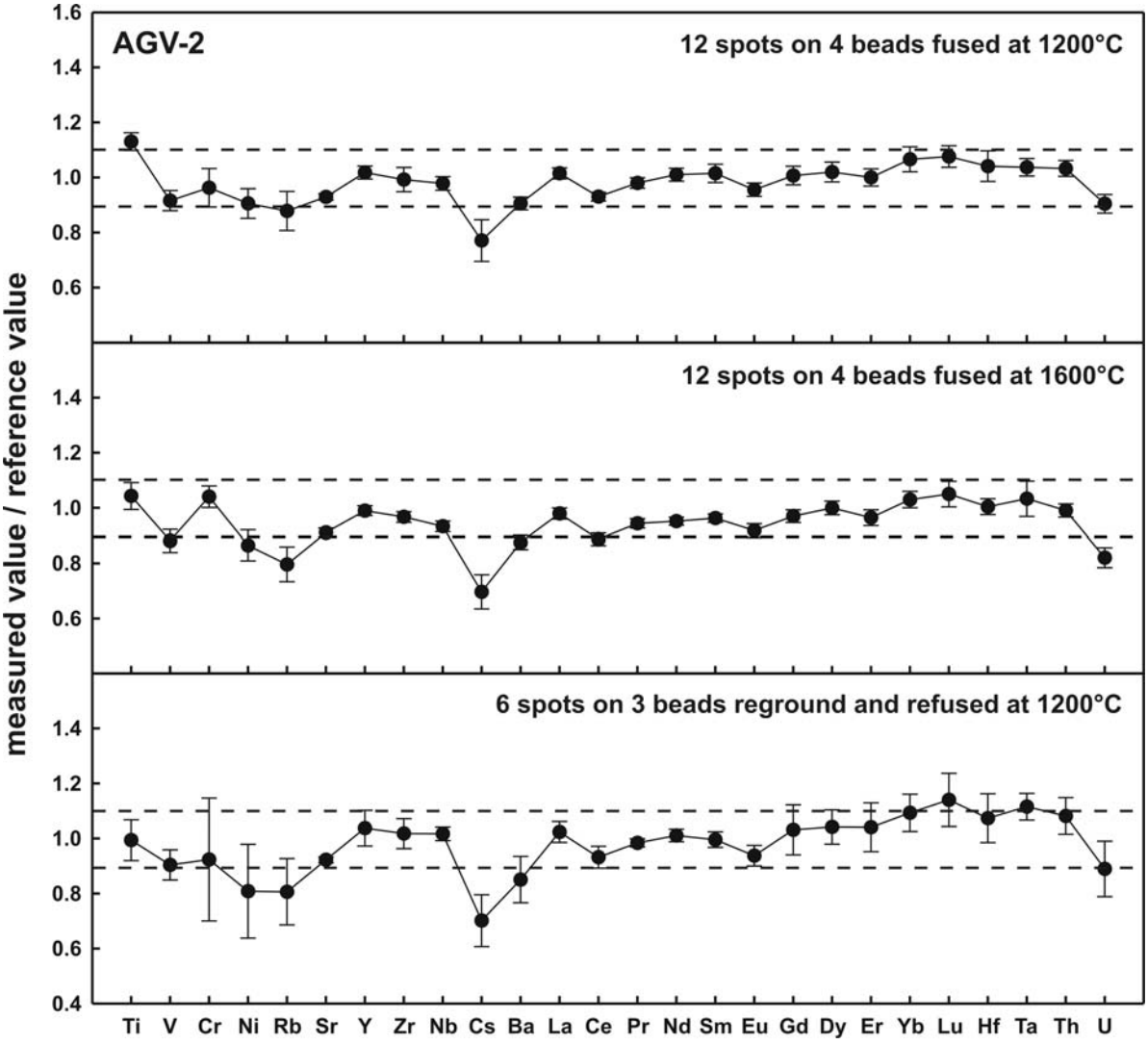

Fig. 2:

Data for reference material AGV-2 presented as the ratio of measured value divided by the reference value. Stippled lines denote 10 % deviation from the reference value. Short melting durations at the lowest temperatures provided the best results for this intermediate rock material.

Table 2: Results obtained for reference material AGV-2. Due to the low SiO_2-content of this sample, excellent recoveries are obtained even at low fusion temperature.

AGV-2								
	reference values		1200°C 4 beads, n=12			1600°C 4 beads, n=12		
	mean	SD	mean	RSD%	rec. %	mean	RSD%	rec. %
Li	**11**	**1**	10.7	9	97	10.9	10	99
Sc	**13**	**1**	15.2	4	117	15.3	3	118
Ti	**6300**	**130**	7122	5	113	6570	8	104
V	**120**	**5**	110	7	92	106	8	88
Cr	**17**	**2**	16.4	13	96	17.7	7	104
Ni	**19**	**3**	17.2	11	91	16.4	11	86
Rb	**66.7**	**3.8**	58.6	14	88	53.1	14	80
Sr	**657**	**4**	610	2	93	598	3	91
Y	**18.8**	**1.5**	19.1	4	102	18.6	3	99
Zr	**225**	**14.1**	223	8	99	218	4	97
Nb	**14.1**	**0.6**	13.8	4	98	13.2	4	93
Cs	**1.25**	**0.08**	0.96	17	77	0.87	16	70
Ba	**1139**	**24**	1031	4	91	997	5	88
La	**36.9**	**1.3**	37.4	3	101	36.1	4	98
Ce	**68.8**	**2.3**	64.0	3	93	61.0	4	89
Pr	**7.79**	**0.31**	7.63	3	98	7.35	3	94
Nd	**30.1**	**0.5**	30.4	4	101	28.6	3	95
Sm	**5.4**	**0.07**	5.48	6	101	5.20	3	96
Eu	**1.53**	**0.04**	1.46	5	96	1.40	5	92
Gd	**4.50**	**0.05**	4.53	6	101	4.36	4	97
Dy	**3.44**	**0.11**	3.51	6	102	3.44	4	100
Er	**1.80**	**0.05**	1.80	6	100	1.74	5	96
Yb	**1.60**	**0.03**	1.71	8	107	1.65	5	103
Lu	**0.24**	**0.01**	0.26	6	108	0.25	8	105
Hf	**4.97**	**0.17**	5.17	9	104	4.99	5	100
Ta	**0.86**	**0.03**	0.89	5	104	0.86	5	103
Pb	**13**	**1**	9.49	28	73	8.58	46	66
Th	**6.05**	**0.22**	6.25	5	103	5.99	4	99
U	**1.82**	**0.11**	1.65	7	90	1.49	8	82

CaO as internal standard measured as ^{43}Ca. All data in $\mu g g^{-1}$. Reference values are averages compiled from the GeoReM database (Raczek et al., 2001,Yu et al., 2003, Kent et al., 2004, Willbold & Jochum, 2005) and from the USGS. rec% = recovery

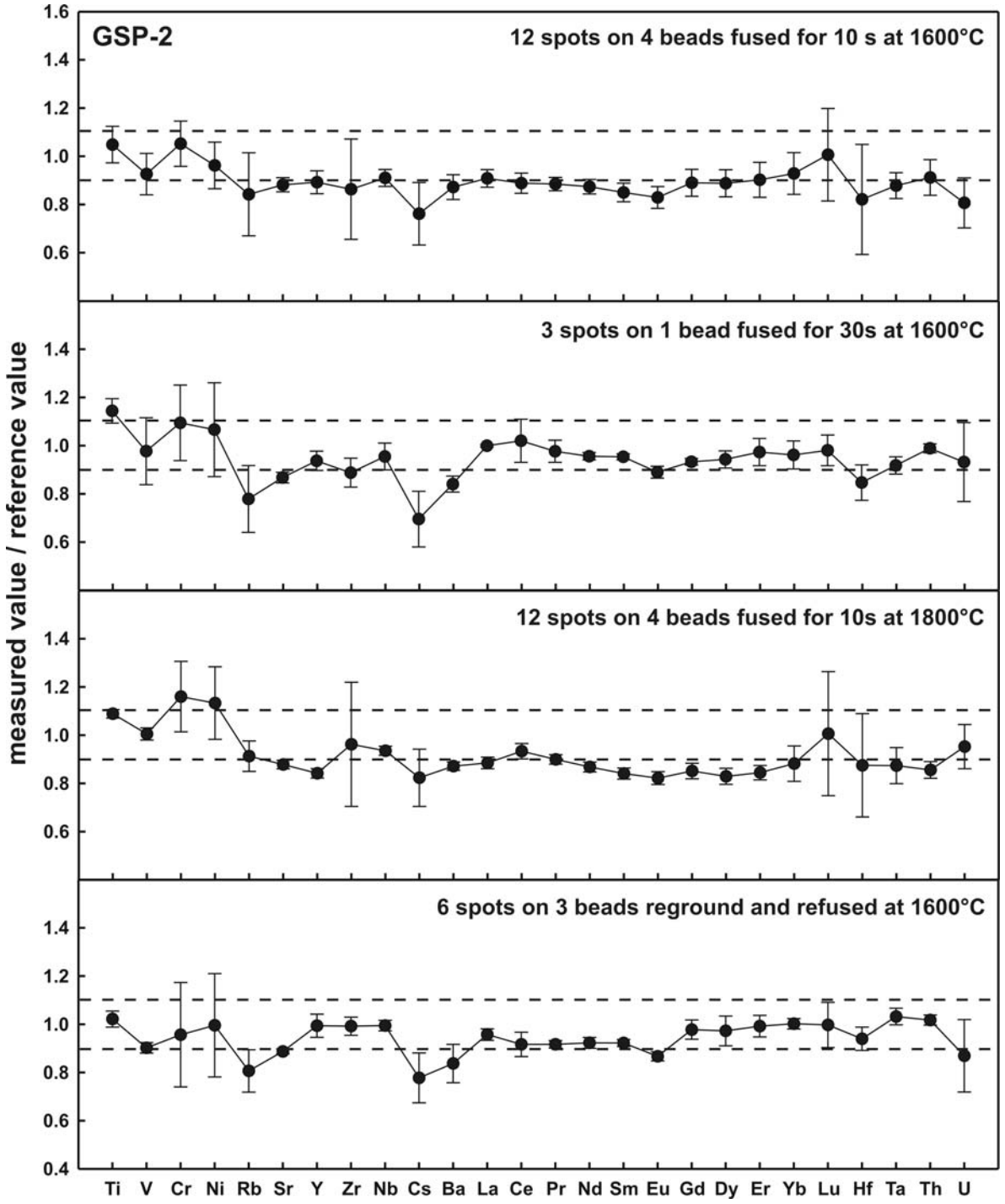

Fig. 3:

Data for reference material GSP-2 presented as ratio of measured value divided by the reference value. Stippled lines denote 10 % deviation from the reference value. Note improvement of results during longer melting (30 s) and after regrinding and remelting.

Table 3: Results obtained for reference material GSP-2. Recoveries are best if a long melting time is applied or if beads are reground and fused again.

GSP-2														
	reference values		1600°C, 10s 4 beads, n=15			1800°C, 10s 2 beads, n=6			1600°C, 30s 1 bead, n=3			reground, 1600°C 3 beads, n=6		
	mean	SD	mean	RSD%	rec. %	mean	RSD%	rec. %	mean	RSD%	rec. %	mean	RSD%	rec. %
Li	**36**	**2**	38.1	13	106	46.4	6	128	34.9	14	97	40.9	4	114
Sc	**6.3**	**0.7**	9.46	12	150	9.93	3	158	8.2	1	131	9.80	5	155
Ti	**3960**	**120**	4151	7	105	4311	2	109	4538	4	115	4045	3	102
V	**52**	**4**	48.2	9	93	52.3	3	101	50.9	14	98	46.9	2	90
Cr	**20**	**6**	21.0	9	105	23.2	13	116	21.9	14	110	19.1	23	96
Ni	**17**	**2**	16.4	10	96	19.3	13	113	18.2	18	107	16.9	22	100
Rb	**247**	**7**	208	20	84	225	7	91	193	18	78	199	11	81
Sr	**241**	**7**	213	3	88	212	2	88	209	3	87	214	1	89
Y	**27.1**	**1.2**	24.2	5	89	22.8	2	84	25.4	4	94	26.9	5	99
Zr	**564**	**13**	487	24	86	543	27	96	502	7	89	560	4	99
Nb	**26.8**	**0.7**	24.4	4	91	25.1	2	94	25.6	6	96	26.7	2	99
Cs	**1.27**	**0.12**	0.97	17	76	1.05	14	82	0.89	17	70	0.99	13	78
Ba	**1373**	**66**	1197	6	87	1197	2	87	1156	4	84	1149	9	84
La	**186**	**11**	169	4	91	165	3	88	186	1	100	178	2	96
Ce	**436**	**26**	387	5	89	407	3	93	445	9	102	400	6	92
Pr	**55**	**5.1**	48.7	3	88	49.5	2	90	53.8	5	98	50.4	2	92
Nd	**215**	**19**	188	3	87	187	2	87	206	2	96	198	2	92
Sm	**27.5**	**1.3**	23.4	5	85	23.1	3	84	26.3	1	96	25.4	2	92
Eu	**2.39**	**0.15**	1.98	5	83	1.96	3	82	2.1	3	89	2.07	2	87
Gd	**13**	**1.3**	11.6	6	89	11.1	4	85	12.2	1	93	12.7	4	98
Dy	**6.12**	**0.37**	5.43	6	89	5.08	4	83	5.78	4	94	5.95	6	97
Er	**2.39**	**0.21**	2.16	8	90	2.02	4	84	2.33	6	97	2.37	4	99
Yb	**1.7**	**0.1**	1.58	9	93	1.50	8	88	1.64	6	96	1.70	2	100
Lu	**0.24**	**0.02**	0.24	19	101	0.24	26	101	0.24	6	98	0.24	9	100
Hf	**15.7**	**1.5**	12.9	28	82	13.7	25	87	13.3	9	85	14.8	5	94
Ta	**0.95**	**0.02**	0.83	6	88	0.83	9	87	0.87	4	92	0.98	3	103
Pb	**42**	**3**	33.7	34	80	22.8	28	54	39.3	25	94	15.5	46	37
Th	**109**	**7**	99.4	8	91	93.3	4	86	108	2	99	111	2	102
U	**2.46**	**0.06**	2.0	13	81	2.34	10	95	2.3	18	93	2.14	17	87

CaO as internal standard measured as ^{43}Ca. All data in $\mu g g^{-1}$. Reference values are averages compiled from the GeoReM database (Jochum & Jenner, 1994, Raczek et al., 2001, Vendemiatto & Enzweiler, 2001, Yu et al., 2003) and from the USGS. rec% = recovery

JG-1a					
	reference values		1800°C, 30s 1 bead, n=3		
	mean	SD	mean	RSD%	rec. %
Li	**79.5**	**4.5**	94.4	5	118
Sc	**6.21**	**0.49**	9.74	3	157
Ti	**1500**	**180**	1557	2	104
V	**22.7**	**3.8**	19.1	3	84
Cr	**17.6**	**4.4**	19.3	10	110
Ni	**6.91**	**1.9**	7.95	15	115
Rb	**182**	**9**	159	5	87
Sr	**183**	**5**	160	1	87
Y	**30.2**	**1.3**	26.9	4	89
Zr	**117**	**9**	119	3	102
Nb	**11.1**	**0.8**	10.5	2	95
Cs	**11.3**	**0.5**	9.6	7	85
Ba	**465**	**7**	408	1	88
La	**21.8**	**1.8**	20.9	12	96
Ce	**46.4**	**2.4**	44.4	11	96
Pr	**5.44**	**0.35**	4.88	9	90
Nd	**20.3**	**1.2**	18.7	13	92
Sm	**4.6**	**0.27**	4.35	5	95
Eu	**0.74**	**0.08**	0.6	7	81
Gd	**4.36**	**0.36**	4.09	5	94
Dy	**4.36**	**0.37**	4.44	2	102
Er	**2.85**	**0.32**	2.75	3	96
Yb	**2.96**	**0.34**	2.85	4	96
Lu	**0.45**	**0.05**	0.46	11	102
Hf	**3.6**	**0.24**	3.98	1	111
Ta	**1.85**	**0.16**	1.67	4	90
Pb	**26.4**	**2.8**	8.3	39	31
Th	**12.8**	**1.6**	12.1	8	95
U	**4.63**	**0.29**	4.13	1	89

Table 4:

Best result obtained for reference material JG-1a. Due to the high SiO_2-content (72.3 wt%) high fusion temperature and a prolonged melting duration had to be applied. At lower temperatures and shorter fusion duration homogeneity was not sufficient. Note that Pb is strongly depleted at these high fusion conditions.

CaO as internal standard measured as ^{43}Ca. All data in $\mu g g^{-1}$. Reference values are averages compiled from the GeoReM database (Jochum & Jenner, 1994, Govindaraju, 1994, Imai et al., 1995, Stix et al., 1996, Dulski., 2001, Boaventura et al., 2002, Ishikawa et al., 2003, Orihashi & Hirata, 2003, Yu et al., 2003) and the GSJ. rec% = recovery

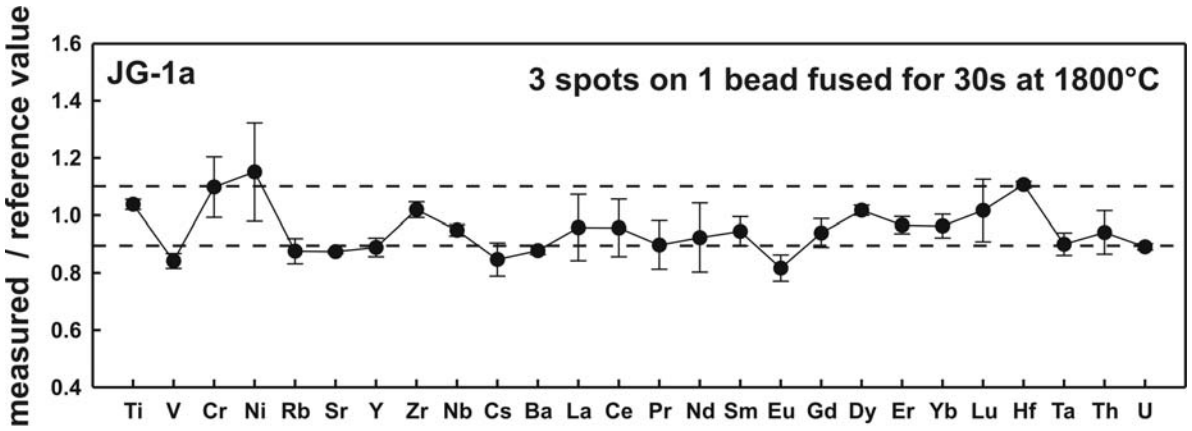

Fig. 4:

Data for reference material JG-1a presented as the ratio of measured value divided by the reference value. Results within 10 % of the reference values for this highly siliceous reference material are only obtained if hot and prolonged melting is applied.

3.2 Comparison of scanning mode ablation with spot ablation

Comparison of line scan and single spot ablation analysis showed no advantage of line scans over spot analyses. Considerably higher Rb and Cs contents (up to 30 %) were obtained in line scan ablations than in spot ablation analyses. Material ablation in scanning mode is confined to the surface of the bead and has been shown to produce larger particles than spot ablations, resulting in high matrix effects and significant contribution to elemental fractionation effects in the ICP (Guillong & Günther, 2002, Kuhn et al., 2004). Large particles may be incompletely ionized in the plasma and elemental fractionation due to preferential ionization of the more volatile elements such as Cs and Rb from the surface of large particles (Kuhn & Günther, 2004) may result. Pb shows contrasting behaviour; it is depleted in the line scans compared to the spot ablation patterns, although it is more volatile than Cs. The time-resolved signal of the spot ablations shows an increase of the Pb signal intensity with increasing depth, indicating that Pb is depleted at the surface of the beads during the melting process. Thus, since line scans only ablate depleted material from the surface, Pb contents are lower than those calculated from spot ablation patterns.

3.3 Application of LA-ICP-MS on glass beads to natural rock samples

For most trace elements analysed, the results by LA-ICP-MS are comparable to those from other methods. Comparison of LA-ICP-MS data of REE and Y contents in a selection of the natural rock samples with SiO_2 of 59 - 85 wt% with data from solution ICP-MS indicates agreement within 10 % (Fig. 5). Larger deviations in one of the samples (a leucosome with 67 wt% SiO_2) are due to the low contents of HREE in this sample (Lu 0.03 $\mu g g^{-1}$). Furthermore, this sample was fused for only 10s at 1600 °C and longer melting could improve agreement with solution-ICP-MS data (Table 5).

Table 5:

Comparison of REE and Y values (mean ± 1SD) of natural rock samples derived by LA-ICP-MS after strip-heater fusion (normal font) with values derived by solution ICP-MS after Li-tetraborate fusion (**bold**). All data in $\mu g g^{-1}$.

sample	**granulite**		**leucosome**		**leucosome**		**sandstone**		**sandstone**	
SiO_2	59.7 wt%		64.3 wt%		67.0 wt%		73.2 wt%		84.8 wt%	
method	LA-ICP-MS	ICP MS	LA-ICP-MS	ICP MS	LA-ICP-MS	ICP MS	LA-ICP-MS	ICP MS	LA-ICP-MS	ICP MS
temperature	1600°C		1600°C		1600°C		1800°C		1800°C	
time	10 s		10 s		10 s		20 s		20 s	
spots	n=6		n=3		n=3		n=6		n=3	
La	16.8±0.5	**17.3**	20.7±1.1	**21.7**	10.2±0.9	**10.7**	13.4±1.1	**13.15**	14.6±0.2	**16.4**
Ce	33.3±0.9	**37.2**	38.1±1.9	**40.9**	15.9±1.8	**16.5**	27.5±2.3	**27.28**	33.8±0.4	**32.9**
Pr	4.14±0.13	**4.49**	4.67±0.14	**5.01**	1.64±0.15	**1.77**	3.09±0.26	**3.07**	3.57±0.07	**3.61**
Nd	17.4±0.6	**17.2**	20.4±0.7	**19.7**	6.02±0.73	**5.79**	11.7±0.9	**11.59**	13.6±0.6	**14.8**
Sm	3.35±0.17	**3.60**	4.66±0.12	**4.76**	0.97±0.17	**0.82**	2.32±0.16	**2.32**	2.86±0.21	**2.91**
Y	15.7±0.45	**16.5**	20.0±0.4	**20.6**	2.28±0.30	**2.34**	13.2±0.2	**13.7**	13.8±0.4	**15.7**
Eu	1.02±0.02	**1.04**	1.51±0.17	**1.53**	0.55±0.02	**0.63**	0.48±0.04	**0.47**	0.61±0.01	**0.65**
Gd	3.17±0.14	**3.19**	4.72±0.09	**4.59**	0.69±0.04	**0.72**	2.25±0.12	**2.19**	2.49±0.14	**2.63**
Dy	2.90±0.1	**2.90**	4.23±0.31	**4.09**	0.49±0.07	**0.44**	2.26±0.09	**2.38**	2.56±0.07	**2.54**
Er	1.66±0.07	**1.59**	2.06±0.07	**1.98**	0.19±0.04	**0.20**	1.31±0.08	**1.39**	1.55±0.11	**1.52**
Yb	1.64±0.05	**1.53**	1.84±0.22	**1.69**	0.19±0.04	**0.18**	1.31±0.11	**1.36**	1.39±0.17	**1.55**
Lu	0.25±0.01	**0.24**	0.24±0.01	**0.23**	0.03±0.02	**0.02**	0.20±0.03	**0.22**	0.22±0.02	**0.24**

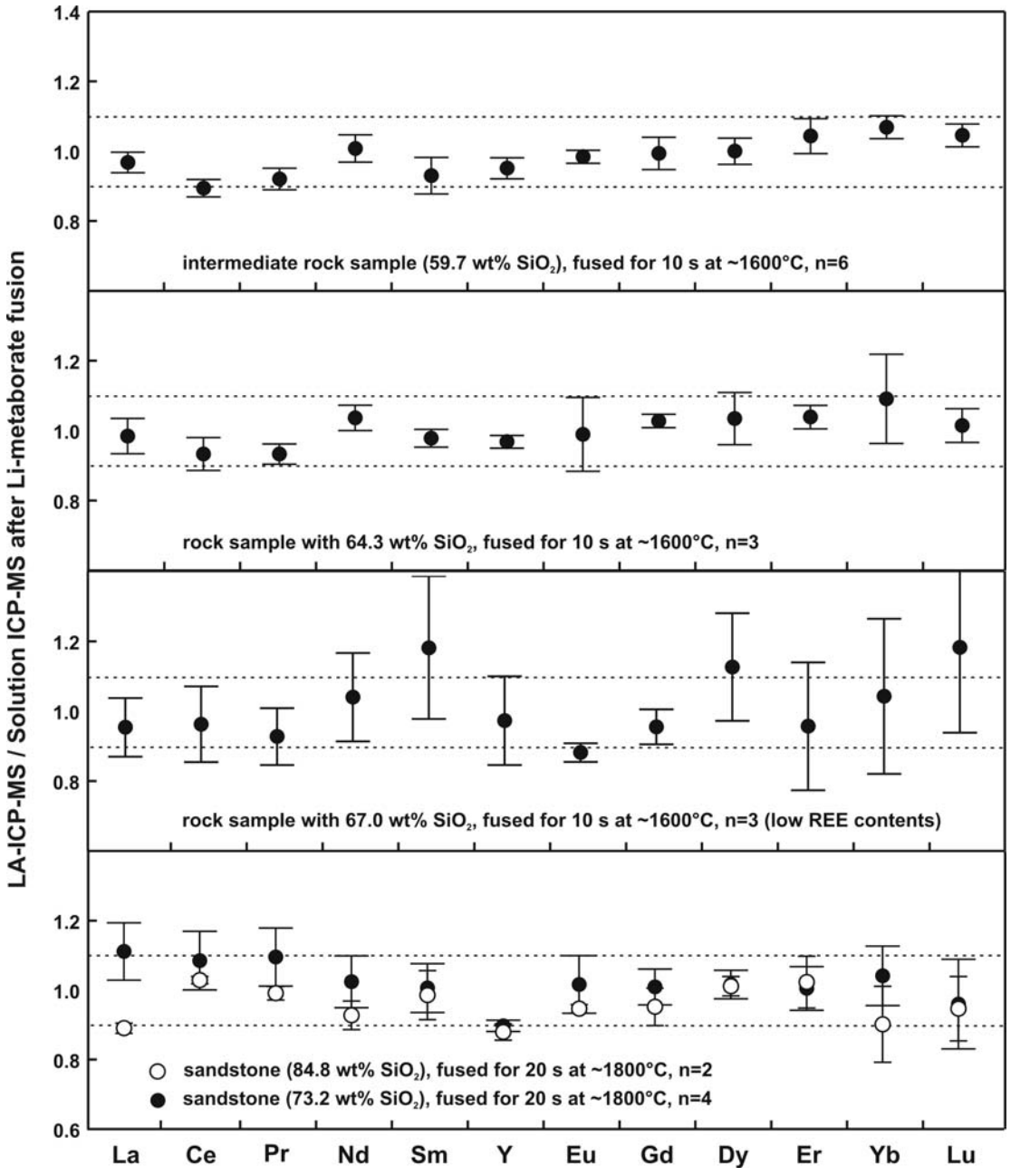

Fig. 5:

LA-ICP-MS values compared to total dissolution ICP-MS values for natural rock samples. The deviation for the methods is less than 10 % (stippled line) even for samples with exceptionally high SiO_2-contents such as sandstones.

There are, however, a few elements for which problems were encountered, namely Sc, Zr, Hf, Pb and Cs. Scandium contents determined by LA-ICP-MS on glass beads in the highly siliceous samples are consistently higher than XRF analyses of powdered rocks and the reference values of standard materials. The difference becomes larger with increasing SiO_2-contents and simultaneously decreasing Sc-contents (Fig. 6). This overestimation of Sc by LA-ICP-MS is not related to the fusion process but most likely results from interferences of $^{28}Si^{17}O$ and $^{29}Si^{16}O$ on isotopic mass 45. This becomes more noticeable in samples with higher SiO_2-contents because this trend generally correlates with decreasing Sc in natural rocks.

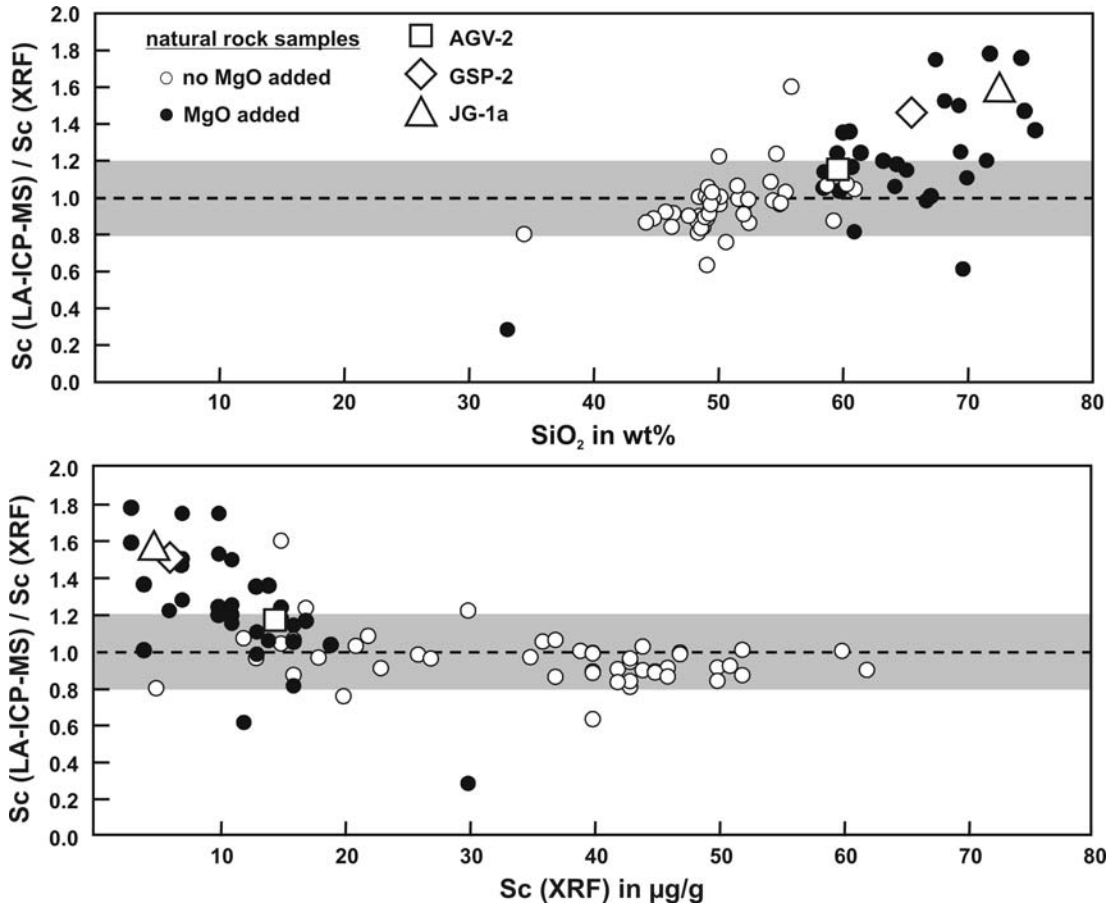

Fig. 6:

Comparison of Sc data obtained by LA-ICP-MS versus XRF-data plotted against (a) SiO_2-content of the samples, and (b) Sc values from XRF. Grey fields indicate agreement within 20 %. The positive deviation of LA-ICP-MS values is due to $^{28}Si^{17}O$ and $^{29}Si^{16}O$ interferences from the Si-rich samples (see text).

The determination of Zr and Hf is problematic in both natural rock samples and geological reference materials (Fig. 7). In most cases, concentrations measured by LA-ICP-MS on glass beads are lower than those determined by XRF. The poor correlation between Zr contents in samples with SiO_2<55wt% and no added MgO results from a mixture of two effects. Firstly, these samples were fused at 1200°C which may have prevented complete melting of small zircon crystals. Secondly, mafic rocks have low Zr contents and some of the scatter is related to inaccuracy of XRF determinations these concentrations. This is supported by mass balance calculations obtained for some of the mafic samples by analyzing Zr and Hf concentrations in constituent minerals of the unmelted rocks and combining them into whole-rock concentrations. Results are in accordance with the LA-ICP-MS data, whereas concentrations obtained by XRF are too high.

3.4 Comparison with alternative methods for trace element analysis of bulk rocks

X-ray fluorescence spectrometry is a standard tool for the determination of a number of trace elements (Rb, Sr, Ba, Zr, Sc, V, Cr, Ni) in geological materials. Our analyses show that the LA-ICP-MS data on glass beads usually agree well with XRF data and deviations are less than 10 % (Fig. 7). At concentrations <20 $\mu g g^{-1}$ the discrepancy increases as detection limits of the XRF method are approached. Highly siliceous samples are more prone to erroneous determination of these elements by XRF since low concentrations of transition metals coincide with high SiO_2-contents of the samples. Therefore we consider the LA-ICP-MS method to be more reliable in the low concentration range.

Both XRF and INAA require larger amounts of sample material than the strip heater method and are capable of analysing a more limited palette of trace elements, resulting in only partial coverage of the elements generally sought by geochemists. Larger samples (ca. 200 mg) are also used for solution ICP-MS, which, in contrast, permits detection of many more elements at ultratrace concentrations (< 0.01 $\mu g g^{-1}$), but these are not generally sought in geological applications. Solution ICP-MS requires more time-consuming acid digestion of samples which may encounter similar problems in the dissolution of accessory minerals.

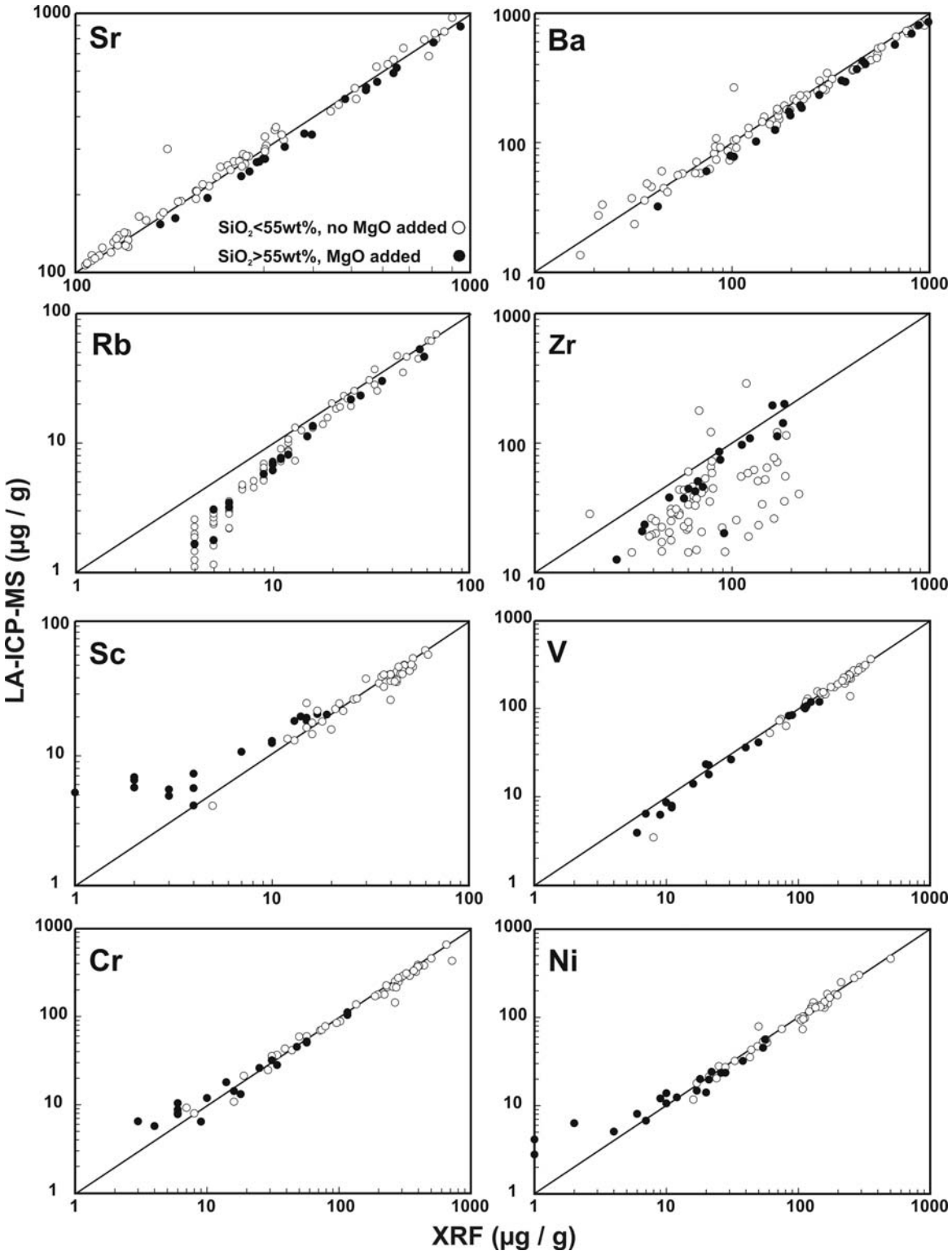

Fig. 7:

Comparison of XRF and LA-ICP-MS values for a large group of natural rock samples. In the low concentration range deviation between the methods may be larger than 10 %; here LA-ICP-MS values are preferred. See text for further discussion.

In summary, the LA-ICP-MS glass bead method developed here enables accurate and precise simultaneous determination of many trace elements in SiO_2-rich whole-rocks by laser sampling for first time. It is a rapid and cheap method which does not require acid digestion in a chemical laboratory, and can be practised on much smaller samples, opening the way to many technical and experimental applications. The palette of elements is larger than available to INAA and XRF, and preparation times are quicker (INAA) or comparable (XRF). Specific problems are encountered with Sc (this applies also to solution ICP-MS), and the volatile elements Pb and Cs. Problems with Zr and Hf can be circumvented by further optimization of melting times and temperatures.

References

Boaventura, G.R., De Oliveira, R.C. & Santelli R.E. (2002). 73 Off-line and on-line determination of eleven rare earth elements in silicate rocks by ICP-AES using Dowex minicolumns for separation of interfering elements in continuous flow systems. *Geostandards Newsletter: The Journal of Geostandards and Geoanalysis* **26**, 63-73.

Dulski, P. (2001). Reference materials for geochemical studies: New analytical data by ICP-MS and critical discussion of reference values *Geostandards Newsletter: The Journal of Geostandards and Geoanalysis* **25**, 87-125.

Eggins, S.M. (2003). Laser ablation ICP-MS analysis of geological materials prepared as lithium borate glasses. *Geostandards Newsletter: The Journal of Geostandards and Geoanalysis* **27**, 147-162.

Fedorowich, J.S., Richards, J.P., Jain, J.C., Kerrich, R. & Fan, J. (1993). A rapid method for REE and trace-element analysis using laser sampling ICP-MS on direct fusion whole-rock glasses. *Chemical Geology* **106**, 229-249.

Govindaraju, K. (1994). 1994 compilation of working values and sample description for 383 geostandards. *Geostandards Newsletter: The Journal of Geostandards and Geoanalysis* **1**, 1-158.

GSJ. Geological survey of Japan, Geochemical Reference Samples DataBase. (http://www.aist.go.jp/RIODB/geostand/).

Guillong, M. & Günther, D. (2002). Effect of particle size distribution on ICP-induced elemental fractionation in laser ablation-inductively coupled plasma-mass spectrometry. *Journal of Analytical Atomic Spectrometry* **17**, 831-837.

Gumann, S., Lahaye, Y. & Brey, G. (2003). Iridium Strip - Rhyolithe enthüllen ihre Details. *Berichte des Europäischen Jahrbuchs für Mineralogie* **15**(1), 72.

Gumann, S. (2004). Sardinian Ignimbrites - Major and Trace Element Composition and Iridium Strip Heater Experiments. *Diploma thesis*, Johann Wolfgang Goethe University, Frankfurt / Main, Germany.

Imai, N., Terashima, S., Itoh, S. & Ando, A. (1995). 1994 compilation of analytical data for minor and trace elements in seventeen GSJ geochemical reference samples "Igneous Rock Series". *Geostandards Newsletter: The Journal of Geostandards and Geoanalysis* **19**(2) 135-213.

Ishikawa, T., Sugimoto, K. & Nagaishi, K. (2003). Determination of rare-earth elements in rock samples by an improved high -performance ion chromatography. *Geochemical Journal* **37**, 671-680.

Jochum, K.P. & Jenner, G.A. (1994). Trace element analysis of Geological Survey of Japan silicate reference materials: Comparison of SSMS with ICP-MS data and a critical discussion of compiled values. *Fresenius' Journal of Analytical Chemistry* **350**, 310-318.

Jochum, K.P., Nohl, U., Herwig, K., Lammel, E., Stoll, B. & Hofmann, A.W. (2005). GeoReM: A new geochemical database for reference materials and standards (http://georem.mpch-mainz.gwdg.de/). *Geostandards and Geoanalytical Research* **29**, 333-338.

Kent, A.J.R., Jacobsen, B., Peate, W., Waight, T. & Baker, J.A. (2004). Isotope dilution MC-ICP-MS rare earth element analysis of geochemical reference materials NIST-SRM 610, NIST SRM 612, NIST SRM 614, BHVO-2G, BHVO-2, BCR-2G, JB-2, WS-E, W-2, AGV-1 and AGV-2. *Geostandards and Geoanalytical Research* **28**, 417-429.

Kuhn, H.-R., Guillong, M. & Günther, D. (2004). Size-related vaporisation and ionisation of laser-induced glass particles in the inductively coupled plasma. *Analytical and Bioanalytical Chemistry* **378**, 1069-1074.

Kuhn, H.-R. & Günther, D. (2004). Laser ablation-ICP-MS: particle size dependent elemental composition studies on filter-collected and online measured aerosols from glass. *Journal of Analytical Atomic Spectrometry* **19**, 1158-1164.

Mareels, J., (2004). ICP-MS analysis, geochemistry, and petrogenesis of granites from the Variscan northern Vogesen (France). *PhD thesis*, 359 pp, Catholic University of Leuven, Netherlands.

Meinhold, G., Kostopoulos, D. & Reischmann, T. (in press). Geochemical constraints on the provenance and depositional setting of sedimentary rocks from the islands of Chios, Inousses and Psara, Aegean Sea, Greece: Implications for the evolution of Palaeotethys. *Journal of the Geological Society of London* **164.**

Nicholls, I.A. (1974). A direct fusion method of preparing silicate rock glasses for energy-dispersive electron microprobe analysis. *Chemical Geology* **14**, 151-157.

Orihashi, Y. & Hirata, T. (2003). Rapid quantitative analysis of Y and REE abundances in XRF glass bead for selected GSJ reference rock standards using Nd-YAG 266 nm UV laser ablation ICP-MS. *Geochemical Journal* **37**, 401-412.

Pearce, N.J.G., Perkins, W.T., Westgate, J.A., Gorton, M.P., Jackson, S.E., Neal, C.R. & Chenery, S.P. (1997). A compilation of new and published major and trace element data for NIST SRM 610 and NIST SRM 612 glass reference materials. *Geostandards Newsletter: The Journal of Geostandards and Geoanalysis* **21**, 115-144.

Raczek, I., Stoll, B., Hofmann, A.W. & Jochum, K.P. (2001). High-precision trace element data for the USGS reference materials BCR-1, BCR-2, BHVO-1, BHVO-2, AGV-1, AGV-2, DTS-1, DTS-2, GSP-1 and GSP-2 by ID-TIMS and MIC-SSMS. *Geostandards Newsletter: The Journal of Geostandards and Geoanalysis* **25**, 77-86.

Stix, J., Gorton, M.P. & Fontaine, E. (1996). Major and trace element analysis of fifteen Japanese igneous reference rocks by XRFS and INAA. *Geostandards Newsletter: The Journal of Geostandards and Geoanalysis* **20**, 87-94.

USGS (2004) Geochemical reference materials and certificates. (http://minerals.cr.usgs.gov/geo_chem_stand/).

Vendemiatto, M.A. & Enzweiler, J. (2001). Routine control of accuracy in silicate rock analysis by X-Ray fluorescence spectrometry. *Geostandards Newsletter: The Journal of Geostandards and Geoanalysis* **25**, 283-291.

Willbold, M. & Jochum, K.P. (2005). Multi-element isotope dilution sector field ICP-MS: A precise technique for the analysis of geological materials and its application to geological reference materials. *Geostandards and Geoanalytical Research* **29**, 63-82.

Yu, Z., Norman, M.D. & Robinson, P. (2003). Major and trace element analysis of silicate rocks by XRF and laser ablation ICP-MS using lithium borate fused glasses: Matrix effects, instrument response and results for international reference materials. *Geostandards Newsletter: The Journal of Geostandards and Geoanalysis* **27**, 67-89.

Part II

– Internal differentiation of the Archean continental crust – Fluid-controlled melting of granulites and TTG-amphibolite associations in Central Finland

Franziska Nehring, Stephen F. Foley, Pentti Hölttä, Alfons van den Kerkhof

Abstract 25

1. Introduction 26

2. Geological setting 27

3. Petrography 29

3.1 Granulites 29

3.2 TTG gneisses and associated amphibolites 32

3.3 Leucosomes 35

4. Metamorphic conditions 35

5. Analytical methods 36

6. Fluid inclusions 37

6.1 Carbonic inclusion 37

6.2 Aqueous inclusions 39

7. Geochemistry 40

7.1 Granulites 40

7.2 TTG gneisses 44

7.3 Amphibolitic gneisses and amphibolite lenses 46

7.4 Leucosomes 46

8. Granulite and migmatite petrogenesis 50

8.1 Fluid regime during partial melting of granulites and amphibolite-banded migmatites 50

8.2 Melt formation in granulites 51

8.2.1 Mafic granulites 51

8.2.2 Intermediate granulites 55

8.3 Melt formation in TTG gneisses 57

8.4 Origin of leucosomes in granulites, TTG gneisses and amphibolites 59

9. Conclusions 64

Appendix A 65

Appendix B 67

References 70

Abstract

Closely associated granulites and upper-amphibolite facies migmatites (tonalitic-trondhjemitic-granodioritic gneisses, amphibolites) from Central Finland record reworking and partial melting of already existing Archean crust during a major tectonothermal event at 2.6-2.7 Ga. Vast amounts of new continental crust formed throughout the Fennoscandian Shield at the same time suggesting a close connection between crustal recycling and crustal growth.

Differences in peak metamorphic P-T-conditions and in the composition of fluid inclusions imply that partial melting in different lithologies was fluid-controlled. Anhydrous mineral assemblages as well as tonalitic melts in granulites formed due to dehydration melting of amphibole. A dry melting regime in granulites is supported by the high abundance of carbonic fluid inclusions in granulites. The geochemistry of the LREE-depleted mafic granulites can be modelled by 10-30 % partial melting of an amphibolitic source rock leaving a garnet-bearing residue. Modal amphibole contents in intermediate granulites are variable. Ratios between modal amphibole and modal clinopyroxene or orthopyroxene imply that the amount of melt produced by the breakdown of amphibole within intermediate granulites was less than 10 % and melting was most likely restricted by the availability of quartz.

Migmatitic TTG gneisses interspersed with amphibolites are the host rocks of granulites and the predominant rock type in the working area. Pressure-temperature estimates for amphibolite lenses in the gneisses yield 660-770°C and 5-6 kbar. These P-T-conditions restrict partial melting to the wet solid us and it is inferred that melting of the gneisses occurred in the presence of a H_2O-rich fluid. Abundant aqueous fluid inclusions and the lack of carbonic inclusions in the gneisses are in accordance with a water-fluxed melting regime.

Leucosomes in CaO-rich mafic granulites and amphibolites have higher Ca / Na ratios than leucosomes in intermediate granulites and TTG gneisses and hence, leucosome composition records the source composition. This implies that the formation of trondhjemites is favoured by partial melting of sodic precursors (TTG gneisses) while melting of the CaO-rich mafic rocks exclusively produces tonalitic melts.

The REE contents in leucosomes from both granulites and migmatitic gneisses are low and both exhibit strong positive Eu anomalies. Petrography as well as geochemistry of leucosomes suggest, that they represent plagioclase-quartz assemblages crystallized early from the melt phase. It also implies that similar plagioclase compositions in leucosomes and adjacent mesosomes record equilibration with the same melt phase percolating along grain boundaries.

1. Introduction

Reworking and partial melting of already existing crust is evident in many Archean crustal sequences. Recycling of continental crust as far back as the late Archean is recorded for instance by zircon ages and isotope data (Nd and Hf isotopes) of rocks from the Superior Province in Canada (Whalen et al., 2002, Bédard, 2006) and from southern China (Zhang et al., 2006). Recent studies by Hawkesworth & Kemp (2006) and Kemp et al. (2006) have shown that zircon crystallization ages can reflect crustal reworking rather than crustal growth. This suggests that global peaks in crustal growth at 2.7 Ga or 1.9 Ga (Condie, 1998) also involve reworking and remelting of older crust.

Archean continental crust predominantly consists of tonalite-trondhjemite-granodiorite (TTG) associations. These primary plutonic rocks have variable field aspects ranging from homogeneous gneisses to highly heterogeneous migmatites (Martin, 1994) due to post-magmatic metamorphic overprint. There is a general consensus that TTG represent derivates of partially melted basaltic crust (Martin, 1993, Drummond & Defant, 1990). However, it is still debated whether melting occurred in a subduction zone setting or at the base of thick basaltic crust (Bédard 2006 and references therein). Tonalitic to trondhjemitic melts have been generated in a variety of melting experiments on mafic source rocks (Johnston, 1986, Beard & Lofgren, 1991, Rushmer, 1991, Rapp et al., 1991, Sen & Dunn, 1994, Wolf & Wyllie, 1994, Patiño Douce & Beard, 1995, Rapp, 1995, Springer & Seck, 1997, Sisson et al., 2005). Moyen & Stevens (2006) demonstrated that melting of slightly enriched, MORB-like basalts is needed to account for TTG characteristics. Garnet and amphibole are required in the residue to induce the strong fractionation of the REE and low Nb / Ta in Archean TTG (Rapp et al., 1991, Martin, 1994, , Foley et al., 2002).

It is generally accepted that most of the TTG crust is primitive and only slightly modified by fractional crystallization (Bédard, 2006). However, melting and recycling of TTG crust under lower-crustal conditions may have operated in most of the high-grade Archean terrains leading to an addition of felsic melt to the continental crust. This is for instance indicated by the abundance of inherited zircon cores well as Nd isotopic constraints that indicate variable contribution of older crustal sources in many TTG suites and greenstone belt volcanics (Stern et al., 1994, Tomlinson et al., 2003, Tomlinson et al. 2004, Whalen et al., 2004).

Reworking of the 3.1-2.7 Ga old basement in Central Finland took place under upper-amphibolite to granulite facies conditions between 2.7-2.63 Ga (Mänttäri & Hölttä, 2002) and

generated partial melts from variable source rocks. In this paper we compare and contrast petrographical, geochemical and fluid-inclusion data in order to constrain the conditions of crustal melting. Modelling of melt and residue compositions allows us to draw some conclusions on the extent of melt formation and crustal recycling. Granulites from the working area are anhydrous residues formed by incongruent dehydration melting reactions in amphibolitic source rocks. Indications for dehydration melting reactions are lacking in upper-amphibolite facies migmatites and we suggest that melting within these rocks could have only occurred if triggered by a hydrous fluid. Thus the availability of water is considered as the controlling factor of melt formation reactions in the lower crust of Central Finland.

2. Geological setting

The working area is part of the Archean Iisalmi block which lies at the SW-margin of the Karelian craton (Fig. 1). The dominate rock types of this area are migmatitic TTG gneisses. Amphibolites occur as schollen, rafts and lenses within the gneisses but also as several meter wide zones. The association of migmatitic TTG gneisses and amphibolites forms the host rock for frequently occurring pyroxene- and garnet-bearing intermediate and mafic granulites. The small granulite blocks are usually bounded by faults but also gradual transitions between granulites and migmatites can be observed. The working area was subdivided into three major units according to the field appearance and mineralogy of the granulites. Those units are the from NW to SE the *Iisalmi-Sukeva* area, the *Varpanen-Pallikäs* area and the *Jonsa* area (Fig. 1).

Fig. 1 (next page):

Generalized geological map of the working area, modified after Hölttä & Paavola (2000). Numbers on the map refer to samples presented in Appendix A and B. Outcrops 031 and 138 are located N and NW of Sukeva, outcrops 131-133 to the east of the Varpanen block. They are not displayed on the map. Shear zones, dolerite dykes, gabbros and granitoid intrusion are of Proterozoic age.

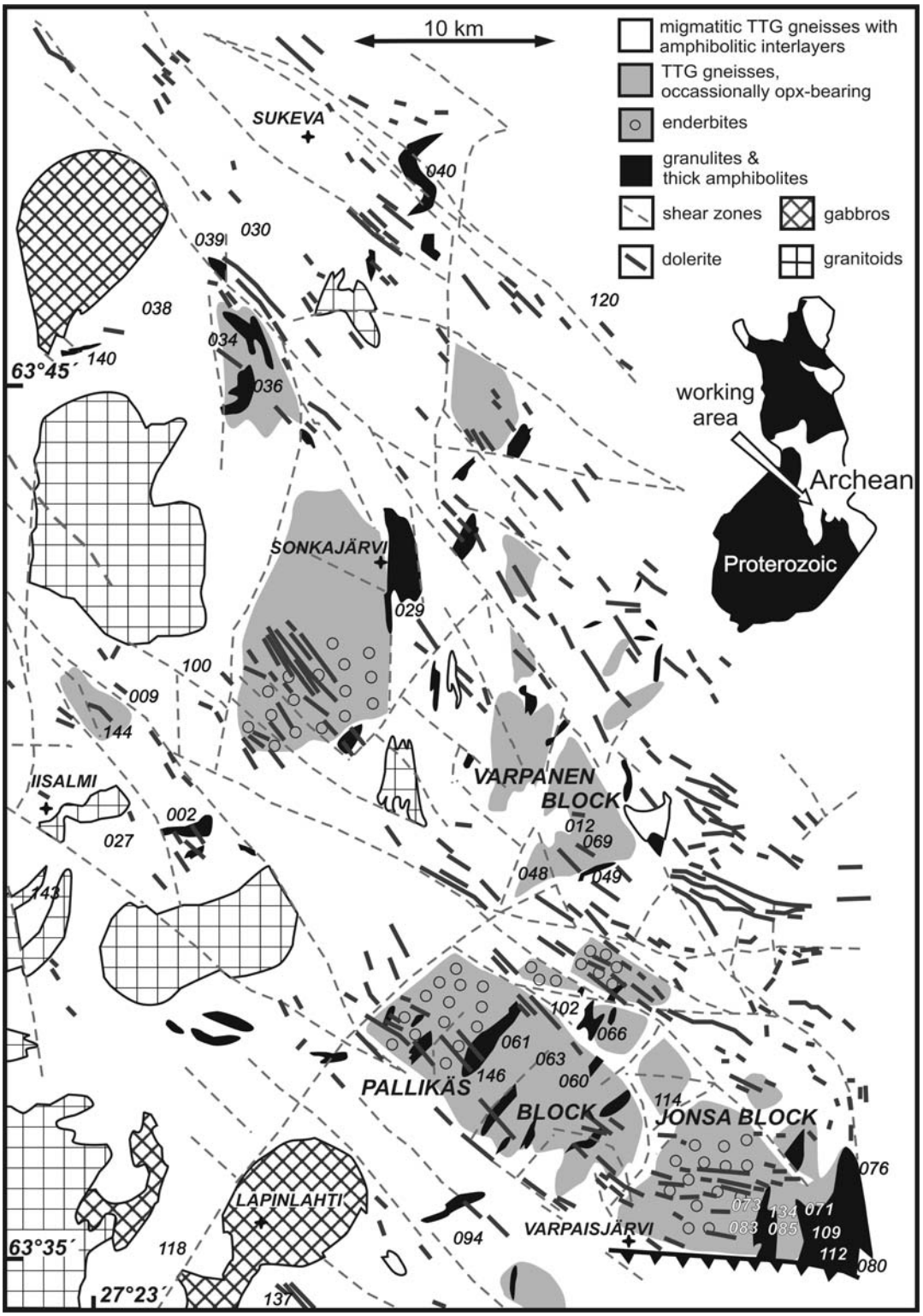
10 km
migmatitic TTG gneisses with amphibolitic interlayers
TTG gneisses, occassionally opx-bearing
enderbites
granulites & thick amphibolites
shear zones
gabbros
dolerite
granitoids
working area
Archean
Proterozoic
SUKEVA
SONKAJÄRVI
IISALMI
VARPANEN BLOCK
PALLIKÄS BLOCK
JONSA BLOCK
LAPINLAHTI
VARPAISJÄRVI
63°45´
63°35´
27°23´
040
039
030
038
034
036
140
120
029
100
009
144
002
027
143
012
069
048
049
102
066
061
063
146
060
114
076
073
134
071
083
085
109
112
080
094
118
137

Fig. 1

Zircon ion microprobe dating as well as Sm-Nd model ages of granulites from the Varpanen area indicate protolith ages of 3.1-3.2 Ga (Hölttä et al., 2000, Mänttäri & Hölttä, 2002). Similarly, mesosomes of TTG gneisses from the western part of the working area have an age of 3.2 Ga (Mänttäri et al. 1998). In contrast, zircon ages of granulites from the Jonsa area are 2.73-2.70 Ga and the Sm-Nd model age is 2.93 Ga (Hölttä et al., 2000). This major age difference between rocks from the NW and SE parts of the working area suggest terrane accretion during the late Archean since metamorphism occurred coevally in both terranes between 2.70-2.63 Ga (Mänttäri & Hölttä, 2002, Hölttä et al., 2000). Igneous enderbites (opx-bearing tonalitic to dioritic igneous rocks) intruded throughout the working area during the early phase of granulite metamorphism. Compositionally similar and contemporaneous leucodioritic igneous rocks lacking orthopyroxene occur in the very north of the working area (Naimakangas type leucodiorites) and to the east of the Varpanen area (Rokanmäki tonalite) (Paavola, 1999, Paavola, 2003).

3. Petrography

3.1 Granulites

Granulitic rocks in the working area display a variety of modal mineralogy ranging from grt-cpx-pl granulites to opx-cpx-pl granulites lacking garnet (mineral abbrevations after Kretz, 1983). Granoblastic grt-cpx-pl±hbl assemblages are typical for the 3.1 Ga granulites from the Iisalmi-Sukeva area (Fig. 2a-d). They resemble occurrences of Archean mafic granulites described by Sawyer (1991), Williams et al. (1995) and Hartel & Pattison (1996) from Canada. In the mafic granulites orthopyroxene is present only as a breakdown product within symplectites around garnet or pseudomorphs after garnet. The rocks show weak layering of lighter and darker zones. Leucosomes are present as thin veins and melt patches (Fig. 2c)

Prograde, granoblastic orthopyroxene is characteristic for the 2.7 Ga intermediate granulites from the Jonsa area. The Jonsa granulites show layering of lighter and darker bands which often interfinger each other (Fig. 2e). Garnet is restricted to single layers (Fig. 2f). The amount of leucosome is typically higher than in mafic granulites (Fig. 2g). Migmatitic mica gneisses and Al-Mg granulites (metasediments) are intercalated with intermediate granulites in the Jonsa area (Hölttä, 1997) but are not considered further in this study.

Field appearance and compositional differences in intermediate granulites suggest a pre-metamorphic layering of broadly andesitic rocks probably resembling volcanic successions. Similar compositional layering of garnet-bearing and garnet-free granulites has been described by Zhao et al. (2000) from the North China craton and Kar et al. (2003) from the Eastern Ghats Granulite Belt in India.

The Varpanen area in between the Iisalmi-Sukeva and the Jonsa area is distinct in comprising both mafic grt-cpx-pl±hbl assemblages and intermediate opx-cpx-pl granulites.

The modal amount of amphibole in granulites is variable. Prograde amphibole is rarely found in mafic granulites from the Iisalmi-Sukeva area. In intermediate granulites amphibole it is always present (Fig. 2h), sometimes as the predominant mafic mineral with only slight overgrowth of pyroxenes while in other samples it is almost completely consumed by growth of pyroxenes and only present as inclusions in clinopyroxene, orthopyroxene or garnet. Variations between amphibole-rich and amphibole-poor or –absent layers may occur within a single outcrop.

Porphyroblastic garnet in mafic granulites reaches grain sizes up to 2-3 cm (Fig. 2d) and contains inclusions of other minerals present in the host rock (mostly amphibole and clinopyroxene). Skeletal garnet intergrown with quartz are sometimes found in contact with leucosomes. Opaque phases such as ilmenite and magnetite are abundant. Biotite is a minor constituent of intermediate granulites from the Jonsa and Varpanen area. Apatite is present as tiny euhedral crystals usually enclosed in plagioclase. Grain size of granulites typically ranges between 0.8-2 mm. Approach to equilibrium is demonstrated in most granulites by granoblastic growth with subhedral to euhedral grain shapes.

Fig. 2 (next page):

Field aspects and mineralogy of mafic and intermediate granulites from the working area. a) Garnet-bearing mafic granulite. b) Melt rich zone in mafic granulite. c) Thin leucosome veins in mafic granulites. d) Thin section of mafic granulite showing garnet surrounded by clinopyroxene. e) Layering in intermediate granulites. e) Melt-rich part of an intermediate granulite adjacent to a garnet-bearing layer. f) Outcrop of intermediate granulite with high abundance of leucosome. h) Clinopyroxene and orthopyroxene overgrowth on amphibole in an intermediate granulite.

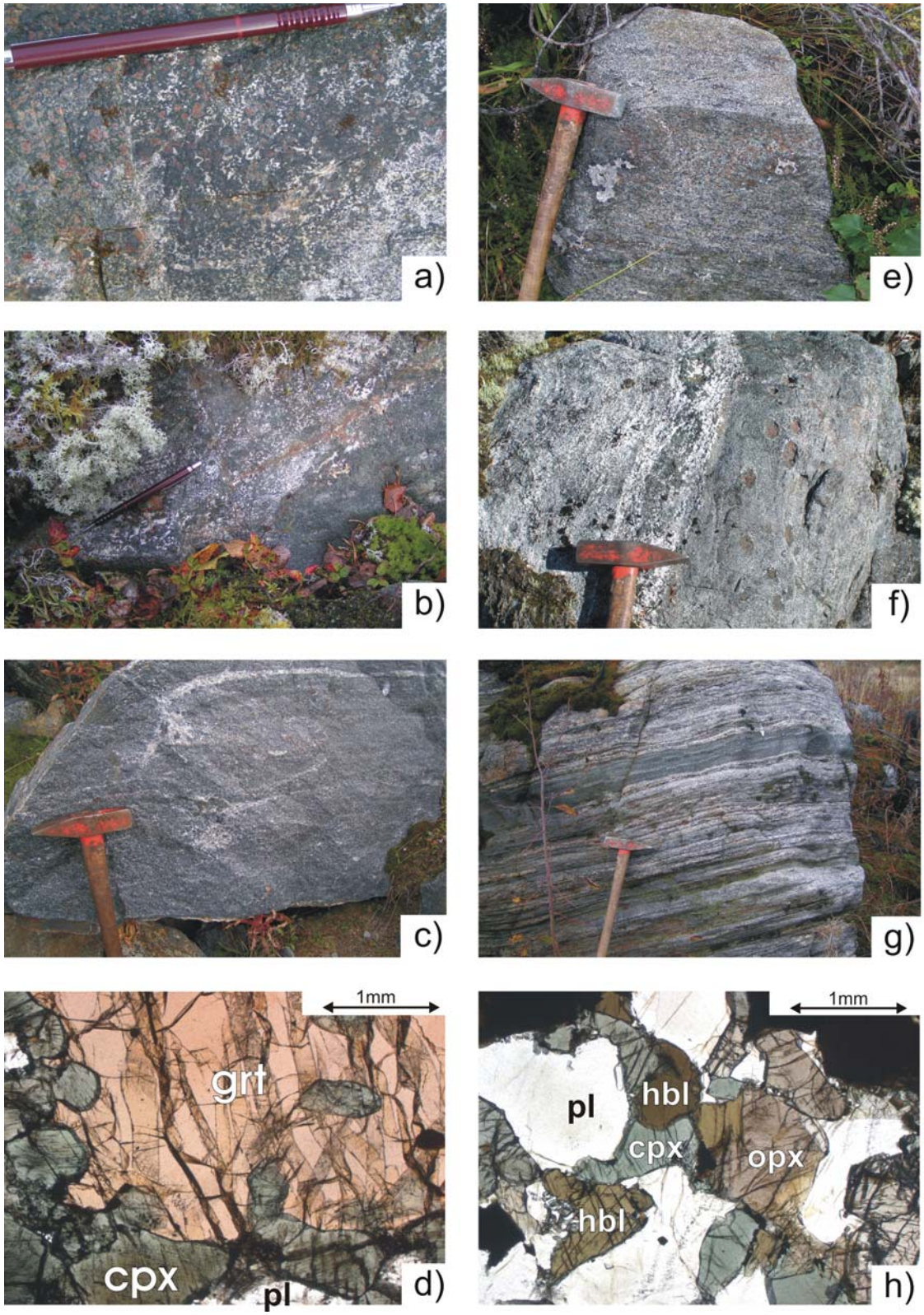

Fig. 2

3.2 TTG gneisses and associated amphibolites

The texture of TTG gneisses varies between metatexites with small scale segregation of melt (Fig. 3a-b) and schlieren migmatites with a higher degree of disaggregation (Fig. 3c-d). Mesosomes of the migmatites are predominantly tonalitic and consist of pl + qtz ± kfs ± amph ± bt ± ep. Mafic minerals make up 10-40 % of the modal mineralogy but either biotite or amphibole can be absent. Clinopyroxene is rarely to be found. Potassic feldspar occurs locally in rocks with elevated potassium contents and correlates with varieties rich in biotite. No anhydrous ferromagnesian phases have been detected in the tonalitic gneisses. Resorption textures (Fig. 4a-b) occur in some migmatites closely associated with granulites and suggest that at least some parts of the migmatite area also experienced P-T-conditions high enough to stabilize garnet or orthopyroxene. Clinopyroxene most likely was present in amphibole-bearing gneisses at peak metamorphism but it is strongly altered to secondary amphibole. The TTG gneisses commonly contain small-scale schollen, lenses and thin layers of amphibolite that consist of up to 90 % mafic minerals (Fig. 3e-f). Amphibole accompanied by biotite is the dominant mafic mineral in these amphibolite layers and lenses. Clinopyroxene can be present but it is usually altered into secondary green, Mg-rich amphibole and only recognizable by shape and colour (Fig. 4c-d). Alteration of prograde brownish amphibole into retrograde greenish or bluish amphibole and epidote is common although rocks that display alteration of clinopyroxene do not necessarily show alteration of amphibole. Plagioclase and quartz occupy interstices between granoblastic, subhedral to euhedral amphibole. Very rarely potassic feldspar occurs in amphibolite lenses that also contain biotite. Amphibolite schollen and lenses are considered as disrupted pre-metamorphic mafic intrusions into the tonalitic basement.

Fig. 3 (next page):

Field aspects of migmatites. a-b) Metatexitic TTG gneisses with stromatic leucosome. c-d) Schlieren migmatites with a high proportion of leucosome and a larger degree of disaggregation compared to the metatexites. e) Amphibolite lenses in migmatitic TTG gneiss. f) Folded amphibolite bands in migmatitic TTG gneiss. g) Stromatic migmatite with amphibolitic mesosome. h) Thick amphibolite containing leucosome parallel to the foliation as well as within a melt patch.

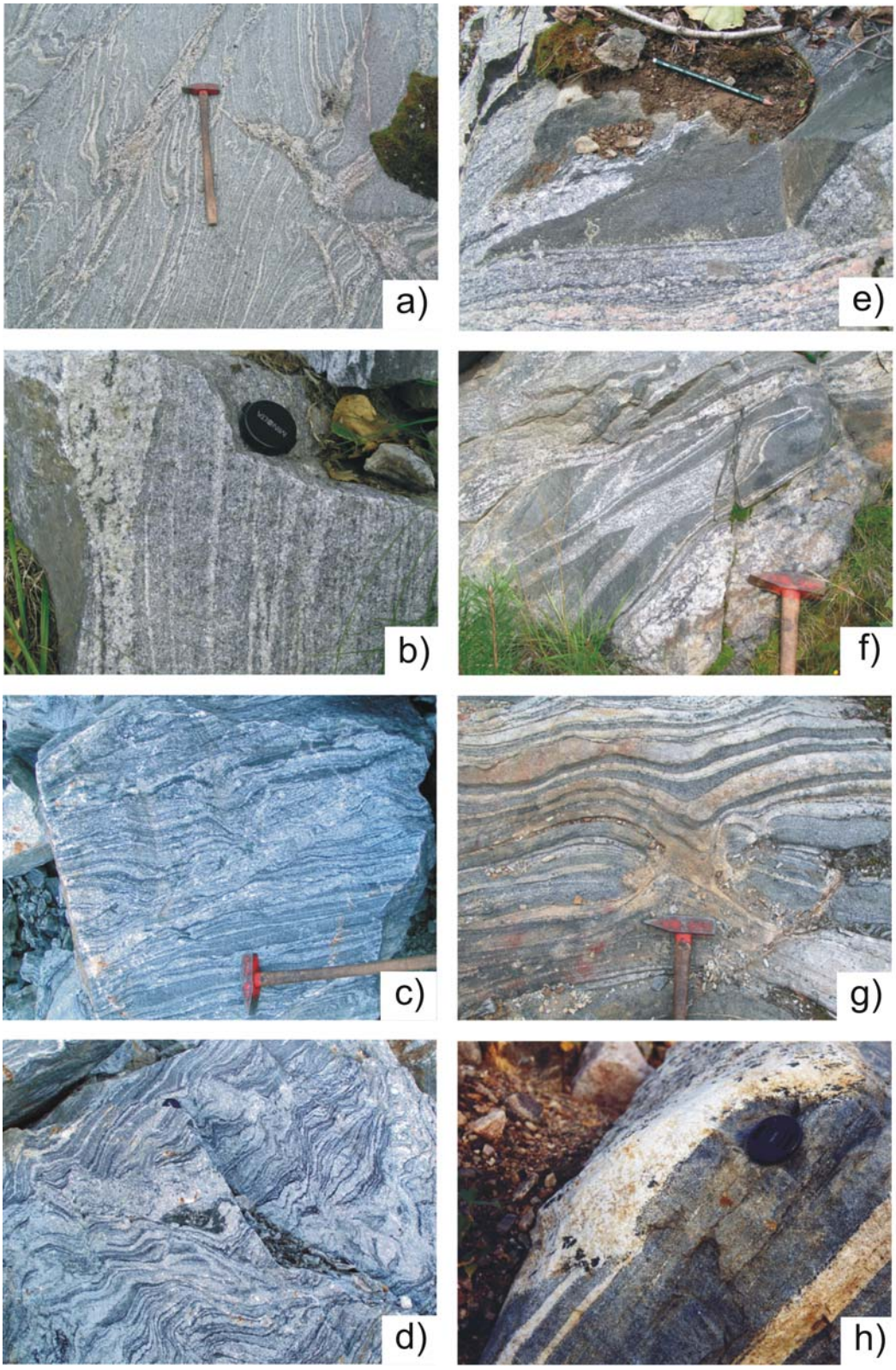

Fig. 3

Much less frequent than amphibolite lenses and schollen are several meter-wide zones of amphibolitic gneisses which are intercalated with the TTG gneisses (Fig. 3g-h). Some of these thick amphibolites may represent retrogressed granulites based on granulites occurrences in the close vicinity and remnants of orthopyroxene or garnet within them. In other localities they seem to represent more mafic constituents of the TTG basement. The thick amphibolites are grouped together although their composition and mineralogy is rather variable.

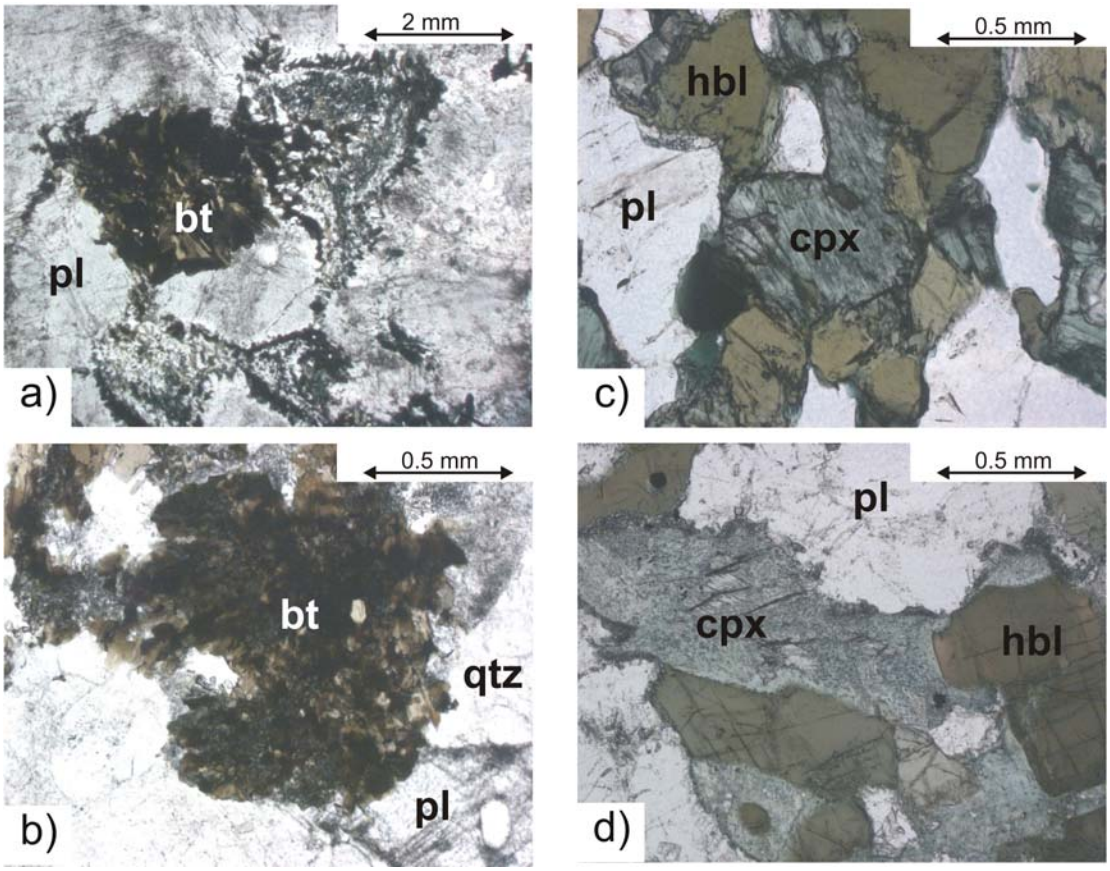

Fig. 4:

(a-b) Resorption textures in migmatitic gneisses closely associated with granulites. Pseudomorphs (4a) and fine-grained clots of biotite (4b) are inferred to represent replacements of former orthopyroxene and garnet. Clinopyroxene in amphibolite lenses (4c) from the migmatite area is usually altered into secondary amphibole (4d).

3.3 Leucosomes

Granulites as well as the lower-grade TTG gneisses and amphibolites contain leucosomes. Leucosomes within the mafic granulites from the Iisalmi-Sukeva area consist of thin veins and small melt patches. Intermediate granulites from Varpanen and Jonsa areas are stromatic with leucosomes forming several cm-thick layers. Additionally, diatexites with a high leucosome / mesosome ratio exist in the Jonsa and Varpanen areas. The amount of leucosome in the TTG gneisses is variable. Some outcrops display features of extensive melting and mobilization with host rock structures being nearly obliterated.

Leucosomes in all lithologies consist of large subhedral to euhedral grains of plagioclase with quartz occupying the interstices between plagioclase grains. Large plagioclase crystals often are disrupted and twinning lamellae are bent indicating deformation after crystallization. Although mafic phases are rare in leucosomes they display the spectrum of the host minerals. Within granulites mafic phases are more abundant in small leucosome patches but are rare in thicker discordant leucosomes. Most mafic phases in leucosomes are considered to be disaggregated crystals from the host but large, euhedral crystals in melt patches represent peritectic phases of the melting reaction.

4. Metamorphic conditions

Peak metamorphic conditions are obtained from grt-cpx-pl-qtz assemblages indicating 9-11 kbar and 800-950°C (Hölttä & Paavola, 2000). The highest pressures were obtained from mafic granulites in the NW of the Iisalmi-Sukeva area, suggesting that deeper proportions of the crust are exhumed in the NW. After peak metamorphism the area experienced decompression and cooling to ca. 7 kbar and 700°C as indicated by garnet decomposition to orthopyroxene and plagioclase.

Mineral compositions within symplectites around garnet or along fractures in garnet give 5.7-7.1 kbar and 590-740°C. Symplectite formation most likely took place during paleoproterozoic overprint and fracturing of the bedrock.

Amphibolites as well as TTG gneisses are poor in P-T-indicators. Amphibole-plagioclase thermometry following Holland & Blundy (1994) was applied in combination with the Al-in-hornblende barometer calibrated by Anderson & Smith (1995). One of the thick amphibolites

within TTG gneisses from the NW of the Iisalmi-Sukeva (outcrop 038) area yielded upper-amphibolite facies P-T-conditions of 660-690°C at 4.8-5.8 kbar and an amphibolite lens from a migmatite outcrop close to Iisalmi (outcrop 009) gives 720-770°C at 4.4-6.0 kbar. Derivation of temperatures for amphibolites followed thermometer B in Holland & Blundy (1994) since it is suitable for silica-undersatured rocks. The Al-in-hornblende barometer was calibrated for the assemblage qtz + kfs + pl + amph + bt + Fe-Ti-oxides + ttn + melt + fluid. Potassic feldspar and biotite are often lacking from the samples. Although Anderson & Smith (1995) stated that the absence of alkali feldspar does not seem to affect the pressure estimations significantly, calculated pressures for the TTG gneisses and amphibolites should be considered with caution. The close relationship with granulites equilibrated under higher pressures and a combined metamorphic evolution suggests that pressure calculations for the amphibolites are minimum estimates.

5. Analytical methods

Samples were analysed for major and a number of trace elements (Cr, Ni, Sc, V, Sr, Rb, Ba and Zr) by XRF at the Institute for Geosciences, University of Mainz. The REE as well as Y, Hf, Nb, Ta, Th and U were analyzed using LA-ICP-MS and solution ICP-MS. Most samples with less than 55 wt% SiO_2 were processed on an Iridium strip heater and the glass beads produced were measured by LA-ICP-MS. For further explanation of this method see Fedorowich et al. (1993) and Jochum et al. (2005). Samples with higher SiO_2 contents were analysed applying Li-metaborate fusion following the method described in Mareels (2004). The solutions obtained after Li-metaborate fusion were analyzed using a VG Elemental Plasma Quad 3 at the University of Mainz, Institute for Geosciences. Thorium determination proved difficult using the method of Mareels (2004) especially at low concentrations in the leucosomes.

Fluid inclusions studies were carried out using a Linkam THMS 600 heating / freezing stage mounted on an Olympus BH-2 microscope in combination with a TP 91 controller. The accuracy is generally about 1°C, for CO_2-melting 0.2°C.

6. Fluid inclusions

Fluid inclusions have been studied in mesosome – leucosome pairs from granulites and TTG gneisses but data are mainly derived from the leucosomes because they provide well preserved quartz grains. The fluid inclusion regime in granulites is dominated by carbonic inclusions while TTG gneisses almost exclusively contain aqueous inclusions.

6.1 Carbonic inclusion

CO_2-inclusion in rocks from the working area are strictly bound to granulite outcrops. They predominately occur in quartz but to a much smaller extent can also be observed in garnet, plagioclase and pyroxene. The inclusions are situated along healed-fracture planes or within stretched and transposed clusters none of which crosscut the crystal boundaries. The CO_2-inclusions are rounded or exhibit negative crystal shape (Fig. 5 a-b). Within garnet they are stretched and form large vermiform and only partly filled cavities. Melting of the CO_2-inclusion occurred instantaneous close to the triple point of pure CO_2 (*Tt* = -56.6°C). The overwhelming majority of inclusions homogenized into the liquid state. The homogenization temperatures (*Th*) range between - 26 and +30°C and have a prominent mode between -5 and +5°C (Fig. 6a). Less prominent peaks occur at -10°C and between +20 and +23°C. Homogenization temperatures below -18°C were found in only one sample from the Varpanen area. Homogenisation temperatures of inclusions in plagioclase and pyroxene agree with those in quartz within the same sample while inclusions in garnet show higher *Th* than those in quartz. This may be due to extensive fracturing of the brittle garnet porhyroblasts during proterozoic movements.

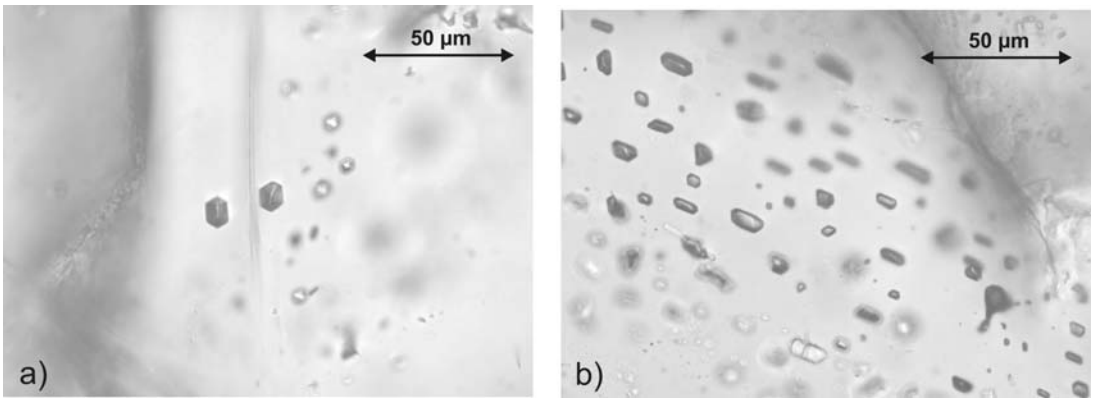

Fig. 5:

Carbonic inclusions in a granulite leucosome. a) Isolated inclusions with negative crystal shape.
b) Large cluster of inclusions.

Densities of CO_2-inclusions are low (σ = 1.05 – 0.75 g / ccm). Using the equation of state of Angus et al. (1976) provided within the computer package *FLUIDS* by Bakker (2003) the lowest homogenization temperature observed of ca. -24°C corresponds to an isochore that intersects the lower part of the P-T-field of peak metamorphism yielding about 8 kbar at 800°C. The inclusions with the lowest homogenization temperatures most likely represent primary, peak metamorphic inclusions. Although they are rare, their presence confirms the experiments of Vityk & Bodnar (1995) which showed that a small percentage of inclusions usually survives overpressure during retrograde uplift. Their occurrence additionally implies that the large group of CO_2-inclusions with lower densities records post-metamorphic resetting. Isochores corresponding to the low-density CO_2-inclusion clearly lie below the P-T-field of granulites yielding pressures of 4-5 kbar or even lower at peak metamorphic temperatures of 800°C (Fig. 6b). Densities of CO_2-inclusion most likely correspond to Paleoproterozoic overprint of the working area for which P-T-conditions were confined to 3.1-5.4 kbar and 540-630°C (Mänttäri & Hölttä, 2002).

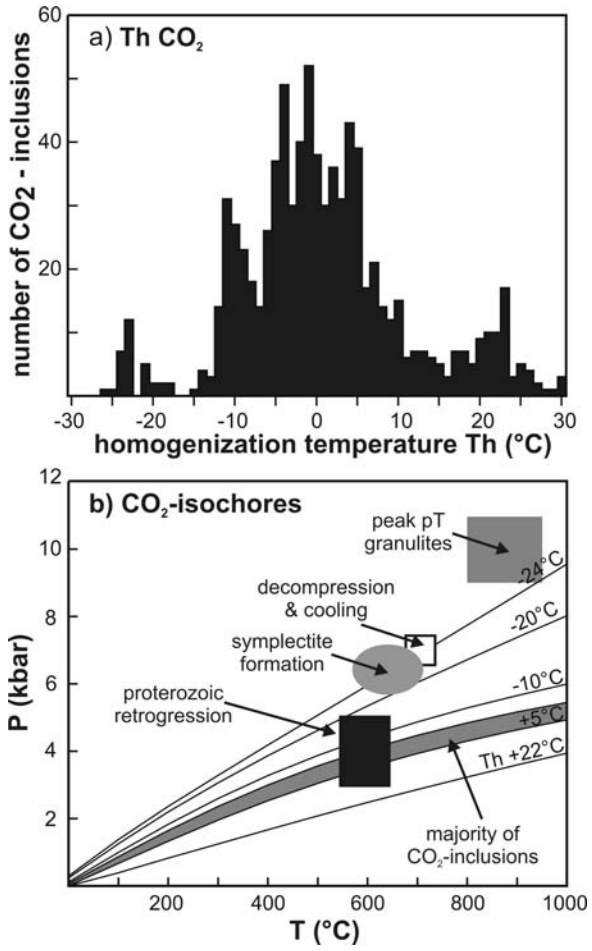

Fig. 6:

Results from studies of CO_2-inclusions.

a) Homogenization temperatures (Th) of most of the inclusions fall in the range between -10°C and +10°C and the corresponding densities are 0.9-1.0 g/cm3. Few inclusions have Th below -20°C and densities of 1.05 g/cm3.

b) Isochores corresponding to observed homogenization temperatures and P-T-conditions of major tectonic events. Most inclusion were reset during Proterozoic overprint of the area. Fluid inclusions with the lowest Th intersect into the P-T-field of granulites and most likely were trapped peak-metamorphic.

6.2 Aqueous inclusions

Aqueous fluid inclusions are abundant in the TTG gneisses. Granulites contain few aqueous inclusions but they become more abundant near fault zones or close to the borders of granulite occurrences.

Aqueous inclusions in both granulites and TTG gneisses are irregularly formed and they occur isolated, as small clusters, within fractures or along grain boundaries (Fig. 7 a-b). They are usually monophase at room temperature. Low salinity aqueous inclusions with melting temperatures close to 0°C are considered as late meteoric waters. Most aqueous inclusions melt in the temperature range between -5 and -15°C (Fig. 8 a & b) corresponding to salinities of 8 - 18 eq. wt% NaCl (Bodnar, 1993). Melting temperatures below -15°C are less frequent but nevertheless they occur and are as low as -46°C in two samples. These brines rarely contain cubic crystals of salt. Final melting temperatures below -21°C suggest the presence of cations such as Ca^{2+}, Mg^{2+} or K^{+}. Within gneisses formation of eutectic melt is sometimes observed at temperatures below -50°C clearly indicating the presence of $CaCl_2$ in the aqueous fluid. Homogenization temperatures have been measured in a few aqueous inclusions of gneiss samples. One group of aqueous inclusions homogenizes at *Th* ~100°C while a second group has *Th* ~250°C. Nevertheless inclusions of both types are closely associated and can not be distinguished by other means.

Age relations of aqueous inclusions are difficult to unravel. High-salinity brines are common in high-grade metamorphic rocks and may be considered as primary although their origin is not fully understood yet. They may evolve by scavenge of water from the fluid phase into silicate melt during anatexis

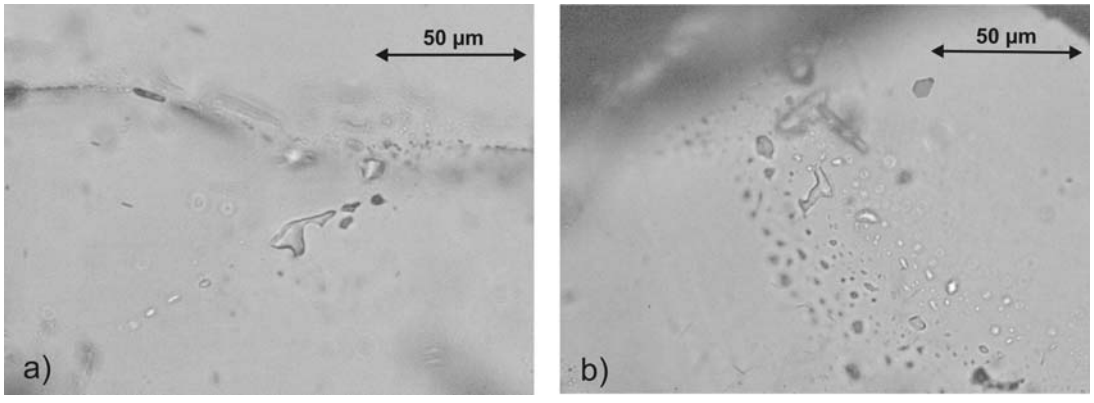

Fig. 7: a) Small cluster of irregularly formed aqueous inclusion in a migmatite leucosome.
b) Larger cluster of aqueous inclusions on a healed fracture plane in a migmatite leucosome.

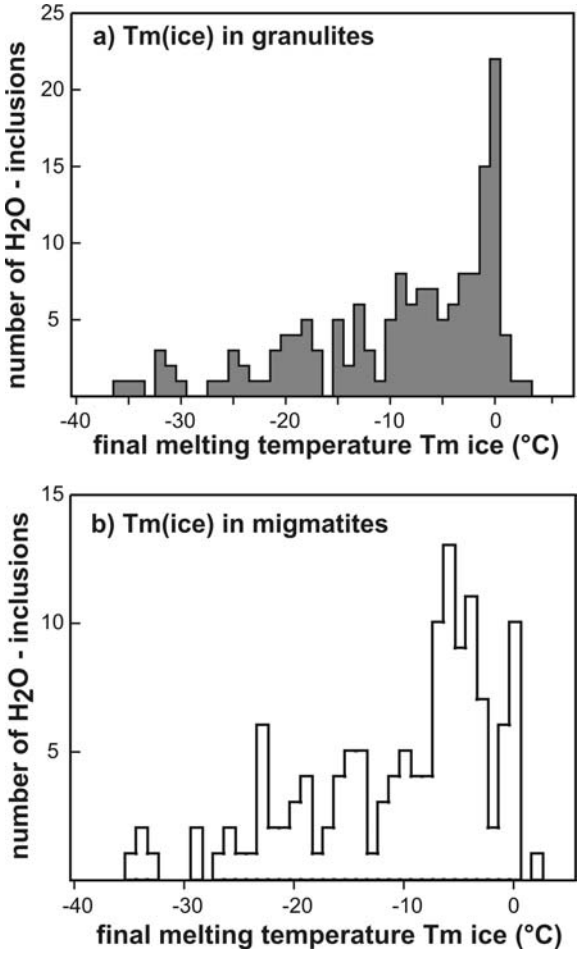

Fig. 8:

Melting temperatures of aqueous inclusions in granulites (a) and upper amphibolite facies migmatites (b).

Fluids with low salinities and melting temperatures close to 0°C are considered as late meteoric waters. In contrast, brines with high salinities and low melting temperatures were probably captured early in the metamorphic history.

7. Geochemistry

7.1 Granulites

Mineralogical varieties of granulite occurrences are associated with compositional differences. Grt-cpx-granulites from the Iisalmi-Sukeva area are mafic with 48-50 wt% SiO_2 (Appendix A), while opx-cpx-granulites from the Jonsa area are intermediate in composition (52-60 wt% SiO_2) (Hölttä, 1997). Mafic granulites usually display steep fractionation trends on variation diagrams (Fig. 9). The most striking feature is their strong enrichment in CaO (8-16 wt%) compared to intermediate granulites (5-11 wt%). A high modal abundances of clinopyroxene (35-50%) correlates with the elevated CaO contents in mafic granulites. Except one location mafic granulites have lower K_2O- (0.05-0.42 wt%) and Na_2O contents (1.2-2.7 wt%) than intermediate granulites (K_2O: 0.26-1.25 wt%, Na_2O: 1.7-4.7 wt%) resulting in higher Ca / (Na+K) ratios. FeO and MgO contents are comparable in mafic and intermediate granulites but are lower in the intermediate granulites with increasing SiO_2.

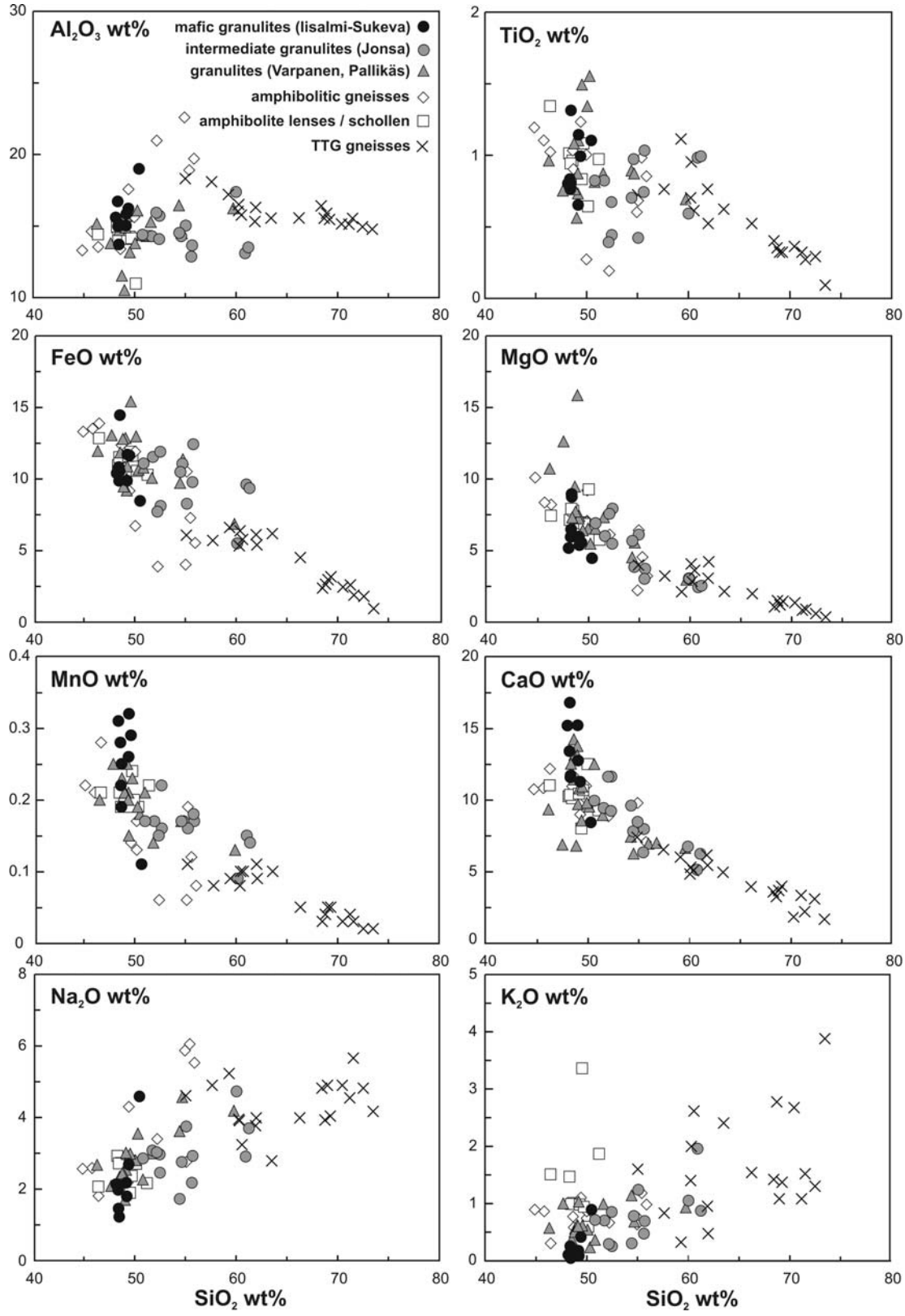

Fig. 9:

Major element variations vs. SiO_2 for main lithologies from the working area.

Plots vs. Mg-number (Mg#) reveal that the intermediate Jonsa granulites show a strong trend of increasing Al_2O_3 and decreasing TiO_2 with increasing Mg# (Fig. 10), whereas this correlation is not observed in mafic granulites. On the contrary, in the mafic granulites from Iisalmi-Sukeva those with Mg# > 50 have lower Al_2O_3 than those with Mg# < 50. Trends in major element variation diagrams for both groups of granulites may indicate fractionation of clinopyroxene and An-rich plagioclase from a mafic precursor although the proportion of the fractionating minerals most likely was different.

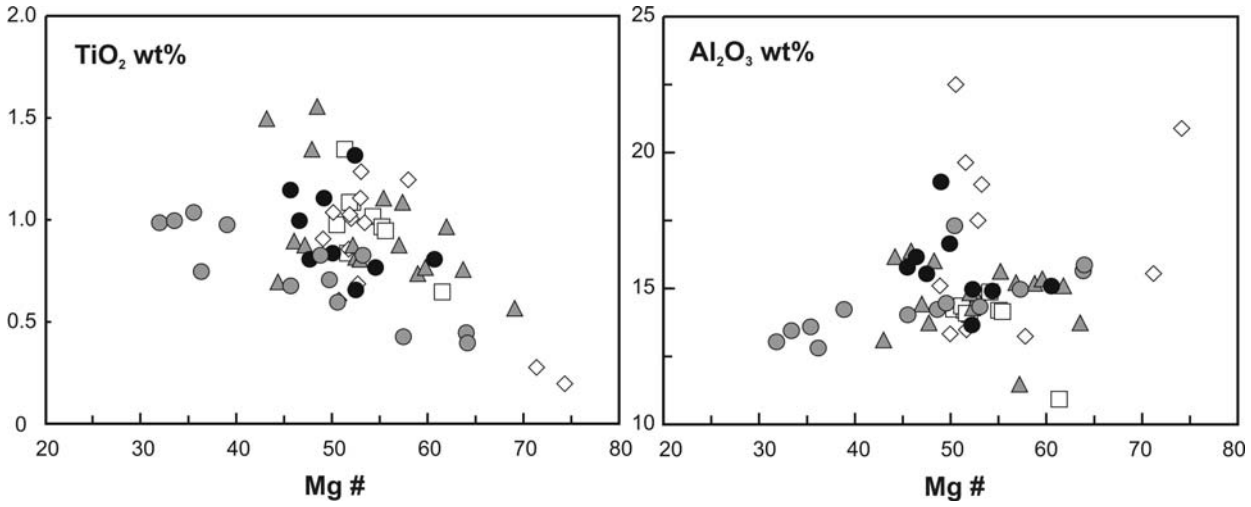

Fig. 10:

TiO_2 and Al_2O_3 vs. Mg# for main lithologies from the working area (symbols as in Fig. 9). Note the linear trends for the intermediate granulites from the Jonsa area and the differences in Al_2O_3 in the mafic granulites from the Iisalmi-Sukeva area.

Granulites from the Varpanen and Pallikäs area show compositional overlap with both groups. According to difference in mineralogy some samples are more similar to grt-cpx-pl granulites from the Iisalmi-Sukeva area, and are also slightly enriched in CaO and follow their characteristic steep fractionation trends, while others are intermediate in composition and resemble opx-cpx-granulites from the Jonsa area. Nevertheless they have higher TiO_2 at comparable Mg # than Jonsa granulites.

Similarly to major element characteristic granulites can be subdivided according to their trace element pattern (Hölttä, 1997), indicating petrogenesis in different settings. Mafic granulites from the Iisalmi-Sukeva area have high Cr, Ni, Sc and V contents (Appendix B, Fig. 11a) and are depleted in incompatible elements with low Rb (< 6ppm), K (< 0.4 wt%), Sr (62-125 ppm) and

Ba (0-36 ppm) contents (Fig. 11b-c). The samples most depleted in K are those with the lowest Rb contents. Intermediate granulites from Jonsa area have comparable Rb contents but K contents are higher than in mafic granulites as well as Sr (230-480 ppm) and Ba (69-780 ppm) contents. Excellent correlation between Ba and K is caused by the amount and composition of Ba and K bearing phases (amphibole, biotite, potassic feldspar) in the rocks.

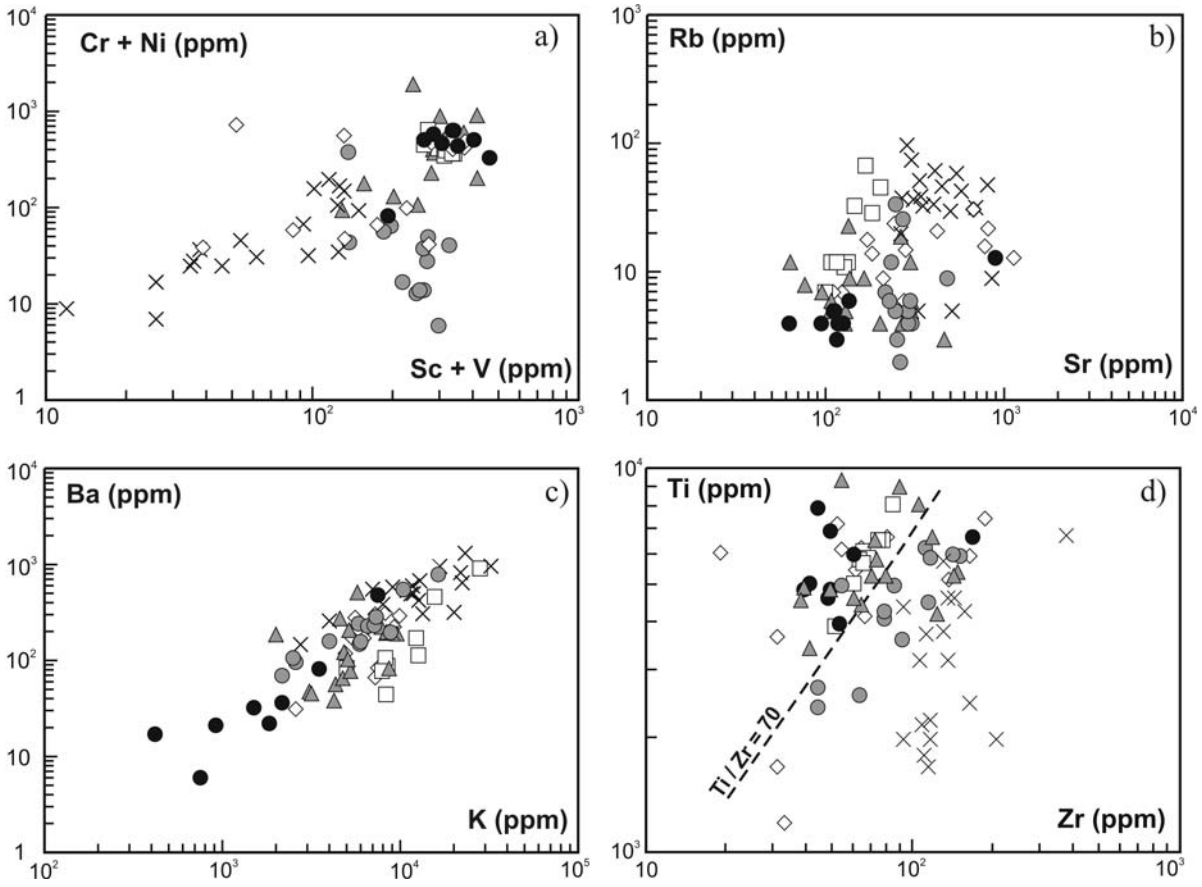

Fig. 11:

Selected trace element plots of compatible and incompatible elements (symbols as in Fig. 9). The low contents of Rb, Ba, Sr and K in the mafic granulites from the Iisalmi-Sukeva area are an indication for melt depletion.

Granulites have overall low U and Th contents (Th < 1 ppm, U < 0.3 ppm). The lowest values are observed in the mafic granulites from Iisalmi-Sukeva and Varpanen areas (Th < 0.2 ppm, U < 0.1 ppm).

Zr values are also low in the Iisalmi-Sukeva samples (< 60 ppm) but are higher in most other granulite occurrences (max. 150 ppm). Hölttä (1997) showed that granulites define two

groups according to their Ti / Zr ratios. Jonsa granulites have Ti / Zr = 40-70 while granulites from other areas besides few exceptions show ratios of 67-180 (Fig. 11d).

Mafic granulites from the Iisalmi-Sukeva area have flat REE-pattern at about 10 times the chondritic value with slight depletion of the LREE. Jonsa granulites have comparable HREE contents but are enriched in the MREE and LREE to variable degrees with La contents of up to 100 times the chondritic value (Fig. 12). REE-patterns of granulites from Pallikäs and Varpanen are flat or LREE enriched. Both types may occur in a single outcrop and flat REE-patterns are restricted to more mafic, garnet-bearing layers.

On multi-element plots intermediate granulites resemble modern island-arc basalts due to negative Nb-Ta, Ti- and Zr-anomalies. Mafic granulites lack such anomalies and broadly resemble tholeiitic basalts.

7.2 TTG gneisses

TTG gneisses are mainly tonalitic with SiO_2 contents between 55 and 73 wt%. They are enriched in Na_2O and K_2O compared to granulites and have low Ca/(Na+K) ratios. All except one are peraluminous. TTG gneisses have considerably lower Sc and V contents than granulites and amphibolites but contain the highest concentrations of Rb and Ba among the studied samples (Fig. 11). Their REE-patterns are strongly fractionated as typical for Archean TTG complexes (Martin, 1994) with La about 100 times chondritic (Fig. 12). Two groups of TTG gneisses can be distinguished according to major and trace element composition. The most striking difference are $(La/Yb)_N = 37\text{-}56$ in group I gneisses and $(La/Yb)_N < 20$ in group II gneisses. This difference is caused by a stronger depletion of the HREE in the first group while LREE contents are alike (Fig. 12). All TTG gneisses from the east of the Varpanen area belong to the first group but also throughout the rest of the working area such strongly fractionated TTG gneisses can be found. Additionally, the two groups can be divided according to their Y contents, which are <8 ppm in group I and 11-32 ppm in group II. Low HREE as well as low Y contents suggest a strong involvement of garnet in the petrogenesis of the first group of TTG gneisses. Although there is compositionally overlap group I gneisses have higher SiO_2 (68-73 wt%) and Na_2O (> 4 wt%) but lower FeO (0.9-3.1 wt%), MgO (0.42-1.56 wt%) and CaO (1.7-4.0 wt%) contents than group II gneisses (SiO_2 55-66 wt%, Na_2O > 4 wt%, FeO 4.5-6.3 wt%, MgO 2.07-4.3 wt%, CaO 3.9-4.7 wt%).

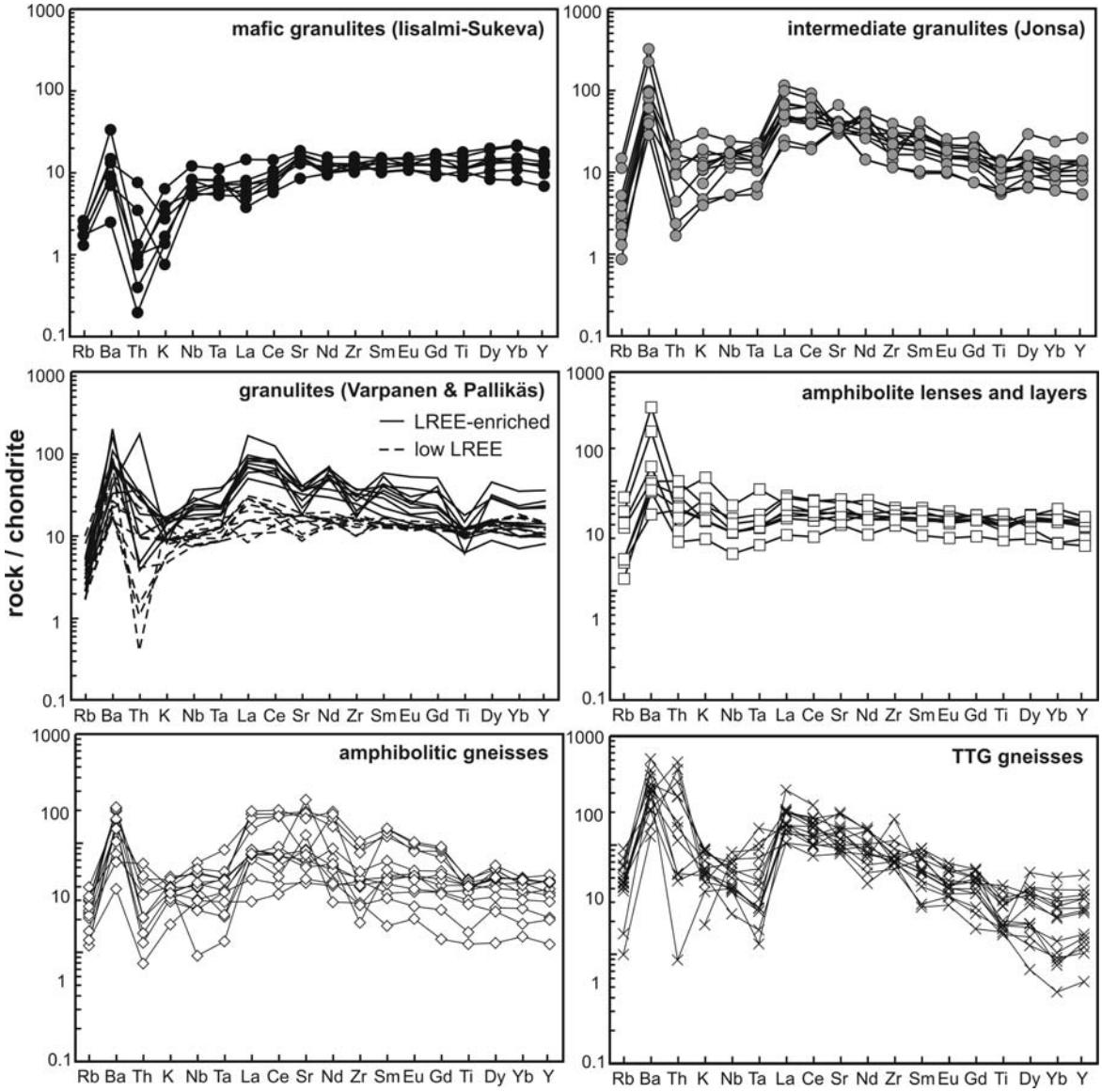

Fig. 12:

Extended trace element diagrams. Intermediate granulites from the Jonsa area as well as LREE-enriched granulites from other granulites block strongly resemble modern island-arc basalts showing distinct negative Nb-Ta, Zr- and Ti-anomalies. Mafic granulites as well as amphibolite lenses and layers from the Iisalmi-Sukeva area correspond to tholeiitic basalts. Note the two groups of TTG gneisses which can be distinguished according to their HREE contents.

7.3 Amphibolitic gneisses and amphibolite lenses

Amphibolite lenses commonly occurring within TTG gneisses have SiO_2 contents 46-51 wt% comparable to mafic granulites but they have slightly lower CaO and MnO and higher FeO and MgO than mafic granulites (Fig. 9). The Al_2O_3 vs. Mg # plot reveals that amphibolite lenses are similar to the low-Al_2O_3 group of the mafic granulites (Fig. 10). All amphibolite lenses have high Cr, Ni, Sc and V contents comparable to mafic granulites but in contrast to the depleted granulites they are also enriched in the incompatible elements Ba, Rb and K (Fig. 11). They have essentially flat REE pattern (Fig. 12).

Amphibolitic gneisses found in the working area have SiO_2 contents between 46-55 wt% and show compositional overlap with all granulite groups. Some of the more intermediate amphibolitic gneisses from the Jonsa and Pallikäs area have low contents of compatible elements comparable to the Jonsa granulites (Fig. 11a). Both, amphibolite lenses / layers and amphibolitic gneisses are enriched in Ba, Rb and K compared to the depleted granulites (Fig. 11b-c). Sr values are low in the amphibolite lenses and layers (< 200 ppm) but higher in the amphibolite bodies (up to 1100 ppm). REE pattern of the amphibolitic gneisses are LREE enriched except one slightly LREE-depleted occurrence (040) from the north of the Iisalmi-Sukeva area which most likely represents a retrogressed mafic granulite (Fig. 12). This is supported by the fact that few relict garnet grains have been observed in this outcrop.

7.4 Leucosomes

SiO_2 contents of leucosomes from granulites and TTG gneisses are 57-80 wt%. SiO_2 contents of less than 60 wt% are rare and occur in samples with a higher amount of entrained mafic phases. In the normative feldspar classification diagram after Barker (1979) leucosomes from granulites are richer in CaO than leucosomes from TTG gneisses. They are tonalitic while migmatite leucosomes cluster along the border between the trondhjemite and tonalite field (Fig. 13). Few leucosomes in either rock type have K_2O contents > 1 wt%. These leucosomes occur if potassic feldspar and biotite are present in the adjacent mesosomes.

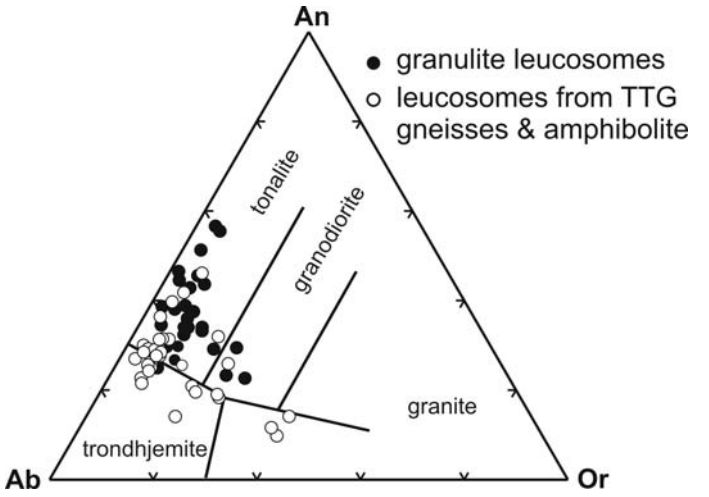

Fig. 13:
Leucosome classification according to the normative feldspar composition of Barker (1979). Granulite leucosomes are displaced towards the Anorthite-apex and classify as tonalites while most leucosomes from TTG gneisses plot along the border of tonalite and trondhjemite field due to lower Ca / Na ratios.

Leucosomes are peraluminous (A/CNK ~ 1.2) and show trends of decreasing Al_2O_3, MgO and FeO vs. SiO_2 and increasing Na_2O and CaO vs. Al_2O_3 (Fig. 14). The latter reflects the abundance and composition of plagioclase in the leucosome. Contents of MgO (< 1.5 wt%) and FeO (< 2 wt%) are low and there is no significant difference in Mg # between leucosomes from TTG gneisses and granulites. However, leucosomes from the TTG gneisses extend to higher Sr (> 600 ppm) as well as higher Rb (> 40 ppm) values than granulite leucosomes. Sr contents in leucosomes correlate with the composition of plagioclase in mesosomes. Thus, high Sr contents in leucosomes occur in granulites with sodic plagioclase as typical for most of the intermediate granulites, whereas low Sr contents are observed in leucosomes from the mafic and more calcic granulites of the Iisalmi-Sukeva area. Similarly, leucosomes hosted by amphibolitic gneisses and amphibolite lenses have lower Sr contents than those hosted by TTG gneisses due to differences in the plagioclase composition of the host rocks (Fig. 15). Rb contents > 30 ppm are connected with Ba > 500 ppm reflecting the involvement of biotite. Zr - contents in leucosomes exhibit a wide scatter between 18 – 340 ppm but are mostly below 150 ppm. Contents of each Sc, Cr, Ni and V in leucosomes are usually lower than 50 ppm. Higher contents of up to 100 ppm reflect the abundance of entrained clinopyroxene and amphibole.

REE-patterns of leucosomes are very variable. La_N ranges between 10-100 and Yb_N may be as low as 0.24, resulting in variable $(La/Yb)_N$ ratios of 5-177. Most leucosomes exhibit a strong positive Eu-anomaly (Fig. 16) demonstrating the influence of plagioclase on the REE-budget of leucosomes. Leucosomes enriched in REE or with rather flat REE-pattern lack an Eu-anomaly and only the most REE-enriched leucosomes show a slight negative Eu-anomaly. Some

leucosomes within granulites have high contents of HREE indicative of the presence of garnet as a peritectic or entrained phase.

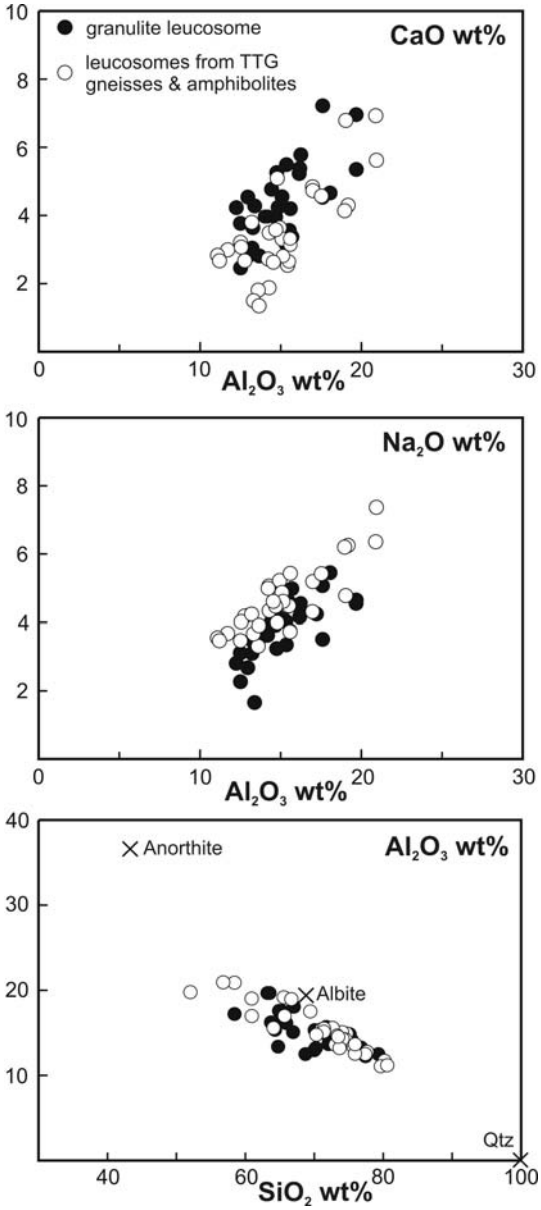

Fig. 14:

Trends of Na_2O and CaO vs. Al_2O_3 and Al_2O_3 vs. SiO_2 for granulite and migmatite leucosomes. The linear trends reflect the importance of plagioclase on leucosome major element composition.

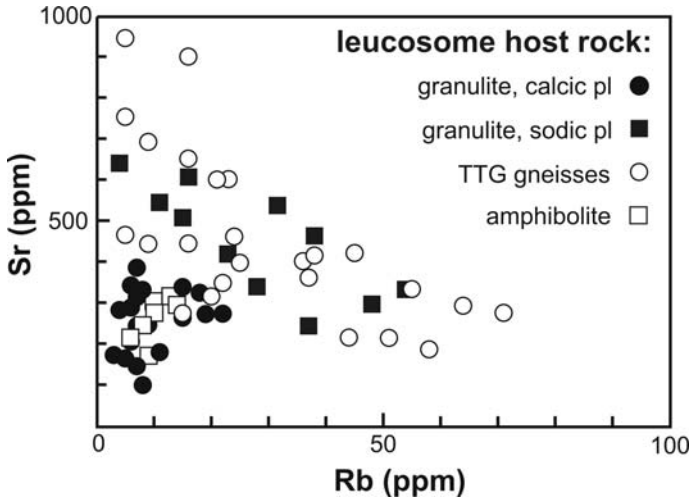

Fig. 15:

Sr vs. Rb contents in leucosomes. Sr contents are usually high in migmatite leucosomes. Low Sr contents among migmatite leucosomes are related to CaO-rich amphibolitic source rocks with low Sr contents. Among granulite leucosomes high Sr contents occur in Na_2O- and Sr-rich intermediate granulites with sodic plagioclase.

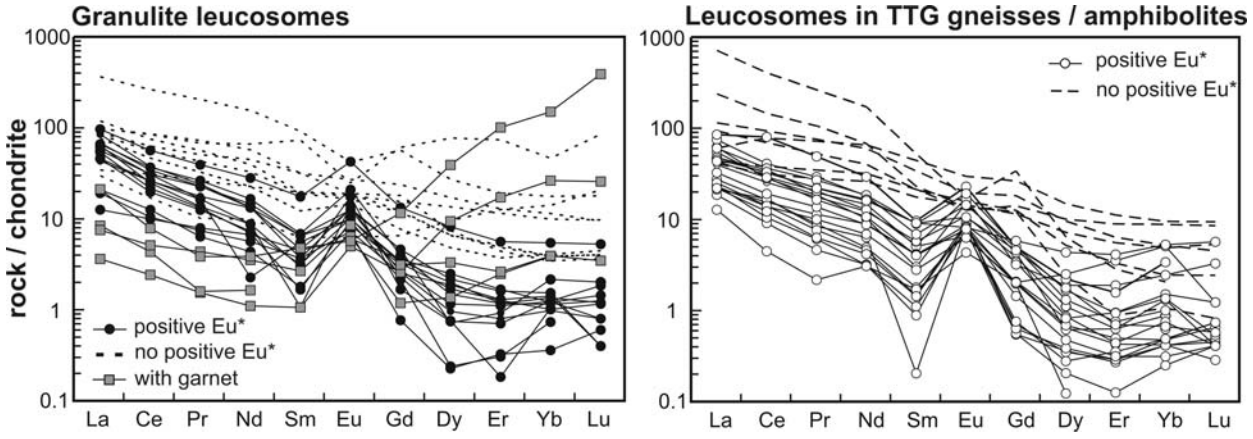

Fig. 16:

Chondrite-normalized REE-pattern for granulite and migmatite leucosomes. Most leucosomes display strong positive Eu-anomalies (Eu*) and have very low HREE contents. Pay attention to small negative Eu-anomalies in the leucosomes richest in REE. High HREE in some granulite leucosomes are related to peritectic garnet.

8. Granulite and migmatite petrogenesis

8.1 Fluid regime during partial melting of granulites and amphibolite-banded migmatites

The major change in fluid composition between upper-amphibolite facies gneisses and granulites closely resembles amphibolite-to-granulite transitions described from other occurences (Touret & Olsen, 1985, Andersen et al., 1997). The overall abundance of carbonic inclusions within granulites from the working area indicates that anhydrous conditions were reached during peak metamorphism. On the contrary, the lack of carbonic inclusions but presence of aqueous inclusion in TTG gneisses and amphibolites point to hydrous conditions during peak metamorphism and migmatisation.

Igneous enderbites occur throughout the working area and contain abundant CO_2-inclusions as well (Poutiainen, 1992). They could be considered as likely sources for the carbonic fluids in granulites. However, CO_2-rich fluids possess a high wetting angle inhibiting large scale fluxes of CO_2 through rocks (Watson & Brenan, 1987). This implies that the CO_2 must have been a constituent of the internal fluid of the granulites at peak metamorphism and was not introduced from the outside. A viable mechanism for fixation of CO_2 in granulites can be release of CO_2 from saline aqueous solutions (brines) upon cooling, entrapment of the CO_2 *in-situ* and escape of the remaining aqueous solution due to a contrasting wetting behaviour (Gibert et al., 1998, Johnson, 1991).

We consider the absence of CO_2-inclusions and the high abundance of aqueous inclusions in TTG gneisses and amphibolites as the main indicators that partial melting and migmatisation within in these rock types took place in the presence of a hydrous fluid under upper-amphibolite facies condition. The gneisses and amphibolites exhibit no indication of dehydration melting reactions but abundant leucosomes suggest intense partial melting. This implies that a H_2O-rich fluid aided melt formation in rocks that could otherwise not have melted at the metamorphic conditions under consideration. According to freezing point depressions, aqueous inclusions contain less than 20 eq. wt% NaCl (Bodnar, 1993). The mole fraction of NaCl in the fluid will therefore be lower than $\boldsymbol{X}_{NaCl} = 0.1$ resulting in $\boldsymbol{a}_{H_2O} = 0.8$ at 10 kbar, which is sufficient for fluid-induced melt formation in the granitic system at temperatures close to 700°C (Aranovich & Newton, 1996).

Alteration of pyroxenes and amphibole is common in all rock types. In granulite areas alteration is restricted to fault zones where late aqueous fluids were able to migrate.

Clinopyroxene forms part of the metamorphic assemblage of the amphibolite lenses in the migmatites but it is extensively altered to secondary amphibole. This indicates pervasive hydration of the migmatite area after peak metamorphism probably triggered by crystallization of hydrous melts. Additionally, dilution of high-salinity aqueous inclusions and formation of new fluid inclusions during retrograde metamorphism at ~1.9 Ga is a likely process.

8.2 Melt formation in granulites

The common depletion of incompatible elements in large Archean granulite terranes (Pride & Mücke, 1980, Vielzeuf et al., 1990, Guernina & Sawyer, 2003) suggests that granulites are residues of melt extraction. The amount of melt extracted from granulite terranes strongly depends on the amount of hydrous phases present at the onset of melting and the melt forming reaction which is mainly controlled by P-T-conditions. Dehydration melting reactions of amphibole have been studied in a variety of petrological experiments thus that the P-T-dependance of melt-forming reactions in mafic and intermediate source rocks are well known. This allows to model observed mineral modes and compositions of granulites from the working area as residues from partial melting of amphibole-bearing source rocks.

8.2.1 Mafic granulites

The modal amount of amphibole in mafic granulites is small (< 10 %). The dry character of the rocks can be accounted for by two scenarios.

i) The igneous precursor of the mafic granulites intruded into the lower to middle crust and never experienced hydration so that the rock was dry at the onset of metamorphism. In this case the mineralogical assemblage of mafic granulites represents re-crystallized igneous minerals and the trace element composition of mafic granulites is a feature inherited from a source rock with a composition comparable to N-MORB pattern. However, porphyroblastic growth and uneven distribution of garnet suggest a formation during metamorphism.

ii) If the rocks were moderately hydrous at the onset of metamorphism (amphibolites) the observed mineral textures indicate that almost all amphibole was exhausted in the formation of clinopyroxene, garnet and melt. In this case, the trace element characteristics of mafic granulites can be modelled as residues of melting of a mafic precursor.

We favour the second option for the petrogenesis of mafic granulites from the Iisalmi-

Sukeva area. The dry solidus of mafic rocks is located between 800-900°C at 5-10 kbar (Beard & Lofgren, 1991, Rushmer, 1991, Sisson et al., 2005). Temperatures in excess of 800°C and pressures of 9-11 kbar were determined for the granulites from the working area and enabled partial melting of mafic rocks in agreement with following general dehydration melting reaction at pressures above 10 kbar (Wolf & Wyllie, 1994; Hartel & Pattison, 1996):

$$\mathit{hbl} + \mathit{pl} + \mathit{qtz} = \mathit{cpx} + \mathit{grt} + \mathit{melt} \quad (1)$$

Hartel & Pattison (1996) predict that garnet is produced in larger amounts than clinopyroxene and that titanite will be an additional crystallizing phase. Titanite is rarely observed and clinopyroxene is always more abundant than garnet in the mafic granulites from the Iisalmi area as deduced from the field appearance, point counting and calculation of modal abundances. This may be attributed to extensive clinopyroxene-formation in this CaO-rich environment according to reaction (2) (Rushmer, 1991) on the prograde path before the rocks entered the stability field of garnet.

$$\mathit{hbl} + \mathit{pl}^1 + \mathit{qtz} = \mathit{cpx} + \mathit{pl}^2 + \mathit{melt} \pm \mathit{ilm} \quad (2)$$

Thus, melt formation may have changed from a garnet-absent reaction to a garnet-present reaction during metamorphism. Alternatively, some of the high amount of clinopyroxene was inherited from the igneous precursor or formed by subsolidus reactions.

Patches and veins of leucosomes as well as low Rb, Ba and K contents within mafic granulites are indicative of the loss of a melt fraction. They are depleted in LREE and have fractionate Th/U ratios which may be an additional feature produced during partial melting. Similar processes have been described by Garrido et al. (2006) for the formation of garnet granulites from the Kohistan Arc Complex by dehydration melting of amphibole-bearing arc plutonics.

Amphibolite lenses and layers abundantly present in TTG gneisses resemble mafic granulites in terms of major elements and compatible trace elements. They have flat REE pattern at roughly 10 times the chondritic value and are enriched in incompatible elements compared to the mafic granulites and thus may be likely source rocks for mafic granulites. We applied a batch melting model using observed modal compositions of mafic granulites as likely residues from

melting of an average amphibolite composition. Partition coefficients derived under conditions appropriate for crustal melting are rare. Klein et al. (2000) report D_{cpx} and D_{grt} in equilibrium with tonalitic liquids at 15 kbar and 1050°C and 900°C, respectively which are consistent with the results from Barth et al. (2002). Amphibole partition coefficients were taken from Klein et al. (1997) since they were obtained in equilibrium with a tonalitic liquid at 900°C and 10 kbar. However, more recent research (Tiepolo et al., 2000) showed that amphibole fractionates Nb from Ta with $^{Amph}D_{Nb} > {}^{Amph}D_{Ta}$. We therefore used $^{Amph}D_{Nb}$ 0.44 and $^{Amph}D_{Ta}$ 0.26 which are suitable for the observed amphibole compositions (Ti_{Tot} 0.2 apfu, Mg# 60). Plagioclase partition coefficients for X_{An} 50 were calculated using the equations given in Bédard (2006).

About 10 % partial melting of an average amphibolite lens leaving 10 % garnet, 35 % plagioclase, 45 % clinopyroxene and 10 % amphibole in the residue is sufficient to explain the trace element pattern of most mafic granulites. Some strongly fractionated mafic granulites require up to 30 % partial melting, higher amounts of residual garnet (30 %) and low amounts of residual plagioclase (20 %) (Fig. 17a). Incidentally, these strongly fractionated granulites report pressures of > 11 kbar which points to an increased incorporation of plagioclase in the melt as observed for instance by Sen & Dunn (1994).

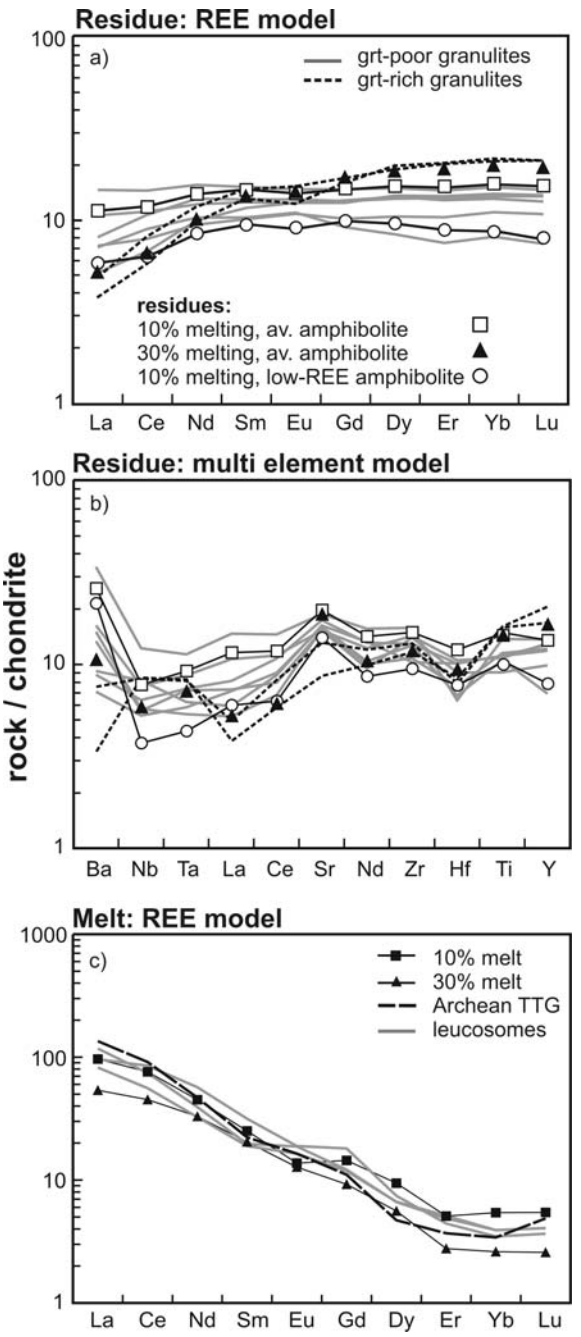

Fig. 17:
Mafic granulites are modelled as residues from partial melting of amphibolites from the working area. Residue mineralogies are constrained for slightly and strongly fractionated mafic granulites and modal abundances were taken from point counting. Model melts are strongly fractionated and resemble typical Archean TTG crust.

Low Ba contents in model residues similar to contents in mafic granulites are only obtained if Ba in the source rock is less than 150 ppm. This requires omission of two biotite rich amphibolite lenses with Ba contents of 454 ppm and 894 ppm from the calculation of an average amphibolite composition. Ba contents <20 ppm as observed in mafic granulites with strongly fractionated REE-pattern are not reproduced by our model (Fig. 17b). They require less Ba in the source as well as total consumption of amphibole and lower modal plagioclase in the residue. Likewise low Sr contents in strongly fractionated mafic granulites are only reproduced by lower source rock Sr contents (~100 ppm) and lower modal plagioclase in the residue (10 %) than applied in the model. A small positive Sr anomaly is observed in slightly fractionated mafic granulites while it is absent from amphibolite lenses and layers considered as precursor-pattern. This anomaly in the granulites is caused by the storage of Sr in residual plagioclase. The lack of a positive Sr-anomaly in strongly fractionated granulites additionally points to an increased incorporation of plagioclase in the melt phase at higher pressures.

Adjustment of Nb and Ta values requires a phase with high D_{Nb} and D_{Ta}. Ilmenite is a common accessory phase in granulites and LA-ICP-MS analyses of ilmenites showed high concentrations of Nb, Ta. Sc and V. Including ilmenite in the melting model yields Nb and Ta contents in good agreement with the mafic granulites. Additionally, ilmenite will retain Ti during melting.

Although trace element modeling works fine, mass balance considerations showed that the actual source rocks of mafic granulites must have been richer in CaO, Al_2O_3, SiO_2 and lower in MgO than the amphibolite lenses from the Iisalmi area. If a supposed loss of 10-20 % tonalitic melt has taken place, the original source rocks of mafic granulites would resemble low Mg-tholeiites.

The high amount of restitic garnet in the mafic granulites will lead to a strong HREE depletion in the corresponding melts. This implies that dehydration melting of amphibolitic source rocks under lower crustal condition leaving garnet-bearing mafic granulites produces strongly fractionated tonalitic melts similar to typical Archean TTGs (Fig. 17c). However, Sr and Eu contents in the melt are strongly controlled by the amount and composition of residual plagioclase. High Sr contents (>250 ppm) as typical for Archean TTG (Martin, 1997, Martin et al. 2005) and the lack of negative Sr- and Eu-anomalies in melts can only arise if plagioclase abundance progressively decreases at pressures above 10 kbar.

8.2.2 Intermediate granulites

The presence of stromatic leucosomes, abundant CO_2-inclusions and low contents of incompatible elements are a sign that also intermediate granulites from the Jonsa and Varpanen experienced dehydration melting. Compared to mafic granulites, in which prograde amphibole is rare, intermediate granulites provide abundant evidence for dehydration melting of amphibole such as overgrowth of pyroxenes on amphibole. Prograde clinopyroxene and orthopyroxene were produced by a reaction similar to reaction (3) found by Patiño Douce & Beard (1995).

$$\mathbf{0.82\ hbl + 0.18\ qtz = 0.08\ pl + 0.45\ cpx + 0.22\ opx + 0.22\ melt + 0.02\ il} \quad \mathbf{(3)}$$

This reaction is consistent with pressures <10 kbar and higher SiO_2-activities in intermediate granulites that facilitate the stability of orthopyroxene. Especially the ratio of cpx / opx observed Patiño Douce & Beard (1995) is very similar to the ratio of these minerals in the intermediate granulites (Table 1). Metamorphism and melting of a layered suite of rocks such as the granulites from the Jonsa and Varpanen area will produce inhomogeneous residues with residue mineralogy depending on source rock composition on the one hand and degree of amphibole-breakdown on the other hand. Accordingly, intermediate granulites exhibit significant variations in the modal mineralogy with plagioclase constituting 30-50 %, amphibole 10-40 % and clinopyroxene 10-30 % of the modal abundance. The high proportion of plagioclase in intermediate granulites indicates that it was stable during partial melting and most likely also formed as a peritectic product as predicted from reaction (3). The garnet-producing reaction (1) is restricted to Fe-rich layers in intermediate granulites but within these layers garnet can make up more than 20 %.

By assuming that all clinopyroxene in the intermediate granulites was produced by the breakdown of amphibole in the presence of quartz (reaction 3) it is possible to calculate the amount of melt that formed due to reaction (3). The melt proportion was small ranging between 5-10 % for most of the samples (Table 1). Since amphibole is still present in most intermediate granulites the rocks are fertile with respect to melt formation. The availability of quartz is considered as the controlling factor of reaction progress. Thus, the reaction stopped as quartz became exhausted.

Table 1

Modal abundances of cpx-opx-granulites and melt fractions calculated according to reaction (3).

sample	method	amph	cpx	opx	pl	kfs	qtz	mgt	ilm	bt	total	melt
012-04 M1	LSR	26	17	9	39			1	1	7	100	6.5
012-04 M2	LSR	22	17	9	41			2	1	7	100	6.5
012-04 M3	LSR	5	27	9	41		3	5	2	7	99	10.0
060-03 b	LSR	29	8	8	39	5	9	2			100	3.0
069-03 M1	LSR	29	25	12	28			2	1	2	99	9.4
076-04 a	LSR	15	27	13	45						100	10.1
080-03 M	LSR	3	24	12	49	2	2		1	7	100	9.0
112-04 M	LSR	25	20	10	43		3				100	7.4
137-04 M	LSR	53	12	3	26		4	2			100	4.5
048-04 b	PC	43	16	7	27			7			100	6.2
102-04a	PC	30	4	3	59		3	1			100	1.7
114-04M	PC	18	12	8	61			2			99	4.4
109-04 b	PC	20	7	4	66			3			100	2.6

LSR – least square regression, PC – point counting, all data in [%]

The low degree of melting in intermediate granulites did not change REE contents significantely so that the observed REE contents will closely approach source composition. Subparallel REE patterns of intermediate granulites additionally indicating that HREE-retaining garnet did not play a significant role in fractionation during partial melting except for some HREE-enriched layers. The consumption of amphibole during partial melting mainly liberates Large Ion Lithophile Elements as well as Nb and Ta. However, the concentration of Nb and Ta in the residue is buffered by the formation of ilmenite. Accessory biotite and unconsumed amphibole buffer Ba contents while the behaviour of Sr is controlled by the presence of plagioclase. Sr contents are generally high in intermediate granulites but positive Sr-anomalies on multi-element-plots are rare. Samples lacking Sr-anomalies or having small negative Sr-anomalies occur more frequently. Variable concentrations of Sr must be inherited from the precursor since Sr remains in the residue due to the large modal abundance and stability of plagioclase.

Melts derived from intermediate granulites mainly inherit the fractionation pattern of their sources but will be more LREE-rich. The HREE will not be fractionated due to the absence of garnet. The shape of the MREE is influenced by the amount of amphibole in the residue. Negative Eu- and Sr-anomalies may be characteristic for melts derived from intermediate

granulites because of high amounts of restitic plagioclase. Altogether, this implies that trace element pattern of partial melts of intermediate granulites formed at pressures below 10 kbar do not resemble typical Archean TTG although - concerning major elements - they are tonalitic.

8.3 Melt formation in TTG gneisses

The mesosomes of migmatitic TTG gneisses are hydrous comprising amphibole and biotite as mafic phases. Clinopyroxene can be additionally present. The lack of anhydrous mineral assemblages indicates that leucosomes in TTG gneisses were not formed due to dehydration melting but that melting at low temperatures was fluxed by a hydrous fluid.

Water-saturated experiments on natural granitoid compositions were conducted at 15 kbar by Carroll & Wyllie (1990) and Johnston & Wyllie (1988) and at 20 kbar by Acosta-Vigil et al. (2006). The melting interval of the trondhjemitic composition used by Johnston & Wyllie (1988) lies between 610-745°C. Carroll & Wyllie (1990) detected the solidus for their tonalite below 700°C at water contents of ~5 wt%. Acosta-Vigil et al. (2006) observed an interconnected melt phase already at 690°C and low degrees of melting. According to Johannes (1984) beginning of melting in the granite system qz-kfs-ab-an-H_2O can be observed between 690°C at 2 kbar and 630°C at 17 kbar.

The stability of plagioclase is greatly lowered in the presence of water. Therefore melting in hydrous quartzofeldspatic compositions starts at temperatures considerably lower than required for dehydration melting and the melt productivity is greatly enhanced in the H_2O-present environment (Beard & Lofgren, 1991).

Plagioclase composition of mesosome and leucosome from TTG gneisses ranges between X_{An} 20-27. Leucosome plagioclase composition is slightly more sodic in some outcrops and virtually the same as mesosome plagioclase composition in other outcrops. Equal plagioclase compositions in leucosomes and mesosomes have often been described from migmatites (Gupta & Johannes, 1982, Whitney & Irving, 1994). This contradicts with plagioclase-melt-equilibria which predict a strong contrast between X_{An} in the residual plagioclase and X_{An} in the melt phase. However, percolation of melt along grain boundaries can lead to equilibration of mesosome and leucosome plagioclase with the same melt phase (Marchildon & Brown, 2001) and similar plagioclase compositions are consequence of that process.

The transition from stromatic migmatites to strongly disaggregated schlieren migmatites

observed in some outcrops of TTG gneisses (Fig. 3c-d), resembles metatexite to diatexite transitions described by White et al. (2005). The amount of melt required to produce diatexites is estimated in the order of 20-40 vol% (Greenfield et al., 1996, Sawyer, 1998). Since most migmatitic gneisses preserve pre-migmatitic structures and classify as metatexites the amount of melt in the system most likely was less than 25 vol%. Redistribution of melt could explain the enrichment of melt and formation of diatexites in some migmatite outcrops. Still, major elements and trace elements of individual leucosome samples reflect the composition of the respective host (Fig. 13 and 15) suggesting that melt loss, melt injection and melt mixing did not play an important role in migmatite petrogenesis.

The origin of the hydrous fluid that induced partial melting of the TTG gneisses at low temperatures is hard to decipher. Small amounts of water present in the TTG gneisses prior to metamorphism will allow low degrees of melting at the wet solidus. White et al. (2005) considered fluid release by subsolidus dehydration reactions in metapelites and metapsammites as a source for fluid enhanced melt production in adjacent gneisses. Metasediments occur in the Jonsa area but are absent from the rest of the working area and are therefore no likely sources for hydrous fluids. Nevertheless, exposed granulites continue to deeper levels as suggested by geophysical data (Korsman et al., 1999). Crystallization of melts derived from dehydration melting of deeper levels of mafic rocks could have released the water required for melting of the TTG gneisses at conditions close to the wet solidus. Still, the migmatization of the gneisses is widespread and pervasive which requires an important flux of aqueous fluid.

Larger intrusive bodies that could represent melts segregated from the migmatitic gneisses are lacking at the present outcrop scale. Small leucodiorite intrusions (Naimakangas leucodiorites) in the very NW of the working area would be likely candidates supported by conventional U-Pb age data on zircons that give 2706±3 Ma (Paavola, 2003). However, neodymium isotopes yield T_{DM} model ages of 2800 Ma (H. Huhma, personal communication), thus showing very limited contribution of older crustal material to the sources of the Naimakangas leucodiorites.

8.4 Origin of leucosomes in granulites, TTG gneisses and amphibolites

The origin of leucosomes has long been debated. It is obvious that they are related to the anatexis of their host rocks but still they may represent minimum melts, equilibrium melts, disequilibrium melts, fractionated melts or cumulates. Comparison of leucosome major element composition with melt compositions generated by Johannes (1989) in the tonalitic system Qtz-(Ab+Or)-An reveals that leucosomes from the working area are poorer in quartz than tonalitic melts at 2 kbar (Fig. 18). Lower quartz contents than in the 2 kbar experiments can be produced by higher pressures that allow plagioclase to enter the melt in a larger proportion than quartz. Migmatite leucosome compositions overlap with melt compositions derived in melting experiments on tonalitic compositions under variable H_2O-activities, temperatures and pressures. All of these experiments yield compositions displaced towards the (Ab+Or)-An join of the triangle (Fig. 18). Furthermore, the removed composition of most granulite leucosomes towards the An-Qtz join clearly shows the influence of the more calcic source rocks.

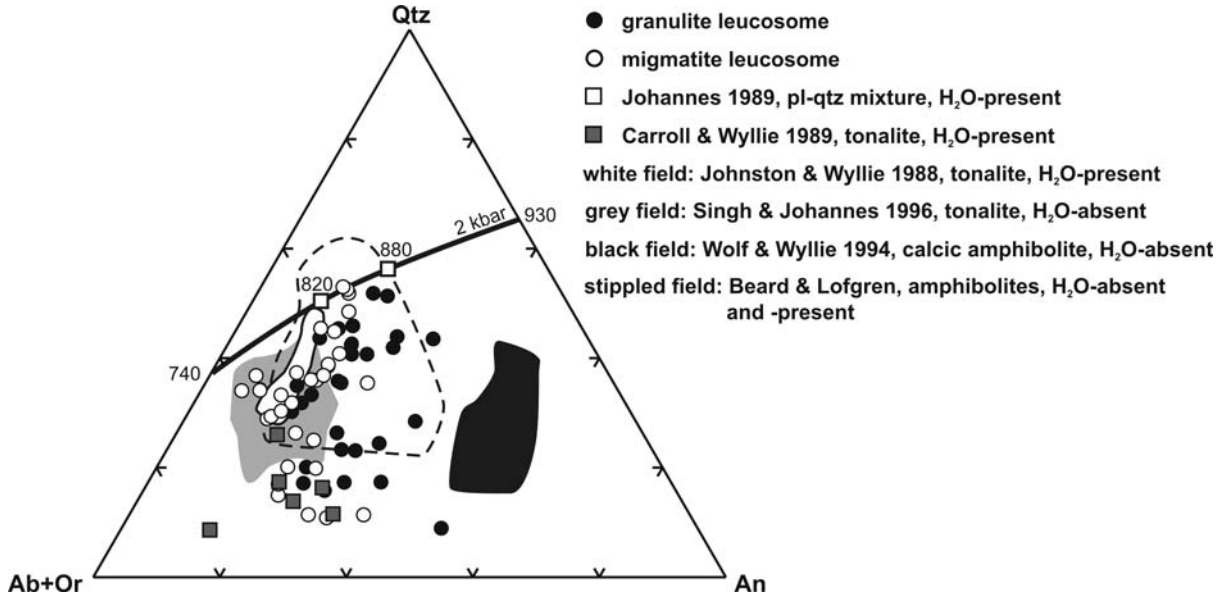

Fig. 18:

Normative An-Qtz-Ab+Or triangular modified after Johannes (1989). Lower qtz contents in leucosomes are consistent with pressures higher than 2 kbar.

Trace element patterns of most leucosomes from granulites and amphibolite-banded migmatites exhibit low total REE-abundances and positive Eu- and Sr-anomalies. The considerable positive Eu- and Sr-peaks on chondrite normalized plots of leucosomes reflect the

strong influence of plagioclase on leucosome composition due to high partition coefficients of plagioclase for Sr and Eu (Blundy & Wood, 1991, Wilke & Behrens, 1999, Bédard, 2006).

Positive Eu- and Sr-anomalies in leucosomes may indicate that plagioclase fractionation was important in their petrogenesis. This implies that leucosomes represent melt migration pathways consisting of plagioclase and quartz crystallized early from a percolating and finally extracted melt phase (Marchildon & Brown, 2001, Solar & Brown, 2001, Sawyer 2001). The assumption involves melt connectivity at small melt fractions as suggested by Brown (1994). The interpretation of leucosomes as plagioclase-quartz-assemblage crystallized from a melt phase is supported by the coarse grain-size and the euhedral shape of plagioclase grains (Brown, 2001). Furthermore, leucosomes are richer in CaO (Fig. 19) but poorer in K_2O at high SiO_2-contents than the vast majority of Archean TTG, pointing to the pronounced input of fractionated plagioclase on leucosome composition. The anhydrous nature and the presence of peritectic phases (grt, cpx, opx) in some granulite leucosomes additionally implies that leucosomes cannot be regarded as segregated melts since crystallization of the hydrous melts will lead to considerable retrogression of the peritectic phases in leucosomes and adjacent mesosomes (White & Powell, 2002).

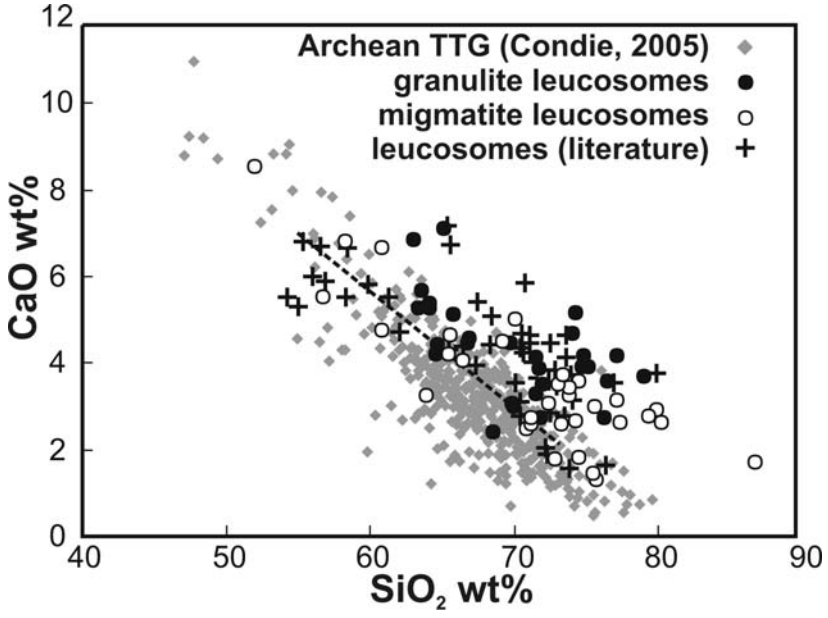

Fig. 19:

Comparison of leucosomes with Archean TTG. The enrichment of CaO in leucosomes compared to Archean TTG points to an increased proportion of CaO-rich fractionated plagioclase. Leucosome data are for leucosomes in mafic rocks (amphibolite, granulite) and are taken from Sawyer (1991), Hansen & Stuk (1993), Williams et al. (1995) and Hölttä (unpublished data). The stippled line indicates the trend in TTG gneisses from the working area.

Several parameters can influence leucosome composition if the fractional crystallization model applies.

1) Composition of the parent melt.
2) Composition of the fractionated plagioclase and changing partition coefficients with changing X_{An}.
3) Degree of fractional crystallization.
5) Amount of fractionating plagioclase and other potential minerals such as quartz or K-feldspar.
6) Entrapment of evolved liquids and entrainment of host rock minerals.
7) Fractionation from already fractionated liquids.

In order to apply a fractional crystallization model we determined the modal abundance of plagioclase in migmatite and granulite leucosomes by least square regressions using appropriate plagioclase compositions. Plagioclase abundances were found to range between 40 – 60 % and a mean value of 50 % was used in modelling. X_{An} in the leucosomes ranges between 20 and 40. We used partition coefficients (Di) in the calculations appropriate for X_{An} 30 after Bédard (2006).

The most arguable variable in the fractional crystallization model for leucosomes is the composition of the parent melt. Two out of 32 migmatite leucosomes analyzed have smooth REE pattern and a major and trace element composition closely resembling the Naimaskangas leucodiorites as well as mesosomes from the TTG gneisses (Table 2). Therefore the two leucosomes as well as an average Naimaskangas leucodiorite and two groups of migmatite mesosomes were used as potential parent melts. Migmatite leucosomes with the lowest REE contents probably represent the most pristine cumulates and degree of fractional crystallization to produce such leucosomes was ~ 10 % (Fig. 20). HREE in leucosomes are slightly higher than could be explained by fractional crystallization of plagioclase alone. Zircon has high D_{HREE} and its crystallization as an accessory phase raises the HREE contents of leucosomes. Alternatively the entrainment of zircon from the host rock produces the same effect.

More complicated processes than simple plagioclase fractionation might have influenced the REE-pattern of most of the other migmatite leucosomes. Their higher REE contents and less pronounced positive Eu-anomalies suggest that they formed by fractionation from an already fractionated liquid or that they contain trapped fractionated melts as suggested by Sawyer (1987). Both processes may equally operate. The amount of evolved melt trapped in the leucosomes is less than 10%.

Table 2

REE contents of possible parent melts serving for crystallization of pl-qtz-leucosomes

parent melt	La	Ce	Nd	Sm	Eu	Gd	Dy	Er	Yb	Lu
				granulites						
melt from 10% melting of amphibolite	*22.87*	*46.53*	*20.60*	*3.71*	*0.77*	*2.87*	*2.32*	*0.81*	*0.87*	*0.13*
granulite leucosome 036-04 L2	22.78	52.21	26.00	4.67	1.06	3.60	1.83	0.71	0.56	0.09
				migmatites						
average orthogneiss, low HREE	*29.81*	*49.87*	*18.66*	*2.79*	*0.71*	*2.30*	*1.05*	*0.41*	*0.35*	*0.03*
average orthogneiss, high HREE	20.00	45.74	25.96	4.95	1.22	3.79	2.86	1.44	1.32	0.19
average Naimaskangas leucodiorite	29.49	63.13	31.99	5.78	1.36	3.96	2.79	1.27	1.13	0.15
migmatite leucosome 128-04 L	26.94	56.80	27.02	4.98	1.09	3.58	2.34	1.01	0.83	0.11
migmatite leucosome 027-03 L	21.98	42.36	18.18	3.10	0.88	2.47	1.27	0.52	0.39	0.06

melts printed in italics were used for the calculations in Fig. 20, data in [ppm]

Leucosome 036-04L2 was used as the parent melt for modelling of the granulite leucosomes because of its good agreement with the 10 % model melt from the partial melting model (Fig. 17c). Additionally, few natural granulite leucosomes preserve equilibrium composition with smoothly but strongly fractionated REE-pattern. Again the whole spread of granulite leucosome composition can only be explained by fractionation from evolved liquids or by entrainment of residual melts and if accessory zircon accounts for the typical trough-shaped pattern of the HREE.

Sr contents of leucosomes are sensitive to the fractional crystallization model since Sr will be effectively removed from the liquid as fractionation progresses. The Sr contents of the respective parent melt for each leucosome is source rock dependant as suggested from Fig. 15 and will strongly influence the Sr-content in the cumulate. Sr contents are usually below 400 ppm in granulite leucosomes. About 30-50 % fractional crystallization are required to account for the observed Sr contents in leucosomes using an initial Sr-content of 300 ppm in the parent melt and $D_{Sr}^{pl} = 6.5$ for X_{An} 30.

Concentrations of other trace elements are strongly dependant on additionally crystallizing phases such as K-feldspar for Ba or biotite for Rb. Small amounts of entrained biotite or amphibole can also explain the contents of Nb, Ta, Sc and V.

The formation of leucosomes by crystallization of plagioclase and quartz from a melt phase involves generation of fractionated liquids. Sawyer (1987) discovered leucosomes in metasediments that represent cumulates and their fractionated melts, respectively. Johannes et al.

(2003) showed that leucosomes in metasediments from southern Finland and small granite sheets intruding the metasedimentary sequence are related as cumulates and evolved liquids.

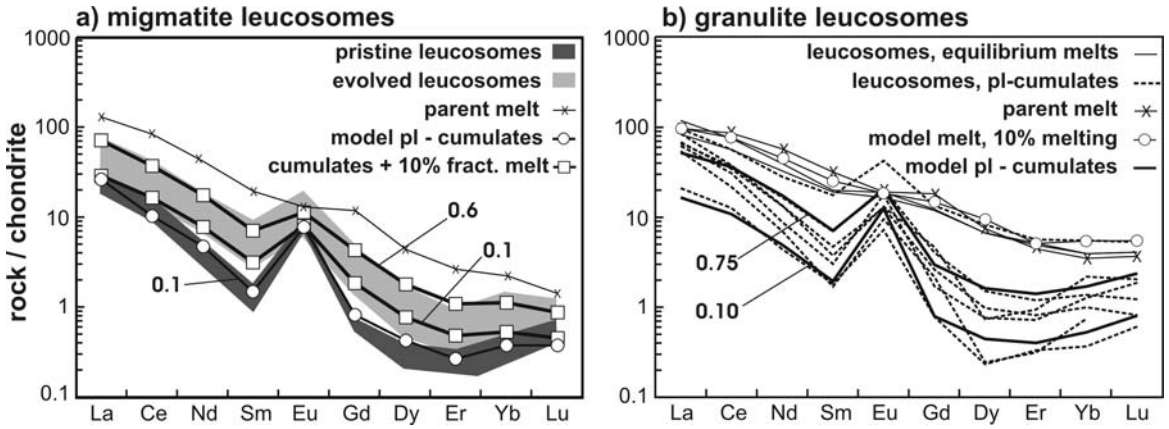

Fig. 20:

Models for leucosome formation by fractional crystallization of equilibrium melts. The bold numbers in the diagrams refer to the degree of fractionation. As parent melt for migmatite leucosomes served the composition of the average migmatitic TTG gneiss with low HREE contents. Leucosome 036-04 L2 was used as the parent melt for granulite leucosomes because of its near equilibrium composition (see 10 % model melt in Fig. 17c). Migmatite leucosomes with low REE contents are consistent with about 10 % fractionation of the parent melt forming cumulates comprising 50 % pl and 50 % qtz. Higher REE contents in migmatite leucosomes require the entrapment of some fractionated liquid or crystallization from already fractionated liquids. Granulite leucosome compositions respond to up to 10-75 % fractional crystallization of the parental liquid.

Residual liquids will have negative Eu- and Sr anomalies. Very few leucosomes with these features have been found in the working area. The lack of residual liquids could be due to incomplete sampling but may also indicate efficient melt loss from the system.

While the crystallization part of leucosome petrogenesis seems to be mainly preserved in the REE patterns, Ca / Na ratios as well as Sr-contents in leucosomes allow conclusions about the source rock composition. Mafic source rocks (amphibolite, granulite) from the working are typically richer in CaO but poorer in Na_2O and Sr than TTG gneisses. These features are imprinted on leucosome compositions from the respective host rocks and thus must also be observable in escaped melts.

9. Conclusions

In this work we present an example of internal differentiation of Archean continental crust by coeval partial melting of middle to lower crustal lithologies. Melt forming reactions in different lithologies strongly depend on the activity of H_2O in the peak-metamorphic fluid. While granulites represent anhydrous residues of dehydration melting of amphibole, low P-T-conditions determinded for migmatitic TTG gneisses and amphibolites require the presence of a hydrous fluid to allow melting at the wet solidus.

About 10-30 % tonalitic melt was produced by melting of an amphibolitic precursor leaving LREE-depleted mafic grt-cpx-granulites as residues. Intermediate cpx-opx-granulites record ~10 % of melting according to the ratio of clinopyroxene / amphibole. TTG gneisses show variable degrees of migmatization. The obliteration of pre-migmatitic structures by disaggregation and the formation of schlieren migmatite indicate that melt production within the gneisses may have been as high as ~25 vol%.

Melting of the TTG gneisses yielded leucosomes that are rich in Na_2O and have an affinity towards trondhjemite while leucosomes within granulites are CaO-rich and classify as tonalites. This indicates that remelting of a Na_2O-rich precursor under conditions that allow plagioclase to take part in the melt forming reaction as in the presence of a hydrous fluid, is a viable mechanism to produce trondhjemitic melts.

Leucosome trace element pattern with strong positive Eu-anomalies reflect the importance of plagioclase in leucosome petrogenesis. These patterns can be reproduced by fractional crystallization of plagioclase, quartz and accessory zircon from a leucocratic melt including the storage of small amounts of fractionated liquid.

Appendix A: Major elements analyses of selected bulk rock samples

sample	loc.	SiO_2	TiO_2	Al_2O_3	FeO	MnO	MgO	CaO	Na_2O	K_2O	total	Mg #
granulites												
002-03 M2	1	48.12	0.81	15.57	10.36	0.31	5.23	15.22	2.14	0.11	97.9	47
029-03 M2	1	49.13	0.66	15.00	9.84	0.26	6.03	15.24	2.18	0.18	98.5	52
034-03 M2	1	49.17	1.15	15.81	11.66	0.32	5.43	12.78	1.80	0.09	98.2	45
036-03 M1	1	48.43	1.32	13.69	14.41	0.25	8.80	11.74	1.23	0.09	100.0	52
140-04 M	1	48.36	0.77	14.94	9.82	0.22	6.54	16.82	1.46	0.05	99.0	54
071-03 M	2	60.89	0.99	13.07	9.57	0.15	2.49	5.16	2.91	1.97	97.2	32
076-04 a	2	52.44	0.45	15.68	8.08	0.16	7.98	11.66	2.46	0.26	99.2	64
076-04 M2	2	54.59	0.98	14.26	11.02	0.17	3.91	7.84	2.76	0.79	96.3	39
076-04 M3	2	51.69	0.83	14.26	11.49	0.17	6.07	9.47	3.08	0.71	97.8	49
080-03 M	2	55.03	0.43	15.00	8.23	0.16	6.17	8.50	3.75	1.25	98.5	57
109-04 a	2	52.41	0.68	14.06	11.86	0.22	5.53	9.26	2.97	0.86	97.9	45
109-04 M1a	2	50.77	0.83	14.36	11.04	0.17	6.97	9.98	2.86	0.72	97.7	53
109-04 M1b	2	55.59	0.75	12.84	9.74	0.18	3.08	6.37	2.18	0.48	91.2	36
112-04 M	2	52.13	0.40	15.90	7.67	0.15	7.62	11.65	3.03	0.30	98.9	64
114-04 M	2	59.99	0.60	17.34	5.46	0.09	3.10	6.77	4.73	1.06	99.1	50
012-03 M1	3	50.26	1.56	16.05	10.61	0.18	5.53	9.56	3.55	0.24	97.5	48
012-04 M1	3	51.59	0.88	15.25	10.03	0.14	7.38	8.97	3.00	1.00	98.2	57
012-04 M2	3	49.16	1.11	15.66	10.83	0.15	7.46	9.73	2.98	1.04	98.1	55
048-03 M1	3	50.76	0.82	14.32	10.74	0.21	6.58	12.53	2.27	0.37	98.6	52
048-04 b	3	49.11	0.74	15.22	9.16	0.21	7.30	13.79	2.54	0.52	98.6	59
048-04 d	3	54.37	0.90	16.41	9.68	0.17	4.58	7.46	3.62	1.15	98.3	46
048-04 g	3	48.47	0.81	14.69	11.80	0.23	7.36	12.56	2.35	0.38	98.7	53
049-03 M	3	49.51	1.50	13.14	15.37	0.23	6.47	8.59	2.99	0.62	98.4	43
049-04 b	3	47.62	0.76	13.77	13.01	0.25	12.67	6.91	2.09	1.01	98.1	64
049-04 d	3	54.64	0.88	14.46	11.34	0.17	5.61	6.28	4.57	0.69	98.6	47
069-03 M2	3	49.09	0.88	14.87	9.98	0.20	6.04	13.14	3.02	0.61	97.8	52
060-03 b	4	56.10	0.46	15.27	8.34	0.17	6.22	6.98	3.93	1.05	98.5	57
063-04 M1	4	49.28	0.92	13.68	12.63	0.22	6.76	10.83	2.85	0.83	98.0	49
063-04 M2	4	49.58	0.90	13.87	12.53	0.22	6.90	10.96	2.56	0.61	98.1	50
066-03 M	4	48.75	0.79	14.04	10.42	0.23	6.94	14.26	2.32	0.31	98.1	54
137-04 M	5	50.14	0.86	14.78	10.90	0.18	7.23	10.18	3.22	1.06	98.6	54
thick amphibolites												
038-03 M1	1	49.94	1.01	14.13	11.87	0.17	7.13	10.09	2.72	0.75	97.8	52
040-03 M	1	46.39	1.03	13.51	13.84	0.28	8.26	12.20	1.81	0.31	97.6	52
120-04 M	1	48.67	0.91	15.13	10.63	0.20	5.68	11.76	2.81	0.59	96.4	49
073-04 M	2	48.59	1.04	13.36	12.33	0.21	6.87	10.97	2.91	0.78	97.1	50
085-03 M1	2	55.03	0.69	15.00	10.47	0.19	6.47	9.82	2.76	0.75	101.2	52
061-03 M	4	45.75	1.11	14.59	13.47	0.21	8.41	10.85	2.59	0.87	97.9	53
061-04 M	4	44.82	1.20	13.27	13.26	0.22	10.15	10.77	2.57	0.90	97.2	58
146-04 b	4	55.85	0.86	19.66	6.11	5.50	0.08	3.27	7.09	5.53	1.0	52
136-05 M1	5	49.95	0.28	15.58	6.68	0.13	9.25	11.01	2.80	0.87	96.6	71
136-05 M2	5	52.17	0.20	20.92	3.84	0.06	6.17	8.89	3.40	0.67	96.3	74
amphibolite lenses / layers												
009-03 M1	1	48.24	1.02	14.90	10.92	0.21	7.19	10.28	2.93	1.48	97.2	54
027-03 M	1	51.16	0.98	14.27	10.25	0.22	5.80	9.31	2.17	1.88	96.0	50
030-03 M1	1	49.49	0.84	14.23	11.86	0.24	7.02	8.04	1.90	3.38	97.0	51
100-03 M	1	48.57	0.97	14.23	11.46	0.19	7.84	10.15	2.73	1.02	97.2	55
128-04 M	1	50.10	0.65	10.96	10.52	0.19	9.33	12.53	2.71	0.60	97.6	61
134-04 M	1	46.37	1.35	14.39	12.80	0.21	7.49	11.05	2.07	1.52	97.3	51
094-03 M1	5	49.25	1.09	14.07	11.56	0.19	6.99	10.47	2.32	0.99	96.9	52
TTG gneisses												
009-04	1	68.40	0.41	16.37	2.34	0.03	1.12	3.61	4.82	1.43	98.3	45
030-04 c	1	60.27	0.96	16.47	6.33	0.10	2.90	5.33	3.91	2.01	99.1	44
031-04 ME	1	68.95	0.33	15.85	2.92	0.05	1.26	3.71	4.90	1.09	99.1	38
138-04 ME	1	71.15	0.33	15.09	2.56	0.04	0.89	3.36	4.55	1.09	97.8	54
143-04 M	1	54.99	0.73	18.27	6.03	0.11	4.04	7.42	4.61	1.61	98.0	37
144-04 ME	1	59.25	1.12	17.16	6.57	0.09	2.17	6.04	5.23	0.33	97.3	53
083-04	2	60.53	0.62	15.73	5.73	0.10	3.67	5.09	3.24	2.63	97.7	51
113-03 M1	2	57.59	0.77	18.05	5.66	0.08	3.28	6.56	4.90	0.84	99.4	40
134-04 ME	2	72.48	0.30	14.91	1.76	0.02	0.65	3.12	4.82	1.31	99.1	46
118-03	5	69.23	0.33	15.42	3.13	0.05	1.52	4.00	4.04	1.38	99.2	51
131-04	5	70.41	0.37	15.11	2.41	0.03	1.41	1.86	4.90	2.69	98.8	52
132-04	5	68.70	0.36	15.51	2.60	0.04	1.56	3.28	3.93	2.79	99.5	48
133-04	5	71.50	0.28	15.50	1.84	0.03	0.96	2.23	5.66	1.53	98.3	45

localities (loc.): 1 – Iisalmi-Sukeva, 2 – Jonsa, 3 – Varpanen, 4 – Pallikäs, 5 - others

Appendix A continued

sample	loc.	SiO_2	TiO_2	Al_2O_3	FeO	MnO	MgO	CaO	Na_2O	K_2O	total	Mg #
granulite leucosomes												
002-03 L	1	63.21	0.11	19.67	2.96	0.08	1.56	6.96	4.55	0.34	99.4	49
034-03 L2	1	74.56	0.02	14.75	1.29	0.07	0.38	5.26	3.24	0.15	99.7	35
036-04 L1	1	75.13	0.03	14.84	0.30	0.01	0.07	4.24	4.15	0.42	99.2	30
036-04 L2	1	64.33	1.08	16.18	4.62	0.08	2.10	5.38	4.16	0.72	98.7	45
071-03 L	2	72.05	0.22	13.67	2.75	0.05	0.70	2.81	3.50	2.63	98.4	31
076-04 L2	2	70.00	0.28	12.96	5.72	0.20	1.46	4.54	2.68	0.47	98.3	31
076-04 L3	2	64.75	0.14	13.38	10.85	0.55	2.72	4.28	1.66	0.23	98.6	31
109-04 L	2	58.43	0.19	17.22	3.43	0.07	3.17	10.81	4.24	0.57	98.1	62
114-04 L	2	67.02	0.18	18.06	1.71	0.03	1.00	4.66	5.45	0.99	99.1	51
012-04 L1	3	71.77	0.35	15.59	1.40	0.01	0.88	4.20	3.77	1.31	99.3	53
012-04 L2	3	63.51	0.47	19.68	2.20	0.02	1.64	5.35	4.65	1.58	99.1	57
012-04 L3	3	64.31	0.56	15.35	5.78	0.09	3.37	5.49	3.35	0.79	99.1	51
048-03 L1	3	77.43	0.29	12.25	1.33	0.03	0.64	4.23	2.81	0.44	99.5	46
048-04 a	3	65.26	1.21	17.60	2.74	0.04	1.08	7.22	3.51	0.38	99.0	41
048-04 c	3	75.40	0.08	14.19	1.06	0.03	0.46	3.97	3.63	0.91	99.7	44
048-04 f	3	79.29	0.13	12.50	0.46	0.01	0.26	3.77	3.11	0.41	99.9	50
069-03 L1	3	66.92	0.44	15.08	4.34	0.07	2.66	4.55	4.14	0.92	99.1	52
069-03 L2	3	65.93	0.36	16.14	3.45	0.06	2.09	5.23	4.45	0.94	98.7	52
063-04 L	4	76.78	0.14	13.27	0.97	0.02	0.43	3.64	3.44	0.83	99.5	44
migmatite leucosomes												
006-04 L	1	74.72	0.07	14.27	0.67	0.01	0.36	1.88	5.06	1.83	98.9	49
009-03 L1	1	74.70	0.03	14.93	0.40	0.01	0.15	3.64	5.22	0.32	99.4	40
009-03 L2	1	73.05	0.33	13.60	1.80	0.03	0.91	1.81	3.31	4.02	98.9	48
027-03 L	1	60.94	0.58	16.97	5.11	0.07	2.62	4.84	4.31	1.94	97.4	48
030-04 b	1	66.67	0.23	18.96	1.38	0.02	0.73	4.14	6.20	0.93	99.3	49
030-04 e	1	74.04	0.18	15.08	0.92	0.01	0.50	3.31	4.87	0.64	99.6	49
031-04 L	1	72.67	0.11	15.59	0.70	0.01	0.32	3.14	5.43	0.70	98.7	45
038-05 L	1	79.66	0.12	11.08	0.90	0.02	0.46	2.83	3.55	0.34	99.0	48
100-04 L2	1	71.38	0.24	15.14	1.95	0.03	1.13	2.81	4.61	1.84	99.1	51
128-04 L	1	65.68	0.46	16.99	3.55	0.06	1.63	4.73	5.19	0.71	99.0	45
144-04 L1	1	75.91	0.46	12.55	2.19	0.02	0.70	3.07	4.02	0.34	99.3	37
144-04 L2	1	58.42	0.24	20.89	3.27	0.06	2.23	6.93	6.36	0.45	98.9	55
085-03 L	2	80.58	0.06	11.20	0.39	0.01	0.10	2.67	3.47	0.58	99.1	32
134-04 L1	2	73.47	0.18	14.54	1.34	0.03	0.49	2.63	4.61	1.97	99.3	40
134-04 L2	2	75.92	0.03	13.65	0.26	0.01	0.03	1.35	3.91	4.29	99.5	17
061-03 L	4	60.91	0.35	19.03	3.87	0.07	2.24	6.79	4.78	0.62	98.7	51
061-04 L	4	52.02	0.91	19.78	6.92	0.11	4.44	8.67	4.94	0.73	98.5	54
094-03 L1	5	64.09	0.60	15.58	4.64	0.07	3.93	3.32	3.73	2.22	98.2	60
094-03 L2	5	74.11	0.09	14.29	1.21	0.03	1.05	3.49	4.34	0.56	99.2	61
120-04 L	5	70.29	0.18	14.78	2.20	0.05	1.07	5.09	4.00	0.37	98.0	47

localities (loc.): 1 – Iisalmi-Sukeva, 2 – Jonsa, 3 – Varpanen, 4 – Pallikäs, 5 - others

Appendix B: Trace element bulk rock analyses of selected samples *(n.a. – not analyzed, b.d. – below detection)*

sample	loc.	Sc	V	Cr	Ni	Rb	Sr	Y	Zr	Nb	Ba	La	Ce	Pr	Nd	Sm	Eu	Gd	Dy	Er	Yb	Lu	Hf	Ta	Th	U
granulite																										
002-03 M2	1	45	263	294	176	4	125	18.5	49	1.52	21	1.91	6.55	1.11	5.96	1.91	0.73	2.52	3.21	2.10	2.17	0.33	1.03	0.10	0.01	0.00
029-03 M2	1	42	222	343	168	5	110	15.4	53	1.34	32	1.72	4.84	0.79	4.32	1.49	0.61	2.02	2.57	1.66	1.77	0.26	0.92	0.10	0.22	0.06
034-03 M2	1	53	353	338	173	4	94	26.1	49	1.98	6	1.15	5.01	0.86	5.43	2.20	0.86	3.40	4.68	3.27	3.40	0.52	0.80	0.11	0.01	0.01
036-03 M1	1	60	405	221	112	4	62	28.3	44	2.01	b.d.	0.90	3.54	0.71	4.48	1.96	0.69	3.20	4.90	3.30	3.51	0.52	0.86	0.11	0.03	0.02
140-04 M	1	43	243	397	189	3	115	10.8	48	1.26	17	1.68	5.48	0.88	4.71	1.53	0.61	1.82	2.06	1.20	1.31	0.18	0.69	0.08	0.10	0.10
071-03 M	2	22	197	7	10	34	247	21.7	150	5.80	776	27.5	56.6	6.43	24.6	4.49	1.22	4.15	3.76	2.17	2.00	0.30	1.83	0.31	0.62	0.09
076-04 a	2	37	161	16	49	3	252	8.45	44	1.27	69	4.99	11.7	1.56	6.55	1.53	0.57	1.50	1.60	0.95	0.97	0.16	0.68	0.09	0.05	0.05
076-04 M2	2	32	231	2	12	4	291	21.8	116	4.11	226	16.0	37.9	4.33	18.1	4.41	1.04	3.36	3.94	2.61	2.23	0.61	2.93	0.25	n.a.	0.11
076-04 M3	2	36	235	6	22	5	290	14.3	85	3.09	147	10.0	29.8	3.31	14.4	3.12	0.89	3.13	2.93	1.64	1.46	0.22	2.42	0.18	n.a.	0.11
080-03 M	2	22	115	228	153	26	271	14.3	63	3.55	540	12.0	24.7	3.04	11.9	2.43	0.71	2.30	2.20	1.31	1.47	0.22	0.37	0.19	0.27	0.04
109-04 a	2	40	233	29	21	12	233	16.8	78	3.76	230	23.5	48.5	5.91	23.1	4.69	1.11	3.96	3.58	1.80	1.61	0.26	3.37	0.27	0.49	0.17
109-04 M1a	2	49	279	20	21	7	216	41.2	54	4.03	155	14.0	38.7	4.85	20.6	6.10	1.43	5.33	7.22	4.57	3.82	0.91	1.46	0.18	n.a.	0.07
109-04 M1b	2	29	225	7	7	5	246	19.6	114	4.07	157	11.0	27.8	3.15	13.6	3.18	0.88	2.91	3.28	2.55	2.05	0.46	2.86	0.27	n.a.	0.10
112-04 M	2	35	151	7	50	2	262	8.39	44	1.25	105	5.85	12.5	1.60	6.58	1.44	0.55	1.50	1.65	0.92	0.98	0.14	0.66	0.07	0.07	0.03
114-04 M	2	13	125	18	26	9	482	12.5	91	4.16	194	10.8	25.0	3.56	15.8	3.20	0.93	2.66	2.30	1.29	1.24	0.19	0.78	0.31	0.37	0.24
012-03 M1	3	32	218	37	71	3	464	23.7	54	5.24	184	15.8	35.0	4.70	22.0	4.90	1.87	5.05	4.55	2.47	2.23	0.33	1.12	0.25	0.08	0.03
012-04 M1	3	40	245	307	101	9	164	37.7	70	4.45	191	21.6	47.5	5.76	23.7	6.18	2.19	6.98	7.52	3.83	3.61	0.50	0.90	0.26	0.83	0.12
012-04 M2	3	36	263	296	126	9	136	58.3	118	5.92	82	14.5	39.5	5.93	29.5	8.89	3.04	10.5	11.5	6.05	5.82	0.79	6.74	0.31	1.08	0.57
048-03 M1	3	45	265	348	150	5	129	15.6	39	3.13	47	4.81	11.5	1.56	7.28	2.02	0.65	2.53	2.79	1.71	1.56	0.25	0.78	0.22	0.04	0.01
048-04 b	3	40	225	384	166	6	107	16.9	64	2.23	56	6.83	13.6	1.69	7.76	2.14	0.72	2.58	3.03	1.88	1.98	0.30	1.23	0.17	0.47	0.14
048-04 d	3	26	177	74	58	19	264	20.7	147	6.50	189	23.6	51.4	6.39	26.0	5.00	1.27	4.52	4.01	2.16	2.14	0.31	1.58	0.50	0.55	0.29
048-04 g	3	44	275	386	168	4	128	15.7	49	2.27	45	3.66	10.3	1.41	6.80	1.97	0.72	2.33	2.89	1.75	1.94	0.28	0.90	0.13	0.03	0.02
049-03 M	3	48	370	130	75	4	269	29.8	89	4.28	205	7.16	19.0	2.76	13.5	3.88	1.26	4.86	5.56	3.38	3.20	0.47	1.20	0.29	0.10	0.03
049-04 b	3	62	355	652	265	23	134	22.9	38	3.94	196	1.98	8.40	1.39	7.36	2.44	0.70	2.81	3.74	2.67	2.97	0.44	0.74	0.21	0.01	0.01
049-04 d	3	17	140	50	130	5	302	17.2	142	5.51	504	19.9	50.8	7.22	31.3	6.10	1.54	4.78	3.70	1.85	1.65	0.29	1.15	0.32	0.11	0.32
069-03 M2	3	40	248	266	108	6	302	20.6	79	2.51	102	40.8	79.1	8.71	32.9	5.46	1.44	4.42	3.91	2.25	2.25	0.33	1.63	0.18	5.22	0.40
060-03 b	4	32	124	307	76	13	266	43.2	66	7.17	407	21.7	54.0	7.36	33.1	8.16	1.42	8.24	8.02	4.40	3.85	0.53	0.79	0.33	0.30	0.13
063-04 M1	4	47	305	188	105	10	76	21.9	60	1.87	53	6.76	12.5	1.44	6.45	2.05	0.75	2.76	3.82	2.54	2.84	0.44	0.99	0.12	0.88	0.11
063-04 M2	4	47	294	197	108	8	70	22.1	59	1.76	37	3.71	7.98	1.12	5.82	1.87	0.72	2.76	3.83	2.48	2.68	0.41	0.95	0.12	0.28	0.06
066-03 M	4	48	271	346	114	4	110	20.3	54	1.82	39	2.51	6.80	1.06	5.56	1.85	0.69	2.54	3.29	2.05	2.10	0.31	1.08	0.12	0.12	0.05
137-04 M	5	39	246	232	125	7	136	19.0	60	2.53	121	7.32	15.9	2.02	8.93	2.44	0.85	2.93	3.46	2.11	2.25	0.33	1.13	0.17	0.65	0.18

localities: 1 – Iisalmi-Sukeva, 2 – Jonsa, 3 – Varpanen, 4 – Pallikäs, 5 – others

Appendix B continued *(n.a. – not analyzed, b.d. – below detection)*

sample	loc.	Sc	V	Cr	Ni	Rb	Sr	Y	Zr	Nb	Ba	La	Ce	Pr	Nd	Sm	Eu	Gd	Dy	Er	Yb	Lu	Hf	Ta	Th	U
thick amphibolites																										
038-03 M1	1	3	36	22	17	18	171	24.6	19	3.66	168	8.2	20.7	2.72	11.8	3.25	0.93	3.84	4.37	2.68	2.66	0.39	1.17	0.22	0.54	0.14
040-03 M	1	50	324	267	155	7	123	23.7	54	2.22	31	2.13	6.78	1.2	6.81	2.41	1.04	3.35	4.21	2.68	2.78	0.41	1.22	0.12	0.05	0.02
120-04 M	1	47	291	262	146	7	110	18	61	1.73	117	4	9.01	0.98	6.4	1.68	0.66	2.33	3.59	2.49	2.46	0.53	1.39	0.16	n.a.	0.21
073-04 M	2	42	239	333	141	6	275	16.6	64	3.56	212	7.94	20.5	2.6	11.2	2.62	1.02	2.81	3.19	1.85	1.98	0.29	1.19	0.17	0.17	0.07
085-03 M1	2	39	236	10	32	9	210	14.1	66	2.28	169	9.15	19.8	2.38	9.95	2.18	0.72	2.34	2.52	1.59	1.52	0.23	1.2	0.16	0.11	0.05
061-03 M	4	51	325	344	147	14	182	24.2	80	3.3	66	8.2	25.8	3.9	18.3	4.2	1.2	4.21	4.44	2.66	2.64	0.38	1.53	0.23	0.76	0.88
061-04 M	4	45	286	324	173	24	243	29.7	52	5.41	83	16.3	60.8	9.8	47.9	10.4	2.68	8.35	6.1	3.05	2.84	0.38	1.34	0.28	0.32	0.44
146-04 b	4	15	118	31	17	16	785	25.6	136	6.42	308	22	60.3	8.92	33.9	9.24	2.07	7.42	5.4	2.53	2.3	0.33	1.04	0.52	0.17	0.16
136-05 M1	5	29	103	336	231	15	281	8.95	31	0.47	299	8	15	1.62	7.22	1.46	0.44	1.42	1.86	1.09	1.19	0.05	0.33	0.04	n.a.	0.07
136-05 M2	5	13	39	436	296	21	423	4.25	33	1.69	276	7	11.2	0.99	4.04	0.67	0.31	0.62	0.69	0.39	0.54	n.a.	0.49	0.08	n.a.	0.16
amphibolite lenses / layers																										
009-03 M1	1	43	280	294	118	33	145	21.9	65	2.71	169	4.12	10.9	1.60	8.03	2.44	0.88	3.19	3.91	2.45	2.48	0.37	1.22	0.17	0.33	0.26
027-03 M	1	37	261	308	108	46	203	23.9	68	3.38	454	6.80	16.3	2.26	10.6	2.93	0.90	3.55	4.16	2.56	2.54	0.38	4.19	0.21	0.48	0.16
030-03 M1	1	44	270	229	121	68	167	26.7	60	5.65	894	5.68	11.9	1.54	7.21	2.25	0.84	3.11	4.34	3.04	3.44	0.52	1.06	0.50	0.98	1.51
100-03 M	1	43	283	280	129	12	133	20.6	63	2.67	87	4.92	12.1	1.70	8.20	2.41	0.79	3.11	3.73	2.28	2.37	0.35	1.43	0.17	0.63	0.24
128-04 M	1	43	230	501	148	7	99	11.9	51	1.45	83	2.43	5.97	0.93	4.73	1.49	0.53	1.96	2.27	1.32	1.30	0.18	0.97	0.11	0.25	0.06
134-04 M	1	30	234	264	190	29	182	14.4	84	3.90	112	7.29	16.7	2.46	12.5	3.24	1.11	3.33	3.03	1.45	1.32	0.19	1.85	0.25	1.35	1.13
094-03 M1	5	46	296	257	109	12	107	23.9	77	2.61	105	4.57	10.8	1.59	8.41	2.68	0.96	3.57	4.47	2.85	2.91	0.44	1.28	0.18	0.91	0.46
TTG gneisses																										
009-04	1	2	33	13	12	34	404	4.88	163	3.71	491	52.9	89.1	10	32.5	4.66	0.85	3.35	1.28	0.4	0.26	0.02	4.77	0.1	14.18	n.a.
030-04 c	1	12	114	19	16	48	813	11.1	130	4.53	942	27.8	61.2	7.87	33.1	5.6	1.39	3.81	2.48	1.08	0.97	0.14	0.4	0.2	2.24	0.14
031-04 ME	1	4	42	16	9	30	503	11.9	116	3.43	573	17.3	36	4.41	16.7	3.26	0.8	2.42	2.19	1.14	1.02	0.13	3.74	0.11	2.65	n.a.
138-04 ME	1	4	22	4	3	39	342	32	205	9.31	192	29.2	52.5	6.08	22.1	4.99	0.79	4.56	5.39	3.35	3.06	0.49	7.5	0.57	11.53	n.a.
143-04 M	1	18	114	96	54	43	579	12.7	92	6.78	303	15.3	37.4	5.21	23.5	4.72	1.29	3.72	2.86	1.36	1.27	0.19	0.72	1.03	0.5	0.59
144-04 ME	1	16	81	8	24	5	514	16.5	375	7.58	145	11.9	28.1	3.63	14.9	3.41	0.98	3.2	2.92	1.64	1.57	0.25	8.74	0.45	n.a.	n.a.
083-04	2	14	113	116	54	59	544	18.3	112	5.76	810	28.3	62.9	8.4	35	6.4	1.25	4.8	3.56	1.83	1.72	0.25	2.75	0.24	0.6	0.13
113-03 M1	2	16	109	75	32	9	860	16.5	135	3.37	545	19.4	48.9	7.02	32.5	6.32	1.59	4.77	3.17	1.56	1.34	0.19	1.32	0.11	0.05	0.02
134-04 ME	2	4	22	8	9	38	268	1.59	110	1.64	528	11.8	21.4	2.02	7.33	1.22	0.49	0.89	0.35	0.19	0.12	0.02	3.34	0.06	0.62	0.27
118-03	5	7	47	23	23	37	311	3.55	92	3.21	487	21	29.8	3.21	9.9	1.33	0.62	1.37	0.69	0.31	0.32	0.04	2.43	0.04	n.a.	n.a.
131-04	5	5	31	15	13	75	303	5.51	116	5.26	635	30.5	54.6	6.36	20.7	3.2	0.78	2.74	1.26	0.47	0.37	0.04	3.8	0.14	5.43	n.a.
132-04	5	2	36	17	20	62	411	6.06	108	5.24	1289	27.7	47.1	5.43	17.9	2.57	0.67	2.41	1.15	0.54	0.51	0.05	3.16	0.33	5.33	n.a.
133-04	5	2	24	10	7	33	352	4.21	114	3.05	416	17	28.8	3.51	12.4	2.18	0.62	1.63	0.88	0.34	0.29	0.02	3.59	0.1	1.56	n.a.

localities (loc.): 1 – Iisalmi-Sukeva, 2 – Jonsa, 3 – Varpanen, 4 – Pallikäs, 5 - others

Appendix B continued *(n.a. – not analyzed, b.d. – below detection)*

sample	loc.	Sc	V	Cr	Ni	Rb	Sr	Y	Zr	Nb	Ba	La	Ce	Pr	Nd	Sm	Eu	Gd	Dy	Er	Yb	Lu	Hf	Ta	Th	U
granulite leucosomes																										
002-03 L	1	10	40	57	22	10	292	5.41	57	0.17	74	1.79	3.17	0.41	1.62	0.40	0.48	0.62	0.82	0.42	0.64	0.09	0.95	0.01	0.01	0.05
034-03 L2	1	7	7	6	12	5	164	21.1	60	0.07	42	0.86	1.50	0.15	0.51	0.16	0.28	0.52	2.32	2.75	4.23	0.63	1.31	0.03	0.09	0.11
036-04 L1	1	2	7	4	4	7	145	2.99	24	0.98	178	13.3	18.8	2.09	6.66	0.97	0.70	0.92	0.54	0.26	0.25	0.01	3.59	0.06	n.a.	n.a.
036-04 L2	1	8	83	78	41	6	342	8.19	292	6.90	239	22.8	52.2	6.68	26.0	4.67	1.06	3.60	1.83	0.71	0.56	0.09	8.23	0.25	n.a.	n.a.
071-03 L	2	3	32	5	1	54	334	1.34	129	1.82	1215	15.0	15.2	1.26	3.99	0.16	0.78	0.46	0.19	0.03	0.17	n.a.	3.45	0.12	1.19	0.16
076-04 L2	2	11	73	5	6	4	282	14.6	86	0.85	203	7.00	10.3	0.94	4.56	0.93	0.35	1.31	2.36	2.03	2.26	0.51	2.12	0.06	n.a.	0.09
076-04 L3	2	24	61	4	3	3	172	82.5	67	0.44	106	5.00	4.85	0.36	1.77	0.71	0.32	2.31	9.54	16.0	23.8	9.43	1.27	0.05	n.a.	0.02
109-04 L	2	27	95	4	10	7	313	93.1	30	1.74	228	23.0	51.3	6.24	30.0	10.7	1.38	12.0	18.8	11.7	7.38	2.07	0.45	0.12	n.a.	0.40
114-04 L	2	4	21	16	18	11	545	2.28	71	1.17	428	10.2	15.9	1.64	6.02	0.97	0.56	0.69	0.50	0.19	0.19	0.03	0.98	0.07	0.20	0.05
012-04 L1	3	3	31	6	10	28	339	1.12	160	1.66	667	14.6	18.8	1.54	4.02	0.45	0.99	0.34	0.19	0.12	0.20	0.05	5.07	0.03	0.06	0.17
012-04 L2	3	7	30	30	33	38	461	10.0	261	4.13	649	22.7	34.3	3.63	12.8	2.58	2.36	2.65	2.02	0.90	0.88	0.13	7.47	0.12	0.26	n.a.
012-04 L3	3	15	85	116	56	6	288	20.0	86	6.07	358	20.7	38.1	4.67	20.4	4.66	1.51	4.72	4.23	2.06	1.84	0.23	2.39	0.26	1.23	0.42
048-03 L1	3	6	49	72	14	7	243	2.49	83	2.26	165	4.53	6.41	0.69	2.58	0.55	0.41	0.50	0.47	0.21	0.23	0.01	2.30	0.19	0.12	n.a.
048-04 a	3	46	296	215	113	6	205	16.7	68	4.77	64	8.11	19.0	2.40	10.4	2.88	1.00	3.07	3.33	1.84	1.60	0.24	1.70	0.36	n.a.	n.a.
048-04 c	3	4	10	6	7	15	263	2.27	87	0.49	225	10.8	16.0	1.51	1.05	0.82	0.56	0.65	0.42	0.21	0.17	0.03	2.69	0.05	0.15	0.19
048-04 f	3	2	20	31	9	11	179	0.34	67	0.16	197	4.95	7.71	0.59	2.01	0.27	0.40	0.16	0.06	0.05	0.06	0.02	1.24	n.a.	0.06	0.05
069-03 L1	3	11	54	89	50	8	331	8.33	125	2.55	605	19.5	34.3	3.97	14.9	2.80	0.92	2.35	1.64	0.82	0.63	0.10	3.59	0.08	n.a.	n.a.
069-03 L2	3	10	59	69	45	7	385	8.46	152	2.34	482	27.9	45.5	5.21	17.9	2.92	1.05	2.42	1.63	0.78	0.63	0.10	3.69	0.07	n.a.	n.a.
063-04 L	4	3	15	4	6	22	273	0.50	133	0.64	237	12.7	13.2	1.22	3.19	0.25	0.53	0.43	0.06	0.05	0.12	0.00	4.53	0.01	n.a.	n.a.
migmatite leucosomes																										
006-04 L	1	1	10	10	11	36	401	1.23	58	0.52	1278	9.32	15.5	1.62	5.57	0.84	0.60	0.76	0.27	0.10	0.14	n.a.	1.65	0.43	1.02	n.a.
009-03 L1	1	b.d.	6	9	4	10	302	0.43	35	0.09	98	4.35	5.55	0.43	1.44	0.16	0.42	0.11	0.09	0.04	0.07	0.01	0.55	0.01	0.49	0.28
009-03 L2	1	3	32	6	6	63	309	1.04	147	4.53	2090	14.6	17.1	1.70	4.64	0.44	0.84	0.85	0.15	0.10	0.21	0.01	5.46	0.16	1.07	n.a.
027-03 L	1	9	82	100	77	55	333	5.72	72	5.22	548	22.0	42.4	4.81	18.2	3.10	0.88	2.47	1.27	0.52	0.39	0.06	1.50	0.14	0.93	0.21
030-04 b	1	b.d.	23	33	11	21	600	1.85	17	2.09	447	11.3	19.7	2.04	7.54	1.34	0.59	0.90	0.43	0.11	0.11	0.01	0.06	0.10	0.90	0.10
030-04 e	1	2	23	13	10	16	444	0.50	161	1.15	485	5.18	7.41	0.58	1.88	0.21	0.47	0.15	0.07	0.06	0.08	0.02	5.01	0.04	0.14	0.30
031-04 L	1	1	11	4	1	16	651	0.82	65	0.66	473	5.22	9.41	1.04	4.05	0.61	0.43	0.40	0.17	0.08	0.08	0.02	1.13	0.02	0.08	0.07
038-05 L	1	3	12	9	8	9	171	0.98	26	1.09	103	5.00	10.2	0.77	2.88	0.03	0.47	0.39	0.03	n.a.	0.10	n.a.	0.37	0.03	n.a.	0.25
100-04 L2	1	5	23	16	8	37	361	1.68	155	2.54	632	55.7	88.6	9.76	30.8	3.38	0.76	2.40	0.59	0.14	0.17	0.02	4.45	0.07	21.31	n.a.
128-04 L	1	10	58	18	9	9	692	11.2	130	4.14	506	26.9	56.8	6.98	27.0	4.98	1.09	3.58	2.34	1.01	0.83	0.11	4.56	0.16	n.a.	n.a.
138-04 L	1	b.d.	8	6	2	51	214	1.12	75	1.41	1431	7.67	11.6	1.26	3.98	0.60	0.48	0.67	0.21	0.07	0.12	0.01	2.81	0.05	n.a.	n.a.
144-04 L1	1	2	32	2	4	5	465	1.47	341	2.67	198	5.42	8.42	0.92	3.12	0.41	0.35	0.41	0.20	0.15	0.24	0.03	9.86	0.17	n.a.	n.a.
144-04 L2	1	16	50	34	20	5	945	8.61	26	1.13	276	9.64	19.0	2.60	11.8	2.58	0.80	2.27	1.75	0.88	0.78	0.13	0.50	0.11	0.14	0.05
085-03 L	2	3	11	3	1	10	276	0.41	48	0.22	374	5.90	8.57	0.70	2.43	0.22	0.51	0.13	0.09	0.05	0.07	0.01	1.18	0.01	0.08	0.09
134-04 L1	2	2	15	8	5	44	215	6.02	105	2.52	327	10.7	20.1	2.01	7.30	1.34	0.45	1.15	1.06	0.65	0.84	0.14	8.48	0.15	1.86	0.81
134-04 L2	2	2	5	4	b.d.	58	186	0.50	46	0.17	963	10.2	17.5	1.51	4.83	0.59	0.44	0.29	0.12	0.05	0.05	0.01	1.38	0.02	5.32	0.55
061-03 L	4	15	74	44	33	9	443	13.6	121	4.76	173	10.3	23.1	3.21	14.4	3.13	0.70	2.77	2.45	1.42	1.41	0.21	0.85	2.02	3.82	7.89
061-04 L	4	23	148	72	44	16	900	19.1	120	3.68	142	14.2	47.3	6.64	29.8	6.52	1.65	5.20	3.61	1.77	1.52	0.23	2.81	0.17	n.a.	n.a.
094-03 L1	5	9	95	46	26	71	275	2.81	175	6.57	609	12.8	17.7	1.89	5.77	0.77	0.93	0.63	0.46	0.30	0.39	0.08	5.29	0.18	n.a.	n.a.
094-03 L2	5	3	17	12	6	14	293	1.54	43	1.11	234	17.6	24.8	2.68	8.24	1.01	0.80	0.96	0.32	0.12	0.16	0.00	1.01	0.04	0.63	n.a.
120-04 L	5	11	47	40	33	8	244	4.52	46	0.49	179	3.00	2.71	0.20	1.39	0.25	0.24	0.40	0.61	0.56	0.81	0.03	0.90	0.04	n.a.	0.09

localities (loc.): 1 – Iisalmi-Sukeva, 2 – Jonsa, 3 – Varpanen, 4 – Pallikäs, 5 – others (n.a. – not analyzed)

References

Acosta-Vigil, A., London, D. & Morgan VI, G. B. (2006). Experiments on the kinetics of partial melting of a leucogranite at 200 MPa H_2O and 690-800°C: Compositional variability of melts during the onset of H_2O saturated crustal anatexis. *Contribution to Mineralogy and Petrology* **151**, 539-557.

Andersen, T., Whitehouse, M. J. & Burke, E. A. J. (1997). Fluid inclusions in Scourian granulites from the Lewisian complex of NW Scotland: Evidence for CO_2-rich fluid in Late Archaean high-grade metamorphism. *Lithos* **40** (2-4), 93-104.

Anderson, J. L. & Smith, D. R. (1995). The effects of temperature and fO_2 on the Al-in-hornblende barometer. *American Mineralogist* **80**, 549-559.

Angus, S., Armstrong, B., de Reuk, K. M., Altunin, V. V., Gadetskii, O. G., Chapela, G. A. & Rowlinson, J. S. (1976). International thermodynamic tables of the fluid state, Carbon Dioxide. *Pergamon* **3,** Oxford.

Aranovich, L. Y. & Newton, R. C. (1996). H_2O activity in concentrated NaCl solutions at high pressures and temperatures measured by the brucite - periclase equilibrium. *Contribution to Mineralogy and Petrology* **125**, 200-212.

Bakker, R. J. (2003). Package FLUIDS 1. Computer programs. *Chemical Geology* **194**, 3-23.

Barker, F. (1979). Trondhjemite: Definition, environment and hypotheses of origin. In: Barker, F. (ed.) *Trondhjemites, Dacites and related rocks*, Elsevier, 1-12.

Barth, M. G., Foley, S.F. & Horn, I. (2002). Partial melting in Archean subduction zones: constraints from experimentally determined trace element partition coefficients between eclogitic minerals and tonalitic melts under upper mantle condiditons. *Precambrian Research* **113**, 323-340.

Beard, J. S. & Lofgren, G. E. (1991). Dehydration melting and water-saturated melting of basaltic and andesitic greenstones and amphibolites at 1, 3 and 6-9 kb. *Journal of Petrology* **32**, 365-401.

Bédard, J. H. (2006). Trace element partitioning in plagioclase feldspar. *Geochimica et Cosmochimica Acta* **70**, 3717-3742.

Bédard J. H. (2006). A catalytic delamination-driven model for coupled genesis of Archaean crust and sub-continental lithospheric mantle. *Geochimica et Cosmochimica Acta* **70**, 1188-1214.

Blundy, J. & Wood, B. (1991). Crystal-chemical controls on the partitioning of Sr and Ba between plagioclase feldspar, silicate melts and hydrothermal solutions. *Geochimica et Cosmochimica Acta* **55**, 193-209.

Bodnar, R. J. (1993). Revised equation and table for determining the freezing point depression of H_2O-NaCl solutions. *Geochimica et Cosmochimica Acta* **57**, 683-684.

Brown, M. (1994). The generation, segregation, ascent and emplacement of granite magma: the migmatite-to-crustally-derived granite connection in thickened orogens. *Earth Science Reviews* **36**, 83-130.

Brown, M. (2001). Orogeny, migmatites and leucogranites: A review. *Proceedings of the Indian*

Academy of Sciences-Earth and Planetary Sciences **110**(4), 313-336.

Carroll, M. R. & Wyllie, P. J. (1990). The system tonalite-H_2O at 15 kbar and the genesis of calc-alkaline magmas. *American Mineralogist* **75**, 345-357.

Condie, K. C. (2005). TTGs and adakites: are they both slab melts? *Lithos* **80**, 33-44.

Condie, K. C. (1998). Episodic continental growth and supercontinents: A mantle avalanche connection? *Earth and Planetary Science Letters* **163**(1-4), 97-108.

Drummond, M. S. & Defant, M. J. (1990). A model for trondhjemite-tonalite-dacite genesis and crustal growth via slab melting - Archean to modern comparisons. *Journal of Geophysical Research-Solid Earth and Planets* **95**(B13), 21503-21521.

Fedorowich, J. S., Richards, J. P., Jain, J. C., Kerrich, R. & Fan, J. (1993). A rapid method for REE and trace-element analysis using laser sampling ICP-MS on direct fusion whole-rock glasses. *Chemical Geology* **106**, 229-249.

Foley, S., Tiepolo, M. & Vannucci, R. (2002). Growth of early continental crust controlled by melting of amphibolite in subduction zones. *Nature* **417**(6891), 837-840.

Garrido, C. J., Bodinier, J.-L., Burg, J.-P., Zeilinger, G., Hussain, S. S., Dawood, H., Chaudhry, S. & Gervilla, F. (2006). Petrogenesis of mafic garnet granulite in the lower crust of the Kohistan Paleo-arc Complex (Northern Pakistan): Implications for intra-crustal differentiation of island arcs and generation of continental crust. *Journal of Petrology* **47**(10), 1873-1914.

Gibert, F., Guillaume, D. & Laporte, D. (1998). Importance of fluid immiscibility in the H_2O-NaCl-CO_2 system and selective CO_2 entrapment in granulites: Experimental phase diagram at 5-7 kbar, 900°C and wetting textures. *European Journal of Mineralogy* **10**, 1109-1123.

Greenfield, J. E., Clarke, G. L., Bland, M. & Clark, D. J. (1996). In-situ migmatite and hybrid diatexite at Mt. Stafford, Central Australia. *Journal of Metamorphic Geology* **14**(4), 413-426.

Guernina, S. & Sawyer, E. W. (2003). Large-scale melt-depletion in granulite terranes: An example from the Archean Ashuanipi Subprovince of Quebec. *Journal of Metamorphic Geology* **21**(2), 181-201.

Gupta, L. N. & Johannes, W. (1982). Petrogenesis of a stromatic migmatite (Nelaug, southern Norway). *Journal of Petrology* **23**(4), 548-567.

Hansen, E. C. & Stuk, M. (1993). Orthopyroxene-bearing, mafic migmatites at Cone Peak, California: evidence for the formation of migmatitic granulites by anatexis in an open system. *Journal of Metamorphic Geology* **11**, 291-307.

Hartel, T. H. D. & Pattison, D. R. M. (1996). Genesis of the Kapuskasing (Ontario) migmatitic mafic granulites by dehydration melting of amphibolite: The importance of quartz to reaction progress. *Journal of Metamorphic Geology* **14**, 591-611.

Hawkesworth, C. J. & Kemp, A. I. S. (2006). Using hafnium and oxygen isotopes in zircons to unravel the record of crustal evolution. *Chemical Geology* **226**, 144-162.

Holland, T. J. H. & Blundy, J. (1994). Non-ideal interactions in calcic amphiboles and their bearing on amphibole-plagioclase thermometry. *Contribution to Mineralogy and Petrology* **116**, 433-447.

Hölttä, P. (1997). Geochemical characteristics of granulite facies rocks in the Archean Varpaisjärvi area, Central Fennoscandian Shield. *Lithos* **40**(1), 31-53.

Hölttä, P., Huhma, H., Mänttäri, I. & Paavola, J. (2000). P-T-t development of Archaean granulites in Varpaisjärvi, Central Finland. II. Dating of high-grade metamorphism with the U-Pb and Sm-Nd methods. *Lithos* **50**, 121-136.

Hölttä, P. & Paavola, J. (2000). P-T-t development of Archaean granulites in Varpaisjärvi, Central Finland. I. Effects of multiple metamorphism on the reaction history of mafic rocks. *Lithos* **50**, 97-120.

Jochum, K. P., Stoll, B., Herwig, K. & Amini, M. (submitted). Trace element and isotope analyses of geo- and cosmochemical samples by laser ablation-sector field-ICPMS. In: Douthitt, C. B. (ed.) *High-Resolution ICP-MS*.

Johannes, W. (1984). Beginning of melting in the granite system Qz-Or-Ab-An-H_2O. *Contribution to Mineralogy and Petrology* **86**, 264-273.

Johannes, W. (1989). Melting of plagioclase-quartz-assemblages at 2 kbar water pressure. *Contribution to Mineralogy and Petrology* **102**, 270-276.

Johannes, W., Ehlers, C., Kriegsman, L. M. & Mengel, K. (2003). The link between migmatites and S-type granites in the Turku area, southern Finland. *Lithos* **68**, 69-90.

Johnson, E. L. (1991). Experimentally determined limits for H_2O-CO_2-NaCl immiscibility in granulites. *Geology* **19**, 925-928.

Johnston, A. D. (1986). Anhydrous P-T phase relations of near-primary high-alumina basalt: Implications for the origin of island arcs and tonalite-trondhjemite series rocks. *Contribution to Mineralogy and Petrology* **92**, 368-382.

Johnston, A. D. & Wyllie, P.J. (1988). Constraints on the origin of Archean trondhjemites based on phase relations of the Nuk Gneiss with H_2O at 15 kbar. *Contribution to Mineralogy and Petrology* **100**, 35-46.

Kar, R., Bhattacharya, S. & Sheraton, J. W. (2003). Hornblende-dehydration melting in mafic rocks and the link between massif-type charnockite and associated granulites, Eastern Ghats Granulite Belt, India. *Contribution to Mineralogy and Petrology* **145**(6), 707-729.

Kemp, A. I. S., Hawkesworth, C. J., Paterson, B. A. & Kinny, P. D. (2006). Episodic growth of the Gondwana supercontinent from hafnium and oxygen isotopes in zircon. *Nature* **439**, 580-582.

Klein, M., Stosch, H.-G. & Seck, H. A. (1997). Partitioning of high field-strength and rare-earth elements between amphibole and quartz-dioritic to tonalitic melts: An experimental working. *Chemical Geology* **138**, 257-271.

Klein, M., Stosch, H. G., Seck, H. A. & Shimizu, N. (2000). Experimental partitioning of high field strength and rare earth elements between clinopyroxene and garnet in andesitic to tonalitic systems. *Geochimica Et Cosmochimica Acta* **64**(1), 99-115.

Korsman, K., Korja, T., Pajunen, M., Virransalo, P., GGT / SVEKA Working Group (1999). The GGT/SVEKA transect: Structure and evolution of the continental crust in the Paleoproterozoic Svecofennian orogen in Finland. *International Geology Review* **41**(4), 287-333.

Kretz, R. (1983). Symbols of rock-forming minerals. *American Mineralogist* **68**, 277-279.

Mänttäri, I. & Hölttä, P. (2002). U-Pb dating of zircons and monazites from Archean granulites in Varpaisjärvi, Central Finland: Evidence for multiple metamorphism and Neoarchean terrane accretion. *Precambrian Research* **118**, 101-131.

Mänttäri, I., Sergeev, S. A., Paavola, J., Pakkanen, L. & Vestin J. (1998). From conventional to ionprobe U-Pb dating of inhomogeneous zircon population: 3.2 Ga basement gneiss, Lapinlahti, Central Finland. *23th Nordiske Vintermode*, 197.

Marchildon, N. & Brown, M. (2001). Melt segregation in late syn-tectonic anatectic migmatites: an example from the Onawa contact aureole, Maine, USA. *Physics and Chemistry of the Earth Part a-Solid Earth and Geodesy* **26**, 225-229.

Mareels, J. (2004). ICP-MS analysis, geochemistry and petrogenesis of granites from the Variscan northern Voges (France), K.U. Leuven.

Martin, H., Smithies, R. H., Rapp, R., Moyen, J.-F., & Champion D. (2005). An overview of adakite, tonalite–trondhjemite–granodiorite (TTG), and sanukitoid: relationships and some implications for crustal evolution. *Lithos* **79**, 1-24.

Martin, H. (1994). The Archean Grey Gneisses and the genesis of continental crust. In: Condie, K.C. (ed.) *Archean Crustal Evolution*. Developments in Precambrian Geology, 205-247.

Martin, H. (1993). The Mechanisms of Petrogenesis of the Archean Continental-Crust - Comparison with Modern Processes. *Lithos* **30**(3-4), 373-388.

Moyen, J.-F. & Stevens, G. (2006). Experimental Constraints on TTG petrogenesis: Implications for Archean Geodynamics. In: Benn, K., Mareschal, J.-C. & Condie, K.C. (ed.) *Archean Geodynamics and Environments*. Washington D.C.: American Geophysical Union, 149-175.

Paavola J. (1999). Pre-Quaternary rocks of the Rautavaara map-sheet area (sheet 3343). In: Geological Survey of Finland (ed.) *Explanation to the maps of Pre-Quaternary rocks.* Espoo.

Paavola J. (2003). Pre-Quaternary rocks of the Vieremä map-sheet area (sheet 3342). In: Geological Survey of Finland (ed.) *Explanation to the maps of Pre-Quaternary rocks.* Espoo.

Patiño Douce, A. E. & Beard, J. S. (1995). Dehydration-melting of biotie gneiss and quartz amphibolite from 3 to 15 kbar. *Journal of Petrology* **36**(3), 707-738.

Poutiainen M. (1992). Fluid inclusions in rocks of the Archean high-grade Varpaisjärvi-Lapinlahti area, Central Finland. Bull Geol Soc Finland 64, 3-12.

Pride, C. & Muecke, G. K. (1980). Rare Earth Element geochemistry of the Scourian Complex N.W. Scotland - Evidence for the granite-granulite link. *Contributions to Mineralogy and Petrology* **73**, 403-412.

Rapp, R. P. (1995). Amphibole-out phase boundary in partially melted metabasalt, its control over liquid fraction and composition, and source permeability. *Journal of Geophysical Research-Solid Earth* **100**, 15601-15610.

Rapp, R. P., Watson, E. B. & Miller, C. F. (1991). Partial melting of amphibolite / eclogite and the origin of Archean trondhjemites and tonalites. *Precambrian Research* **51**, 1-25.

Rushmer, T. (1991). Partial melting of two amphibolites: contrasting experimental results under fluid-absent conditions. *Contribution to Mineralogy and Petrology* **107**, 41-59.

Sawyer, E. W. (1987). The role of partial melting and fractional crystallization in determining discordant migmatite leucosome compositions. *Journal of Petrology* **28**, 445-473.

Sawyer, E. W. (1991). Disequilibrium melting and rate of melt-residuum separation during migmatization of mafic rocks from the Grenville front, Quebec. *Journal of Petrology* **32**, 701-738.

Sawyer, E. W. (1998). Formation and evolution of granite magmas during crustal reworking: The significance of diatexites. *Journal of Petrology* **39**(6), 1147-1167.

Sawyer, E. W. (2001). Melt segregation in the continental crust: distribution and movement of melt in anatectic rocks. *Journal of Metamorphic Geology* **19**(3), 291-309.

Sen, S. K. & Dunn, T. (1994). Dehydration melting of a basaltic composition amphibolite at 1.5 and 2 GPa: implications for the origin of adakites. Contribution to Mineralogy and Petrology **117**, 394-409.

Sisson, T. W., Ratajeski, K., Hankins, W. B. & Glazner, A. F. (2005). Voluminous granitic magmas from common basaltic sources. *Contribution to Mineralogy and Petrology* **148**, 635-661.

Solar, G. S. & Brown, M. (2001). Petrogenesis of migmatites in Maine, USA: Possible source of peraluminous leucogranite in plutons? *Journal of Petrology* **42**(4), 789-823.

Springer, W. & Seck, H.A. (1997). Partial fusion of basic granulites at 5 to 15 kb: implications for the origin of TTG magmas. *Contribution to Mineralogy and Petrology* **127**, 30-45.

Stern, R. A., Percival, J. A. & Mortensen, J. K. (1994). Geochemical evolution of the Minto block: a 2.7 Ga continental magmatic arc built on the Superior proto-craton. *Precambrian Research* **65**, 115-153.

Tiepolo, M., Vannucci, R., Oberti, R., Foley, S., Bottazzi, P. & Zanetti, A. (2000). Nb and Ta incorporation and fractionation in titanian pargasite and kaersutite: crystal-chemical constraints and implications for natural systems. *Earth and Planetary Science Letters* **176**, 185-201.

Tomlinson, K. Y., Davis, D. W., Stone, D., & Hart, T. R. (2003). U-Pb age and Nd isotopic evidence for Archean terrane development and crustal recycling in the south-central Wabigoon subprovince, Canada. *Contribution to Mineralogy and Petrology* **144**, 684-702.

Tomlinson, K. Y., Stott, G. M., Percival, J. A. & Stone, D. (2004). Basement terrane correlations and crustal recycling in the western Superior Province: Nd isotopic character of granitoid and felsic volcancic rocks in the Wabigoon subprovince, N. Ontario, Canada. *Precambrian Research* **132**, 245-274.

Touret, J. L. R. & Olsen, S. N. (1985). Fluid inclusions in migmatites. In: Ashworth, J.R. (ed.) *Migmatites*, Blackie and Son, pp. 265-286.

Vielzeuf, D., Clemens, J. D., Pin, C. & Moinet, E. (1990). Granites, granulites and crustal differentiation. In: Vielzeuf, D. & Vidal, P. (ed.) *Granulites and Crustal Evolution*, Kluwer Academic Publisher, 59-85.

Vityk, M. O. & Bodnar, R. J. (1995). Do fluid inclusion in high grade metamorphic terranes

preserve peak metamorphic density during retrograde decompression. *American Mineralogist* **90**, 641-644.

Watson, E. B. & Brenan, J. M. (1987). Fluids in the Lithosphere. 1. Experimentally determined wetting characteristics of CO_2-H_2O fluids and their implications for fluid transport, host rock physical properties and fluid inclusion formation. *Earth and Planetary Science Letters* **85**, 497-515.

Whalen, J. B., Percival, J. A., McNicoll, V. J. & Longstaffe, F. J. (2002). A mainly crustal origin for tonalitic granitoid rocks, Superior Province, Canada: Implications for late Archean tectonomagmatic processes. *Journal of Petrology* **43**(8), 1551-1570.

Whalen, J. B., Percival, J. A., McNicoll, V. J. & Longstaffe, F. J. (2004). Geochemical and isotopic (Nd-O) evidence bearing on the origin of late- to post-orogenic high-K granitoid rocks in the Western Superior Province: implications for late Archean tectonomagmatic processes. *Precambrian Research* **132**, 303-326.

White, R. W., Pomroy, N. E. & Powell, R. (2005). An in-situ metatexite-diatexite transition in upper amphibolite facies rocks from Broken Hill, Australia. *Journal of Metamorphic Geology* **23**, 579-602.

White, R. W. & Powell, R. (2002). Melt loss and the preservation of granulite facies mineral assemblages. *Journal of Metamorphic Geology* **20**(7), 621-632.

Whitney, D. L. & Irving, A. J. (1994). Origin of K-poor leucosomes in a metasedimentary migmatite complex by ultrametamorphism, syn-metamorphic magmatism and subsolidus processes. *Lithos* **32**, 173-192.

Wilke, M. & Behrens, H. (1999). The dependence of the partitioning of iron and europium between plagioclase and hydrous tonalitic melt on oxygen fugacity. *Contribution to Mineralogy and Petrology* **137**(1-2), 102-114.

Williams, M. L., Hammer, S., Kopf, C. & Darrach, M. (1995). Syntectonic generation and segregation of tonalitic melts from amphibolite dikes in the lower crust, Striding-Athabasca mylonite zone, northern Saskatchewan. *Journal of Geophysical Research-Solid Earth* **100**, 15717-15734.

Wolf, M. B. & Wyllie, P. J. (1994). Dehydration-melting of amphibolite at 10 kbar - the Effects of Temperature and Time. *Contribution to Mineralogy and Petrology* **115**(4), 369-383.

Zhang, S.-B., Zheng, Y.-F., Wu, Y.-B., Zhao, Z.-F., Gao, S. & Wu, F.-Y. (2006). Zircon U-Pb age and Hf isotope evidence for 3.8 Ga crustal remnant and episodic reworking of Archean crust in South China. *Earth and Planetary Science Letters* **252**, 56-71.

Zhao, G. C., Wilde, S. A., Cawood, P. A. & Lu, L. Z. (2000). Petrology and P-T path of the Fuping mafic granulites: Implications for tectonic evolution of the central zone of the North China craton. *Journal of Metamorphic Geology* **18**(4), 375-391.

Part III

Trace element partitioning in the granulite facies.

Franziska Nehring, Stephen F. Foley, Pentti Hölttä

Abstract 78

1. Introduction 79

2. Geological setting and metamorphism 80

3. Petrography 82

3.1 Mafic granulites 82

3.2 Intermediate granulites 83

4. Methods 85

5. Sample description and bulk rock geochemistry 86

6. Mineral chemistry 87

6.1 Amphibole 87

6.2 Clinopyroxene 89

6.3 Orthopyroxene 92

6.4 Garnet 92

6.5 Plagioclase 92

6.6 Biotite 94

6.7 Ilmenite and magnetite 94

6.8 Apatite 95

7. Discussion 96

7.1 Mass balance calculations 96

7.2 Rare earth element partitioning between coexisting minerals and melt 96
7.2.1 Amphibole / Clinopyroxene REE-partitioning **96**
7.2.2 Garnet / Clinopyroxene REE-partitioning **100**
7.2.3 REE in orthopyroxene **102**
7.2.4 REE partitioning into plagioclase **103**
7.2.5 The role of apatite **104**
7.3 Partitioning of the High Field Strength Elements (HFSE) 106
7.4 Large Ion Lithophile Elements (LILE) 109
7.5 Transition metals 111
7.6 Th and U 113

8. Implications for melting within the lower crust 115
8.1 Melt composition in equilibrium with granulitic residues 115
8.2 Metasomatism of minerals in residual granulites 118
8.3 The importance of ilmenite for Nb/Ta ratios in coexisting melts 119

9. Conclusions 120

Appendix A 122

Appendix B 123

References 125

Abstract

Analyses of trace elements in mineral phases of granulites provide important information about the trace element distribution in the lower crust. Since granulites are considered as residues of partial melting processes, trace element characteristics of granulite mineral phases record mineral / melt equilibria.

LA-ICP-MS was applied to the principal mineral phases (amph, pl, cpx, opx, grt, ap, il) of mafic and intermediate granulites from Central Finland, which experienced P-T-conditions of 800-950°C at 9-11 kbar during a major collisional event in the late Archean. The analyses indicate that equilibrium was attained between most mineral phases except for garnet in mafic granulites that is only in equilibrium with its immediate surrounding and hence exerts limited influence on the bulk partition coefficient. Accessory phases are important in hosting REE (apatite), HFSE (ilmenite) and transition metals (ilmenite, magnetite).

The comparison of the LA-ICP-MS data with published values as well as the application of predictive models were used to formulate a set of $D^{mineral/melt}$ values that is applicable for trace element modelling under lower crustal conditions. The relationship between mineral trace element contents and leucosomes with compositions close to equilibrium melts provides additional constraints on mineral / melt partitioning.

The D-values derived in this study are broadly similar to magmatic partition coefficients for intermediate melt compositions. They provide a self-consistent set of D-values for Sc, V, Cr and Ni between clinopyroxene, amphibole, garnet, orthopyroxene, ilmenite and magnetite which was lacking in the literature so far. In addition, they emphasize the strong impact that ilmenite exerts on the distribution of Nb and Ta. As a consequence, ilmenite has to be included into further discussions about the role of melting of mafic source rocks as the driving mechanism for Archean crust generation.

Trace element characteristics of tonalitic melts in equilibrium with mafic and intermediate granulites are different from the typical Archean crustal association of tonalites-trondhjemites-granodiorites (TTG) concerning Sr contents and REE fractionation. Melts in equilibrium with granulitic residues are therefore not considered as important contributors to Archean crust formation.

1. Introduction

The genesis of the Archean continental crust has been a matter of debate during the past decades. Models for continental crust production focus on the melting of basaltic source rocks in a subduction zone setting (Drummond & Defant, 1990, Martin, 1994) or at the base of thickened lower crust (Smithies, 2000, Bédard, 2006a). In contrast, the further differentiation of the continental crust by metamorphism and partial melting has attracted much less attention although understanding crustal melting processes and redistribution of trace elements during crustal melting will have significant implications for the geochemical evolution of the continental crust.

High temperature anatexis within the middle to lower crust is a direct consequence of the incongruent melting of hydrous minerals (muscovite, amphibole, biotite) leaving an anhydrous granulitic residue and generating significant amounts of granitoid melts. Widespread granulite terranes typically occur in the deeply eroded Archean proportions of the continents (see Vielzeuf & Vidal, 1990 and references therein) which suggests that crustal melting was important in Archean crust differentiation and recycling. So far the behaviour of trace elements in granulites is poorly understood and very few sets of partition coefficients exist that were experimentally derived under granulite facies conditions (800-900°C, 7-10 kbar) for minerals in equilibrium with tonalitic-andesitic liquids (Brenan et al., 1995, Klein et al., 1997, Klein et al., 2000, Hilyard et al., 2000, Barth et al., 2002) and usually either garnet, amphibole or orthopyroxene are lacking in the run products.

Another approach to gain fundamental insight into trace element redistribution in the granulite facies is to study trace element contents of minerals from well equilibrated mineral assemblages from partially molten rocks. Mafic and intermediate granulites from Central Finland provide excellent opportunities for *in-situ* trace element determination by LA-ICP-MS. They have simple, well equilibrated mineral parageneses; containing garnet in addition to amphibole and clinopyroxene at pressures >10 kbar and orthopyroxene at lower pressures and elevated SiO_2 contents as the main facies indicators. Partition coefficients between coexisting minerals are almost identical among different lithologies which points to a close approach to equilibrium during partial melting. Accessory phases (apatite, ilmenite, magnetite) are major carriers of Nb, Ta, REE and the transition metals. They may act as reservoirs of these elements in the deep continental crust.

All of the granulite lithologies contain patches, veins and layers of quartzofeldspatic leucosome which are considered as remnants of melt derived from anatexis of the mafic and

intermediate source rocks. Although the leucosomes provide important evidence of partial melting, their usability for constraining the trace element partitioning between granulitic residues and melt is mainly hampered by the uncertainty regarding whether leucosomes are equilibrium melts or not. Appearance and compositions of most leucosomes is actually more consistent with the crystallization of plagioclase and quartz from a percolating and finally extracted melt phase along melt migration pathways (Marchildon & Brown, 2001, Solar & Brown, 2001). Conclusions about the partitioning between minerals and tonalitic melts under lower crustal conditions must hence be drawn carefully by using rarely occurring leucosomes with a more melt like composition while the comparison of the distribution of trace elements between coexisting minerals with published data on mineral / mineral partitioning offers another possibility for the compilation of a self-consistent set of mineral / melt partition coefficients applicable for modelling trace element scenarios during crustal melting of mafic and intermediate rocks.

2. Geological setting and metamorphism

Samples under consideration were collected from fault-bounded granulite blocks cropping out within amphibolite-facies migmatites between Sukeva, Iisalmi and Varpaisjärvi in Central Finland (Fig. 1). The Archean bedrock is cut by large NW-trending shear zones developed during Proterozoic thrusting of the Iisalmi block to the NE.

According to zircon ion microprobe dating, mafic granulites from the NW-part of the working area (Iisalmi-Sukeva and Varpanen area) have protolith ages of 3.1-3.2 Ga (Hölttä et al., 2000). Intermediate granulites from the SE of the working area (Jonsa area) have minimum protolith ages of 2.73-2.70 Ga (Mänttäri & Hölttä, 2002). The age difference between the NE and the SW granulites most likely indicates terrane accretion during the late Archean. Granulite metamorphism accompanied by partial melting occurred coevally in both terranes between 2.70-2.63 Ga (Hölttä et al., 2000, Mänttäri & Hölttä, 2002).

Detailed description of metamorphic reactions and determination of the P-T-path for the mafic and intermediate granulites from the working area is given in Hölttä & Paavola (2000). Peak metamorphic conditions are obtained from grt-cpx-pl-qtz assemblages indicating 9-11 kbar and 800-950°C. The highest pressures were obtained from mafic granulites in the NW of the Iisalmi-Sukeva area. After peak metamorphism, the area experienced decompression and cooling to ca. 7 kbar and 700°C as indicated by garnet decomposition to orthopyroxene and plagioclase.

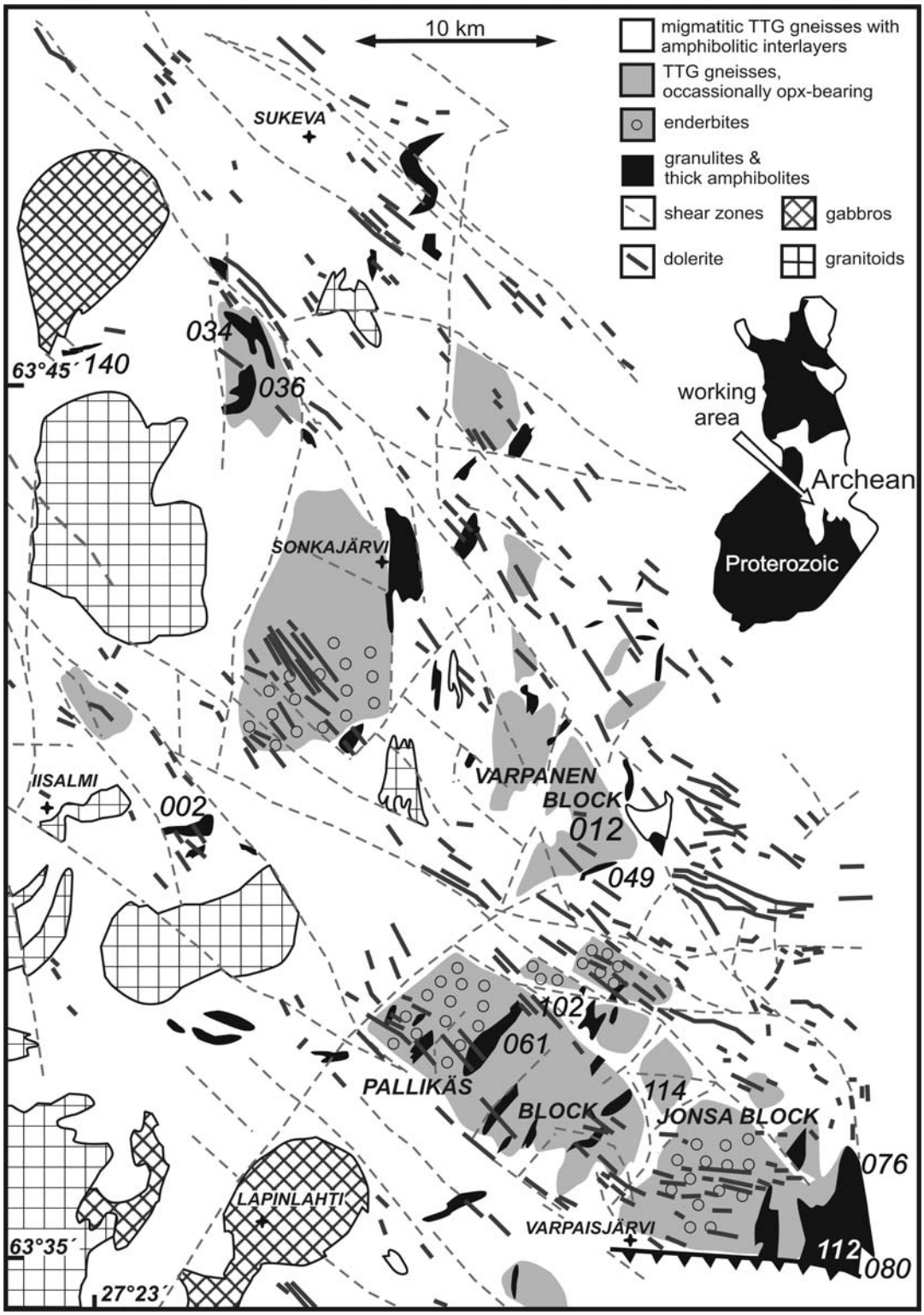

Fig. 1:

Schematic geological map of the working area. Numbers indicate outcrops where samples were collected.

Opx-pl-symplectites formed at P-T-conditions of 5.7-7.1 kbar and 590-740°C around garnet or along fractures in garnet during proterozoic overprint and fracturing of the bedrock.

3. Petrography

3.1 Mafic granulites

Granoblastic grt-cpx-pl±hbl assemblages are typical for the 3.1 Ga mafic granulites of the NW part of the working area (Iisalmi-Sukeva) (Fig. 2). Qtz is absent from these rocks. Within the Varpanen block mafic and intermediate granulites are intercalated. They resemble garnet-bearing mafic granulites described by Sawyer (1991), Williams et al. (1995) and Hartel & Pattison (1996). Orthopyroxene is present as a breakdown product within symplectites around garnet or pseudomorphs after garnet. Single grains of prograde amphibole are enclosed by clinopyroxene or garnet while retrograde amphibole forms rims on garnet or clinopyroxene. Garnet is porphyroblastic and reaches grain sizes up to 2-3 cm. It commonly contains inclusions of other minerals present in the host rock (mostly cpx). Ilmenite and magnetite are common accessory phases in mafic granulites.The peak mineral assemblage and mineral textures suggest that mafic granulites from the Iisalmi-Sukeva area formed by the following general dehydration-melting reaction (Wolf & Wyllie, 1994; Hartel & Pattison, 1996):

$$hbl + pl \pm qtz = cpx + grt + melt \quad (1)$$

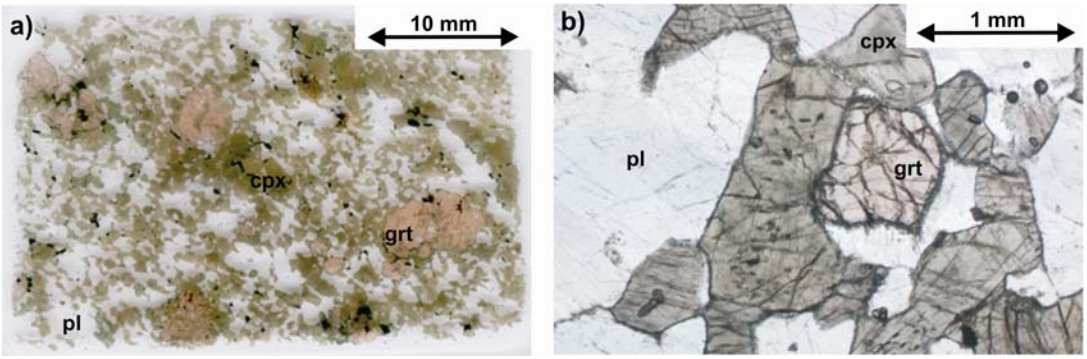

Fig. 2:

Photomicrographs of mafic granulites showing granoblastic growth of garnet in contact with clinopyroxene. Black specks in Fig. 2a are oxide phases. Brown specks in the large clinopyroxene in Fig. 2b are ilmenite.

Hartel & Pattison (1996) predict that garnet is produced in a larger amount than clinopyroxene in reaction (1). However, clinopyroxene is always more abundant than garnet in the Finnish mafic granulites as deduced from the field appearance, point counting and calculation of modal abundances (Table 1). This may be attributed to formation of clinopyroxene in CaO-rich rocks on the prograde path according to reaction (2) (Rushmer, 1991) before the rocks entered the stability field of garnet.

$$\mathbf{hbl + pl^1 + qtz = cpx + pl^2 + melt \pm ilm} \quad \mathbf{(2)}$$

(pl^2 more calcic than $pl^{1)}$

Alternatively the precursor of mafic granulites may not have been fully hydrated before metamorphism and some clinopyroxene is recrystallized from the igneous precursor. However, the lack of relict cores as well as low Mg# of clinopyroxene which reflect Mg# in coexisting amphibole point to a metamorphic origin.

3.2 Intermediate granulites

Prograde, granoblastic orthopyroxene is characteristic for the 2.7 Ga intermediate granulites of the Jonsa block (Fig. 1). The modal mineralogy of intermediate granulites varies significantly, with plagioclase constituting 30-50%, amphibole 10-40% and clinopyroxene of 10-30% of the modal abundance (Fig. 3, Table 1). Orthopyroxene is usually present in approximately half the amount of clinopyroxene. Garnet in intermediate granulites is restricted to Fe-rich and more mafic layers but within these layers it can make up more than 20%. Field appearance and compositional differences suggest a pre-metamorphic layering of broadly andesitic rocks probably resembling volcanic successions. Similar compositional layering of garnet-bearing and garnet-free granulites has been described by Zhao et al. (2000) from the North China craton and Kar et al. (2003) from the Eastern Ghats Granulite Belt in India.

The opx-producing reaction in typical opx-cpx-granulites was likely similar to reaction (3) (Patiño Douce & Beard, 1995).

$$\mathbf{amph + qtz = pl + cpx + opx + melt + ox} \quad \mathbf{(3)}$$

The stability of orthopyroxene in the Jonsa area is facilitated by pressures < 10 kbar and higher SiO_2-activities compared to the Iisalmi-Sukeva area. The exhaustion of quartz during the reaction progress left amphibole partially unconsumed.

Opaque phases such as ilmenite and magnetite are abundant in all types of granulite while biotite occurs as a minor constituent of intermediate granulites only. Accessory apatite is present as tiny euhedral crystals enclosed in plagioclase.

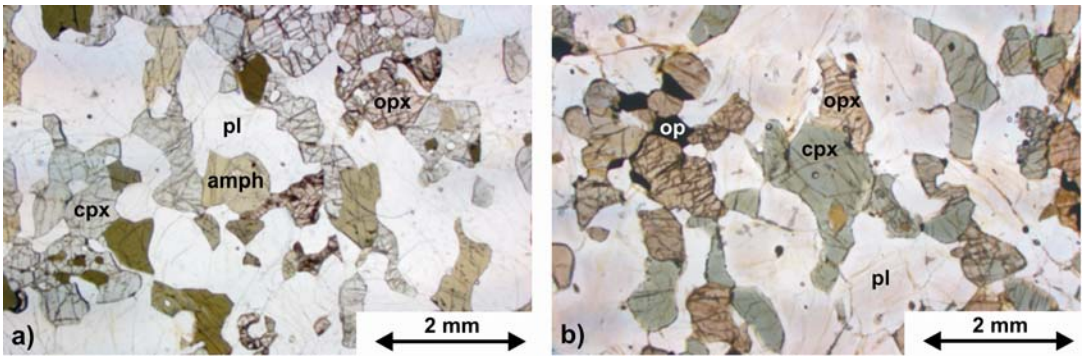

Fig. 3:

Photomicrographs of intermediate opx-cpx-granulites. Fig. 3a shows an amphibole-rich granulite while amphibole is almost completely consumed in Fig. 3b.

Table 1
Modal abundances of minerals in granulites calculated from point counting and least squares regression.

sample	sample type	sample area	amph	cpx	opx	plg	kfs	grt	qtz	mgt	il	bt	total
061M	amphibolite	Pallikäs	68	6	-	24	-	-	-	2	0	-	100
002M2	grt-cpx	Iisalmi - Sukeva	6	43	-	38	-	11	-	1	1	-	100
034M2	grt-cpx	Iisalmi - Sukeva	-	38	-	40	-	20	-	1	1	-	100
036M1*	grt-cpx	Iisalmi - Sukeva	15	33	-	17	-	28	3	1	2	-	99
140M	grt-cpx	Iisalmi - Sukeva	2	50	-	40	-	5	-	2	1	-	100
012M1	grt-cpx	Varpanen	6	19	11	55	-	1	-	4	3	-	99
049M	grt-cpx	Varpanen	14	20	12	38	-	8	1	3	1	2	99
076M1	grt-cpx	Jonsa	22	15	1	35	-	6	15	3	1	1	99
076a	opx-cpx	Jonsa	15	27	13	45	-	-	-	-	-	-	100
080 M	opx-cpx	Jonsa	3	24	12	49	2	-	2	-	1	7	100
112M	opx-cpx	Jonsa	25	20	10	42	-	-	3	-	-	-	100
102a	opx-cpx	Jonsa	30	4	3	59	-	-	3	1	-	-	100
114M	opx-cpx	Jonsa	18	12	8	61	-	-	-	2	-	-	99

* Mass balances for sample 036 M1 were difficult to accomplish due to a high abundance of symplectites and retrograde opx

4. Methods

All geochemical analyses were performed in the laboratories of the Department of Geosciences, Johannes Gutenberg-University, Mainz, Germany. Bulk rock analyses were accomplished for major and a number of trace elements (Cr, Ni, Sc, V) by XRF. All other trace elements were obtained by fusion of rock powder on an Iridium strip heater and analyses of the glasses by LA-ICP-MS. For further explanation of this method see Part I of the thesis, Fedorowich et al. (1993) and Jochum et al. (2005).

Analyses for mineral chemistry were conducted with a JEOL JXA 8900 RL electron microprobe using wavelength dispersive analysis and a range of natural and synthetic standards. The data were corrected using the CITZAF procedure (Armstrong, 1995).

In-situ trace element measurements were performed with an Agilent 7500ce quadrupole ICP-MS coupled with a NewWave Research UP-213 laser ablation unit. The analyses were made using Argon as plasma and carrier gas except for orthopyroxene and plagioclase which were analyzed with a He/Ar mixture. Data acquisition was accomplished in a rapid, peak-jumping mode with one point per peak at 10 ms dwell time. Before each analysis, background measurements were performed for 60 s. Plasma conditions were adjusted to oxide formation rates below 0.5 % (monitored using the 248/232 mass ratio), thus no further oxide corrections were necessary. Either ^{43}Ca or ^{44}Ca were used as internal standards for amphibole, clinopyroxene, garnet, plagioclase and apatite. Si^{29} served as internal standard for orthopyroxene. Certified glass reference material NIST SRM 612 was the external standard and data reduction was carried out using the software “Glitter”. The elemental concentrations of NIST SRM 612 used for standardization were taken from Pearce et al. (1997) except for Zr in NIST SRM 612 for which the preferred values given in the GeoReM database (http://georem.mpch-mainz.gwdg.de/) was used. Instrument performance and stability were monitored by repeated measurements of USGS basaltic reference glass BCR-2G during the analytical sessions. The precision on BCR-2G over the course of this study was better than 10 % for all elements and accuracies are within 5 % except for Zr, Hf and Ni (10 %). Detection limits in the argon mode are lower than 0.05 $\mu g g^{-1}$ except for Sc (0.2 $\mu g g^{-1}$), Cr (1 $\mu g g^{-1}$), Ni (0.2 $\mu g g^{-1}$), V and Ba (0.1 $\mu g g^{-1}$).

5. Sample description and bulk rock geochemistry

Samples numbered 002M2, 034M2, 036M1 and 140M from the Iisalmi-Sukeva area in the NW of the working area are typical grt-cpx-granulites. Sample 036M1 contains discrete grains of prograde brown amphibole while the other samples only contain retrograde green amphibole. Mafic granulite 002M2 is distinct in containing small equally distributed garnet grains instead of large granoblastic ones. Compositionally, grt-cpx-granulites resemble tholeiitic basalts. They have SiO_2 of 48- 49 wt%, CaO-contents between 12 and 17 wt%, a high amount of compatible elements Sc, V, Ni and Cr and exibit LREE depletion (Table 2, Fig. 4).

The Varpanen area (Fig. 1) comprises both grt-cpx-granulites as well as opx-cpx-granulites. Two grt-cpx-granulites from this area (012M1 and 049M) were studied. They closely resemble the Iisalmi-Sukeva granulites but are slightly richer in SiO_2 and Na_2O and poorer in CaO. Both samples have higher absolute REE abundance than the Iisalmi-Sukeva samples (Fig. 4).

Intermediate opx-cpx-granulites are typical for the Jonsa area in the SE of the working area. Three samples were taken from granulite patches within diatexite (080M, 102a, 114M) and two further samples stem from coarse grained, several metres wide granulite bodies (076a, 112M). Sample 080M contains biotite while amphibole is rare. Sample 114M has a SiO_2-content close to 60 wt% which was most likely raised by infiltration of melt into the granulite patch. The same may hold true for sample 102a since both were taken from similar settings. The intermediate granulites characteristically have low contents of compatible elements. They are LREE enriched with $(La/Yb)_N$ between 3.5 and 6 (Fig. 4). The LREE enrichment as well as negative Nb-Ta and Zr-Hf anomalies suggest that intermediate granulites have arc-related precursor rocks.

One garnet-bearing sample (076M1) was collected in the Jonsa area. The skeletal garnet from this sample is intergrown with plagioclase and quartz suggesting growth in a melt-rich environment. This is also suggested by prevailing amphibole that could resulting from back-reaction between hydrous melt and pyroxenes. The sample is LREE-enriched and has very low Cr and Ni contents.

Additionally, an amphibolite (061M) was collected in order to provide constraints on mineral compositions prior to partial melting. The amphibolite comprises amph-cpx-pl with clinopyroxene being much less abundant than amphibole. The amphibolite has similar major elements as well as Cr and Ni contents to mafic granulites from the Iisalmi-Sukeva area. Nevertheless the REE pattern is closer to the LREE enriched patterns of most intermediate granulites.

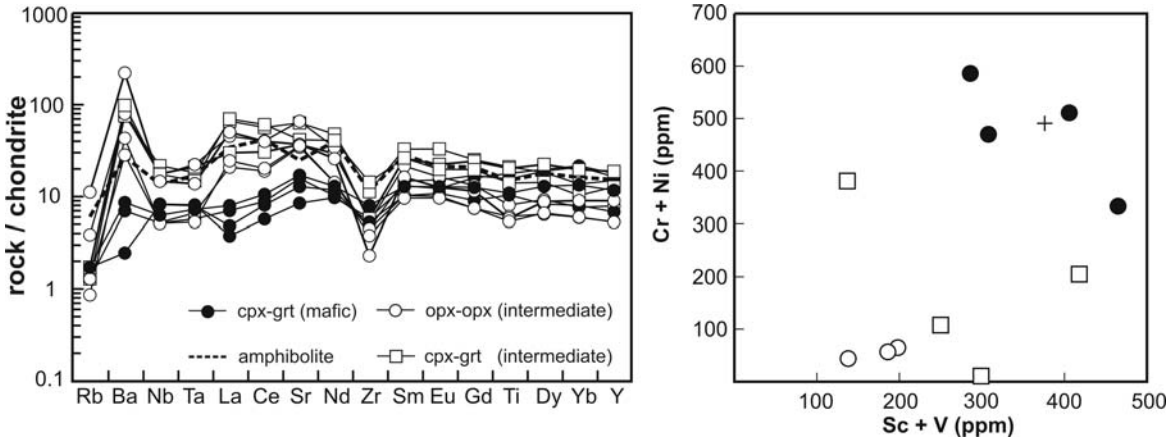

Fig. 4:

Bulk rock trace element pattern. Note the clear distinction between intermediate granulites and mafic granulites. LREE-enrichment, negative Nb-Ta anomalies and low contents of compatible elements in intermediate granulites could be related to an arc-setting of the precursor rocks. Contrasting with this are the geochemical features of mafic granulites which resemble tholeiitic basalts.

6. Mineral chemistry

6.1 Amphibole

Only amphibole inferred to be prograde was analysed and analyses were recalculated after Leake et al. (1997). Amphiboles are ferropargasitic, pargasitic and edenitic in composition with only minor in-sample variation (Appendix A). An exception is sample 036M1 where amphibole enclosed in garnet has higher X_{Mg} than larger amphibole grains lacking contact with garnet. Compared to amphibole in thick granulite bodies with low K_2O (0.64-0.85 wt%) contents, amphibole from granulite patches within diatexite (080M, 102a, 114M) are enriched in K_2O (1.5-1.8 wt%) due to equilibration of the amphibole with a melt-rich environment. The lowest K_2O contents in amphibole are found in mafic granulite 036M1 (~0.4 wt%). If amphibole is present in the samples it is the major bearer of trace elements (Appendix B) and bulk rock trace element pattern is usually mirrored by the amphibole pattern. The REE pattern are rather flat with obvious LREE depletion in sample 036M1 and 034M2 (Fig. 5c-d) and slight LREE enrichment in intermediate granulites (Fig. 6-7). HREE depletion occurs in amphibole enclosed in garnet (Fig. 5c) and in amphibole from garnet-bearing sample 076M1 (Fig. 6d). REE are markedly enriched and a strong negative Eu-anomaly appears in amphibole from granulite patches in diatexite outcrops (Fig. 7c-e).

Table 2:
Bulk rock major-oxide and trace element data for studied samples (values in italics by XRF, other trace elements by LA-ICP-MS). Additionally, the composition of a leucosome from outcrop 036 is given, which was used in the calculations of mineral / melt partition coefficients.

	amphi-bolite	grt-cpx-granulites (Iisalmi – Sukeva)				grt-cpx- gran. (Varpanen)		opx-cpx-(grt)- granulites (Jonsa)					leuco-some
	061M	002M2	034M2	036M1	140M	012M1	049M	076M1	076a	080M	112M	114M	036L2
SiO_2	45.8	48.1	49.2	48.4	48.4	50.3	49.5	55.7	52.4	55.0	52.1	60.0	75.1
TiO_2	1.11	0.81	1.15	1.32	0.77	1.56	1.50	1.04	0.45	0.43	0.40	0.60	0.03
Al_2O_3	14.6	15.6	15.8	13.7	14.9	16.1	13.1	13.6	15.7	15.0	15.9	17.3	14.8
Fe_2O_3*	15.0	11.5	12.9	16.0	10.9	11.8	17.1	13.7	9.0	9.1	8.5	6.1	0.33
MnO	0.21	0.31	0.32	0.25	0.22	0.18	0.23	0.17	0.16	0.16	0.15	0.09	0.01
MgO	8.41	5.23	5.43	8.8	6.54	5.53	6.47	3.78	7.98	6.17	7.62	3.1	0.07
CaO	10.9	15.2	12.8	11.7	16.8	9.56	8.59	8.00	11.7	8.50	11.7	6.77	4.24
Na_2O	2.59	2.14	1.8	1.23	1.46	3.55	2.99	2.93	2.46	3.75	3.03	4.73	4.15
K_2O	0.87	0.11	0.09	0.09	0.05	0.24	0.62	0.7	0.26	1.25	0.30	1.06	0.42
P_2O_5	0.10	0.04	0.04	0.07	0.04	0.39	0.12	0.12	0.04	0.05	0.07	0.13	b.d.
total	99.3	99.0	99.5	101.6	100.1	98.7	100.1	99.6	100.1	99.4	99.7	99.7	99.2
Sc	*51*	*45*	*53*	*60*	*43*	*32*	*48*	*36*	*37*	*22*	*35*	*13*	8
V	*325*	*263*	*353*	*405*	*243*	*218*	*370*	*263*	*161*	*115*	*151*	*125*	83
Cr	*344*	*294*	*338*	*221*	*397*	*37*	*130*	*b.d.*	*16*	*228*	*7*	*18*	78
Ni	*147*	*176*	*173*	*112*	*189*	*71*	*75*	*11*	*49*	*153*	*50*	*26*	41
Rb	12.5	1.02	1.46	1.11	0.67	0.40	1.99	1.01	0.42	25.3	0.89	5.77	6.00
Sr	188	131	100	59	116	444	262	309	268	282	271	467	342
Y	24.2	18.5	26.1	28.3	10.8	23.7	29.8	20.2	8.45	14.3	8.39	12.6	10.0
Zr	44.7	30.9	17.7	22.5	20.4	43.7	22.3	55.1	17.2	8.90	14.6	20.2	292
Nb	3.30	1.52	1.98	2.01	1.26	5.24	4.28	4.24	1.27	3.55	1.25	4.16	6.90
Ba	71.1	27.5	18.6	7.88	13.6	194	218	233	58.2	452	91.6	174	239
La	8.20	1.91	1.15	0.90	1.69	15.8	7.16	16.7	4.99	12.0	5.85	10.8	22.8
Ce	25.8	6.55	5.01	3.54	5.48	35.0	19.0	37.5	11.7	24.7	12.5	25.0	52.2
Pr	3.90	1.11	0.86	0.71	0.88	4.70	2.76	4.56	1.56	3.04	1.60	3.56	6.68
Nd	18.3	5.96	5.43	4.48	4.71	22.0	13.5	18.8	6.55	11.1	6.58	15.8	26.0
Sm	4.20	1.91	2.20	1.96	1.53	4.90	3.88	3.92	1.53	2.43	1.44	3.20	4.67
Eu	1.20	0.73	0.86	0.69	0.61	1.87	1.26	1.12	0.57	0.71	0.55	0.93	1.06
Gd	4.21	2.52	3.40	3.20	1.82	5.05	4.86	3.95	1.50	2.31	1.50	2.66	3.60
Dy	4.44	3.21	4.68	4.90	2.06	4.55	5.56	3.54	1.60	2.20	1.65	2.30	1.83
Er	2.66	2.11	3.27	3.30	1.20	2.47	3.38	1.93	0.95	1.31	0.92	1.29	0.710
Yb	2.64	2.17	3.40	3.51	1.31	2.23	3.20	1.67	0.97	1.47	0.98	1.24	0.560
Lu	0.38	0.33	0.52	0.52	0.18	0.33	0.47	0.24	0.16	0.22	0.14	0.19	0.090
Hf	1.53	1.03	0.80	0.86	0.69	1.12	1.20	1.66	0.68	0.37	0.66	0.78	8.23
Ta	0.23	0.10	0.11	0.11	0.08	0.25	0.29	0.20	0.09	0.19	0.07	0.31	0.250
Th	0.76	0.01	0.01	0.03	0.10	0.08	0.10	0.13	0.05	0.27	0.07	0.37	n.a.
U	0.89	0.01	0.01	0.02	0.10	0.03	0.03	0.05	0.05	0.04	0.03	0.24	n.a.

* - sample 076M1 is the only grt-bearing sample from the Jonsa area

Amphibole in the mafic granulite 036M1 has very low Ba, Rb and Sr contents of <14ppm, <4ppm and 20-40 ppm respectively (Appendix B). High Ba and Sr in amphibole are observed in garnet-bearing samples 012M1, 076M1 and 049M while enrichment of Rb occurs in amphibole from samples 080M, 102a and 114M. In the amphibole from amphibolite 061M the highest Rb-contents found (~14 ppm) correlate with high Th and U contents.

The variability of Cr, Ni, Sc and V contents in amphibole from the different settings is attributed to the different petrologic origin of the precursor rocks. Amphibole is the major Nb and Ta hosting phase besides ilmenite and rarely occurring biotite.

6.2 Clinopyroxene

Clinopyroxene is mainly augite and diopside with X_{Mg} between 0.6-0.8 (Appendix A). No systematic variation in X_{Mg} between mafic and intermediate granulites was observed.

Clinopyroxene REE patterns are very similar to those of amphibole in the same sample but the absolute amount of REE is about 2-4 times lower (Fig. 5-7). A similar distribution between amphibole and clinopyroxene is also observed for V, Cr, Ni, Sr, Y, Th and U. Contents of Sc, Zr and Hf are equal in amphibole and clinopyroxene but contents of Rb, Ba, Nb and Ta are much lower in clinopyroxene (Appendix B, Fig. 7f-k). Due to the low abundance or even absence of amphibole in grt-cpx-granulites, clinopyroxene is the major REE-hosting phase in these rocks.

Clinopyroxene has very homogeneous major element composition but trace elements exhibit some varieties. Clinopyroxene intergrown with large garnet porphyroblasts exhibit depletion from Gd to Lu while clinopyroxene in the matrix further away from the porphyroblasts have flat HREE patterns (Fig. 5b-c, Fig. 6b-c). All analysed clinopyroxene is HREE depleted within samples 002M2 (Fig. 5a) and 140M (Fig. 5d). The HREE-distribution between clinopyroxene and garnet suggest that although full homogenization of the major elements was achieved under granulite facies conditions the HREE failed to equilibrate probably because of slow intergranular diffusion.

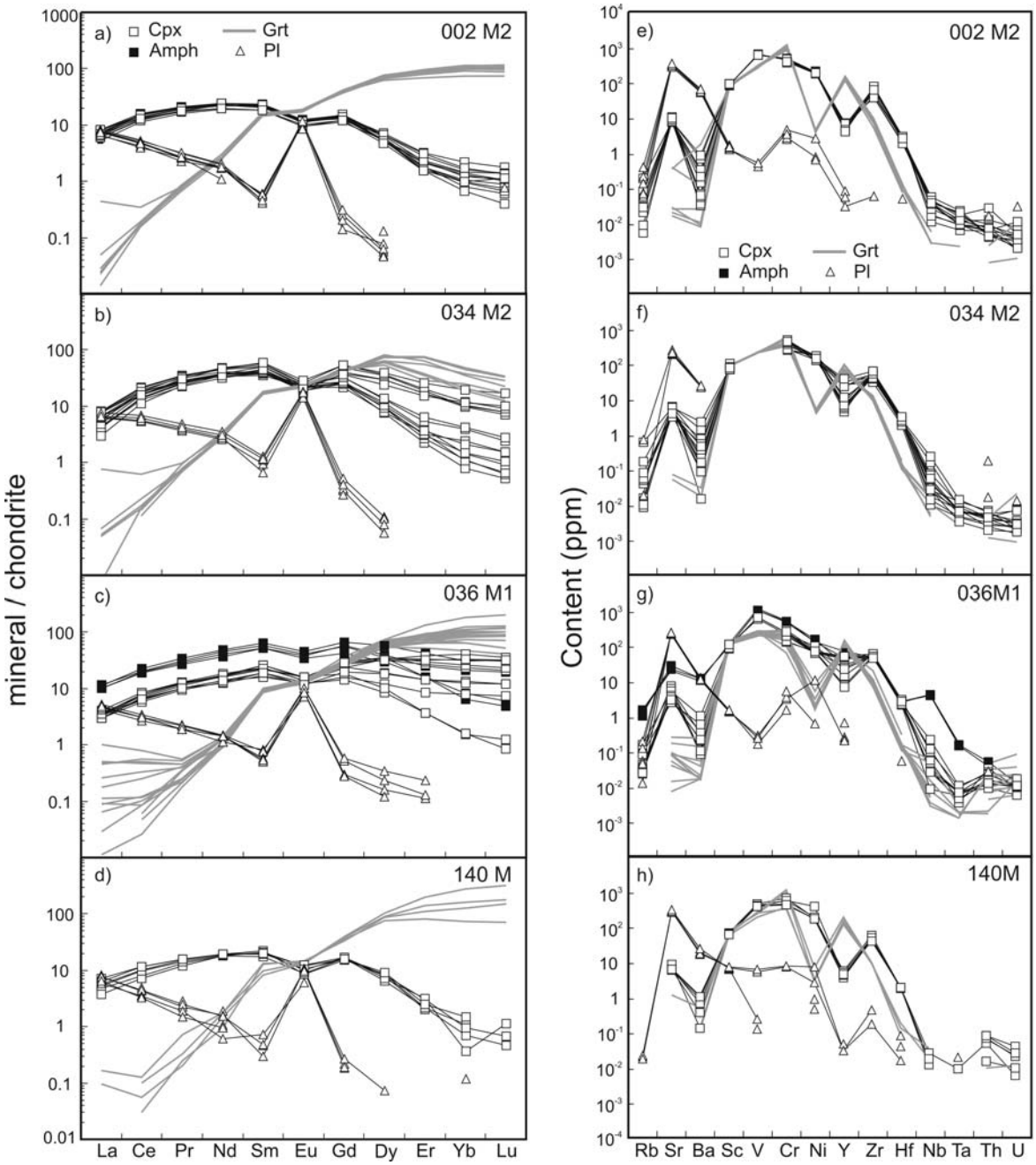

Fig. 5:

Trace element patterns of mineral phases from mafic granulites. REE-pattern on the left hand site are normalized to chondrite while multi-element patterns on the right side display the the concentration of trace elements in ppm. Note the variability of HREE contents in cpx and amphibole associated with garnet.

Symbols: filled squares – amphibole, white squares – cpx, triangles – plagioclase, grey lines - garnet

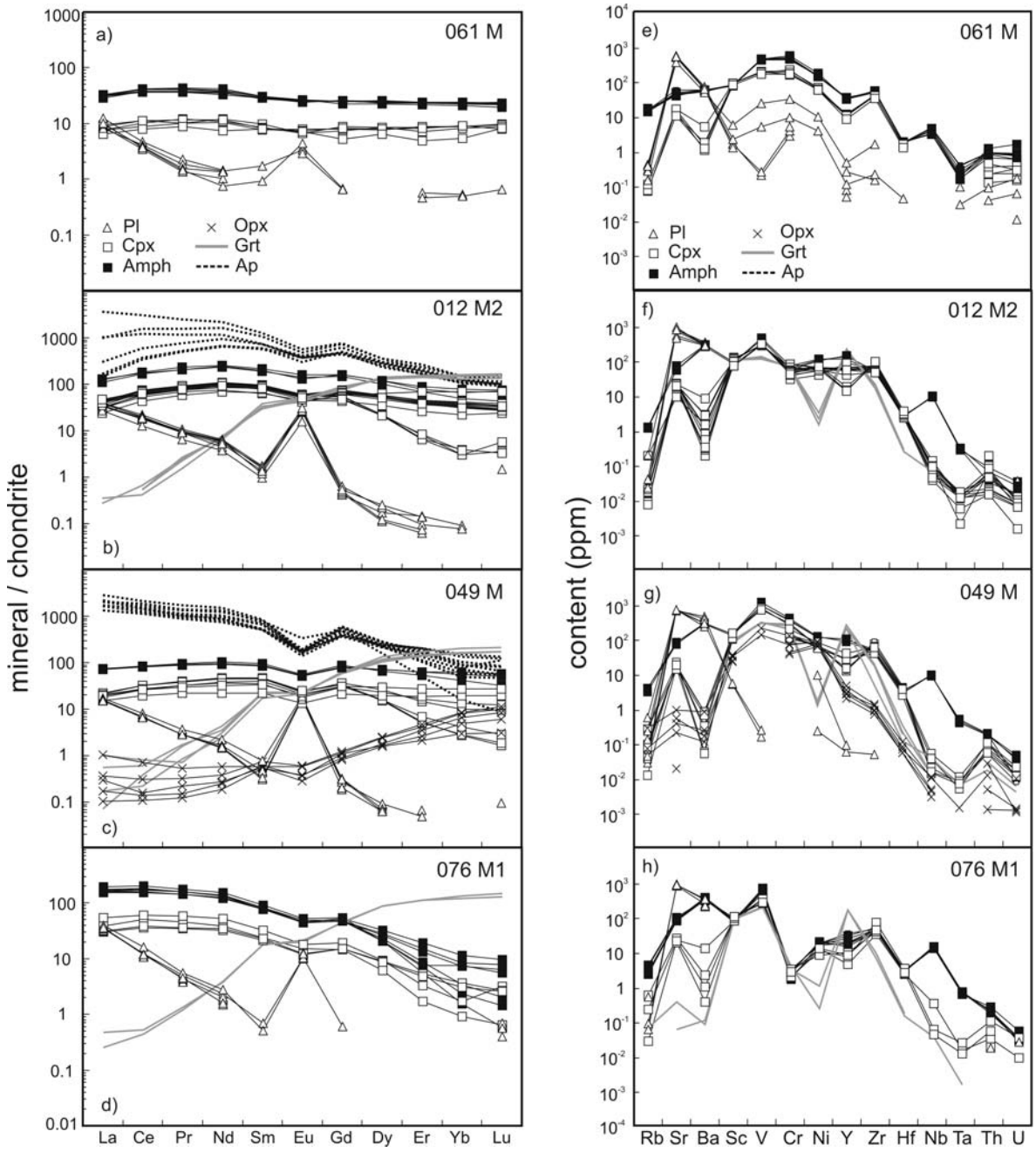

Fig. 6:

Trace element patterns of mineral phases from the amphibolite and intermediate, garnet-bearing granulites. Note the high abundance of REE in apatite in samples 012M2 and 049M.

Symbols: filled squares – amphibole, white squares – clinopyroxene, triangles – plagioclase, grey lines – garnet, crosses – orthopyroxene, stippled lines - apatite

6.3 Orthopyroxene

Orthopyroxene has X_{Mg} of 0.5-0.7. Its overall low contents of trace elements (Appendix B) suggests limited control of orthopyroxene on the bulk partitioning except for the transition metals. REE contents in opx increase with increasing atomic number but even HREE contents are not higher than 10 times the chondritic value. (Fig. 7a-e).

6.4 Garnet

Garnet has X_{Alm} 0.5-0.62, X_{Prp} 0.13-0.33 and X_{Grs} 0.15-0.28. REE contents in garnet strongly increase with atomic number (Appendix B) except for garnet in sample 034M2 which exhibits decreasing contents of HREE from Dy to Lu. While the MREE contents are consistent within one sample, LREE as well as HREE exhibit some variations. The LREE are commonly below detection limits but sample 036M1 shows that especially La and Ce contents can be quite variable (Fig. 5). This likely reflects the remaining influence of the mineral which garnet has replaced (amph, plg, cpx) and is a further indication that the REE did not fully equilibrate between garnet and the surrounding matrix. In addition to the strong influence on the HREE, garnet contributes significantly to the Sc, V, Cr and Y budget (Fig. 5e-h).

6.5 Plagioclase

Plagioclase exhibits more variation in the major element composition than the other minerals. Plagioclase in mafic granulites from the Iisalmi-Sukeva area has X_{An} 0.53-0.7 in correspondence to the CaO-rich bulk composition. Plagioclase from the two wide granulite bodies in the Jonsa area have X_{An} of 0.47-0.53 while otherwise plagioclase has X_{An} of 0.26-0.33. The most sodic plagioclase occurs in granulite patches within diatexite. It is possible that the plagioclase within these samples experienced addition of alkalies from the melt-rich host as is also suggested by elevated K_2O contents of the amphibole from these samples.

Plagioclase is strongly enriched in Sr and also contains high amounts of Ba (Appendix B). The LREE exhibit little variation within one sample indicating a close approach to equilibrium. They are strongly fractionated with La_N / Sm_N between 10 and 60 and a prominent positive Eu-anomaly is developed in all samples (Fig. 5-7). HREE contents in plagioclase commonly lie below the detection limits.

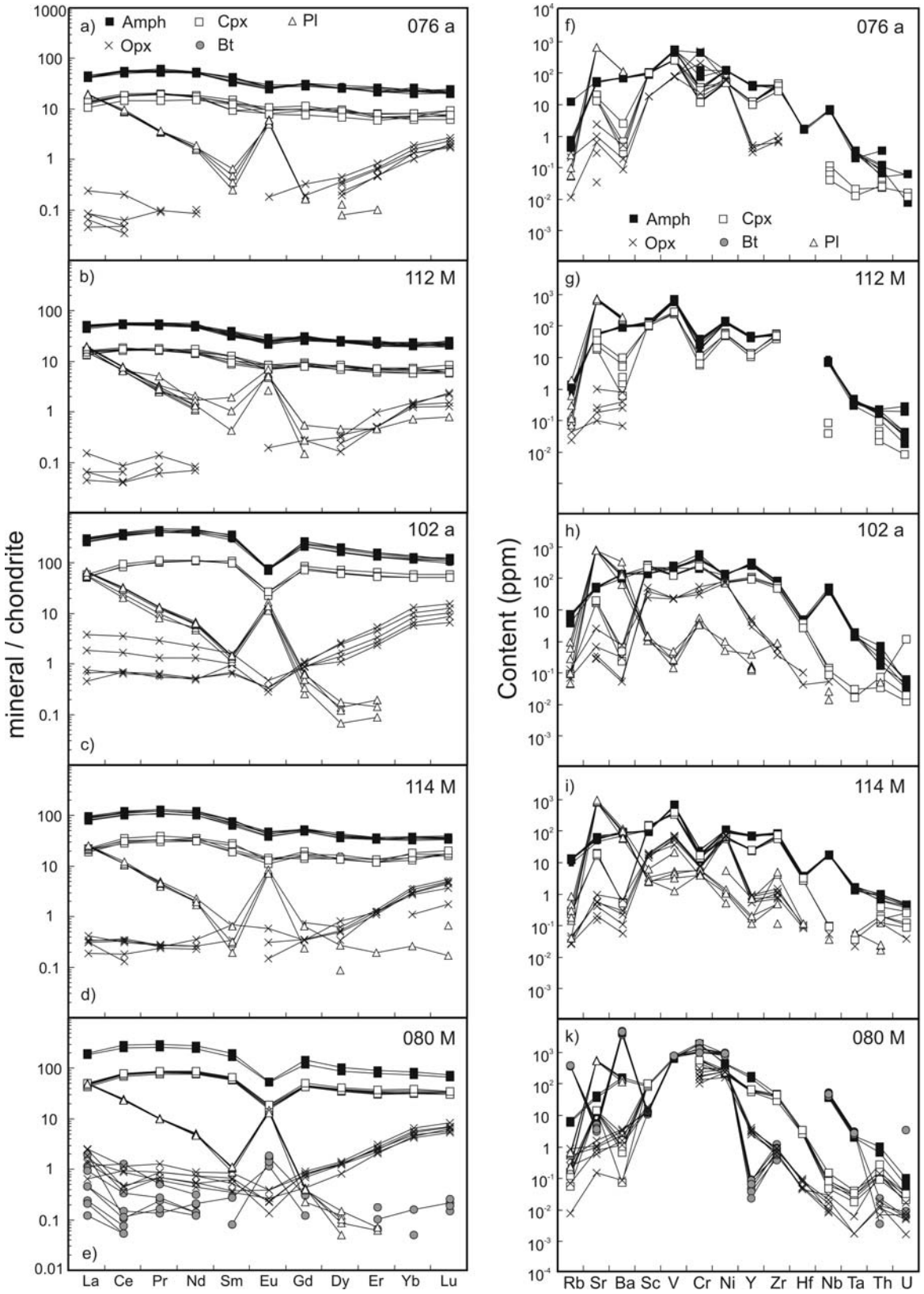
a) Amph Cpx Pl
Opx Bt
076 a
b)
112 M
102 a
c)
114 M
d)
080 M
e)
mineral / chondrite
La Ce Pr Nd Sm Eu Gd Dy Er Yb Lu
f)
076 a
Amph Cpx
Opx Bt Pl
g)
112 M
h)
102 a
i)
114 M
k)
080 M
Content (ppm)
Rb Sr Ba Sc V Cr Ni Y Zr Hf Nb Ta Th U

Fig. 7

Fig. 7 (previous page):

Trace element patterns of mineral phases from opx-cpx-granulites. Note the enrichment of REE and negative Eu-anomalies in samples 102a and 080M (granulite patches in diatexite).

Symbols: filled squares – amphibole, white squares – clinopyroxene, triangles – plagioclase, grey circles – biotite, crosses – orthopyroxene,

6.6 Biotite

Biotite occurs as well developed needles and tabular grains in sample 080M. It is also present but much less common in sample 102a. X_{Mg} of biotite in sample 080M is 0.55-0.58 and slightly higher in sample 102a with 0.57-0.60. Due to grain size biotite was analyzed by LA-ICP-MS in sample 080M only. Biotite has no function in controlling the REE in the specific sample (Fig. 7e). Still it contributes significantly to the V, Cr, Ni, Nb and Ta budget and controls the behaviour of Rb and Ba (Fig. 7k) in the specific sample.

6.7 Ilmenite and magnetite

Oxide phases are abundant in all groups of granulites. Ilmenite and magnetite occur together as irregularly formed blebs with rounded grain boundaries. Broad lamellae of ilmenite in magnetite are observed in sample 076M1 suggesting exsolution of the phases upon cooling. Oxides were analysed by EPMA in several samples but grains large enough for analysis by LA-ICP-MS were only found in samples 012M1, 036M1 and 140M.

Ilmenite consist of 50-53 wt% TiO_2, 45-48 wt% FeO (Appendix A) and contains less than 1 wt% MgO and MnO. The TiO_2 content of magnetite is <0.5 wt%. Both minerals contain significant amounts of V, Cr and Ni but only ilmenite shows affinity towards the High Field Strength Elements (HFSE) and incorporates Sc, Nb, Ta as well as small amounts of Zr (Appendix B, Fig. 8). Nb and Ta contents are at least one order of magnitude higher than contents in amphibole and biotite. This implies that ilmenite significantly influences the Nb and Ta budget.

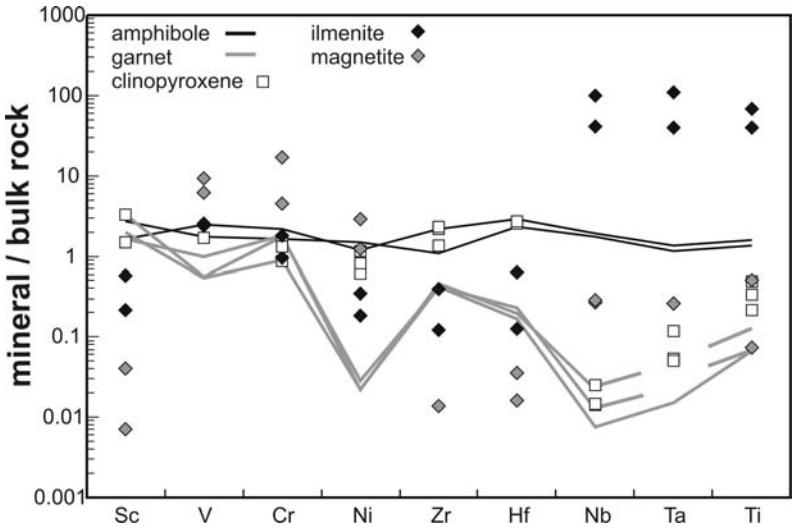

Fig. 8:

Comparison of trace element contents in ilmenite and magnetite to contents in major mineral phases. Only samples in which ilmenite and magnetite were analysed are displayed (012M2, 036M1 and 140M). Nb and Ta are strongly enriched in ilmenite while V, Cr and Ni show preference for magnetite.

6.8 Apatite

Apatite occurs as small euhedral crystals enclosed in plagioclase and along grain boundaries between plagioclase and other minerals. Apatite grains are larger and more abundant in granulites from the Varpanen and Jonsa area than in mafic granulites from the Iisalmi-Sukeva area which is in agreement with higher bulk rock P_2O_5 contents (Table 2). Due to the small grain size apatites were only analysed in samples 012M1 and 049M. Apatites from both samples show only small variation in major elements with CaO 54-56 wt% and P_2O_5 40-42 wt%. Halogen contents are made up exclusively of fluorine (~3 wt%) in sample 049M while sample 012M1 contains 0.4-0.8 wt% chlorine in addition to ~2 wt% fluorine. The sum of Si and Na makes up less than 0.1 apfu which indicates limited amount of substitution on the Ca-site in apatite. LA-ICP-MS analyses showed that LREE and MREE as well as Th and U are strongly incorporated in apatite (Appendix B , Fig. 6b-c). Sample 012M1 shows increasing compatibility of Nd, Sm and Gd compared to La and Ce while within sample 049M the chondrite-normalized pattern slightly decreases from La to Sm. Both samples exhibit negative Eu-anomalies which is more pronounced in sample 049M.

7. Discussion

7.1 Mass balance calculations

Mass balance calculations were accomplished in order to see whether the trace element budget of the samples is hosted by the major mineral phases alone or if accessory phases contribute significantly to the trace element budget. Villaseca et al. (2003) observed that accessory phases are sparse in lower crustal granulites and that major phases incorporate high amounts of trace elements. They proposed a major redistribution of trace elements between accessory and major mineral phases during lower crustal granulite facies metamorphism. Contrasting with this is the concentration of trace element-bearing accessory minerals in residual material (melanosomes) during the upper-amphibolite facies as described in Watt et al. (1996).

Modal mineralogy of the samples (Table 1) has been estimated from point counting as well as from least squares calculations based on the major element composition of the bulk rock and the respective mineral composition obtained by microprobe analysis. Point counting either overestimates or underestimates the amount of garnet in mafic granulites because of the presence or absence of large granoblastic garnet grains within a thin section. Results from the least squares method are considered as more reliable for this rock type. The addition of quartz is necessary for granulite patches within diatexite (114M, 080M) and sample 076M1 where some leucosome may not have been totally separated from the bulk rock sample.

Mass balance considerations also indicated that all REE-enriched samples require the presence of an additional REE-rich phase. Apatite is an important carrier of the REE and it has been observed especially in intermediate granulites. About 0.8 wt% apatite is sufficient to fulfill mass balances for the REE in intermediate granulites. The concentrations of V, Cr and Ni strongly depend on amount and composition of magnetite and ilmenite. Ni is often underestimated by up to 50 %. This suggest that Ni may be hosted in an additional phase such as pyrite or chalcopyrite which have been detected but not analyzed in most of the samples.

7.2 Rare earth element partitioning between coexisting minerals and melt

7.2.1 Amphibole / Clinopyroxene REE-partitioning

The trivalent REE partition in the crystal-chemically analogous 8-fold M4-site in amphibole and the M2-site in clinopyroxene where they substitute for Ca (Bottazzi et al., 1999). HREE-contents of amphibole and clinopyroxene within grt-bearing samples are variable. Pairs of amphibole and

clinopyroxene were chosen that were not affected by the presence of garnet for the calculation of $D^{amph/cpx}$. Observed $D_{REE}^{amph/cpx}$ are 2-5 using mineral pairs that are in textural equilibrium with one another (Fig. 9). This is in accordance with $D_{REE}^{amph/cpx}$ found by Schröter (2006) in a granulite facies mafic sill from East Antarctica and with values reported by Storkey et al. (2005) from a metabasite of the Arunta block, Australia. Pride & Mücke (1981) reported $D_{REE}^{amph/cpx} \sim 2$ for granulites from the Scourian Complex in Scotland. $D_{REE}^{amph/cpx} > 3$ have also been reported by Witt-Eickschen & Harte (1994) for peridotite xenoliths from the East-Eifel.

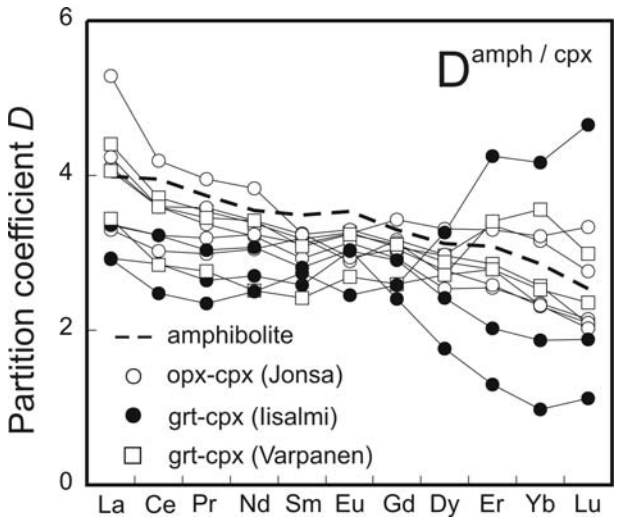

Fig. 9:
REE partition coefficients between amphibole and clinopyroxene. $D^{amph/cpx}$ is larger than 2 for all samples.

In contrast, $D_{REE}^{amph/cpx} \sim 1$ was reported from xenoliths of pyroxenite (Zack et al., 1997), hornblendite (Orejana, et al. 2006), lherzolite (Chazot et al., 1996) and peridotite (Ionov & Hofmann, 1995, Glaser et al., 1999). Witt-Eickschen & Harte (1994) claim that incorporation of the REE into clinopyroxene increases as its Na-content increases because of a more flexible behaviour of the M2-site at higher Na-contents. In addition, Hill et al. (2000) observed a positive correlation between the incorporation of the HFSE and – to a lesser extend – of the REE into clinopyroxene with increasing CaTs-component in clinopyroxene. Clinopyroxene from the Finnish granulites characteristically has lower jadeite component as well as lower CaTs-component compared to clinopyroxenes for which $D_{REE}^{amph/cpx} \sim 1$ was reported (Fig. 10) and both may contribute to low incorporation of the REE into clinopyroxene.

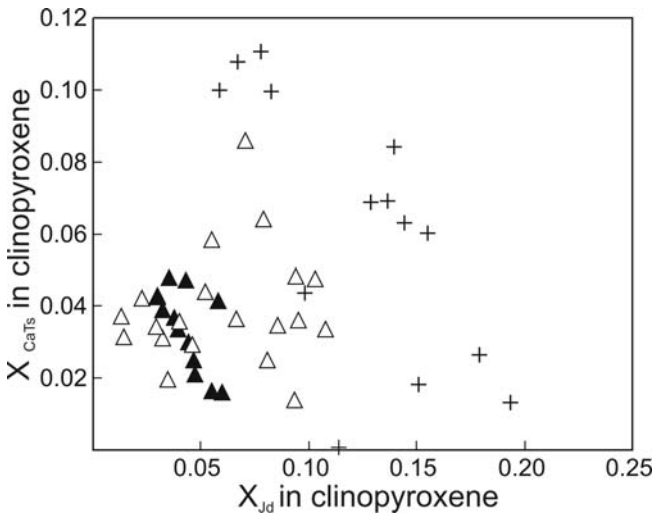

Fig. 10:
CaTs and Jd components in clinopyroxene calculated after Cawthorn & Collerson (1974). Crosses are for clinopyroxenes for which $D_{REE}^{amph/cpx} \sim 1$ have been reported (see text for references). Triangles are for clinopyroxenes with $D_{REE}^{amph/cpx} > 1$ (black triangles – this study, white triangles – literature, see text). REE partitioning into clinopyroxene seems to be favoured by high Jd and high CaTs components.

Klein et al. (1997), as well as Witt-Eickschen & Harte (1994), observed constant $D_{REE}^{amph/cpx}$ for all REE. In this study a constant $D_{REE}^{amph/cpx}$ of ~3 was only found in the two opx-cpx-granulite bodies from the Jonsa area (samples 076a and 112M). Within the other samples $D_{REE}^{amph/cpx}$ decreases between La and Lu from >4 to 2 (Fig. 9) which may indicate slightly increased compatibility of the LREE in amphibole compared to clinopyroxene.

Granulites from the working area are migmatitic and depleted in incompatible elements, suggesting that they experienced melt extraction during granulite facies metamorphism. It is therefore appealing to calculate $D_{REE}^{cpx/melt}$ using the predictive model for crystal-melt partitioning developed by Blundy & Wood (1994). The model was refined by Wood & Blundy (1997) for the REE-partitioning between clinopyroxene and anhydrous silicate melt incorporating pressure and temperature as well as compositional effects. The equations given in Wood & Blundy (1997) yield reasonable results for the optimum radius of the REE-hosting lattice site $r_0^{3+} = 1.03$ Å and for the Young's modulus $E_x^{3+} = 284$ GPa at 900°C and 10 kbar. On the contrary, the calculations for the strain free partition coefficient (D_0^{3+}) for the REE hosting site yield values between 2 and 3 which are high compared to experimentally derived D_0^{3+} in similar systems that range between 0.6 and 2 (Green & Pearson, 1985, Hill et al., 2000, Klein et al., 2000, Barth et al., 2002). Using the calculated D_0^{3+} would result in high $D_{REE}^{cpx/melt}$ and even higher $D_{REE}^{amph/melt}$ because the partitioning between amphibole and clinopyroxene is $D_{REE}^{amph/cpx} \sim 3$. The overestimation of D_0^{3+} in clinopyroxene could be due to the effect of H_2O on crystal-melt partitioning of trace elements

(Wood & Blundy, 2002) since the presence of H_2O suppresses the activities of all other components in the melt. The immediate melts produced by amphibole-dehydration melting are hydrous as is also inferred by back-reaction along leucosomes. If the corrections for melt H_2O-contents given in Wood & Blundy (2002) are used, about 6 wt% H_2O in the melt are required to suppress the mean calculated anhydrous $D_0^{3+} \sim 2.6$ to a value of 1.3 which is in better accordance with experimental data. This is in agreement with melt H_2O-contents between 3-10 wt% observed in dehydration melting experiments of amphibolites (Beard & Lofgren, 1991, Sen & Dunn, 1994, Patiño Douce & Beard, 1995). However, firm constraints on H_2O-contents of melts from the Finnish granulites are lacking and therefore the experimentally derived $D_0^{cpx} = 1.05$ from Klein et al. (2000) was used for the calculation of D_i. Thereby calculated $D_{REE}^{cpx/melt}$ are higher than published values for clinopyroxene in equilibrium with basaltic melts (Hauri et al., 1994, Hart & Dunn, 1993) but smaller than values from Barth et al. (2002) for eclogitic minerals in equilibrium with tonalitic melt (Fig. 11a). They are in accordance with elemental ratios calculated from clinopyroxene and some very rarely occurring tonalitic leucosomes with fractionated REE-pattern close to what could be expected from melting of garnet-bearing mafic source rocks (Martin, 1994). Such leucosomes allow direct determination of $D_{REE}^{cpx/melt}$ by using the observed mean $D_{Eu}^{cpx/melt} = 0.74$ for the estimation of D_0^{3+}. A lower $D_0^{3+} = 0.86$ and therefore also slightly decreased $D_{REE}^{cpx/melt}$ are obtained by this calculation (Table 4).

$D_{REE}^{amph/melt}$ may be calculated by using the lattice site parameters for amphibole given in Klein et al. (1997). In their experiments D_0^{3+} in amphibole decreases from 2.66 at 800°C to 1.7 at 900°C. The higher D_0^{amph} is more likely to apply for our dataset since it yields better consistence with our observation that $D_{REE}^{amph/melt} \sim 3 \times D_{REE}^{cpx/melt}$ (Table 4). By applying this formulation good agreement with $D_{REE}^{amph/melt}$ from low temperature experiments with andesitic-tonalitic melt composition (Nicholls & Harris, 1980, Sisson, 1994, Klein et al., 1997, Hilyard et al., 2000) was obtained (Fig. 11b).

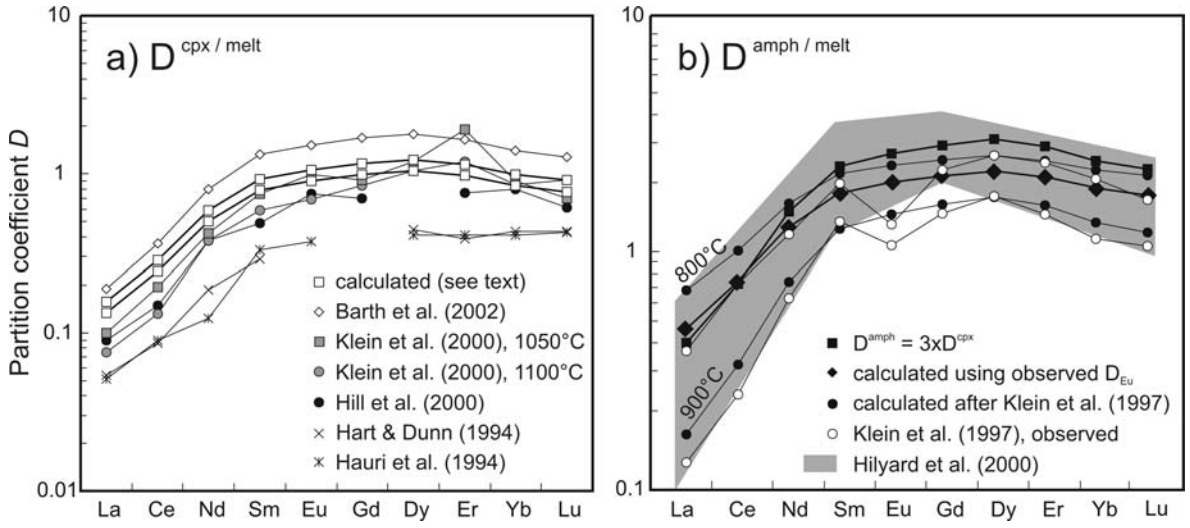

Fig. 11:

REE mineral melt partition coefficients constrained for clinopyroxene and amphibole. Calculated $D_{REE}^{cpx/melt}$ were derived by applying the predictive model of Wood & Blundy (1997). The lower calculated $D_{REE}^{cpx/melt}$ (Fig. 11a) are obtained by using the observed Eu-partitioning between clinopyroxene and a leucosome from outcrop 036. Values for tonalitic melts (Barth et al., 2002, Klein et al., 2000), andesitic melts (Hill et al., 2000) and basaltic melts (Hart & Dunn, 1994, Hauri et al., 1994) are given for comparison. $D_{REE}^{amph/melt}$ calculated as $3xD_{REE}^{cpx/melt}$ (Fig. 11b) yields values comparable to the low temperature (800°C) experiments from Klein et al. (1997). Calculations using $D_{Eu}^{cpx/melt}$ as a proxy for D_0^{3+} as well as E_X^{3+} and r_0^{3+} from Klein et al. (1997) gives values intermediate between the 800°C and 900°C experiments and are consistent with values from Hilyard et al. (2000) experimentally derived at 900-940°C and 2-5 kbar.

7.2.2 Garnet / Clinopyroxene REE-partitioning

Mineral / melt partition coefficients for garnet and other minerals can be obtained by using the observed trace element ratios between a given mineral and clinopyroxene the same way as for the calculation of $D_{REE}^{amph/melt}$. This approach can easily be adopted for two garnet-bearing mafic granulites which show coherent REE concentrations in clinopyroxene and garnet throughout the sample (samples 002M2 and 140M). Within the other garnet-bearing samples clinopyroxene and amphibole enclosed in garnet or intergrown with garnet have lower HREE concentration than matrix clinopyroxene (Fig. 12a). $D_{HREE}^{grt/cpx}$ therefore varies over an order of magnitude in some

samples as shown for instance by sample 049M with $D_{HREE}^{grt/cpx}$ between 8-85. The most plausible explanation for the variation of $D_{HREE}^{grt/cpx}$ within one sample and between different samples is a lack of equilibrium between garnet and the bulk matrix. Garnet probably started to grow late after most of the clinopyroxene already formed. Slow diffusion of REE through the matrix (Skora et al., 2006) may have prevented equilibration so that garnet only seized REE from its immediate surrounding. The well equilibrated assemblage in sample 002M2 may have been favoured by small but equally distributed garnet grains.

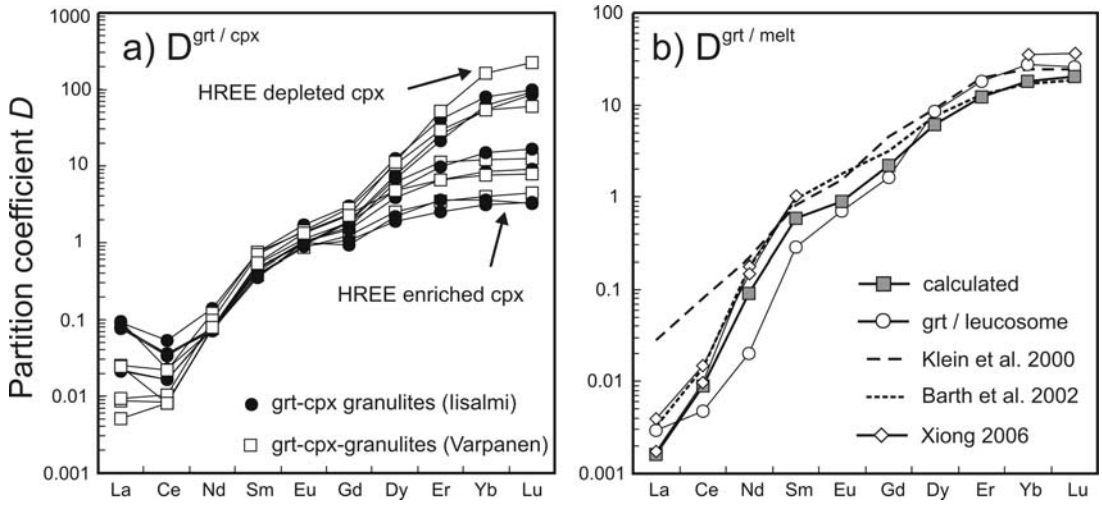

Fig. 12:

REE partitioning between garnet and clinopyroxene (Fig. 12a) are diverse due to the variation in HREE contents of clinopyroxene enclosed in garnet. Therefore, $D_{REE}^{grt/melt}$ were not calculated using the grt / cpx ratio. Instead, $D_{Eu}^{grt/melt} = 0.9$ from the garnet / leucosome ratio together with E_X^{3+}=570 GPa and $r_0^{3+} = 0.95$ Å calculated according to van Westrenen et al. (2000) were applied for the derivation of $D_{REE}^{grt/melt}$. Experimental $D_{REE}^{grt/melt}$ for tonalitic melts given by Klein et al. (2000) for 900°C and 15 kbar, by Barth et al. (2002) for 1000-1040°C and 18 kbar and Xiong (2006) for 900-1100°C and 10-20 kbar are plotted for comparison (Fig. 12b).

As a consequence of the variable $D_{HREE}^{grt/cpx}$, $D_{REE}^{grt/melt}$ calculated from $D_{REE}^{cpx/melt}$ also varies widely. Samples 002M2 and 140M, with an overall depletion of HREE in clinopyroxene, yield $D_{Yb}^{grt/melt}$ of 68 and 140 respectively. In contrast, HREE-enriched clinopyroxene yields $D_{Yb}^{grt/melt}$ as low as ~3. Because of the size of the granulite bodies and the uneven distribution of garnet

porphyroblasts within them it is considered as a better approach to bracket $D_{REE}^{grt/melt}$ by experimental data and calculations according to the elastic strain model. Since $D_{Eu}^{cpx/grt} \sim 1$ within all samples $D_{Eu}^{grt/melt}$ equals $D_{Eu}^{cpx/melt}$ that was calculated between 0.9 and 1.06 depending on which model was chosen. $D_{Eu}^{grt/melt} = 0.9$ can be used together with $r_0^{3+} = 0.95$ Å and $E_x^{3+} \sim 570$ GPa calculated with the van Westrenen et al. (2001) model since these variables only depend on garnet composition. Feeding the variables into the Brice equation yields $D_{REE}^{grt/melt}$ that are within the range of data in tonalitic melt systems from Klein et al. (2000), Barth et al. (2002) and Xiong (2006). They are also consistent with the ratio in garnet from sample 036M1 and the equilibrium leucosome composition from the same outcrop (Fig. 12b).

7.2.3 REE in orthopyroxene

REE contents in orthopyroxene increase from the LREE to the HREE (Fig. 13). For the LREE and the MREE the opx / cpx ratio ranges from 0.005 to 0.03 with considerable scatter for each element, while for the HREE the scatter diminishes and opx / cpx increases to 0.3 (Fig. 13a). Similar distribution coefficients between cpx and opx are also known from different geological settings, for instance from exsolution lamella of opx in cpx in peridotites (Hellebrand et al., 2005). REE-contents in orthopyroxene presented here are lower than values reported from other orthopyroxene occurrences equilibrated under granulite facies conditions (Pride & Muecke, 1981, Schröter et al., 2004, Clarke et al., 2007). As a consequence $D_{REE}^{opx/melt}$ calculated as $D_{REE}^{cpx/melt} \times D_{REE}^{opx/cpx}$ are low with values for $D_{La}^{opx/melt} \sim 0.002$ and $D_{Lu}^{opx/melt} \sim 0.20$ (Table 4). Our values of $D_{REE}^{opx/melt}$ (Fig. 13b) are comparable to partition coefficients determined for basaltic systems (Irving & Frey, 1984, Colson et al., 1988, McKenzie & O'Nions, 1991, Cawthorn, 1996, Schwandt & McKay, 1998) but lower than those for andesites (Schnetzler & Philpotts, 1970, Luhr & Carmichael, 1980, Bacon & Druitt, 1988, Nielsen et al., 1992, Dunn & Sen, 1994).

Orthopyroxene in the intermediate opx-cpx-granulites is produced via amphibole breakdown in about half the proportion of clinopyroxene. Since both clinopyroxene and orthopyroxene host less REE than amphibole, redistribution of the trace elements from amphibole into clinopyroxene and orthopyroxene must have involved the presence of an additional REE-bearing phase (apatite) or a melt phase. Preferential sequestering of REE into apatite compared to orthopyroxene could be a reason for the very low REE contents in orthopyroxene reported here.

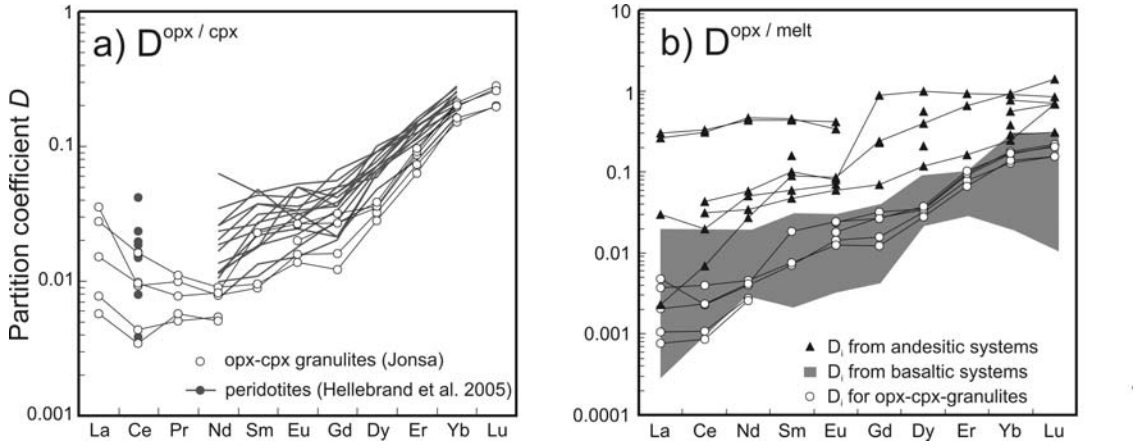

Fig. 13:

$D_{REE}^{opx/cpx}$ in the Finnish opx-cpx-granulites (Fig. 13a) are comparable but slightly lower than ratios known from peridotites indicating very limited partitioning of REE into orthopyroxene. $D_{REE}^{opx/melt}$ calculated from the observed opx / cpx ratio are therefore low and coincide rather with values known from basaltic than from intermediate systems (Fig. 13b).

7.2.4 REE partitioning into plagioclase

REE partitioning into plagioclase has not been studied extensively but increasing $D_{REE}^{pl/melt}$ with decreasing anorthite-content are expected from natural and experimental data (Bédard, 2006). However, the dependance of plagioclase REE contents within the X_{An}-range of our samples (0.25-0.7) is rather blurred. LREE contents in clinopyroxene are well constrained and La as well as Eu concentrations in plagioclase are similar to concentrations in clinopyroxene from the same sample, with $D_{La}^{pl/cpx} = 1.14 \pm 0.2$ and $D_{Eu}^{pl/cpx} = 0.69 \pm 0.15$ (Fig. 14a). The ratio of pl / cpx were used to determine $D_{REE}^{pl/melt}$ from the calculated $D_{REE}^{cpx/melt}$ (Table 4). Bédard (2006b) compiled experimental and natural partition coefficients from several authors and used them to parameterize r_0^{3+}, E_x^{3+} and D_0^{3+}. Calculations using the regression from Bédard (2006b) are therefore applicable for comparison of our data to the broad range of published values. Partition coefficients for the LREE into plagioclase in our rocks are clearly lower than most of the published values. Even lower values for the LREE but similar Eu-values are derived from the plagioclase / leucosome ratio. Nevertheless our data are consistent with the values given in Dunn

& Sen (1994) for basaltic and andesitic systems (Fig. 14b). Partitioning of Eu into plagioclase depends on the redox state of the system during partial melting since incorporation of Eu^{2+} into plagioclase is strongly preferred over incorporation of Eu^{3+}. Wilke & Behrens (1999) made a detailed study of Eu-partitioning into plagioclase as a function of oxygen fugacity. The degree of enrichment of Eu over Sm in the plagioclases from our rocks is similar to the data from Wilke & Behrens (1999) determined at 850°C and at log fO_2 ~ -12, close to the Ni-NiO buffer.

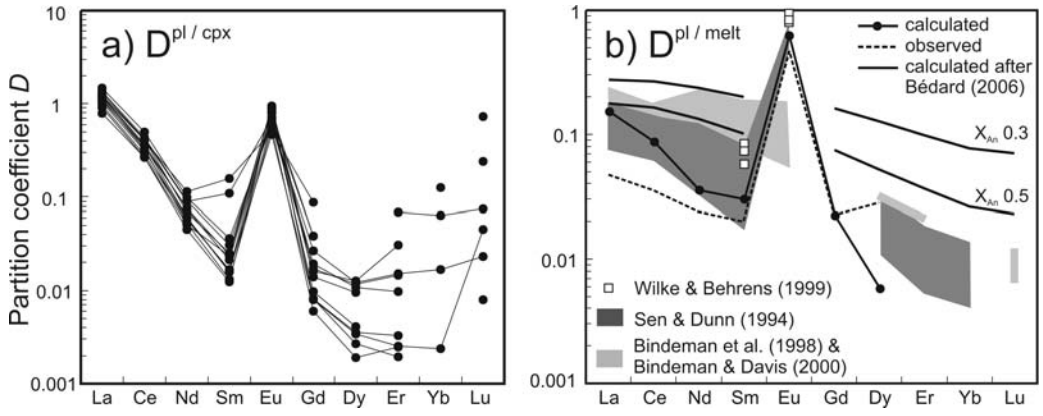

Fig. 14:

Fig. 14a shows the partitioning of REE between plagioclase and clinopyroxene. Note that La and Eu contents in plagioclase equal contents in cpx. $D_{REE}^{pl/melt}$ were calculated using the pl / cpx ratio and the pl / leucosome ratio (Fig. 14b). This approach precludes a dependence of $D_{REE}^{pl/melt}$ on X_{An} in plagioclase as suggested by Bédard (2006b). The values are lower than those calculated after Bédard et al. (2006), Bindeman & Davies (2000) and Bindeman et al. (1998) but are in good agreement with values from Dunn & Sen (1994) experimentally derived in basaltic to andesitic systems at 1 bar and 1100-1200°C. Also shown is the Sm and Eu partitioning after Wilke & Behrens (1999) for a haplotonalitic melt at 850°C, 5 kbar and log fO_2 controlled at the Ni-NiO buffer.

7.2.5 The role of apatite

It is well known that apatite incorporates large amounts of the REE via the substitutions $REE^{3+} + Si^{4+} \leftrightarrow Ca^{2+} + P^{5+}$ and $REE^{3+} + Na^{+} \leftrightarrow 2Ca^{2+}$ (Rønsbo, 1989). Experimental work by Watson & Green (1981) and Prowatke & Klemme (2006) as well as studies of natural occurrences (Nagasawa, 1970, Paster et al., 1974, Luhr et al., 1984, Fujimaki, 1986, Mahood & Stimac, 1990, Sha & Chappell, 1999) demonstrated the influence of melt composition on the

REE partitioning into apatite and showed that partition coefficients for the REE and other highly-charged cations increase with increasing degree of polymerization of the melt.

The ap / cpx ratio was used to calculate $D_{REE}^{ap/melt}$ (Table 4). Sample 012M1 contains apatite with variable LREE contents and three different apatite compositions and the mean clinopyroxene composition were used for the calculation (Fig. 15a). $D_{REE}^{ap/melt}$ derived from this sample have a convex upward pattern centered between Sm and Gd which becomes increasingly flat as the LREE content of the apatite increases. Calculations of $D_{REE}^{ap/melt}$ for sample 049M are hindered by the variable HREE contents in both clinopyroxene and apatite. Combining specific apatite analyses with complementary clinopyroxene analyses yields rather flat $D_{REE}^{ap/melt}$ pattern. $D_{REE}^{ap/melt}$ in both samples fall into the range of experimental partition coefficients for basaltic andesites from Prowatke & Klemme (2006) as well as Watson & Green (1981) although the typical convex upward pattern from the experiments is not reproduced by our data (Fig. 15b). The simple calculation of $D_{REE}^{ap/melt}$ by using the mineral / leucosome ratio gives higher partition coefficients for the HREE due to the strongly fractionated nature of the leucosome.

Apatite from both samples has a negative Eu-anomaly which is small in 012M1 (Eu / Eu*~0.55-0.75) but more evident in 049M (Eu / Eu*~0.3). Apatite grains are usually enclosed in plagioclase and preferential incorporation of Eu into plagioclase could be a reason for the negative Eu-anomaly in apatite. Additionally, the apatite structure prefers Eu^{3+} over Eu^{2+} thus that the uptake of Eu into apatite might have been hindered by the oxidation state of the system.

The model for the REE partitioning into apatite is mostly hampered by the comparison with partition coefficients for garnet. Within sample 012M1 Yb and Lu contents in apatite are similar to contents in garnet while garnet from sample 049M contains about twice as much Yb and Lu as apatite. Consequently, $D_{Yb,Lu}^{ap/melt} \sim D_{Yb,Lu}^{grt/melt}$ for sample 012M1 and $D_{Yb,Lu}^{ap/melt} \sim 0{,}5 \times D_{Yb,Lu}^{grt/melt}$ for sample 049M is expected. Concerning the calculated garnet partition coefficients, the relationship $D_{Yb,Lu}^{ap/melt} \sim 0{,}5 \times D_{Yb,Lu}^{grt/melt}$ in sample 049M is only valid if the ratio of the apatite and the clinopyroxene with the lowest HREE contents is used. For sample 012M1 calculated garnet partition coefficients are too high to be consistent with the apatite partition coefficients. Again, it supports the idea that garnet exerts a limited control on partitioning between minerals in the bulk matrix and that the D_{REE}^{grt} given in Table 4 may be too high for the system under consideration.

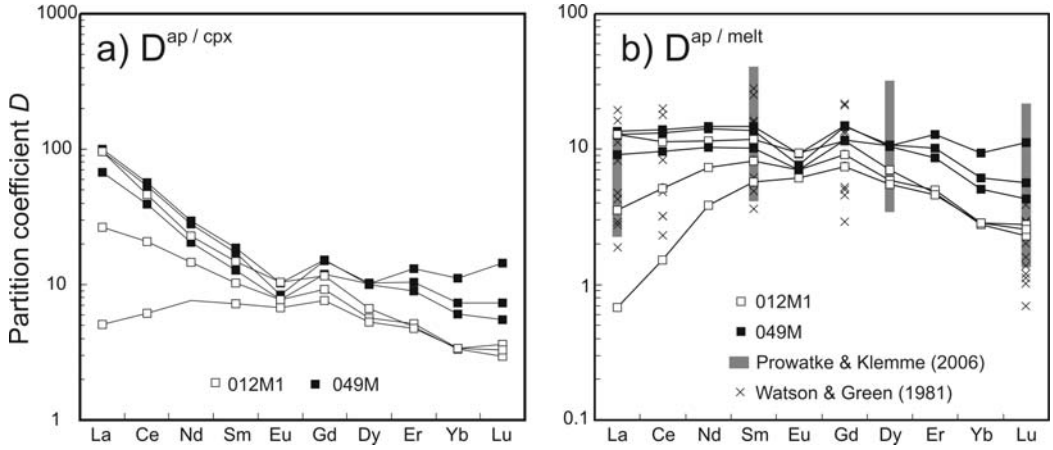

Fig. 15:

REE contents in both apatite and clinopyroxene are variable and therefore different $D_{REE}^{ap/cpx}$ can be calculated for one sample (Fig. 15a). Accordingly, $D_{REE}^{ap/melt}$ calculated as $D_{REE}^{ap/cpx}$ multiplied by $D_{REE}^{cpx/melt}$ are variable (Fig. 15b) but broadly fall into the range of values from Prowatke & Klemme (2006) and Watson & Green (1981). The spread of $D_{REE}^{ap/melt}$ from both references is explained by increasing partitioning into apatite with evolving melt compositions.

7.3 Partitioning of the High Field Strength Elements (HFSE)

Zr and Hf follow Ti in the analogous M1-site in clinopyroxene and the M2-site in amphibole with 6-fold coordination where they are involved in the local charge balance of tetrahedral Al (Tiepolo et al., 2001). In agreement with this are the observed $D^{amph/cpx}$ ~1 for Zr and Hf. Tiepolo et al. (2000) state that Nb and Ta partition into the M1-site in amphibole where they contribute to the charge-balance of dehydrogenation instead of being incorporated alongside with Zr and Hf into the M2-site. This is consistent with low concentrations of Nb and Ta in clinopyroxene where the high-charge cations can only substitute for Ti on M2. Amphibole from the working area equilibrated under high temperatures in the granulite facies and have experienced dehydrogenation which allows increased incorporation of Nb and Ta. Consequently, samples from the working area have high $D_{Nb}^{amph/cpx}$ between 100 and 400 and $D_{Ta}^{amph/cpx}$ between 16 and 60. Nb and Ta partitioning into clinopyroxene is therefore negligible.

Niobium partition coefficients for amphibole in equilibrium with a tonalitic or andesitic

melt generally range from 0.2-0.7 (Klein et al., 1997, Brenan et al., 1995, Hilyard et al., 2000, Xiong, 2006). This is in good accordance with the amphibole / leucosome ratio from sample 036M1 that gives $D_{Nb}^{amph/melt} = 0.55$. Tiepolo et al. (2000) also found that amphibole with low Mg# are able to fractionate Nb from Ta and they developed an equation that relates $D_{Nb/Ta}^{amph/melt}$ to the total titanium content and the Mg# of the amphibole. Applying that equation to the average amphibole composition in the Finnish granulites (Mg# 0.58 ± 0.07, Ti_{tot} 0.22 ± 0.07 apfu) yields a mean $D_{Nb/Ta}^{amph/melt}$ of 1.53 and furthermore $D_{Ta}^{amph/melt} = 0.36$. Amphibole from sample 114 M has elevated Ta-contents in amphibole such that $(Nb^{amph}/Ta^{amph})_N$ = 0.6, while for all other samples the ratio is 1.0-1.8. This implies that amphibole from sample 114 M must have equilibrated with a slightly Ta enriched melt.

Biotite was only analyzed within one sample (080 M) but measurements clearly showed that Nb and Ta concentrations are slightly higher than in amphibole from the same sample (Fig. 16). Since $D_{Nb}^{amph/bt} = 0.81$ and $D_{Ta}^{amph/bt} = 0.74$ partition coefficients for biotite may be calculated as $D_{Nb}^{bt/melt} = 0.68$ and $D_{Ta}^{bt/melt} = 0.51$. The availability of experimentally-derived partition coefficients for biotite is limited. Most data stem from phenocryst-matrix measurements in highly potassic and siliceous systems (Ewart & Griffin, 1994, Nash & Crecraft, 1985, Bea et al., 1994) and are much higher than the values from this work, while data for phlogopite in equilibrium with lamprophyric or lamproitic melts are about a magnitude smaller (Foley et al., 1996, Schmidt et al., 1999). The self-consistency of the values from this study is therefore considered as a better approach for understanding and describing trace element distribution during crustal melting.

The role of both amphibole and biotite in controlling the Nb and Ta budget is limited because of the presence of ilmenite within the granulites. Nb and Ta are strongly partitioned into ilmenite presumably due to coupled substitutions with Ti^{4+} and Fe^{2+} (Ewart & Griffin, 1994). Nb and Ta contents in ilmenite are 20-30 times higher than in amphibole in sample 036M1 and 30-40 times higher in sample 012M1. Ilmenite / melt partition coefficients for Nb and Ta will therefore lie between 12 and 18 which is consistent with the ilmenite / leucosome ratio. These values are obviously higher than $D_{Nb}^{il/melt}$ and $D_{Ta}^{il/melt}$ of ~2 experimentally determined by Zack & Brumm (1998) and Klemme et al. (2006). Nevertheless, they are lower than $D_{(Nb,Ta)}^{il/melt} \sim 50-85$ calculated from phenocryst-matrix relationships in rhyolitic systems (Stimac & Hickmott, 1994, Ewart &

Griffin, 1994). Comparing ilmenite composition with the leucosome composition from sample 036M1 indicates that ilmenite prefers to incorporate Ta over Nb as also suggested by Storkey et al. (2005) and Klemme et al. (2006).

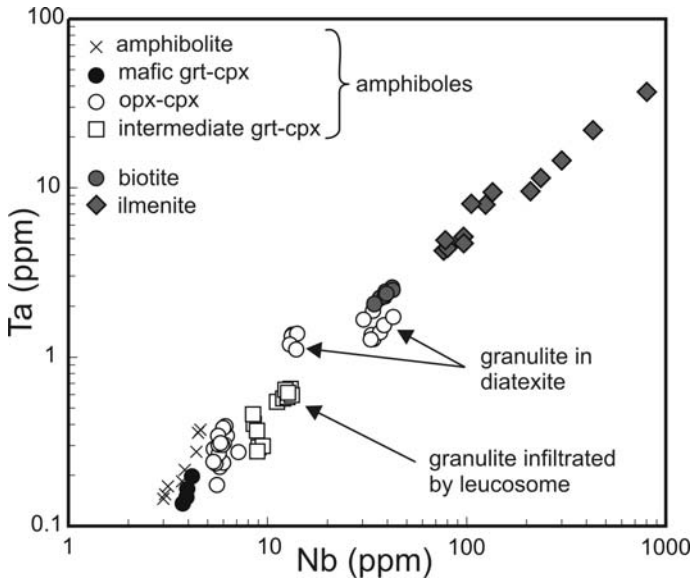

Fig. 16:

Nb and Ta contents in the major Nb-Ta hosting phases amphibole, biotite and ilmenite. Both elements are strongly enriched in ilmenite and slightly enriched in biotite compared to amphibole. Elevated Nb and Ta contents are also observed in amphiboles that equilibrated in a melt-rich environment (granulite patches in diatexite).

Partition coefficients for Zr in amphibole are calculated using the equation given by Dalpé & Baker (2000) that relates Zr partitioning to the Ti and Al contents on the M2 site. Dalpé & Baker (2000) do not distinguish between Ti on the M1 and M2 site and their model is actually made for systems under upper mantle conditions. But applying their model to our amphibole compositions gives a mean $D_{Zr}^{amph/melt} = 0.17$ which is in excellent agreement with the amphibole / leucosome ratio from sample 036M1 (0.15-0.18). These values are lower than experimentally derived values in tonalitic-andesitic systems (Brenan et al., 1995, Klein et al., 1997, Hilyard et al., 2000) which are mainly 0.26-0.9. There are two likely explanations for this phenomenon. First of all, the equation of Dalpé & Baker (2000) is suitable for upper mantle conditions (15-25 kbar, 1200°C) but increased partitioning of Zr into amphibole occurs at lower temperatures and pressures as suggested by the other experimental data. Secondly, the leucosome contains inherited zircon grains from the host rock. Therefore the Zr content of the leucosome

bulk composition might be higher than the Zr content of the original melt phase which would lead to a decreased amphibole / melt ratio. Slightly higher $D_{Zr}^{amph/melt}$ between 0.2 and 0.3 may therefore be more appropriate. In addition $D_{Zr}^{amph/melt}$ and $D_{Zr}^{cpx/melt}$ should match since concentrations of Zr in both minerals is approximately the same. Hill et al. (2000) suggested low incorporation of the HFSE in clinopyroxene with low CaTs-component which is in concordance with the clinopyroxene composition of our samples. Their $D_{Zr}^{cpx/melt}$ of 0.28 closely matches values by Klein et al. (2000) and could be a more realistic partition coefficient for our samples.

Looking at chondrite normalized Zr / Hf in amphibole and clinopyroxene it becomes obvious that $Hf_N \sim 1.5 - 2.5 \times Zr_N$. This is in agreement with $D_{Hf}^{mineral/melt} > D_{Zr}^{mineral/melt}$ for both amphibole and clinopyroxene found in the literature (Brenan et al., 1995, Klein et al., 1997, Klein et al., 2000, Hill et al., 2000, Dalpé & Baker, 2000, Hilyard et al., 2000, Xiong, 2006). The Hf partition coefficient for amphibole and clinopyroxene from the mineral / leucosome ratio is ~ 0.3. It would be about twice as high using literature data (see above).

Garnet prefers Zr over Hf and thereby fractionates these elements the other way round compared to amphibole and clinopyroxene. The ratio of Zr_{grt} / Zr_{cpx} is about 0.2 suggesting very low $D_{Zr}^{grt/melt}$ in the range of 0.03-0.06 according to which $D_{Zr}^{cpx/melt}$ is chosen. These values strongly contrast with published $D_{Zr}^{grt/melt}$ that are about one magnitude higher. However, low $D_{Zr}^{grt/cpx}$ or $D_{Zr}^{grt/amph}$ have been reported from other occurrences of mafic granulites (Storkey et al., 2005, Schröter et al., 2004, Schröter, 2006).

Zr and Hf contents in both ilmenite and biotite are even lower than those in garnet and therefore their in influence on melt composition is negligible.

7.4 Large Ion Lithophile Elements (LILE)

Amphibole, plagioclase and apatite are the main hosts for Sr, Ba and Rb. Amphibole incorporates Ba and Rb on the large A-site in amphibole where they substitute for K and Na while Sr is restrained to the M4-site together with Ca and the REE. Within plagioclase all LILE substitute for Ca. An overall increase in Sr and Ba contents in the plagioclases from our samples correlates with decreasing anorthite content of the plagioclases. This is related to the greater elasticity of the albite crystal lattice allowing increased incorporation of Sr and Ba (Blundy & Wood, 1991).

Equations for the determination of $D_{Sr}^{pl/melt}$ and $D_{Ba}^{pl/melt}$ are given by Blundy & Wood (1991), Bédard (2006b) and Bindeman et al. (1998). The regression from Bédard (2006b) is founded on the largest dataset and was therefore used for the calculation of $D_{Sr}^{pl/melt}$ and $D_{Ba}^{pl/melt}$. Mafic granulites have X_{An} 0.5-0.7 while intermediate granulites have more albitic plagioclase with X_{An} 0.25-0.5. Corresponding $D_{Sr}^{pl/melt}$ therefore vary between 2.7 and 7.3 while $D_{Ba}^{pl/melt}$ range between 0.2 and 1.2.

The observed amphibole / leucosome ratio was not used for the calculations of $D_{Sr}^{amph/melt}$ since leucosomes in most cases represent fractionated plagioclase-quartz assemblages. Even the leucosome with the more melt-like composition almost certainly contains fractionated plagioclase as indicated by a high Sr-content. However, consistent $D_{Sr}^{amph/pl}$ between 0.08-0.1 were observed in most samples with slight exception for granulite patches in diatexite (0.068). Hence Sr is incompatible in the amphibole of all our samples and $D_{Sr}^{amph/melt}$ falls in the range 0.3-0.6 which is in agreement with experimental as well as phenocryst-matrix data (Sisson, 1994, Brenan et al., 1995). $D_{Ba}^{amph/pl}$ is usually ~1 suggesting $D_{Ba}^{amph/melt}$ in the same range as $D_{Ba}^{pl/melt}$. Exceptions are the intermediate but rather calcic granulite bodies 076a and 112M with $D_{Ba}^{amph/pl} = 0.6$. Ba concentration in biotite from sample 080M are about 30 times higher than in plagioclase or amphibole which demands $D_{Ba}^{bt/melt} \sim 30$. Such high $D_{Ba}^{bt/melt}$ is not to be found in the literature were $D_{Ba}^{bt/melt}$ are usually smaller than 10. Nevertheless, it mirrors the extremely wide gap between Ba concentrations in biotite on the one side and amphibole and plagioclase on the other side.

Apatite contains about 1/3 of the amount of Sr as plagioclase from the same sample. The plagioclase from the two samples in which apatite was analysed has X_{An} 0.35-0.4 and a corresponding $D_{Sr}^{pl/melt} \sim 5.5$. $D_{Sr}^{ap/melt}$ is therefore 1.7, similar to experimental data from Prowatke & Klemme (2006) for partitioning between apatite and a basaltic andesite and to data from Watson & Green (1981). Barium contents in apatite are negligible low.

The small amount of Rb present in the samples is almost entirely incorporated into amphibole, except the samples containing biotite. Very low Rb contents are found in the garnet-bearing granulites as well as in the calcic granulite bodies. This could be attributed to low Rb-contents in the source rocks before granulite formation but may also be a feature formed during

melt extraction. Rb-depletion by melt extraction is a feasible process since amphibole from the amphibolite which experienced only limited partial melting are enriched in Rb (14 ppm) compared to amphibole from the residual granulites (<5 ppm) although otherwise the geochemical features are similar. Amphibole from granulite patches within diatexite has higher Rb-contents (5-9 ppm) than amphibole from larger granulite bodies. Refertilization of this amphibole in the melt-rich environment could be a viable process as is also suspected from the elevated potassium contents of those samples. Low ratios of $(Rb/Sr)_N$ and $(Rb/Ba)_N$ in the melt depleted granulites suggest that $D_{Rb}^{amph/melt}$ is about one order of magnitude smaller than $D_{Sr}^{amph/melt}$ and $D_{Ba}^{amph/melt}$. Additionally, $D_{Rb}^{bt/amph}$ within sample 080M is ~55 suggesting that $D_{Rb}^{amph/melt}$ is smaller than 0.1 taken into consideration that most values for $D_{Rb}^{bt/melt}$ fall into the range 1-6 (Mahood & Hildreth, 1983, Nash & Crecraft, 1985, Ewart & Griffin, 1994, LaTourrette et al., 1995, Foley et al., 1996, Schmidt et al., 1999).

7.5 Transition metals

Sc, V, Cr and Ni are hosted by all mineral phases except for plagioclase and apatite. The relationships are complex but some simple conclusions can be drawn. Table 3 shows that the distribution of the transition metals among the principal minerals is consistent and applies at low concentrations of transition metals in intermediate granulites as well as at high concentrations in mafic granulites. It also demonstrates that partitioning of Ni into garnet is negligible, and that orthopyroxene incorporates much smaller amounts of Sc, Cr and V than the other minerals but similar amounts of Ni. Incorporation of Sc, Cr and V into amphibole is about 2 times higher compared to clinopyroxene while Sc is equally distributed between the two minerals. Similar mineral/mineral ratios have been reported from other occurrences of mafic granulites (Storkey et al., 2005, Schröter, 2006). It is difficult to constrain partitioning in magnetite since the concentrations of V, Cr and Ni vary largely within one sample. Even though, the results indicate that concentrations of V, Cr and Ni are 3-10 times higher in magnetite than in clinopyroxene.

There are no well constrained partition coefficients for the transition metals and the spread in the published values is large and erratic. Most of the published values were derived from phenocryst-matrix compositions where bulk matrix effects are difficult to constrain and phenocrysts and matrix may be far out of equilibrium. Also, simultaneous determination of

partition coefficients for all of the four elements are not to be found. Further experimental work on this group of elements is strongly required. Because of the absence of well constrained partitioning data the values given in Table 4 are considered as a good approach for a consistent set of partition coefficients. The consistency of $D^{mineral/mineral}$ with ratios calculated as $D^{mineral/melt} / D^{mineral/melt}$ (Table 3) indicates that the leucosome used for the calculations indeed represent a largely unmodified melt batch. Nevertheless, some of the values are in conflict with published data. For instance $D^{amph/melt}$ for the transition metals from Sisson (1994) agree with our data in having $D_{Sc}^{amph/melt} \sim 2D_{Cr}^{amph/melt}$ but their $D_{V}^{amph/melt}$ are lower than the $D_{Sc}^{amph/melt}$ which is not observed in our data. Similar to our data, experimental partition coefficients from Dostal et al. (1983) yield $D_{Cr}^{amph/melt} \sim 2 * D_{Ni}^{amph/melt}$ but their $D_{V}^{amph/melt}$ are lower. The observation that within garnet $D_{Sc}^{grt/melt}$ is larger than $D_{V}^{grt/melt}$ and $D_{Cr}^{grt/melt}$ is supported by Hauri et al. (1994) and Sisson & Bacon (1992) although there is a large gap between the absolute values.

Table 3

Mineral / clinopyroxene ratios and $D^{mineral/melt}$ for the transition metals. $D^{mineral/melt}$ were calculated from the mineral / leucosome relationship in outcrop 036. $D^{opx/melt}$ were calculated from the overall ratio of opx / cpx and $D^{bt/melt}$ from the bt / cpx ratio in sample 080M since both minerals are not part of the peak metamorphic assemblage in sample 036M1. Ratios between $D^{mineral/melt}$ and $D^{cpx/melt}$ are in good agreement with $D^{mineral/cpx}$ indicating that the distribution of the transition metals in the leucosome from outcrop 036 closely approaches equilibrium.

	$D^{mineral/cpx}$				$D^{mineral/leucosome}$				$D^{mineral/melt} / D^{cpx/melt}$			
	Sc	**V**	**Cr**	**Ni**	**Sc**	**V**	**Cr**	**Ni**	**Sc**	**V**	**Cr**	**Ni**
cpx	1	1	1	1	11	7.3	2.5	1.7	1	1	1	1
grt	0.8-1.2	0.4-0.6	1-2	0.02-0.05	14.5	2.6	2.5	0.06	1.3	0.36	1	0.04
amph	0.8-1.2	1.6-2.5	1-3	1.6-2.5	11	12	6	3.2	1	1.6	2.5	1.9
opx	0.15-0.25	0.16-0.5	0.2-0.5	1	*2.7*	*2*	*1*	*1.7*				
bt	0.15	2.2	2.5	3.6	*1.6*	*13*	*6.3*	*6.1*				
il	0.15-0.3	1	1-1.7	0.2-0.3	4	12	3	0.5	0.4	2	1.2	0.3

Our data confirm that the transition metals are compatible in amphibole, clinopyroxene, orthopyroxene, garnet, biotite and ilmenite except for Ni in garnet. The values are lower than partition coefficients for high-silica melts (rhyolites, trachytes) but higher than most of the basaltic data. This could imply that the minerals equilibrated with an intermediate melt composition.

7.6 Th and U

Th and U contents below 0.1 ppm are typical for mafic, garnet-bearing granulites as well as the two large opx-cpx-granulite bodies. This indicates depletion by melt extraction since both elements are incompatible in the major mineral phases. The amphibolite and the granulite patches from diatexite outcrops are enriched with Th and U contents between 0.24 and 0.8, consistent with enrichment of these samples in other incompatible elements. Concentrations of both Th and U are close to the detection limits in garnet, clinopyroxene, plagioclase, biotite and ilmenite. Amphibole contains up to 0.8 ppm Th and U in the amphibolite. Apatite has the highest Th (3-8 ppm) and U contents (2-4.5 ppm) and will already influence the bulk rock contents if present just in small amounts.

Table 4: Mineral / melt partition coefficients (D_i) constrained in this study.

	cpx		amph		grt	opx	bt	pl		ap				ilm
			min	max				min	max					
Sr			0.3	0.6				2.7	7.3	1.7				
Ba			0.2	1.2			30	0.2	1.2					
Rb			0.01	0.1			3 - 6							
Sc	11		11		15	2.7	1.6							4
V	7.3		12		2.6	1.1	13							12
Cr	2.5		6		2.5	1.0	6.3							3
Ni	1.7		3.2		0.06	1.7	6.1							0.5
Nb			0.55				0.68							12-18
Ta			0.36				0.51							12-18
Zr	0.17	*0.28*	0.17	*0.28*	0.06									
Hf	0.30	*0.60*	0.30	*0.60*										

	D_0 1.05 W&B	D (Eu) W&B	cpx / leuco	3 * cpx	D (Eu) Klein	D (Eu) West.	grt / leuco	opx / cpx		pl / leuco	pl / cpx	012M1 min	012M1 max	049M min	049M max	
La	0.13	0.11	0.04	0.40	0.45	0.002	0.003	0.002		0.048	0.154	0.7	13	11	16	
Ce	0.25	0.20	0.09	0.74	0.72	0.009	0.003	0.002		0.036	0.088	15	11	12	17	
Nd	0.50	0.41	0.26	1.5	1.3	0.09	0.02	0.004		0.024	0.036	4	12	13	19	
Sm	0.79	0.65	0.59	2.4	1.8	0.58	0.28	0.007		0.020	0.031	6	12	13	18	
Eu	0.90	0.74	0.74	2.7	2.0	0.90	0.69	0.019		0.47	0.63	6	9	8	13	
Gd	0.99	0.81	0.89	3.0	2.1	2.2	1.6	0.023		0.023	0.023	8	12	14	17	
Dy	1.1	0.86	1.23	3.1	2.2	6.1	8.4	0.033		0.029	0.006	6	7	10	11	
Er	0.97	0.80	0.83	2.9	2.1	12	18	0.087		0.035	0.011	5	5	9	9	
Yb	0.84	0.69	0.44	2.5	1.9	18	27	0.156			0.014	3	3	4	6	
Lu	0.77	0.63	0.29	2.3	1.8	20	26	0.188			0.067	2	3	3	5	

Italic values are compiled from the literature. D_i that are not given are low and will have no significant impact on melt composition. Inferred minimum and maximum values are given for Rb, Sr and Ba in amphibole and plagioclase as well as for the REE in apatite. See text for further explanation.

W&B – Wood & Blundy (1997), Klein – Klein et al. (1997), West. – van Westrenen et al. (2001), leuco – leucosome.

8. Implications for melting within the lower crust

8.1 Melt composition in equilibrium with granulitic residues

Our data allow broad conclusions about melting of mafic to intermediate igneous precursors under lower crustal conditions. The partition coefficients constrained here are similar to D-values for intermediate compositions (andesitic, tonalitic). Although the observed remnants of partial melts (leucosomes) have high SiO_2-contents between 65-75 wt% none of the observed D-values are as high as expected from phenocryst-matrix distribution coefficients in evolved magmatic systems.

The modal abundances given in Table 1 and the mineral / melt partition coefficients constrained previously (Table 4) were used for the calculation of bulk rock partition coefficients. This shows that during anatexis of mafic and intermediate igneous precursors Rb, Ba, Th, U, Nb, Ta, Zr and Hf are strongly incompatible in the granulitic residue. Sr is compatible in the intermediate granulites because of the low anorthite component of the plagioclase and its high modal abundance. Melts in equilibrium with the plagioclase-rich granulites will therefore be depleted in Sr. The compatibility of Sr becomes lower in the more Ca-rich mafic granulites but the bulk partition coefficient for Sr will remain larger than 1 except for the mafic granulites with the most anorthitic plagioclase and the lowest plagioclase contents. These observations are in accordance with the results of Foley et al. (2002) which claim that only Ca-rich plagioclase with $D_{Sr}^{pl/melt} = 2$ and low modal amounts of plagioclase (<15 %) can account for the observed Sr contents in TTG. This requires melting in the pressure range > 10 kbar. The retention of Sr in granulites due to high modal abundances of plagioclase precludes granulites from being volumetrically important precursors of TTG crust since high Sr contents are a key attribute of TTG. This is demonstrated by modelling non-modal batch melting of a mafic amphibolite (Fig. 17a-b) and an intermediate LREE-enriched amphibolite from the working area (Fig. 17c-d). Tonalitic melts from the mafic amphibolite modelled by using the garnet-producing melting reactions given in Sen & Dunn (1994) broadly resemble Archean leucodiorites from the working area. Marked differences between the leucodiorites and model melts are the low Sr-contents in model melts indicating that the leucodiorites cannot represent unmodified melts of the mafic granulites. Still, the leucosome from outcrop 036 indicates that melts with elevated Sr contents and more strongly fractionated REE-pattern are present but they can only be generated in batches of granulite with the highest garnet and lowest plagioclase contents and may be volumetrically insignificant.

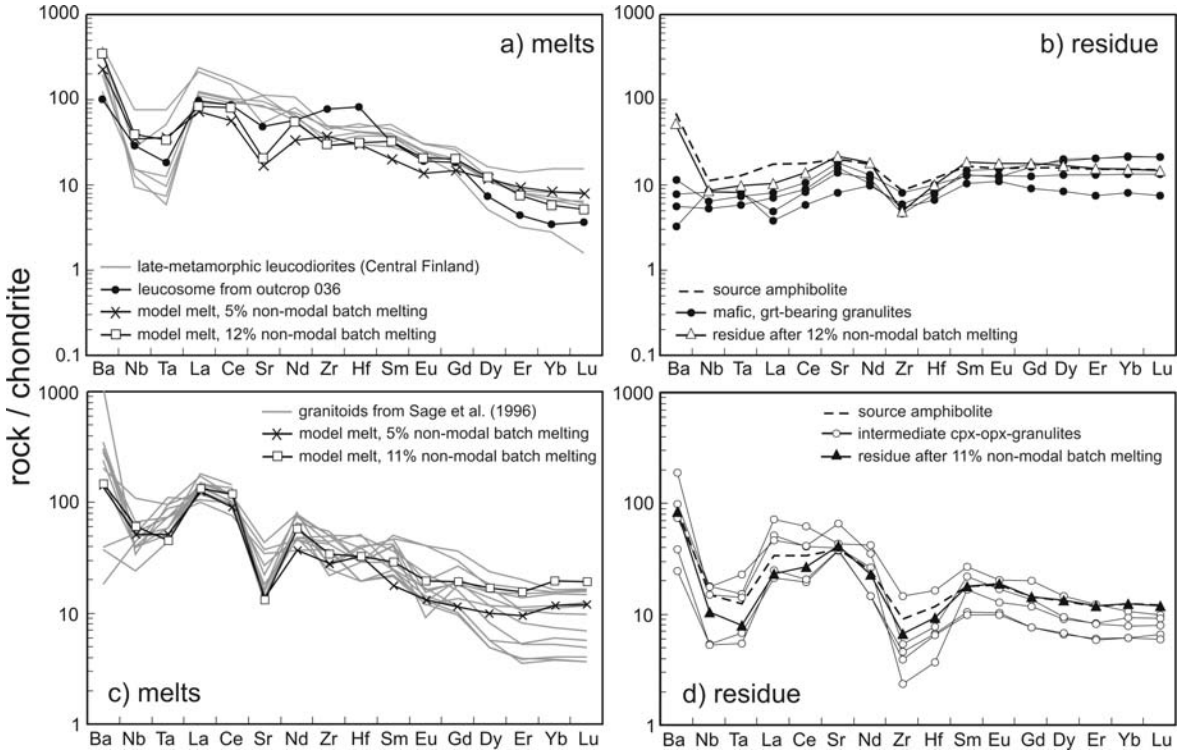

Fig. 17:

Modelling of melt (17a) and residue (17b) composition by melting of an average Archean amphibolite from the Iisalmi area using the partition coefficients constrained in this study (Table 4) and the garnet-producing melting reactions in Sen & Dunn (1994). Modelled residue match the composition of mafic grt-bearing granulites although the Ba content in the source seems to be too high. Model melts are compared to late-metamorphic leucodiorites from the working area. The major difference is the negative Sr-anomaly in model melts that develops due to the high abundance of residual plagioclase in granulites. Thus, granulites are excluded as rocks from which leucodiorites may have been extracted. It also implies that the source of leucodiorites was free of plagioclase or that hydrous melting of plagioclase released Sr into the melt phase (see Part II). Melting of a LREE-enriched amphibolite leaving opx-cpx-granulites as residues was modelled (Fig. 17c-d) using the melting reaction from Patiño Douce & Beard (1995). Again a negative Sr anomaly appears in model melts due to restitic plagioclase. Model melts are similar to granitoid rocks described by Sage et al. (1996) but are unlike than most of the typical Archean TTG

Within mafic granulites, the presence of garnet dictates the bulk compatibility for the HREE suggesting coexistence with a strongly fractionated, HREE-depleted partial melt. However, our analyses demonstrated that garnet may have grown late during peak metamorphism and failed to equilibrate with the bulk matrix. Corresponding melts may therefore have been less influenced by the presence of garnet than is expected at first sight from its modal abundance. Thus, melting models may overestimate the degree of REE-fractionation in melts by simply applying high garnet / melt partition coefficient. Trace element analyses of minerals are therefore crucial to demonstrate equilibrium conditions and draw conclusions on melt compositions.

The intermediate granulites are considered as residues of ~10 % melting of intermediate amphibole-bearing source rocks (see Part II). This is inferred from modal abundances of amphibole, clinopyroxene and orthopyroxene and comparison with experimental data from Patiño Douce & Beard (1995). Model melts have strong negative Sr-anomalies due to the albitic composition of plagioclase and elevated HREE contents because of the absence of garnet (Fig. 17c). Such melts are not typical for Archean TTG assemblages but are reported for instance by Sage et al. (1996) from the Superior Province, Canada. Sage et al. (1996) attribute the geochemical features of these rocks to significant contamination of mantle melts by ancient sialic crust. Still, the geochemical characteristics as well as the small scale occurrence of these rocks could also be explained by small amounts of melting of intermediate arc-crust leaving a granulitic, plagioclase-rich residue.

All of the transition metals are compatible in the granulitic residues, especially if the presence of another Ni-bearing phase (pyrite, chalcopyrite) is considered. The transition metals therefore record the origin of the igneous precursor rocks and reflect the primitive, oceanic nature of the mafic granulites and the evolved character of the intermediate granulites. Together with the age data this strongly supports the hypothesis that in the working area igneous rocks from an oceanic setting and an arc-setting were merged during a collisional event that culminated in granulite facies metamorphism and partial melting.

8.2 Metasomatism of minerals in residual granulites

Elevated REE-contents as well as prominent negative Eu-anomalies in amphibole and clinopyroxene from granulite patches within diatexite contrast with flat amphibole and clinopyroxene patterns from large granulite bodies in the same area. Amphibole from these patches additionally have elevated Rb, Y, Nb, Ta and Th values. Leucocratic batches of the diatexites as well as of most of the leucosomes from other outcrops have geochemical attributes that are consistent with plagioclase and quartz crystallization from a percolating melt phase (see Part II). The large degree of crystallization necessary to produce the amount of the fractionated plagioclase and quartz for building up leucocratic diatexite outcrops will produce evolved melts with prominent negative Eu-anomalies.

Metasomatism and equilibration of the small granulite patches with such late-stage, highly fractionated melts could explain the enriched trace element pattern of the minerals in the small granulite patches (Fig. 18). Remnants of such fractionated, residual melts are occasionally found among leucosomes but their restricted occurences suggests that most of the evolved melts have left the system

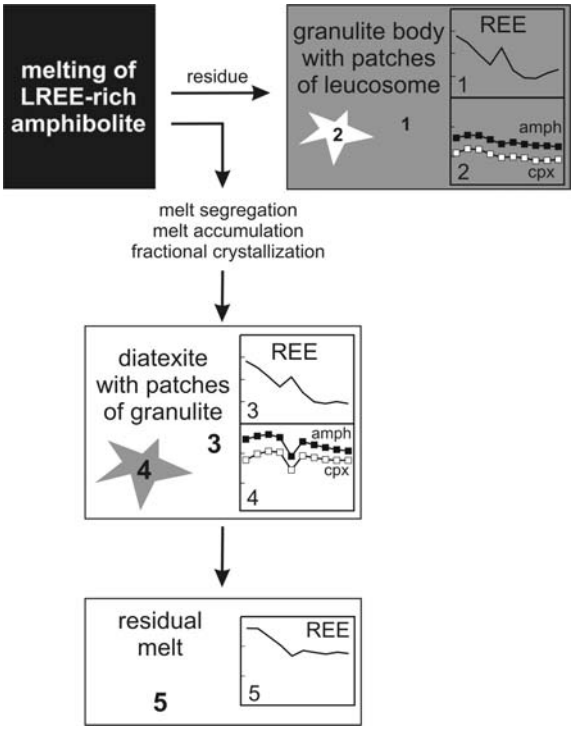

Fig. 18:
Sketch for visualizing development of different REE pattern in amphibole and clinopyroxene in different granulite outcrops. Melting of an LREE-rich amphibolite leaves melt-depleted granulites (1) with small patches of leucosome (2). Most of the melt segregated from the source area and fractionation of plagioclase and quartz from the melt occurred producing diatexites (3). Disrupted pieces of granulite were transported in the melt phase and minerals equilibrated with the melt (4). Evolved melts largely escaped the system (5).

8.3 The importance of ilmenite for Nb/Ta ratios in coexisting melts

The fractionation of Nb from Ta during the course of melting of mafic source rocks has often discussed as the major key for understanding the generation of Archean TTG-crust (Foley et al., 2002, Rapp et al., 2003). Archean TTG-crust characteristically has sub-chondritic Nb/Ta which requires a mineral phase that preferentially incorporates Nb over Ta. Amphibole has $D^{Nb/Ta} > 1$ while in Ti-phases (rutile, titanite, ilmenite) $D^{Nb/Ta} < 1$ occurs. Therefore low Nb/Ta can be expected in melts that are in equilibrium with an amphibole-bearing residue but high Nb/Ta are inferred when amphibole is absent and Nb/Ta is controlled by Ti-phases. During amphibole-dehydration melting of mafic to intermediate source rocks within the lower crust the modal abundance of amphibole constantly decreases. Significant amounts of Ti contained in amphibole are liberated upon amphibole breakdown and become available for the formation of Ti-phases such as ilmenite. Thus, the ratio of amphibole / ilmenite may become crucial in the mafic granulites where amphibole almost reacted out and ilmenite is present in modal abundances of up to 1 wt%. A non-modal batch melting model was applied to model Nb/Ta in melts in dependence of amphibole and ilmenite abundance in the residue. The model relies on melting reactions given in Sen & Dunn (1994) and allows incremental increase of ilmenite up to 1 wt% during melting. Two amphibolites were modelled, being different in their modes of amphibole (52 and 33 %) and clinopyroxene (8% and 25%) prior to melting (Fig. 19). The concentration of Nb and Ta in the amphibolite (061M) were used as a source content. According to our calculations, Nb/Ta smaller than the chondritic value (<18) is favoured by low degrees of melting and a high amount of residual amphibole as is expected when qtz controls the reaction progress. However, the observed modes of the mafic granulites are more consistent with lower amounts of amphibole prior to melting as applied in the second model scenario. In this case amphibole quickly becomes exhausted and Nb/Ta in melts rises steeply. A melting degree <10 % that leaves more than 10 % amphibole in the residue is required to retain Nb/Ta in melts <18. Since the melting reaction that left the mafic granulites went further and exhausted almost all amphibole, the last batches of melt produced likely had elevated Nb/Ta. In the case that ilmenite or another Ti-phase such as titanite was already present at the onset of melting Nb/Ta in the melt is buffered within a more restricted range during melting.

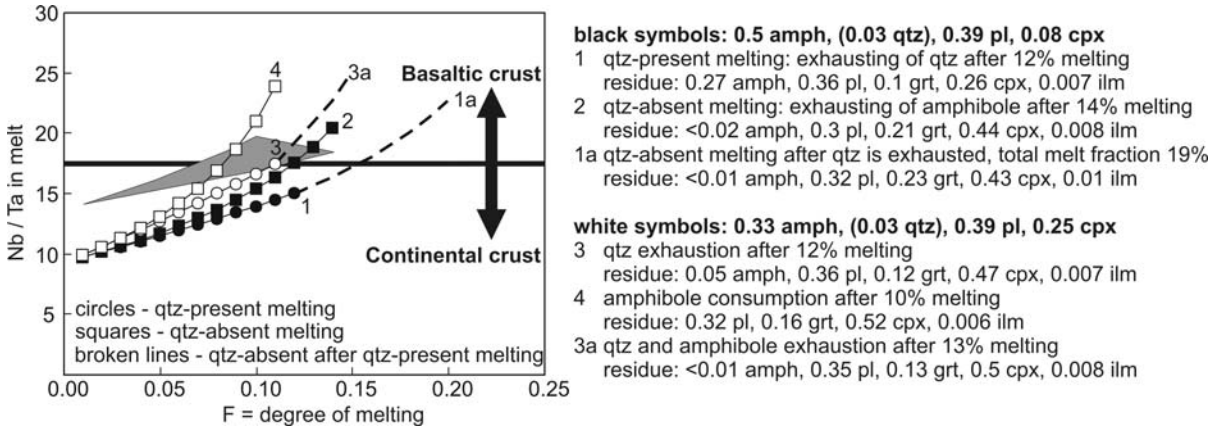

Fig. 19:

Models for Nb/Ta ratios in melts of mafic granulites as a function of degree of melting using a non-modal batch melting model and weight proportion melting reactions given in Sen & Dunn (1994). Two scenarios have been modelled. In both models ilmenite increases incrementally with degree of melting. The first scenario (black symbols) starts with 50 % modal amphibole in the source. Modelled residues do not agree with observed modes of mafic granulites (Table 1), leaving to much amphibole or producing to much garnet. The second scenario (white symbols) uses only 33 % modal amphibole and elevated cpx-contents produced by sub-solidus reactions. This starting mode yields residues in good agreement with observed granulite modes. However, the smaller abundance of amphibole leads to a steeper increase of Nb/Ta in coexisting melts. At the beginning of anatexis melts with low Nb/Ta are produced but the ratio increases as melting progresses due to decreasing amphibole and increasing ilmenite contents. The last batches of melt may therefore have higher Nb/Ta ratios than typical for continental crust. The grey field shows how Nb/Ta in the melt evolves if 1% ilmenite is already present in the starting composition.

9. Conclusions

In-situ trace element determination of minerals from mafic and intermediate granulites were used to monitor partial melting processes within the middle to lower crust. The LA-ICP-MS analyses report equilibrium partitioning between peak metamorphic phases except for minerals that grew together with garnet in small microdomains. A self-consistent set of $D^{mineral/mineral}$ and $D^{mineral/melt}$ values was constrained, using predictive models, experimental data and rarely occurring leucosomes with preserved melt composition. The uniform $D^{mineral/mineral}$ for REE, HFSE and transition metals among the principal minerals of compositionally diverse granulites imply that

they can be easily adopted for other granulite occurrences, giving a clear impression of trace element distribution in the lower crust. $D^{mineral/melt}$ defined in this study are applicable for low pressure, high temperature partial melting and intermediate melt compositions. Non-modal melting models using these $D^{mineral/melt}$ show that partial melts of amphibolites leaving mafic and intermediate granulites as residues at melting degrees <15% will be different from typical Archean TTG-crust by having negative Sr-anomalies due to high amounts of plagioclase in the residues. However, the models demonstrate what kind of melts can be expected from crustal melting of such source rocks and help to distinguish them from magmatic rocks derived under plagioclase-absent conditions.

Analyses of the accessory phases apatite and ilmenite strongly stress their importance in controlling certain trace elements during metamorphism and melting. Ilmenite incorporates high amounts of Nb and Ta. Its role may become crucial as the amount of amphibole progressively diminishes during dehydration melting so that ilmenite becomes the major host for Nb and Ta and consequently controls Nb / Ta ratios in coexisting melts.

Our data also allow us to recognize processes that are related to melt segregation and fractionation. Diatexites are migmatites in which a high amount of melt lead to the obliteration of pre-metamorphic. Although the leucocratic parts of the diatexites have residual features and consist mainly of cumulated plagioclase and quartz, minerals in granulite patches within diatexites record the presence of an evolved melt. This evolved melt was produced by fractional crystallization of plagioclase and quartz from the original melt phase. Thus the remaining melt experienced enrichment of elements incompatible in plagioclase (K, REE, Rb, Y, Nb, Ta) but became depleted in Eu and Sr. The geochemical characteristics of that melt phase became imprinted on the minerals of the granulite patches before segregation from the system. Taken into consideration the above mentioned melting models this implies a small but noticeable contribution of granulite melting to Archean crust formation.

Appendix A: Representative electron microprobe analyses of major mineral phases.

sample	type	phase	SiO_2	TiO_2	Al_2O_3	FeO	MnO	MgO	CaO	Na_2O	K_2O	total
061M	amphi-bolite	amph	42.6	1.61	11.7	15.9	0.27	11.4	11.3	1.73	1.15	98.0
		cpx	50.1	0.18	3.39	11.6	0.45	12.0	20.4	0.79	0.12	99.1
		pl	57.2	-	26.7	0.11	-	0.02	8.32	6.75	0.16	99.3
002M2	grt-cpx granulite	cpx	50.0	0.46	3.53	12.3	0.21	10.9	22.2	0.48	-	100.3
		grt	38.4	0.08	21.3	26.3	1.61	3.86	9.96	0.02	0.01	101.8
		pl	53.5	-	29.2	0.20	0.01	0.01	12.0	4.96	0.10	100.0
034M2	grt-cpx granulite	cpx	50.2	0.34	3.02	11.2	0.26	11.9	22.0	0.41	-	99.6
		grt	38.5	0.09	21.4	25.5	1.09	6.03	8.00	-	-	100.7
		pl	54.5	-	29.6	0.05	-	0.01	11.4	5.00	0.05	100.7
036M1	grt-cpx granulite	amph	44.1	1.76	11.1	14.9	0.14	12.6	11.3	2.06	0.37	98.6
		cpx	51.9	0.29	3.04	10.1	0.23	13.2	22.3	0.42	-	101.6
		grt	39.3	0.07	21.8	25.5	0.83	7.29	6.84	0.01	-	101.8
		pl	53.7	-	29.8	0.10	0.02	0.02	12.7	4.70	0.03	101.0
		il	0.79	50.1	0.20	46.4	0.58	1.19	0.02	0.04	0.02	99.6
		mgt	0.34	0.67	0.59	90.6	0.04	0.15	0.02	0.01	-	94.5
140M	grt-cpx granulite	cpx	51.3	0.37	2.98	11.3	0.19	11.9	22.2	0.45	0.01	100.8
		grt	37.3	0.09	21.1	26.0	1.08	4.97	8.27	-	-	99.0
		pl	51.0	-	31.7	0.10	-	0.01	13.9	3.59	0.02	100.3
		il	0.03	52.8	0.01	45.8	0.80	0.37	0.01	0.01	-	100.0
012M1	grt-cpx granulite	amph	43.9	2.09	11.5	13.8	0.23	12.9	11.7	1.57	0.98	99.2
		cpx	51.1	0.32	3.56	10.6	0.34	12.7	21.8	0.60	0.01	101.0
		grt	39.2	0.12	21.7	25.4	1.34	7.92	6.41	0.01	0.01	102.1
		pl	57.7	0.01	26.5	0.06	0.02	-	8.78	6.87	0.10	100.2
		il	0.03	50.4	0.02	47.4	1.18	0.67	0.01	0.01	-	99.8
		mgt	0.08	0.12	0.28	92.6	0.02	0.06	-	0.03	-	93.9
049M	grt-cpx granulite	amph	41.3	3.07	12.0	19.8	0.13	8.77	11.3	1.73	1.66	100.2
		cpx	51.0	0.28	2.72	14.7	0.24	11.3	20.4	0.61	-	101.3
		grt	38.4	0.08	21.3	29.6	1.28	4.71	6.59	0.01	-	102.1
		opx	50.9	0.05	0.86	32.9	0.64	16.1	0.76	0.01	-	102.2
		pl	60.0	0.01	25.3	0.04	0.03	0.01	7.22	7.71	0.34	100.6
076M1	grt-cpx granulite	amph	41.6	3.24	11.8	19.7	0.13	8.54	11.3	1.83	1.62	100.0
		cpx	51.0	0.23	2.48	13.5	0.27	10.9	21.7	0.64	0.01	100.7
		grt	38.4	0.04	21.1	29.6	1.46	4.23	7.11	0.01	0.01	101.9
		pl	59.5	0.01	24.8	0.07	0.01	0.01	7.18	7.62	0.35	99.6
076a	opx-cpx granulite	amph	44.1	1.79	10.9	14.2	0.16	12.4	11.4	1.58	0.70	97.4
		cpx	51.8	0.25	2.76	9.54	0.29	13.3	21.9	0.55	-	100.4
		opx	52.3	0.06	1.57	24.5	0.61	21.5	0.51	0.03	0.01	101.1
		pl	54.6	0.01	27.8	0.10	0.02	0.01	10.8	5.34	0.18	99.0
112M	opx-cpx granulite	amph	44.6	1.55	10.8	13.8	0.16	12.7	11.3	1.49	0.74	97.2
		cpx	50.8	0.21	2.79	9.39	0.28	13.0	22.2	0.52	0.02	99.4
		opx	52.3	0.06	1.57	24.3	0.65	21.4	0.58	0.03	0.01	101
		pl	54.8		28.0	0.07		0.01	9.56	6.06	0.19	98.8
080M	opx-cpx granulite	amph	42.2	2.20	11.7	15.7	0.15	10.8	11.4	1.54	1.68	97.9
		bt	36.6	4.90	14.4	17.1	0.06	12.6	-	0.08	9.72	96.5
		cpx	51.5	0.17	2.24	11.3	0.28	12.6	21.0	0.65	-	99.8
		opx	51.3	0.06	1.15	27.9	0.61	19.0	0.52	0.01	0.01	100.6
		pl	58.9	-	25.0	0.08	0.03	0.01	6.67	7.59	0.49	98.8
102a	opx-cpx granulite	amph	42.7	2.12	11.1	16.4	0.31	10.6	11.4	1.44	1.51	97.6
		cpx	52.1	0.16	2.30	11.0	0.51	12.4	21.5	0.83	-	100.8
		opx	51.8	0.06	1.36	26.7	1.12	18.4	0.60	0.02	0.02	100.1
		pl	61.5		24.8	0.03		0.01	5.75	8.36	0.23	100.7
114M	opx-cpx granulite	amph	42.8	2.05	11.1	15.2	0.26	11.8	11.4	1.62	1.58	97.7
		cpx	52.3	0.18	2.25	11.9	0.51	13.6	19.5	0.77	0.01	101.1
		opx	52.3	0.04	1.06	24.6	1.04	21.3	0.51	0.03	0.01	100.9
		pl	61.1		25.0	0.12		0.01	6.13	8.26	0.25	100.9

Appendix B: LA-ICP-MS analyses of mineral phases. Minerals numbered 1-3 show the variation in the REE content within one sample. n.a. not analyzed

sample	mineral	Sc	V	Cr	Ni	Rb	Sr	Y	Zr	Nb	Ba	La	Ce	Nd	Sm	Eu	Gd	Dy	Er	Yb	Lu	Hf	Ta	Th	U
061M amphib.	amph	73.7	419	454	143	14.1	43.3	31.9	48.8	3.781	53.2	7.17	22.5	16.0	4.12	1.35	4.70	5.64	3.52	3.51	0.522	1.71	0.234	0.858	0.815
	cpx	84.8	175	178	58.3	0.083	12.8	9.83	37.2	-	2.07	1.80	5.69	4.52	1.18	0.383	1.42	1.81	1.14	1.23	0.206	1.39	-	0.262	0.259
	pl	2.35	7.04	10.0	6.47	0.290	468	0.181	0.634	-	58.3	2.23	2.32	0.518	0.186	0.193	0.126	-	0.079	0.079	0.015	0.041	0.058	0.060	0.074
002M2 grt-cpx granulite	cpx	81.1	558	395	178	0.046	7.77	4.80	53.9	0.031	0.199	1.78	9.19	11.1	3.40	0.680	2.93	1.53	0.371	0.215	0.027	2.30	0.012	0.008	0.004
	grt	72.2	264	917	3.87	-	0.177	124	7.17	0.004	0.251	0.162	0.503	1.55	2.56	1.14	8.70	19.0	15.1	17.4	2.68	0.101	0.002	0.004	0.003
	pl	1.35	0.423	3.02	1.22	0.094	287	0.051	0.055	-	56.2	1.93	3.16	0.848	0.083	0.645	0.048	0.020	0.011	-	0.020	0.045	-	0.015	0.028
034M2 grt-cpx granulite	cpx 1	81.6	n.a.	440	176	0.135	5.99	7.86	57.3	0.059	0.371	1.56	10.8	17.5	6.04	1.22	5.33	2.51	0.587	0.324	0.032	2.87	0.009	0.005	0.004
	cpx 2	90.2	n.a.	452	159	0.085	4.55	32.7	51.9	0.072	0.776	0.999	8.55	17.8	7.26	1.29	8.81	7.82	3.00	1.93	0.234	2.78	0.007	0.004	0.003
	grt 1	101	242	554	5.00	-	0.040	77.2	12.0	0.010	0.018	0.008	0.087	1.36	2.57	1.26	8.58	15.6	6.52	3.95	0.395	0.162	0.001	0.001	0.001
	grt 2	100	255	539	4.82	-	0.035	99.2	11.0	0.011	0.033	0.095	0.196	1.30	2.59	1.28	8.18	17.3	10.7	6.97	0.769	0.130	0.003	0.004	0.011
	pl	n.a.	n.a.	n.a.	n.a.	0.777	236	n.a.	n.a.	n.a.	25.9	1.55	3.56	1.32	0.144	0.900	0.070	0.021	-	-	-	n.a.	n.a.	n.a.	n.a.
036M1 grt-cpx granulite	amph 1	91.2	974	474	146	1.07	25.6	27.0	51.7	3.92	11.3	2.40	11.3	16.7	7.50	1.91	8.32	7.36	2.51	1.03	0.120	2.36	0.148	0.049	0.012
	amph 2	93.6	985	441	125	1.41	20.8	41.8	49.5	3.75	11.2	2.35	11.9	18.3	7.55	2.10	11.4	9.66	3.94	3.33	0.482	2.55	0.136	0.036	-
	amph 3	111	1075	508	126	1.39	18.3	66.8	44.4	3.95	9.57	2.60	13.9	22.3	9.56	2.49	13.1	14.3	6.63	4.89	0.778	2.46	0.166	-	0.011
	cpx 1	82.9	547	128	64.4	0.053	6.27	6.92	47.0	0.020	0.084	0.822	4.57	6.70	2.74	0.780	3.22	2.26	0.591	0.248	0.026	1.99	0.006	0.013	0.010
	cpx 2	94.6	587	236	78.2	0.087	4.99	19.1	50.9	0.038	0.646	0.803	4.16	6.77	2.92	0.695	3.91	4.00	1.94	1.79	0.257	2.38	0.005	0.018	0.010
	cpx 3	93.8	540	217	61.7	0.040	3.05	45.3	48.5	0.092	0.282	0.772	4.30	7.25	3.40	0.821	5.45	8.11	5.09	4.98	0.698	2.43	0.007	0.018	0.010
	grt	117	217	197	2.48	-	0.079	101	9.54	0.015	0.054	0.064	0.154	0.521	1.33	0.733	5.85	15.4	12.8	15.4	2.35	0.145	0.002	0.014	0.019
	pl	1.36	0.215	3.11	5.44	0.081	216	0.313	-	-	10.8	1.09	1.87	0.625	0.093	0.499	0.082	0.052	0.025	-	-	0.050	-	0.030	-
	il	34.6	977	212	20.6	-	-	0.107	8.80	82.1	-	0.320	0.197	0.116	-	0.349	-	-	-	0.034	0.014	0.543	4.35	0.005	0.011
	mgt	2.45	2476	990	320	-	-	1.41	0.313	0.576	-	0.091	0.228	0.258	0.359	0.054	0.570	0.390	0.238	0.392	0.032	0.045	0.043	0.004	0.005
140M grt-cpx granulite	cpx	64.0	407	516	215	-	6.76	4.51	47.1	0.018	0.717	1.22	5.60	8.08	2.81	0.553	3.03	1.83	0.382	0.144	0.018	1.88	0.010	0.061	0.021
	grt	69.2	238	711	4.13	-	0.603	149	9.54	0.028	0.307	0.031	0.047	0.651	1.54	0.729	6.86	20.3	19.7	23.7	4.10	0.136	-	0.012	0.012
	pl	6.71	2.95	7.72	2.83	0.021	283	0.036	0.307	-	20.1	1.61	2.32	0.558	0.071	0.496	0.042	0.018	-	0.018	-	0.046	0.020	-	-
	il	9.39	611	715	66.5	-	-	0.276	2.50	124	-	-	0.186	-	0.059	-	-	-	0.043	0.094	0.035	0.086	8.69	0.009	0.036
012M1 grt-cpx granulite	amph	85.9	374	60.7	104	1.18	58.1	127	47.5	9.12	270	27.6	105	109	29.3	7.80	30.1	27.2	12.3	10.1	1.52	2.56	0.289	0.059	0.024
	cpx1	103	285	55.4	56.7	0.036	18.8	57.0	59.0	0.077	1.62	8.72	39.7	42.6	12.5	3.02	12.8	12.7	6.59	5.82	0.824	2.81	0.012	0.039	0.008
	cpx2	70.6	297	46.4	64.0		18.9	14.7	87.5			10.2	38.3	42.5	12.0	2.95	10.0	5.26	1.16	0.548	0.103	3.03		0.116	70.6
	grt	106	122	64.0	2.03	0.213	-	205	18.2	0.065	-	0.076	0.331	3.24	4.82	2.63	15.9	32.0	22.6	23.4	3.74	0.257	-	-	0.118
	il	44.4	1032	70.4	19.6	-	-	0.360	22.6	396	-	1.89	1.83	0.517	0.187	0.048	0.087	0.057	0.251	0.402	0.092	1.49	18.9	0.550	0.037
	mgt	0.340	2026	630	88.3	-	-	0.070	0.026	1.39	-	0.223	0.282	0.187	0.300	0.025	0.110	0.049	0.044	0.067	-	0.027	0.097	-	0.001
	pl	n.a.	n.a.	n.a.	n.a.	0.070	700	n.a.	n.a.	n.a.	288	8.35	11.2	2.44	0.211	1.41	0.102	0.044	0.017	0.014	0.037	n.a.	n.a.	n.a.	n.a.
	ap 1	-	8.76	-	3.31	-	214	389	-	0.048	1.05	834	1844	979	185	31.4	148	84.9	32.0	19.4	2.45	-	-	4.28	2.21
	ap 2	-	12.8	-	0.670	-	232	361	0.593	0.174	0.550	232	828	624	128	23.4	118	71.9	34.1	19.7	2.97	-	-	5.29	2.38
	ap 3	-	6.45	-	3.52	-	209	329	0.459	-	4.38	44.2	245	326	89.5	20.4	96.6	67.1	31.1	19.8	2.72	-	-	2.71	1.85

Appendix B continued

Sample	mineral	Sc	V	Cr	Ni	Rb	Sr	Y	Zr	Nb	Ba	La	Ce	Nd	Sm	Eu	Gd	Dy	Er	Yb	Lu	Hf	Ta	Th	U
049M grt-cpx granulite	amph 1	131	1101	380	111	3.49	73.9	80.7	40.5	8.85	264	17.3	52.5	47.1	14.3	3.10	17.3	16.2	8.38	6.74	0.808	2.83	0.367	0.160	0.035
	amph 2	127	885	331	106	3.17	68.2	94.2	44.1	8.49	265	16.9	50.2	43.1	12.7	2.96	15.9	17.4	10.1	9.48	1.35	2.82	0.431	0.176	0.038
	cpx 1	102	n.a.	111	65.8	0.136	16.2	12.3	69.7	0.015	0.112	4.87	18.3	19.7	6.53	1.32	6.52	3.85	0.922	0.517	0.052	3.81	0.007	0.067	0.010
	cpx 2	131	705	255	60.9	0.073	16.1	24.2	49.9	0.041	0.770	5.03	18.5	18.7	5.94	1.15	6.68	5.99	2.47	1.90	0.270	3.41	0.007	0.079	0.016
	cpx 3	122	n.a.	161	64.7	0.152	14.9	31.0	46.1	0.024	0.453	4.16	13.9	12.6	4.11	0.914	5.13	6.05	3.63	3.76	0.573	2.86	0.007	0.074	0.015
	grt	82.1	282	211	1.38	-	0.062	206	13.9	0.020	-	0.106	0.311	1.52	3.10	1.27	12.2	28.9	23.9	28.2	4.46	0.198	0.006	0.022	0.005
	opx	27.7	150	64.5	68.7	0.118	0.378	2.86	0.933	0.006	0.308	0.094	0.178	0.153	0.089	0.025	0.205	0.490	0.545	0.998	0.191	0.068	0.001	3.39	0.043
	pl	4.96	0.185	-	4.53	0.155	643	0.069	0.045	-	301	3.71	4.45	0.771	0.069	0.976	0.050	0.019	0.008	-	0.002	-	-	-	-
	ap 1	-	4.83	-	12.7	0.155	300	156	24.4	113	0.004	330	716	403	83.5	10.2	77.4	39.1	12.1	5.77	0.755	1.12	0.023	4.85	2.74
	ap 2	-	7.24	-	15.0	0.558	191	288	1.28	47.7	-	480	993	527	102	9.72	100	61.3	25.8	13.9	1.98	-	-	7.39	4.22
	ap 3	-	3.54	-	2.29	0.265	185	339	0.495	0.523	0.014	418	795	372	76.3	9.40	77.9	60.6	32.4	22.7	3.17	-	0.007	7.17	4.09
076M1 grt-cpx granulite	amph	72.0	521	2.42	16.0	2.69	77.3	19.9	38.6	12.4	290	37.7	99.0	57.1	11.2	2.48	9.24	5.68	1.64	0.913	0.110	2.55	0.600	0.187	0.030
	cpx	85.0	263	2.18	9.90	0.253	19.4	6.66	40.9	0.131	3.56	8.57	26.6	16.9	3.53	0.761	3.00	1.92	0.573	0.355	0.053	2.37	0.016	0.046	0.019
	grt	78.8	175	3.21	0.569	0.060	0.193	140	6.90	0.033	0.086	0.082	0.282	1.65	2.51	1.10	8.48	20.2	17.0	19.4	3.16	0.142	0.001	-	0.002
	pl	n.a.	n.a.	n.a.	n.a.	0.200	724	n.a.	n.a.	n.a.	238	7.78	7.08	0.856	0.084	0.599	0.115	-	-	-	0.013	n.a.	n.a.	n.a.	n.a.
076a opx-cpx granulite	amph	80.2	444	92.3	101	2.14	45.2	33.7	33.4	5.65	60.3	9.85	32.0	22.9	5.44	1.44	5.80	6.18	3.62	3.54	0.509	n.a.	0.247	0.106	0.037
	cpx	84.6	221	16.8	43.2	-	13.5	10.0	33.9	0.063	0.851	2.99	10.6	7.52	1.71	0.499	1.83	2.08	1.08	1.12	0.184	n.a.	0.015	0.025	0.012
	opx	15.8	65.9	205	52.9	0.097	0.754	0.347	0.670	n.a.	0.224	0.023	0.046	0.041	-	0.010	0.050	0.074	0.094	0.223	0.050	n.a.	n.a.	n.a.	n.a.
	pl	n.a.	n.a.	n.a.	n.a.	0.088	542	n.a.	n.a.	n.a.	93.3	4.36	5.25	0.749	0.062	0.299	0.032	0.025	0.016	-	-	n.a.	n.a.	n.a.	n.a.
112M opx-cpx granulite	amph	86.4	474	21.7	101	0.874	41.5	33.5	40.9	5.98	72.5	11.4	33.4	22.3	5.04	1.35	5.64	6.05	3.55	3.40	0.534	n.a.	0.322	0.143	0.068
	cpx	80.0	201	6.93	41.3	0.070	21.9	9.57	35.3	0.050	3.83	3.39	10.4	6.90	1.61	0.416	1.64	1.83	1.08	1.06	0.160	n.a.	-	0.037	0.007
	opx	n.a.	n.a.	n.a.	n.a.	0.027	0.305	n.a.	n.a.	n.a.	0.299	0.020	0.036	0.035	-	0.011	0.053	0.066	0.099	0.224	0.045	n.a.	n.a.	n.a.	n.a.
	pl	n.a.	n.a.	n.a.	n.a.	0.418	510	n.a.	n.a.	n.a.	134	4.16	4.29	0.623	0.177	0.288	0.064	-	-	-	-	n.a.	n.a.	n.a.	n.a.
080M opx-cpx granulite	amph	73.2	552	1485	372	5.38	33.5	136	34.8	32.1	123	46.3	168	121	27.2	3.03	26.7	23.6	13.8	12.9	1.73	n.a.	1.78	0.724	0.069
	bt	10.8	624	1013	747	318	3.57	0.055	0.590	39.7	3527	0.166	0.166	0.086	0.027	0.090	0.042	-	0.018	0.017	0.005	n.a.	2.39	0.012	0.730
	cpx	76.2	n.a.	436	199	0.118	11.7	50.3	33.8	0.071	0.963	11.3	46.7	37.6	9.29	0.968	9.11	9.31	5.42	5.53	0.808	2.51	0.025	0.133	0.023
	opx	12.8	n.a.	157	208	0.307	0.725	2.72	0.625	0.014	1.72	0.405	0.434	0.296	0.083	0.016	0.147	0.304	0.403	0.844	0.163	0.059	0.003	0.194	0.030
	pl	n.a.	n.a.	n.a.	n.a.	0.394	458	n.a.	n.a.	n.a.	117	11.8	14.6	2.26	0.154	0.787	0.074	0.025	0.010	-	-	-	-	-	-
102a opx-cpx granulite	amph	142	180	334	109	5.34	42.7	237	60.21	36.4	107	69.7	233	197	49.9	4.26	48.1	45.8	24.3	20.6	2.85	3.59	1.43	0.333	0.044
	cpx	203	107	214	63.6	0.084	15.9	85.0	47.11	0.110	0.410	13.2	55.6	51.4	15.4	1.45	15.8	16.5	9.40	8.91	1.36	2.97	0.022	0.052	0.360
	opx	32.8	19.5	35.0	66.3	0.091	0.753	3.58	0.471	0.051	0.272	0.367	0.906	0.469	0.148	0.020	0.194	0.470	0.596	1.45	0.270	0.068	-	-	-
	pl	1.16	0.263	3.46	0.685	0.303	636	0.178	-	0.019	127	15.1	17.9	2.75	0.203	0.800	0.096	0.032	0.023	-	-	-	-	0.046	-
114M opx-cpx granulite	amph	78.7	466	15.2	77.0	9.53	44.1	53.1	62.54	13.8	64.9	20.7	67.9	51.1	10.7	2.39	10.1	9.51	5.53	5.72	0.872	2.85	1.26	0.682	0.368
	cpx	107	280	12.4	48.3	0.227	14.7	19.2	50.60	0.082	0.443	4.88	18.9	14.9	3.29	0.725	3.22	3.50	1.99	2.46	0.432	2.36	0.041	0.183	0.143
	opx	14.1	43.6	5.21	52.5	0.030	0.446	0.634	0.855	-	0.229	0.075	0.183	0.123	0.076	0.019	0.088	0.136	0.193	0.503	0.113	0.080	0.019	0.105	0.218
	pl	2.78	5.67	4.01	1.58	0.275	643	0.255	0.40	0.032	65.8	5.73	6.71	0.905	0.053	0.441	0.087	0.043	0.030	0.041	0.010	0.101	0.053	0.020	-

References

Armstrong, J. T. (1995). CITZAF: a package of correction programs for the quantitative electron microbeam X-ray analysis of thick polished materials, thin films, and particles. *Microbeam Analysis* 4, 177-200.

Bacon, C. R. & Druitt, T. H. (1988). Compositional evolution of the zoned calcalkaline magma chamber of Mount-Mazama, Crater Lake, Oregon. *Contributions to Mineralogy and Petrology* **98**(2), 224-256.

Barth, M. G., Foley, S.F. & Horn, I. (2002). Partial melting in Archean subduction zones: constraints from experimentally determined trace element partition coefficients between eclogitic minerals and tonalitic melts under upper mantle condiditons. *Precambrian Research* **113**, 323-340.

Bea, F., Pereira, M. D. & Stroh, A. (1994). Mineral / leucosome trace-element partitioning in a peraluminous migmatite (a laser ablation-ICP-MS study). *Chemical Geology* **117**, 291-312.

Beard, J. S. & Lofgren, G. E. (1991). Dehydration melting and water-saturated melting of basaltic and andesitic greenstones and amphibolites at 1,3 and 6-9 kb. *Journal of Petrology* **32**, 365-401.

Bédard, J. H. (2006a). A catalytic delamination-driven model for coupled genesis of Archaean crust and sub-continental lithospheric mantle. *Geochimica et Cosmochimica Acta* **70**, 1188-1214.

Bédard, J. H. (2006b). Trace element partitioning in plagioclase feldspar. *Geochimica et Cosmochimica Acta* **70**, 3717-3742.

Bindeman, I. N., Davies, A. M. & Drake, M. J. (1998). Ion microprobe study of plagioclase-basalt experiments at natural concentration levels of trace elements. *Geochimica et Cosmochimica Acta* **62**(7), 1175-1193.

Blundy, J. & Wood, B. (1991). Crystal-chemical controls on the partitioning of Sr and Ba between plagioclase feldspar, silicate melts and hydrothermal solutions. *Geochimica et Cosmochimica Acta* **55**, 193-209.

Blundy, J. & Wood, B. (1994). Prediction of crystal-melt partition-coefficients from elastic-moduli. *Nature* **372**(6505), 452-454.

Bottazzi, P., Tiepolo, M., Vannucci, R., Zanetti, A., Brumm, R., Foley, S. F. & Oberti, R. (1999). Distinct site preferences for heavy and light REE in amphibole and the prediction of D-Amph/L(REE). *Contributions to Mineralogy and Petrology* **137**(1-2), 36-45.

Brenan, J. M., Shaw, H. F., Ryerson, F. J. & Phinney, D. L. (1995). Experimental determination of trace element partitioning between pargasite and a synthetic hydrous andesitic melt. *Earth and Planetary Science Letters* **135**, 1-11.

Cawthorn, R. G. (1996). Models for incompatible trace-element abundances in cumulus minerals and their application to plagioclase and pyroxenes in the Bushveld Complex. *Contributions to Mineralogy and Petrology* **123**(1), 109-115.

Cawthorn, R. G. & Collerson, K. D. (1974). The recalculation of pyroxene end-member parameters and the estimation of ferrous and ferric iron content from electron microprobe

analyses. *American Mineralogist* **59**, 1203-1208.

Chazot, G., Menzies, M. A. & Harte, B. (1996). Determination of partition coefficients between apatite, clinopyroxene, amphibole, and melt in natural spinel lherzolites from Yemen: Implications for wet melting of the lithospheric mantle. *Geochimica Et Cosmochimica Acta* **60**(3), 423-437.

Clarke, G. L., White, R. W., Lui, S., Fitzherbert, J. A. & Pearson, N. J. (2007). Contrasting behaviour of rare earth and major elements during partial melting in granulite facies migmatites, Wuluma Hills, Arunta Block, central Australia. *Journal of Metamorphic Geology* **25**(1), 1-18.

Colson, R. O., McKay, G. A. & Taylor, L. A. (1988). Temperature and composition dependencies of trace-element partitioning - olivine melt and low-Ca pyroxene melt. *Geochimica et Cosmochimica Acta* **52**(2), 539-553.

Dalpé, C. & Baker, D. R. (2000). Experimental investigation of large-ion-lithophile-element-, high-field-strength-element- and rare-earth-element- partitioning between calcic amphibole and basaltic melt: the effects of pressure and oxygen fugacity. *Contributions to Mineralogy and Petrology* **140**(2), 233-250.

Dunn, T. & Sen, C. (1994). Mineral / matrix partition coefficients for orthopyroxene, plagioclase and olivine in basaltic to andesitic systems: A combined analytical and experimental study. *Geochimica et Cosmochimica Acta* **58**(2), 717-733.

Dostal, J., Dupuy, C., Carron, J. P., Le Guen de Kerneizon, M. & Maury, R. C. (1983). Partition coefficients of trace elements: application to volcanic rocks of St. Vincent, West Indies. *Geochimica et Cosmochimica Acta* **47**, 525-533.

Drummond, M. S. & Defant, M. J. (1990). A model for trondhjemite-tonalite-dacite genesis and crustal growth via slab melting - Archean to modern comparisons. *Journal of Geophysical Research-Solid Earth and Planets* **95**(B13), 21503-21521.

Ewart, A. & Griffin, W. L. (1994). Application of proton-microprobe data to trace element partitioning in volcanic rocks. *Chemical Geology* **117**, 251-284.

Fedorowich, J. S., Richards, J. P., Jain, J. C., Kerrich, R. & Fan, J. (1993). A rapid method for REE and trace-element analysis using laser sampling ICP-MS on direct fusion whole-rock glasses. *Chemical Geology* **106**, 229-249.

Foley, S.F., Tiepolo, M. & Vannucci, R. (2002). Growth of early continental crust controlled by melting of amphibolite in subduction zones. *Nature* **417**, 837-840.

Foley, S. F., Jackson, S. E., Fryer, B. J., Greenough, J. D. & Jenner, G. A. (1996). Trace element partition coefficients for clinopyroxene and phlogopite in an alkaline lamprophyre from Newfoundland by LAM-ICP-MS. *Geochimica et Cosmochimica Acta* **60**(4), 629-638.

Fujimaki, H. (1986). Partition-Coefficients of Hf, Zr, and Ree between zircon, apatite, and liquid. *Contributions to Mineralogy and Petrology* **94**(1), 42-45.

Glaser, S. M., Foley, S. F. & Günther, D. (1999). Trace element compositions of minerals in garnet and spinel peridotite xenoliths from the Vitim volcanic field, Transbaikalia, eastern Siberia. *Lithos* **48**, 263-285.

Green, T. H. & Pearson, N. J. (1985). Rare earth element partitioning between clinopyroxene and

silicate liquid at moderate to high pressure. *Contributions to Mineralogy and Petrology* **91**, 24-36.

Hart, S. R. & Dunn, T. (1993). Experimental cpx / melt partitioning of 24 trace elements. *Contributions to Mineralogy and Petrology* **113**, 1-8.

Hartel, T. H. D. & Pattison, D. R. M. (1996). Genesis of the Kapuskasing (Ontario) migmatitic mafic granulites by dehydration melting of amphibolite: The importance of quartz to reaction progress. *Journal of Metamorphic Geology* **14**, 591-611.

Hauri, E. H., Wagner T. P. & Grove T. L. (1994). Experimental and natural partitioning of Th, U, Pb and other trace elements between garnet, clinopyroxene and basaltic melts. *Chemical Geology* **117**, 149--167.

Hellebrand, E., Snow, J. E., Mostefaoui, S. & Hoppe, P. (2005). Trace element distribution between orthopyroxene and clinopyroxene in peridotites from the Gakkel Ridge: A SIMS and NanoSIMS study. *Contributions to Mineralogy and Petrology* **150**(5), 486-504.

Hill, E., Wood, B. J. & Blundy, J. D. (2000). The effect of Ca-Tschermaks component on trace element partitioning between clinopyroxene and silicate melt. *Lithos* **53**(3-4), 203-215.

Hilyard, M., Nielsen, R. L., Beard, J. S., Patiño-Douce, A. & Blencoe, J. (2000). Experimental determination of the partitioning behavior of rare earth and high field strength elements between pargasitic amphibole and natural silicate melts. *Geochimica et Cosmochimica Acta* **64**(6), 1103-1120.

Hölttä,P., Huhma, H., Mänttäri, I. & Paavola, J. (2000). P-T-t development of Archaean granulites in Varpaisjärvi, Central Finland. II. Dating of high-grade metamorphism with the U-Pb and Sm-Nd methods. *Lithos* **50**, 121-136.

Hölttä, P. & Paavola, J. (2000b). P-T-t development of Archaean granulites in Varpaisjärvi, Central Finland. I. Effects of multiple metamorphism on the reaction history of mafic rocks. *Lithos* **50**, 97-120.

Ionov, D. A. & Hofmann, A. W. (1995). Nb-Ta rich mantle amphiboles and micas: Implications for subduction-related metasomatic trace element fractionations. *Earth and Planetary Science Letters* **131**, 341-356.

Irving, A. J. & Frey, F. A. (1978). Distribution of trace elements between garnet megacrysts and host volcanic liquids of kimberlitic to rhyolitic composition. *Geochimica et Cosmochimica Acta* **42**, 771-787.

Jochum, K. P., Stoll, B., Herwig, K. & Amini, M. (2005). Trace element and isotope analyses of geo- and cosmochemical samples by laser ablation-sector field-ICPMS. In *High-Resolution ICP-MS* (ed. C. B. Douthitt).

Kar, R., Bhattacharya, S. & Sheraton, J. W. (2003). Hornblende-dehydration melting in mafic rocks and the link between massif-type charnockite and associated granulites, Eastern Ghats Granulite Belt, India. *Contributions to Mineralogy and Petrology* **145**(6), 707-729.

Klein, M., Stosch, H. G., Seck, H. A. & Shimizu, N. (2000). Experimental partitioning of high field strength and rare earth elements between clinopyroxene and garnet in andesitic to tonalitic systems. *Geochimica et Cosmochimica Acta* **64**(1), 99-115.

Klein, M., Stosch, H.-G. & Seck, H. A. (1997). Partitioning of high field-strength and rare-earth

elements between amphibole and quartz-dioritic to tonalitic melts: An experimental study. *Chemical Geology* **138**, 257-271.

Klemme, S., Günther, D., Hametner, K., Prowatke, S. & Zack, T. (2006). The partitioning of trace elements between ilmenite, ulvospinel, annalcolite and silicate melts with implications for the early differentiation of the moon. *Chemical Geology* **234**(3-4), 251-263.

LaTourrette, T., Hervig, R. L.& Holloway, J. R. (1995). Trace-Element partitioning between amphibole, phlogopite, and basanite Melt. *Earth and Planetary Science Letters* **135**(1-4), 13-30.

Leake, B. E. (1997). Nomenclature of amphiboles: Report of the subcommittee on amphiboles of the international mineralogical association, commission on new minerals and mineral names. *The Canadian Mineralogist* **35**, 219-246.

Luhr, J. F., Carmichael, I. S. E. & Varekamp, J. C. (1984). The 1982 eruptions of El Chichón volcano, Chiapas, Mexico: Mineralogy and petrology of the anhydrite-bearing pumices. *Journal of Volcanology and Geothermal Research* **23**, 69-108.

Luhr, J. F. & Carmichael, I. S. E. (1980). The Colima Volcanic Complex, Mexico. *Contributions to Mineralogy and Petrology* **71**, 343-372.

Mahood, G. A. & Stimac, J. A. (1990). Trace-element partitioning in pantellerites and trachytes. *Geochimica et Cosmochimica Acta* **54**, 2257-2276.

Mahood, G. A. & Hildreth, E. W. (1983). Large partition coefficients for trace elements in high-silica rhyolites. *Geochimica et Cosmochimica Acta* **47**, 11-30.

Mänttäri, I. & Hölttä, P. (2002). U-Pb dating of zircons and monazites from Archean granulites in Varpaisjärvi, Central Finland: Evidence for multiple metamorphism and Neoarchean terrane accretion. *Precambrian Research* **118**, 101-131.

Marchildon, N. & Brown, M. (2001). Melt segregation in late syn-tectonic anatectic migmatites: an example from the Onawa contact aureole, Maine, USA. *Physics and Chemistry of the Earth Part A - Solid Earth and Geodesy* **26**, 225-229.

Martin, H. (1994). The Archean grey gneisses and the genesis of continental crust. In *Archean Crustal Evolution* (ed. K. C. Condie), pp. 205-247. Developments in Precambrian Geology.

McKenzie, D. & O'Nions R. K. (1991). Partial melt distributions from inversion of rare earth element concentrations. *Journal of Petrology* **32**, 1021-1091.

Nagasawa, H. (1970). Rare Earth concentrations in zircon and apatite and their host dacite and granites. *Earth and Planetary Science Letters* **9**, 359-364.

Nash, W. P. & Crecraft, H. R. (1985). Partition coefficients for trace elements in silicic magmas. *Geochimica et Cosmochimica Acta*(49), 2309-2322.

Nicholls, I. A. & Harris, K. L. (1980). Experimental rare earth element partition coefficients for garnet, clinopyroxene and amphibole coexisting with andesitic and basaltic liquids. *Geochimica et Cosmochimica Acta* **44**, 287-308.

Nielsen, R. L., Gallahan, W. E. & Newberger, F. (1992). Experimentally determined mineral-melt partition coefficients for Sc, Y and REE for olivine, orthopyroxene, pigeonite,

magnetite and ilmenite. *Contributions to Mineralogy and Petrology* **110**, 448-499.

Orejana, D., Villaseca, C. & Paterson, B. A. (2006). Geochemistry of pyroxenitic and hornblenditic xenoliths in alkaline lamprophyres from the Spanish Central System. *Lithos* **86**, 167-196.

Paster, T. P., Schauwecker, D. S. & Haskin, L. A. (1974). The behavior of some trace elements during solidification of the Skaergaard layered series. *Geochimica et Cosmochimica Acta* **38**(10), 1549-1577.

Patiño Douce, A. E. & Beard, J. S. (1995). Dehydration-melting of biotite gneiss and quartz amphibolite from 3 to 15 kbar. *Journal of Petrology* **36**(3), 707-738.

Pearce, N. J. G., Perkins, W. T., Westgate, J. A., Gorton, M. P., Jackson, S. E., Neal, C. R. & Chenery, S. P. (1997). A compilation of new and published major and trace element data for NIST SRM 610 and NIST SRM 612 glass refernce materials. *Geostandards Newsletter* **21**(1), 115-144.

Pride, C. & Muecke, G. K. (1981). Rare earth element distributions among coexisting granulite facies minerals, Scourian Complex, NW Scotland. *Contributions to Mineralogy and Petrology* **76**, 463-471.

Prowatke, S. & Klemme, S. (2006). Trace element partitioning between apatite and silicate melts. *Geochimica et Cosmochimica Acta* **70**(17), 4513-4527.

Rapp, R. P., Shimizu, N. & Norman, M. D. (2003). Growth of early continental crust by partial melting of eclogite. *Nature* **425**, 605-609.

Rønsbo, J. G. (1989). Coupled substitutions involving REEs and Na and Si in apatites in alkaline rocks from the Ilímaussaq intrusion, South Greenland, and the petrological implications. *American Mineralogist* **74**, 896-901.

Rushmer, T. (1991). Partial melting of two amphibolites: Contrasting experimental results under fluid-absent conditions. *Contributions to Mineralogy and Petrology* **107**, 41-59.

Sawyer, E. W. (1991). Disequilibrium melting and rate of melt-residuum separation during migmatization of mafic rocks from the Grenville front, Quebec. *Journal of Petrology* **32**, 701-738.

Schmidt, K. H., Bottazzi, P., Vannucci, R. & Mengel, K. (1999). Trace element partitioning between phlogopite, clinopyroxene and leucite lamproite melt. *Earth and Planetary Science Letters* **168**, 287–299.

Smithies, R. H. (2000). The Archaean tonalite-trondhjemite-granodiorite (TTG) series is not an analogue of Cenozoic adakite. *Earth and Planetary Science Letters* **182**(1), 115-125.

Schnetzler, C. C. & Philpotts, J. A. (1970). Partition coefficients of rare-earth elements between igneous matrix material and rock-forming mineral phenocrysts; II. *Geochimica et Cosmochimica Acta* **34**(3), 331-340.

Schröter, F. C. (2006). Mineral trace element distribution in amphibolite and granulite facies mafic rocks. Ph.D. thesis. The University of Sydney, Sydney, 85 pp..

Schröter, F. C., Stevenson, J. A., Daczko, N. R., Clarke, G. L., Pearson, N. J. & Klepeis, K. A. (2004). Trace element partitioning during high-P partial melting and melt-rock interaction; an example from northern Fiordland, New Zealand. *Journal of Metamorphic*

Geology **22**(5), 443-457.

Schwandt, C. S. & McKay, G. A. (1998). Rare earth element partition coefficients from enstatite/melt synthesis experiments. *Geochimica et Cosmochimica Acta* **62**(16), 2845-2848.

Sen, S. K. & Dunn, T. (1994). Dehydration melting of a basaltic composition amphibolite at 1.5 and 2 GPa: Implications for the origin of adakites. *Contributions to Mineralogy and Petrology* **117**, 394-409.

Sisson, T. W. (1994). Hornblende-melt trace-element partitioning measured by ion microprobe. *Chemical Geology* **117**, 331-344.

Sisson, T. W. & Bacon, C. R. (1992). Garnet / high-silica rhyolite trace element partition coefficients measured by ion microprobe. *Geochimica et Cosmochimica Acta* **56**, 2133-2136.

Skora, S., Baumgartner, L. P., Mahlen, N. J., Johnson, C. M., Pilet, S. & Hellebrand, E. (2006). Diffusion-limited REE uptake by eclogite garnets and its consequences for Lu-Hf and Sm-Nd geochronology. *Contributions to Mineralogy and Petrology* **152**, 703-720.

Solar, G. S. & Brown, M. (2001). Petrogenesis of migmatites in Maine, USA: Possible source of peraluminous leucogranite in plutons? *Journal of Petrology* **42**(4), 789-823.

Stimac, J. & Hickmott, D. (1994). Trace-element partition-coefficients for ilmenite, orthopyroxene and pyrrhotite in rhyolite determined by micro-Pixe analysis. *Chemical Geology* **117**(1-4), 313-330.

Storkey, A. C., Hermann, J., Hand, M. & Buick, I. S. (2005). Using in situ trace-element determinations to monitor partial-melting processes in metabasites. *Journal of Petrology* **46**(6), 1283-1308.

Tiepolo, M., Bottazzi, P., Foley, S. F., Oberti, R., Vannucci, R. & Zanetti, A. (2001). Fractionation of Nb and Ta from Zr and Hf at mantle depths: The role of titanian pargasite and kaersutite. *Journal of Petrology* **42**(1), 221-232.

van Westrenen, W., Wood, B. J. & Blundy, J. D. (2001). A predictive thermodynamic model of garnet-melt trace element partitioning. *Contributions to Mineralogy and Petrology* **142**(2), 219-234.

Vielzeuf, D., & Vidal, P. (ed.) (1990). *Granulites and Crustal Evolution*, pp. 600. Kluwer Academic Publisher.

Villaseca, C., Romera, C. M., De la Rosa, J. & Barbero, L. (2003). Residence and redistribution of REE, Y, Zr, Th and U during granulite-facies metamorphism: behaviour of accessory and major phases in peraluminous granulites of central Spain. *Chemical Geology* **200**(3-4), 293-323.

Watson, E. B. & Green, T. H. (1981). Apatite/liquid partition coefficients for the rare earth elements and strontium. *Earth and Planetary Science Letters* **56**, 405-421.

Watt G. R., Burns I. M. & Graham G. A. (1996). Chemical characteristics of migmatites: Accessory phase distribution and evidence for fast melt segregation rates. *Contributions to Mineralogy and Petrology* **125**, 100-111.

Wilke, M. & Behrens, H. (1999). The dependence of the partitioning of iron and europium

between plagioclase and hydrous tonalitic melt on oxygen fugacity. *Contributions to Mineralogy and Petrology* **137**(1-2), 102-114.

Williams, M. L., Hammer, S., Kopf, C. & Darrach, M. (1995). Syntectonic generation and segregation of tonalitic melts from amphibolite dikes in the lower crust, Striding-Athabasca mylonite zone, northern Saskatchewan. *Journal of Geophysical Research-Solid Earth* **100**, 15717-15734.

Witt-Eickschen, G. & Harte, B. (1994). Distribution of trace elements between amphibole and clinopyroxene from mantle peridotites of the Eifel (western Germany): An ion-microprobe study. *Chemical Geology* **117**, 235-250.

Wolf, M. B. & Wyllie, P. J. (1994). Dehydration-melting of amphibolite at 10 kbar - the effects of temperature and time. *Contributions to Mineralogy and Petrology* **115**(4), 369-383.

Wood, B. & Blundy, J. (2002). The effect of H_2O on crystal-melt partitioning of trace elements. *Geochimica et Cosmochimica Acta* **66**(20), 3647-3656.

Wood, B. J. & Blundy, J. D. (1997). A predictive model for rare earth element partitioning between clinopyroxene and anhydrous silicate melt. *Contributions to Mineralogy and Petrology* **129**(2-3), 166-181.

Xiong, X. L. (2006). Trace element evidence for growth of early continental crust by melting of rutile-bearing hydrous eclogite. *Geology* **34**(11), 945-948.

Zack, T. & Brumm, R. (1998). Ilmenite / liquid partition coefficients of 26 trace elements determinded through ilmenite / clinopyroxene partitioning in garnet pyroxenites. *The 7th International Kimberlite Conference*, 986-988.

Zack, T., Foley, S. & Jenner, G. A. (1997). A consistent partition coefficient set for clinopyroxene, amphibole and garnet from laser ablation microprobe analysis of garnet pyroxenites from Kakanui, New Zealand. *Neues Jahrbuch für Mineralogische Abhandlungen* **172**(1), 23-41.

Zhao, G. C., Wilde, S. A., Cawood, P. A. & Lu, L. Z. (2000). Petrology and P-T path of the Fuping mafic granulites: implications for tectonic evolution of the central zone of the North China craton. *Journal of Metamorphic Geology* **18**(4), 375-391.